frontiers | Research Topics

Enhancement of photosynthesis through light utilization in plants and crops

Edited by
Jose R. Peralta-Videa, Sina Fallah and Meijian Yang

Published in
Frontiers in Plant Science

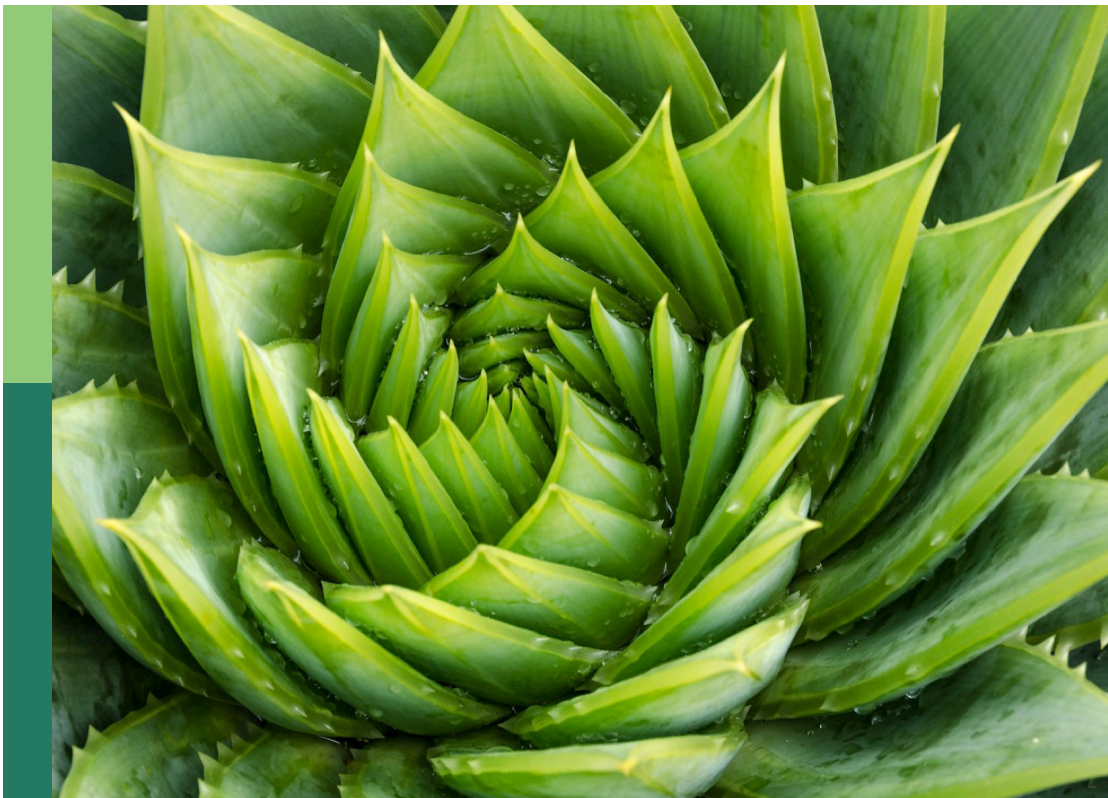

ISSN 1664-8714
ISBN 978-2-8325-6401-1
DOI 10.3389/978-2-8325-6401-1

About Frontiers

Frontiers is more than just an open access publisher of scholarly articles: it is a pioneering approach to the world of academia, radically improving the way scholarly research is managed. The grand vision of Frontiers is a world where all people have an equal opportunity to seek, share and generate knowledge. Frontiers provides immediate and permanent online open access to all its publications, but this alone is not enough to realize our grand goals.

Frontiers journal series

The Frontiers journal series is a multi-tier and interdisciplinary set of open-access, online journals, promising a paradigm shift from the current review, selection and dissemination processes in academic publishing. All Frontiers journals are driven by researchers for researchers; therefore, they constitute a service to the scholarly community. At the same time, the *Frontiers journal series* operates on a revolutionary invention, the tiered publishing system, initially addressing specific communities of scholars, and gradually climbing up to broader public understanding, thus serving the interests of the lay society, too.

Dedication to quality

Each Frontiers article is a landmark of the highest quality, thanks to genuinely collaborative interactions between authors and review editors, who include some of the world's best academicians. Research must be certified by peers before entering a stream of knowledge that may eventually reach the public - and shape society; therefore, Frontiers only applies the most rigorous and unbiased reviews. Frontiers revolutionizes research publishing by freely delivering the most outstanding research, evaluated with no bias from both the academic and social point of view. By applying the most advanced information technologies, Frontiers is catapulting scholarly publishing into a new generation.

What are Frontiers Research Topics?

Frontiers Research Topics are very popular trademarks of the *Frontiers journals series*: they are collections of at least ten articles, all centered on a particular subject. With their unique mix of varied contributions from Original Research to Review Articles, Frontiers Research Topics unify the most influential researchers, the latest key findings and historical advances in a hot research area.

Find out more on how to host your own Frontiers Research Topic or contribute to one as an author by contacting the Frontiers editorial office: frontiersin.org/about/contact

Enhancement of photosynthesis through light utilization in plants and crops

Topic editors

Jose R. Peralta-Videa — The University of Texas at El Paso, United States
Sina Fallah — Shahrekord University, Iran
Meijian Yang — Cornell University, United States

Citation

Peralta-Videa, J. R., Fallah, S., Yang, M., eds. (2025). *Enhancement of photosynthesis through light utilization in plants and crops*. Lausanne: Frontiers Media SA.
doi: 10.3389/978-2-8325-6401-1

Table of contents

05 Editorial: Enhancement of photosynthesis through light utilization in plants and crops
Sina Fallah, Meijian Yang and Jose R. Peralta-Videa

08 LHCA4 residues surrounding red chlorophylls allow for fine-tuning of the spectral region for photosynthesis in *Arabidopsis thaliana*
Xiuxiu Li, Lixia Zhu, Jince Song, Wenda Wang, Tingyun Kuang, Gongxian Yang, Chenyang Hao and Xiaochun Qin

20 Photosynthesis in rice is increased by CRISPR/Cas9-mediated transformation of two truncated light-harvesting antenna
Daniel Caddell, Noah J. Langenfeld, Madigan JH. Eckels, Shuyang Zhen, Rachel Klaras, Laxmi Mishra, Bruce Bugbee and Devin Coleman-Derr

32 Light means power: harnessing light spectrum and UV-B to enhance photosynthesis and rutin levels in microtomato plants
Iury Henrique Almeida Lima, Arthur Almeida Rodrigues, Erika Crispim Resende, Fábia Barbosa da Silva, Fernanda dos Santos Farnese, Lucas de Jesus Silva, Márcio Rosa, Mateus Neri Oliveira Reis, Layara Alexandre Bessa, Thales Caetano de Oliveira, Ana Helena Januário and Fabiano Guimarães Silva

44 Effect of red and blue light versus white light on fruit biomass radiation-use efficiency in dwarf tomatoes
Xinglin Ke, Hideo Yoshida, Shoko Hikosaka and Eiji Goto

55 Response of stomatal conductance, transpiration, and photosynthesis to light and CO_2 for rice leaves with different appearance days
Yuping Lv, Linhui Gu, Runze Man, Xiaoyin Liu and Junzeng Xu

68 Investigating the influence of varied ratios of red and far-red light on lettuce (*Lactuca sativa*): effects on growth, photosynthetic characteristics and chlorophyll fluorescence
Xueting Bi, Hong Xu, Chaowei Yang, Haoran Zhang, Wei Li, Wei Su, Mingtao Zheng and Bingfu Lei

82 Cell size differences affect photosynthetic capacity in a Mesoamerican and an Andean genotype of *Phaseolus vulgaris* L.
Andrew Ogolla Egesa, C. Eduardo Vallejos and Kevin Begcy

98 Reducing red light proportion in full-spectrum LEDs enhances runner plant propagation by promoting the growth and development of mother plants in strawberry
Jian Chen, Fang Ji, Rongwei Gao and Dongxian He

111 Lowering the target daily light integrals following days with excessive lighting can reduce lettuce production costs
Andres M. Mayorga-Gomez, Marc W. van Iersel and Rhuanito Soranz Ferrarezi

126 Laser biospeckle as a method to investigate the short-term effects of far-red light on an arugula (*Eruca sativa* Mill) plant
Hibiki Igarashi, Takeshi Baba, Kairi Takemura, Takahiro Kono, Hirofumi Kadono, Jun Yamada and Uma Maheswari Rajagopalan

frontiers | Frontiers in Plant Science

TYPE Editorial
PUBLISHED 19 May 2025
DOI 10.3389/fpls.2025.1569835

OPEN ACCESS

EDITED AND REVIEWED BY
Xinguang Zhu,
University of Chinese Academy of Sciences, Beijing, China

*CORRESPONDENCE
Jose R. Peralta-Videa
jperalta@utep.edu

RECEIVED 01 February 2025
ACCEPTED 16 April 2025
PUBLISHED 19 May 2025

CITATION
Fallah S, Yang M and Peralta-Videa JR (2025) Editorial: Enhancement of photosynthesis through light utilization in plants and crops. *Front. Plant Sci.* 16:1569835. doi: 10.3389/fpls.2025.1569835

Editorial: Enhancement of photosynthesis through light utilization in plants and crops

Sina Fallah[1], Meijian Yang[2] and Jose R. Peralta-Videa[3]*

[1]Department of Agronomy, Faculty of Agriculture, Shahrekord University, Shahrekord, Iran, [2]Center for Climate Systems Research (CCSR), Columbia Climate School, Columbia University, New York, NY, United States, [3]Department of Chemistry and Biochemistry, Chemistry and Computer Science Building, The University of Texas at El Paso, El Paso, TX, United States

KEYWORDS

photosynthesis, light intensity (irradiance), daily light integral (dli), light spectrum, monochromatic light

Editorial on the Research Topic

Enhancement of photosynthesis through light utilization in plants and crops

The essential role of light in photosynthesis was discovered nearly two and a half centuries ago by the Dutch physician Jan Ingen-Housz, who demonstrated that plants exposed to light restore oxygen (Stirbet et al., 2020). In 1872, Jean Senebier et al. demonstrated that CO_2 was needed to restore O_2 in light-exposed plants (Shevela et al., 2019). Since then, thousands of articles have been written describing the role of light in photosynthesis.

Crop production is reduced due to changes in photosynthesis, which is affected by environmental conditions, such as CO_2 excess/depletion or water shortage. He and Matthews (2023) mentioned that the elevated CO_2 concentration impacted photosynthesis and reduced yield in soybeans. Water and fertilizer supply also affect photosynthesis and yield. Chastain et al. (2014) evaluated the effects of water deficit on net photosynthesis and lint production in a two-year field experiment with three cotton (*Gossypium hirsutum*) cultivars. The cultivars were ground in a dryland with only rainfall or well-watered during the growing season. The authors found that under water deficit, there was a decrease in stomatal conductance and an increase in photorespiration, resulting in a reduction of net photosynthesis and lint yield (in only one of the seasons).

Cultivation in a controlled environment can help combat climate uncertainties and maintain food supplies in regions with limited arable land. However, this requires a specific structure to improve and maintain photosynthesis (Niu and Masabni, 2018). This Research Topic contains 10 articles discussing key factors impacting photosynthesis and crop production under controlled conditions. Six of these articles discussed different effects of the light spectrum, mainly red and far-red light effects. One presented the impact of cell size on photosynthesis. Another examined the interaction of CO_2 with light, and the others discussed different aspects of photosynthesis and plant growth, such as light intensity. Light intensity affects photosynthesis in different manners depending on the type of plant. There has been inconsistency in the number of days that plants can tolerate low daily light integral (DLI) days after exposure to a high DLI day of natural light. Previous reports referred to a single day, which practically eliminates the use of supplemental light. Mayorga-Gomez

et al. experimented with lettuce (*Lactuca sativa*) plants exposed to a high DLI day (22.5 mol/m^{2}*day) followed by a varying number of low DLI days. They reported that lettuce plants exposed to one day of high DLI can endure multiple days of low DLI, which may result in reduced energy consumption. CO_2 concentration and light intensity affect photosynthesis, stomatal conductance, and leaf transpiration. Lv et al. reported that increased photosynthetically active radiation in rice rapidly increases stomatal conductance, transpiration, and net photosynthesis. Conversely, increasing the CO_2 concentration gradually decreases stomatal conductance and transpiration, but photosynthesis increases linearly and slowly as leaf development increases until stabilization. However, CO_2 absorption by leaves depends on several factors, including variations in light and CO_2 volume. Ogolla Egesa et al. reported that cell size is another factor influencing the photosynthetic rate. They studied Mesoamerican and Andean common beans and found that the former has smaller epidermal cells with higher stomatal density, which allows higher water and CO_2 conductance. This helps the plants to increase chlorophyll and protein content.

Another light parameter to consider is the spectrum. Changes in the red and far-red spectra have been shown to affect plant development differently. Bi et al. evaluated the effects of changes in the ratio of red to far-red light on biochemical parameters and the nutritional quality of lettuce. They compared the effects of 450 nm blue light + 650 nm red light (control) with 650 nm red light + 730 nm far-red light in a 3:2 ratio (F3). They found that plants exposed to F3 had significantly higher net photosynthetic rate, stomatal conductance, leaf area, aboveground fresh weight, vitamin C, and total soluble sugars. The duration of far-red light, which affects phytochrome, impacts plant development. Igarashi et al. illuminated leaves of arugula for 120–300 sec with LED light of 735 nm (far-red) and 635 nm (red) plus a laser light of 852 nm to produce biospeckles for rapid evaluation of far-red influence. They found that brief exposure to far-red light increased internal activity compared with prolonged exposure. They also found that the response of one-month-old leaves was better than that of three-month-old leaves. Chen et al. reported that reducing red light in full-spectrum LEDs has a significant impact on the growth of the propagation remains of strawberries. White LEDs increased the total dry mass of runner plants by 83%compared to red and blue LEDs. On the other hand, Ke et al. cultivated Micro-Tom and Rejina tomatoes exposed to monochromatic red light, a red/blue light ratio = 3, and white light at 300 μmol/m^{2}*s. The monochromatic red light photosynthetic rate resulted in the lowest radiation use efficiency. The highest proportion of blue light (up to 25%) resulted in the highest photosynthetic rate and radiation use efficiency. Blue light produced the best effects on fruit. Similar results were reported by Almeida Lima et al. on microtomato plants exposed for 12 h to blue light at 300 μmol/m^{2}*s and 3.7 W/m^{2} UV-B for 1 h daily. These plants had the highest photosynthetic rates and fruits with the highest rutin content compared to red and white light. Lv et al. stated that crop production may increase under suboptimal conditions by improving far-red utilization. This is because only a tiny portion of far-red light is used in photosynthesis. On the other hand, Caddell et al. mentioned that antenna assembly component genes CpSRP43, CpSRP54a, and their paralog, CpSRP54b, have a high photosynthetic contribution to chlorophyll content. This impacts plants that grow in mixed communities.

The articles included in this Research Topic contribute to a better understanding of the many facets that light plays to enhance photosynthesis and improve plant growth under controlled conditions. There are still several aspects to be studied, such as the varietal response and the effects of light on plants exposed to nanoagrochemicals.

Author contributions

JP: Writing – original draft. SF: Writing – review & editing. MY: Writing – review & editing.

Funding

The author(s) declare that no financial support was received for the research and/or publication of this article.

Conflict of interest

The authors declare that the research was conducted in the absence of any commercial or financial relationships that could be construed as a potential conflict of interest.

The author(s) declared that they were an editorial board member of Frontiers, at the time of submission. This had no impact on the peer review process and the final decision.

Generative AI statement

The author(s) declare that no Generative AI was used in the creation of this manuscript.

Publisher's note

References

Chastain, D. R., Snider, J. L., Collins, G. D., Perry, C. D., Whitaker, J., and Byrd, S. A. (2014). Water deficit in field-grown Gossypium hirsutum primarily limits net photosynthesis by decreasing stomatal conductance, increasing photorespiration, and increasing the ratio of dark respiration to gross photosynthesis. *J. Plant Physiol.* 171, 1576–1585. doi: 10.1016/j.jplph.2014.07.014

He, Y., and Matthews, M. L. (2023). Seasonal climate conditions impact the effectiveness of improving photosynthesis to increase soybean yield. *Field Crops Res.* 296, 108907. doi: 10.1016/j.fcr.2023.108907

Niu, G., and Masabni, J. (2018). Plant Production in Controlled Environments. *Horticulturae*. 4, 28. doi: 10.3390/horticulturae4040028

Shevela, D., Bjorn, L. O., and Govindjee, (2019). *Photosynthesis: Solar Energy for Life* (Singapore: World Scientific Publishing).

Stirbet, A., Lazár, D., Guo, Y., and Govindjee, G. (2020). Photosynthesis: Basics, history and modelling. *Ann. Bot.* 126, 511–537. doi: 10.1093/aob/mcz171

frontiers | Frontiers in Plant Science

TYPE Original Research
PUBLISHED 17 January 2023
DOI 10.3389/fpls.2022.1118189

OPEN ACCESS

EDITED BY
Deqiang Duanmu,
Huazhong Agricultural University, China

REVIEWED BY
Xiaoling Xu,
Hangzhou Normal University, China
Haijun Liu,
Washington University in St. Louis, United States

*CORRESPONDENCE
Xiaochun Qin
bio_qinxc@ujn.edu.cn

SPECIALTY SECTION
This article was submitted to Photosynthesis and Photobiology, a section of the journal Frontiers in Plant Science

RECEIVED 07 December 2022
ACCEPTED 30 December 2022
PUBLISHED 17 January 2023

CITATION
Li X, Zhu L, Song J, Wang W, Kuang T, Yang G, Hao C and Qin X (2023) LHCA4 residues surrounding red chlorophylls allow for fine-tuning of the spectral region for photosynthesis in *Arabidopsis thaliana*. *Front. Plant Sci.* 13:1118189. doi: 10.3389/fpls.2022.1118189

LHCA4 residues surrounding red chlorophylls allow for fine-tuning of the spectral region for photosynthesis in *Arabidopsis thaliana*

Xiuxiu Li[1,2], Lixia Zhu[2], Jince Song[2], Wenda Wang[3], Tingyun Kuang[3], Gongxian Yang[1], Chenyang Hao[1] and Xiaochun Qin[2*]

[1]School of Chemistry and Chemical Engineering, University of Jinan, Jinan, China, [2]School of Biological Science and Technology, University of Jinan, Jinan, China, [3]Photosynthesis Research Center, Key Laboratory of Photobiology, Institute of Botany, Chinese Academy of Sciences, Beijing, China

Improving far-red light utilization could be an approach to increasing crop production under suboptimal conditions. In land plants, only a small part of far-red light can be used for photosynthesis, which is captured by the antenna proteins LHCAs of photosystem I (PSI) through the chlorophyll (Chl) pair *a*603 and *a*609. However, it is unknown how the energy level of Chls *a*603–*a*609 is fine-tuned by the local protein environment *in vivo*. In this study, we investigated how changing the amino acid ligand for Chl *a*603 in LHCA4, the most red-shifted LHCA in *Arabidopsis thaliana*, or one amino acid near Chl *a*609, affected the energy level of the resulting PSI-LHCI complexes *in situ* and *in vitro*. Substitutions of the Chl *a*603 ligand N99 caused a blue shift in fluorescence emission, whereas the E146Q substitution near Chl *a*609 expanded the emission range to the red. Purified PSI-LHCI complexes with N99 substitutions exhibited the same fluorescence emission maxima as their respective transgenic lines, while the extent of red shift in purified PSI-LHCI with the E146Q substitution was weaker than in the corresponding transgenic lines. We propose that substituting amino acids surrounding red Chls can tune their energy level higher or lower *in vivo*, while shifting the absorption spectrum more to the red could prove more difficult than shifting to the blue end of the spectrum. Here, we report the first *in vivo* exploration of changing the local protein environment on the energy level of the red Chls, providing new clues for engineering red/blue-shifted crops.

KEYWORDS

photosystem I, LHCI, LHCA4, red Chl, red shift, blue shift

Introduction

Oxygenic photosynthesis uses light energy to convert carbon dioxide and water into carbohydrates and oxygen, sustaining almost all life activities on Earth. Photosynthesis is initiated with the light reactions, whereby light energy is captured and transferred to induce the charge separation in the reaction centers of photosystem I (PSI) and photosystem II (PSII), leading to the generation of reducing power as NADPH and metabolic energy as ATP. In vascular plants, PSI and PSII have a common general organization including a core complex moiety (PSI core or PSII core) and an outer antenna complex moiety (LHCI for PSI or LHCII for PSII). These two super-complexes are thus called PSI-LHCI and PSII-LHCII. Notably, their spectroscopic properties are substantially different: PSI can use light at wavelengths longer than 700 nm, whereas PSII cannot, even though they both use chlorophyll *a* (Chl *a*) as their major light-harvesting pigment (Croce and van Amerongen, 2014). This red shift in the absorption forms of PSI-LHCI expand the range of light-harvesting capacity into the near far-red region of the light spectrum, which is important for at least two major aspects. First, because far-red light is enriched in shaded environments, these red forms are helpful in harvesting light within or under a canopy (Rivadossi et al., 1999; Chen and Blankenship, 2011). Second, these red-shifted Chls greatly affect the excitation energy transfer within PSI-LHCI due to their low energy (Croce and van Amerongen, 2013). Therefore, a better understanding of the mechanism of these red forms of PSI-LHCI associated with Chl *a* is important for tuning the spectral region and regulating the excitation energy transfer of photosystems.

In vascular plants, the red spectral forms of PSI-LHCI are associated with a small number of low-energy Chl molecules (so-called red Chls) that absorb photons at wavelengths longer than 700 nm (Croce and van Amerongen, 2013). These red Chls bound to different sites of PSI-LHCI can have different energy levels that can be determined by fluorescence emission spectroscopy at low temperature (77K fluorescence). The PSI core complex contains 14 subunits (PsaA–L, PsaN, and PsaO) and 98 Chl *a* molecule (with six belonging to the electron transfer chain cofactors, while the other 92 function as antenna pigments) (Mazor et al., 2015; Qin et al., 2015) and shows a major fluorescence emission peak at 720 nm rather than two peaks at 685 nm and 695 nm as seen with PSII due to the existence of several red Chls (Satoh, 1986; Bassi and Simpson, 1987; Qin et al., 2006). The outer antenna complex associated with PSI (LHCI) is composed of four antenna proteins, LHCA1 to LHCA4, which are organized in the order LHCA1-LHCA4-LHCA2-LHCA3 from PsaG to PsaK, forming a crescent shape surrounding the PSI core on the PsaG–PsaF–PsaJ–PsaK side (Ben-Shem et al., 2003) and enhancing the PSI absorption cross section. These LHCA antenna proteins belong to the light-harvesting chlorophyll *a*/*b* protein superfamily (LHCs), which also includes the antenna proteins of PSII (LHCBs) (Buchel, 2015). Different LHC proteins share a similar fold, characterized by three major transmembrane helices (TMHs), B, C, and A, from their N- to C-terminal ends, and have conserved Chl- and carotenoid-binding sites (Qin et al., 2015). However, the most striking feature of LHCAs when compared to LHCBs is the presence of red Chl molecules in LHCAs (Croce and van Amerongen, 2013). These red Chls are critical for the fluorescence properties of LHCAs: While LHCBs have an absorption maximum in the range of 660–680 nm and an emission maximum at about 685 nm (Nussberger et al., 1994), the incorporation of the four LHCAs into PSI confers PSI-LHCI with an emission peak at about 735 nm, thus representing a red shift of about 50 nm compared to LHCB (Croce, 2015). Many studies have explored the mechanistic basis of these energy levels and the origin of the red Chl forms in individual LHCAs.

Work focusing on the spectral characteristics of the red Chls in LHCAs can be divided into two stages. In the 1980s, LHCI was often isolated as two fractions: LHCI-730 (the LHCA1-4 heterodimer) and LHCI-680 (a monomer or heterodimer composed of LHCA2 and LHCA3), named according to their fluorescence emission maxima (Kuang et al., 1984; Knoetzel et al., 1992). However, it was later found that a native LHCA2-LHCA3 heterodimer showed red-shifted fluorescence emission with a maximum around 730 nm, suggesting that LHCI-680 may not reflect the true native state of the heterodimer, as evidenced by the loss of the red shift, perhaps as a consequence of treatment with detergents during isolation (Wientjes and Croce, 2011). As several pigments are involved in the interaction between adjacent LHCAs and between LHCI and the PSI core (Qin et al., 2015), it was impossible to separate individual LHCAs without pigment loss (Ballottari et al., 2004), which prompted the use of reconstituted LHCA proteins with pigments (rLHCAs) for further study near the end of the 1990s. The four rLHCAs, rLHCA1–4, showed discrepancies in their fluorescence emission properties (Schmid et al., 1997; Schmid et al., 2002; Castelletti et al., 2003): rLHCA1 and rLHCA2 showed peaks at 686 and 701 nm, respectively, while rLHCA3 and rLHCA4 exhibited red-shifted peaks at 725 and 730 nm, respectively, demonstrating that 1) the energy level of the red Chls differed in different rLHCAs and 2) that rLHC4 had the most red-shifted absorption form.

It is important to reveal how the energy level of red Chls is regulated. Two excitonically coupled Chl *a* molecules are bound to the Chl-binding sites of A603 and B609 (nomenclature as described by Liu et al., 2004), corresponding to A5 and B5 according to Kühlbrandt et al. (1994), and were shown to be responsible for the red forms by means of site-directed mutagenesis of each rLHCA (Morosinotto et al., 2002; Morosinotto et al., 2003). We previously solved the crystal structure of the PSI-LHCI complex from garden pea (*Pisum sativum*) at 2.8-Å resolution in 2015 and recently improved the initial structure to 2.4-Å resolution (Qin et al., 2015; Wang et al., 2021). The PSI-LHCI structure illustrated how each LHCA binds to a pair of Chls (Chl *a*603– *a*609), which were suggested to be red Chls. The pair is the only Chl forming a connection between each LHCA and the PSI core at the stromal side, they occupy key positions in the excitation energy transfer (EET) pathway. Coupled with the lower energy level of red Chls, 90% of the energy absorbed by LHCI goes through the Chl *a*603-Chl *a*609 pair (Croce et al., 1996) and needs to be transferred across a high energy state to reach PSI core and be used for the primary reaction of PSI (Croce and van Amerongen, 2013). At the luminal pigment layer, in LHCA1, LHCA2, and LHCA4, a Glu residue near Chl *a*609 and located within helix C interacts with the C7-formyl group of Chl *b*607 *via* hydrogen bonds, while Chl *b*607 is the closest Chl molecule to Chl *a*603. In LHCA3 and LHCA4 with the most red-shifted emissions, the central ligand for Chl *a*603 is an Asn residue, while the central ligand for Chl *a*603 is a His residue in LHCA1 and LHCA2, which have weakly red-shifted emissions. By contrast, Chl *a*609 always coordinates with a Glu residue. In addition,

based on pigment-pigment and pigment-protein interactions it was suggested that the porphyrin head of Chl *a*609 is more stable geometrically than Chl *a*603, and Chl *a*603 may be more likely to undergo conformational modulation. In spite of the high-resolution structures and some *in vitro* studies based on monomeric rLHCAs (Morosinotto et al., 2003; Wientjes et al., 2012), whether and how the protein matrix affects the energy level of the lowest energy state *in vivo* have not been reported.

In this study, we selected LHCA4, whose reconstituted form possesses the most red-shifted fluorescence emission among all rLHCAs, as the target protein, and focused on the effect of replacing the Asn(N)99 residue coordinating with Chl *a*603 and the Glu(E)146 residue located near Chl *a*609 to investigate the energy level of intact and mutant pigment-protein complexes *in vivo* (Figure S1). Accordingly, we generated a series of transgenic lines in Arabidopsis expressing constructs encoding single-point mutations in LHCA4 and determined their physiological and biochemical characteristics. In addition, we isolated and analyzed PSI-LHCI particles from the wild type and transgenic lines. We demonstrate here that all substitutions of the N99 residue in LHCA4 led to a blue shift in the fluorescence emission, indicative of the disruption of the red forms, while the E146Q mutation caused a shift red in the fluorescence emission, indicating an enhancement of the red shift. This is the first report of mutations in LHCA to be characterized *in vivo* in an effort to analyze the effects of protein micro-environments on the energy level of red Chls, which provides a new perspective of the regulation of these red Chl forms *in vivo*.

Materials and methods

Plant material and growth conditions

The Arabidopsis (*Arabidopsis thaliana*) accession Columbia-0 (Col-0) was used for all experiments. Plants (the wild type and mutants) were grown for 45 days in a growth chamber in 45% relative humidity, at 21°C, with a photoperiod of 16 h light/8 h dark under 110–130 μmol photons m^{-2} s^{-1}. The environment was strictly controlled. For all measurements, only fully expanded mature leaves were used from the 4th to the 7th pair of leaves depending on the time and condition.

The *lhca4* mutant was prepared by CRISPR/Cas9-mediated gene editing, and the vector used was pHSE401 (Xing et al., 2014). The plant vector used to introduce transgenes with point mutations was pMDC83 harboring the cauliflower mosaic virus (CaMV) 35S promoter. Single nucleotide mutations were introduced by overlapping PCR. The sequence of the Arabidopsis genome was obtained from the TAIR website (https://www.arabidopsis.org/). Plasmids with the correct sequence were transformed into Agrobacterium (*Agrobacterium tumefaciens*) (strain GV3101), which were then employed for plant transformation. Transgenic plants were obtained after Agrobacterium infection by floral dipping, and lines homozygous for each transgene were identified in the T2 generation. See Table S1 for a list of all primers.

Thylakoid isolation and PSI-LHCI purification

Thylakoid isolation from Arabidopsis leaves was performed according to a previous report (Croce et al., 1996) with some modifications. Thylakoid membranes were prepared immediately after plant leaves were harvested. For every 10 g of leaves, 100 mL of solution A (20 mM Tricine-NaOH pH 7.8, 0.3 M sucrose, 5 mM $MgCl_2$) was added and the tissues were crushed with a blender. The resulting cell and chloroplast suspension was then centrifuged at 7,000 × g for 7 min at 4°C. The supernatant was discarded, and the green pellet was resuspended in solution B (20 mM Tricine-NaOH, pH 7.8, 5 mM $MgCl_2$) and then centrifuged at 20,000 × g for 10 min to obtain the thylakoid membrane in a JA14 rotor (Beckman) at 4°C. The chlorophyll concentrations were calculated from the absorbances at 645 and 663 nm of an 80% (v/v) acetone extract (Arnon, 1949).

PSI-LHCI purification was performed according to a published report (Ballottari et al., 2004). The thylakoid membrane was solubilized 1% (v/v) n-dodecyl β-D-maltoside (β-DDM) at 0.5 mg Chl/mL in an ice bath for 30 min. The insolubilized materials were removed by centrifugation at 40,000 × g for 15 min, and the supernatant was loaded onto a 0.3 M–0.9 M continuous sucrose density gradient (containing 20 mM Tricine-Tris, pH 7.5, 0.015% β-DDM) and centrifuged at 243,500 × g for 16 h at 4°C in an SW40Ti rotor (Beckman).

SDS-PAGE and immunoblot analyses

The polypeptide compositions of samples were analyzed by SDS–PAGE. Samples were treated with a sample buffer containing 2% (w/v) lithium dodecyl sulfate, 60mM dithiothreitol and 60mM Tris-HCl (pH 8.5) at 60°C for 10min, and subjected to SDS–PAGE with a 16% gel containing 7.5M urea as previously described (Ikeuchi and Inoue). Total protein or isolated PSI-LHCI samples were used for SDS–PAGE. Total proteins were extracted using IP lysis buffer (50 mM Tris-HCl, pH 7.5, 150 mM NaCl, 1mM EDTA, 10% lycerol and 0.1% Trition X-100) with freshly added PMSF (phenylmethysulphonyl fluoride, 2mM) and protease inhibitor cocktail (Roche). Following SDS-PAGE, proteins were transferred to a PVDF membrane (0.45 μm). Membranes were blocked in Tris-buffered solution containing 0.05% Tween 20 (TBS-T) and 5% (w/v) nonfat dry milk for 1 h at room temperature. All antibodies used in this study were purchased from Phyto AB. For primary antibodies of LHCA4 (PhytoAB), TBS-T solutions containing 1% (w/v) nonfat dry milk were prepared to a dilution of 1:10,000 and incubated overnight at 4°C. Subsequently, the membrane was washed three times for 10 min each time in TBS-T. For secondary antibodies, the membrane was incubated for 40 min at room temperature using a goat anti-rabbit IgG (H + L), horseradish peroxidase conjugate (PhytoAB) in TBS-T containing 1% (w/v) nonfat dry milk at a final antibody dilution of 1:10,000. The membrane was then washed three times for 10 min in TBS-T. An ECL luminescence solution was evenly placed over the membrane and incubated for 5 s, and then luminescence was immediately detected with a Tanon-5200 instrument.

Low-temperature fluorescence spectroscopy

Low-temperature (77K) fluorescence emission spectra were recorded using a F-4700 instrument (HITACHI). The excitation wavelength was 440 nm, and emission was detected in the 600- to 800-nm range. Excitation and emission slit widths were set to 3 nm. Samples were dissolved in 50% (v/v) glycerol, 10 mM Tricine-NaOH (pH 7.5), and 0.015% (v/v) β-DDM. The final concentration of Chls in the sample was 1 μg/mL.

Absorption spectrometry

Absorption spectra were recorded using a U-3900H spectrophotometer (HITACHI). All PSI-LHCI samples were finally diluted to 4 μg/mL and detected in the 350- to 750-nm range. Samples were dissolved in 10 mM Tricine-NaOH (pH 7.5) and 0.015% β-DDM.

Measurement of chlorophyll fluorescence induction kinetics curves

Activities of PSII and PSI were measured using a dual-wavelength pulse-amplitude-modulated fluorescence monitoring system (Dual-PAM-100, Walz, Effeltrich, Germany), and all materials were subjected to dark adaptation for 30 min before determination. Parameters were automatically calculated by the Dual-PAM-100 software during the measurement (Klughammer and Schreiber, 2008). First, the minimal fluorescence after dark adaptation (Fo), the maximum fluorescence (Fm) and the maximal change in $P700^+$signal (Pm) was determined using a saturation pulse (10,000 μmol photons m^{-2} s^{-1} for 0.3 s). Plants were then continuously illuminated with actinic light (111 μmol photons m^{-2} s^{-1}) for 5 min, and saturating pulses were imposed every 20 s. The maximum fluorescence (Fm'), the maximum $P700^+$signal (Pm') in the light-adapted state, and the steady state fluorescence (F) and $P700^+$signal (P) during actinic illumination were measured. The actinic light was removed, and the minimal fluorescence level in the light-adapted state (Fo') was determined by illuminating the leaf with a 3-s pulse of far-red light. The quantum yields of energy conversion in PSI and PSII were calculated with the following equations: Y(I) = (Pm' – P)/Pm (Li et al., 2021); Y(II) = (Fm' – F)/Fm' (Klughammer and Schreiber, 2008; Suzuki et al., 2011).

Pigment analysis

The pigments were extracted with 80% (v/v) acetone and analyzed by high-performance liquid chromatography (HPLC) (Thermo Fisher, UltiMate 3000). The liquid phase system and the pigment separation method were as previously described (Angeler and Schagerl, 1997).

Results

Single amino acid substitutions at the N99 residue of LHCA4 cause a blue shift of the far-red fluorescence emission *in vivo*

We selected four amino acids out of the possible 19 to replace the N99 residue of LHCA4 based on three criteria: 1) stability of the mutant protein, 2) the coordination of the central Mg atom in the mutant protein, and 3) previous *in vitro* results. Accordingly, we calculated the predicted protein stability of LHCA4 harboring a substitution of N99 with one of the other 19 amino acids. We thus selected two mutants each with high and low values: cysteine (C) and methionine (M) for high values, and glycine (G) and histidine (H) for low values (Table S2). H is the most common amino acid that provides a ligand to the central Mg atom in Chl (Li et al., 2022); moreover, *in vitro* assays indicated that the N99H mutation still binds to Chl *a*603 (Morosinotto et al., 2003). The other three mutated residues (G, C, and M) might use their main-chain carbonyls to function as ligands to the central Mg atom of Chl *a*603.

To remove any contribution from endogenous LHCA4, we generated an *lhca4-1* mutant by clustered regularly interspaced short palindromic repeat (CRISPR)/CRISPR-associated nuclease 9 (Cas9)-mediated gene editing. To this end, we designed two single guide RNAs (sgRNAs) targeting sequences in *LHCA4*, leading to the isolation of a knockout mutant in the T_2 generation, *lhca4-1*, harboring a 229-bp deletion in *LHCA4* predicted to introduce a premature stop codon after 63 amino acids (Figure 1A). The *lhca4-1* mutant had a very similar appearance as the wild-type (WT) Col-0 under normal growth conditions (Figure 1B). Importantly, both *LHCA4* transcript levels and LHCA4 abundance in *lhca4-1* were much lower or undetectable, respectively, indicating that the *lhca4-1* mutant is likely a null allele (Figures 1C, D). We determined the fluorescence emission properties of leaves from the WT and *lhca4-1* by low-temperature (77K) fluorescence spectroscopy and observed a clear difference between the two genotypes, with a fluorescence emission maximum of 735 nm in the WT and 730 nm in *lhca4-1*(Figures 1E, and Figure S2A). The loss of LHCA4 therefore caused a 5-nm blue shift, which is consistent with a previous report (Zhang et al., 1997).

To explore the *in vivo* properties of the four selected LHCA4 variant proteins above (N99G, N99C, N99H, and N99M), we placed their respective coding sequences under the control of the strong cauliflower mosaic virus (CaMV) 35S promoter and introduced each construct into the *lhca4-1* mutant. We also introduced the wild-type version of the *LHCA4* coding sequence (N99N) into *lhca4-1* as a control line. We confirmed that all transgenes are present in the *lhca4-1* background (Figure S3). We observed no phenotypic differences between the WT and the five types of transgenic lines (Figure 2A). An immunoblot assay indicated that LHCA4 abundance in the transgenic lines is comparable to that in the WT (Figure 2B), and reverse transcription quantitative PCR (RT-qPCR) showed that the relative *LHCA4* expression leaves are higher in the transgenic lines than in the WT (Figure 2C). We also determined the effects of the single amino acid substitutions on fluorescence emission using leaves from each transgenic line and the WT by low-temperature (77K)

10.3389/fpls.2022.1118189

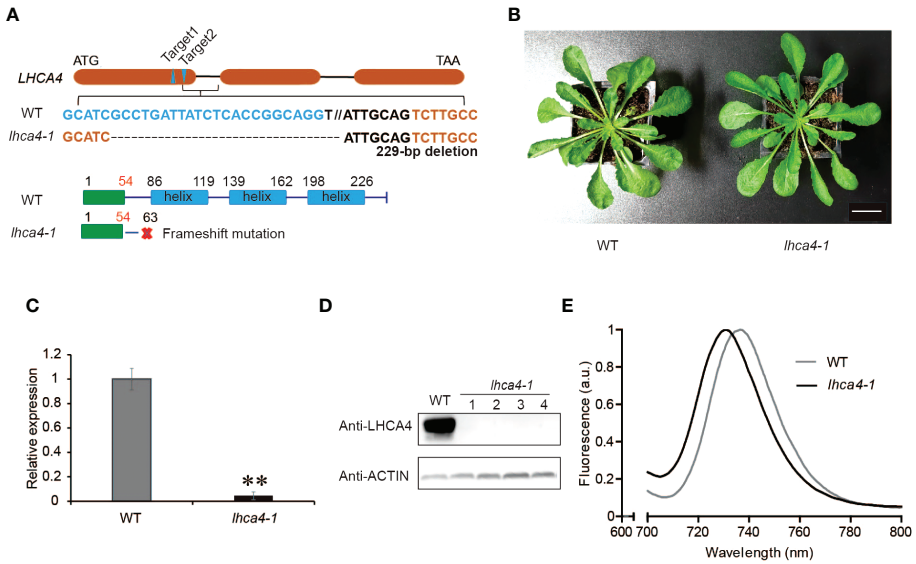

FIGURE 1
Characterization of the *lhca4-1* mutant. **(A)** Schematic diagram of the *LHCA4* locus showing the target sites of sgRNAs to generate the *lhca4-1* mutant. **(B)** Representative rosette phenotype of the wild type (WT) and *lhca4-1* (scale bars = 2 cm). **(C)** Relative *LHCA4* expression levels as detected by reverse transcription quantitative PCR (RT-qPCR) analysis in the WT and *lhca4-1* (using the two-tailed Student's t-test; **significant at $P < 0.01$). **(D)** LHCA4 abundance in the WT and four *lhca4-1* plants, as detected by immunoblotting. ACTIN served as loading control. **(E)** Low-temperature (77K) fluorescence emission spectra (excitation at 440 nm) of the WT and *lhca4-1*. The spectra were normalized to their maximal emission, which was set to 1.

fluorescence spectroscopy. The control line, harboring the *35S:LHCA4*(*N99N*) transgene, showed a fluorescence emission maximum at 735 nm (Figure 2D and Figure S2A), which was identical to that in the WT. By contrast, all other transgenic lines carrying the variant constructs 35S:*LHCA4*(*N99G*), *35S:LHCA4*(*N99C*), *35S:LHCA4*(*N99H*), and *35S:LHCA4*(*N99M*) showed similar fluorescence emission spectra peaking at 730 nm, as in the *lhca4-1* mutant (Figures 2E-H and Figure S2A). We concluded that all substitutions at residue N99 in LHCA4 cause a blue shift in the fluorescence emission of the variant LHCA4 protein, indicating that the excited-state energy level of the red Chls in variant LHCA4s increased when compared to LHCA4 in the WT and the *N99N* control line. While the point mutations almost had no effect on the potential photosynthetic performance, we observed little change in the Chl fluorescence parameters Y(I) and Y(II) in all of the substitutions compared to the control line (Figure 2I), indicating that the photochemical quantum yields of PSI and PSII were maintained well based on the fact that the pigment network within PSI was almost unchanged. In addition, high-performance liquid chromatography (HPLC) analysis showed no significant differences among the WT, the control *N99N* line, and the other transgenic lines in their pigment/Chl *a* ratio (Figure 2J). These results suggest that mutating N99 in LHCA4 to G, C, H, or M has little effect on plant phenotypes and photochemical vitality, although we detected a distinct effect on the energy level of red Chls in LHCA4.

The PSI-LHCI complex of *LHCA4* transgenic lines includes LHCA4

To assess whether the variant LHCA4 proteins were assembled into the PSI-LHCI complex in the transgenic lines, we isolated PSI samples through sucrose density gradient ultracentrifugation of detergent-treated thylakoid membranes (Figure 3A). The WT thylakoid membrane separated into three major bands, corresponding to dissociated antenna proteins (Band 1), PSI core and PSII core (Band 2), and PSI-LHCI (Band 3) based on SDS-PAGE of each fraction (Figure 3 and Figure S4). Band 3 was much wider and darker than Band 2, suggesting that most of the PSI core is in a large super-complex associated with antenna proteins. Notably, the *lhca4-1* mutant had no visible Band 3, with Band 1 migrating at the same position in the gradient as in the WT, while Band 2 was much darker than in the WT. SDS-PAGE and immunoblot analyses determined that LHCA2 and LHCA3, but not LHCA1 or LHCA4, comprise Band 2 (Figure S4). For all transgenic lines expressing LHCA4 variants at N99, we detected all three bands at the same position as in the WT. However, the Chl contents of Bands 2 and 3 differed between the transgenic lines and the WT, with Band 2 having 21–60% more Chls than the WT and Band 3 accumulating about 20% less Chls than the WT, yielding a darker Band 2 and lighter Band 3 in the transgenic lines (Table S3). Band 2 from the mutants contained PSI core proteins and part of LHCA proteins (Figure S4), while Band 3 contained all four LHCA proteins (LHCA1 to LHCA4), as determined by SDS-PAGE and immunoblot analysis (Figures 3B, C). Therefore, although most of the PSI core assembled into a full-size PSI-LHCI complex, we speculate that a small fraction of PSI failed to fully assemble with LHCI due to the absence of LHCA4 and migrated into Band 2, thus explaining its higher Chl contents. To assess whether the lower intensity of Band 3 in the transgenic lines expressing the *LHCA4* variants was a consequence of the mutations, we tested the *N99N* control line under the same conditions and observed a pattern similar to that of the transgenic lines (Figure 3A, Table S3), suggesting that the decrease in fully assembled PSI-LHCI complex (Band 3) is not a consequence of the point mutations but may instead be caused by the

10.3389/fpls.2022.1118189

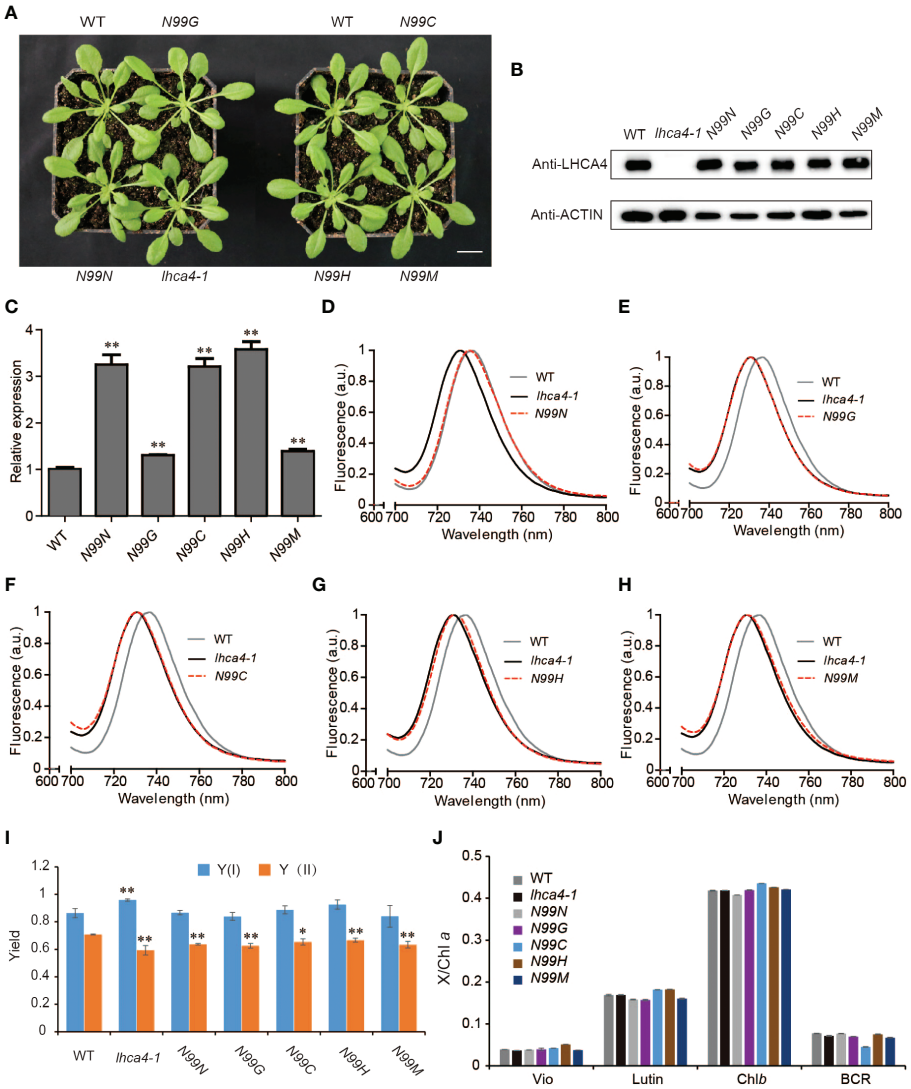

FIGURE 2
Phenotypic and physiological characterization of plants with single amino acid substitutions at N99 in LHCA4. **(A)** Representative photograph of the WT, *lhca4-1*, the control line *35S:LHCA4*(*N99N*), and four lines harboring LHCA4 point mutations in the *lhca4-1* mutant background: *35S:LHCA4* (*N99G*), *35S:LHCA4*(*N99C*), *35S:LHCA4*(*N99H*), and *35S:LHCA4*(*N99M*) (scale bars = 2 cm). **(B-C)** LHCA4 protein abundance analyzed by immunoblots. Anti-ACTIN antibodies were used for the immunoblots assays. **(B)** and relative *LHCA4* expression levels detected by RT-qPCR (using the two-tailed Student's t-test; **significant at P < 0.01) **(C)** in 5-week-old plants from the WT, *lhca4-1*, the control line, and the LHCA4 point mutants. **(D-H)** 77K fluorescence emission spectra for the WT, *lhca4-1*, and *35S:LHCA4*(*N99N*) **(D)**; *35S:LHCA4*(*N99G*) **(E)**; *35S:LHCA4*(*N99C*) **(F)**; *35S:LHCA4*(*N99H*) **(G)**; and *35S:LHCA4*(*N99M*) **(H)**. The excitation wavelength was 440 nm. **(I-J)** Chl fluorescence parameters of Y(I) and Y(II) (using the two-tailed Student's t-test; *significant at P < 0.05, **significant at P < 0.01). **(I)** and pigment composition **(J)** in the WT, *lhca4-1*, the control line, and the four LHCA4 point mutant lines.

introduction of the transgene. We thus propose that the single amino acid substitutions at the N99 residue in LHCA4 did not affect its binding to the PSI core.

Single amino acid substitutions at the N99 residue in LHCA4 cause a blue shift of the far-red fluorescence emission of PSI-LHCI

To explore how the amino acid substitutions introduced in LHCA4 at the N99 residue affected the spectroscopic properties of PSI-LHCI, we measured the absorption spectra and the low-temperature fluorescence emission spectra of PSI-LHCI isolated from WT and N99 mutant plants. PSI-LHCI from the WT and all *LHCA4* transgenic lines showed similar room temperature absorption spectra (Figure 4A), although they differed in their low-temperature fluorescence emission spectra (Figures 4B-E, Figure S2B). Indeed, PSI-LHCI isolated from the WT had a fluorescence emission peak at 732 nm, exhibiting a 3-nm blue shift compared to its 77K fluorescence profile when embedded in thylakoid membranes. PSI-LHCI isolated from the control line *N99N* showed a fluorescence emission peak at 732.2 nm, which was similar to that seen for PSI-LHCI in WT plants (Figure 4B). By contrast, all four transgenic lines with point mutations in N99 showed fluorescence emission peaks at 730.6 nm (*N99G*, Figure 4B), 730 nm (*N99C*, Figure 4C), 730.4 nm (*N99H*, Figure 4D), and 729.8 nm (*N99M*, Figure 4E), with an ~2-nm blue shift compared

10.3389/fpls.2022.1118189

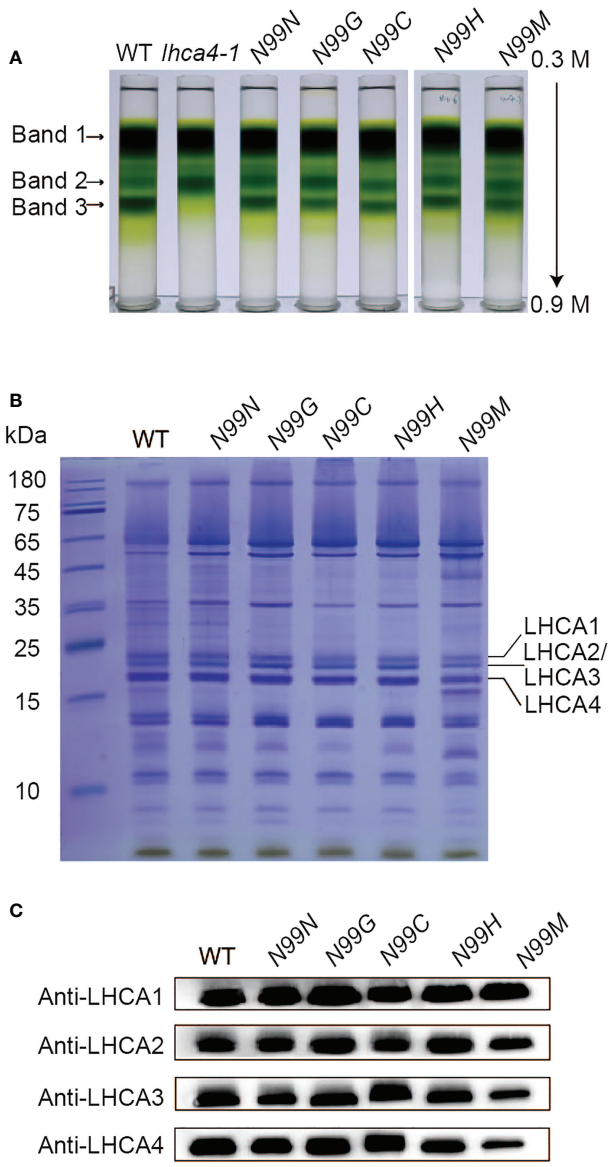

FIGURE 3
Isolation and characterization of PSI-LHCI from N99 point mutant lines. **(A)** Sucrose density gradient ultracentrifugation of detergent-treated thylakoid membranes isolated from the WT, *lhca4-1*, the control, and N99 point mutant lines. The lowest band, labeled Band 3, was collected and analyzed. **(B-C)** Polypeptide composition of Band 3 as analyzed by Coomassie staining after SDS-PAGE (samples corresponding to 2.5 μg Chl were loaded per lane). **(B)** and immunoblot analysis with antibodies against LHCA1, LHCA2, LHCA3, and LHCA4 **(C)**.

to PSI-LHCI from WT plants and the *N99N* control line. This result suggested that replacing N99 with G, C, H, or M in LHCA4 causes a moderate blue shift that is difficult to detect at room temperature by absorption spectroscopy due to the low ratio of red Chls. The observed blue shift in the red Chl forms may reflect a change in the geometrical arrangement of Chl *a*603, which would lead to a concomitant change in the interaction between Chl *a*603 and Chl *a*609. Another possibility is that no Chl molecule bound to the Chl *a*603 site due to the mutated residue at position 99, leaving only Chl *a*609 to bind, which would abolish the far-red absorption of the PSI-LHCI complex. We conclude that the native N99 residue of intact LHCA4 gives rise to the strongest far-red absorption and greatest red shift, while other residues at this position decrease the far-red absorption of the complex.

Changing E146 to Q in LHCA4 broadens the far-red emission window into the red

The *in vitro* assays determined that the E146Q substitution in LHCA4 resulted in a strongly red-shifted emission by 10 nm, from 731 to 741 nm relative to the WT (Wientjes et al., 2012), indicating that E146 might be a candidate to broaden the absorption properties of PSI-LHCI complexes toward the red region of the spectrum *in vivo*. To determine how the replacement of E146 by Q in LHCA4 would affect the far-red absorption *in vivo*, we introduced the *35S:LHCA4* (*E146Q*) construct into the *lhca4-1* mutant and obtained two transgenic lines with a WT appearance: *35S:LHCA4*(*E146Q*)*-1* and *35S:LHCA4*(*E146Q*)*-5* (Figure 5A and Figure S3). Immunoblot and RT-qPCR analysis indicated that *35S:LHCA4*(*E146Q*)*-1* has a lower LHCA4(E146Q) abundance than LHCA4 in the WT, while *35S:LHCA4*(*E146Q*)*-5* accumulated more LHCA4(E146Q) than LHCA4 in the WT (Figures 5B, C). However, their pigment composition and potential photosynthetic performance were similar to those of the WT (Figures 5D, E). Moreover, the leaves of *E146Q* transgenic lines showed different low-temperature fluorescence spectra, as evidenced by their respective emission maxima and the full width at half maximum (FWHM) values. Indeed, the emission maximum of leaves from line *E146Q-5* was 735.2 nm, which was very close to that of the WT (735.6 nm), while the emission maximum of leaves from line *E146Q-1* was 732 nm, 2 nm red-shifted than that of the *lhca4-1* mutant (Figure 5F). In addition, the FWHM values in lines *E146Q-1* and *E146Q-5* were 32.6 and 34 nm, respectively, both of which covering a larger window than the WT (30 nm) or the *lhca4-1* mutant (30.6 nm) (Figure 5F). To more clearly illustrate the difference between line *E146Q-5* and the WT, we calculated the difference spectrum between the two genotypes and multiplied the results by five to raise the amplitude. We observed two positive peaks, one from 710 to 735 nm with a maximum at 721 nm, and the other from 745 to 800 nm with a maximum at 766 nm (Figure 5F). Therefore, although the emission maximum of line *E146Q-5* was similar to that of the WT, its emission peak was broader by increasing the emission at the two above regions when compared to the WT. The region with the peak at 766 nm indicated that line *E146Q-5* has greater absorption in a more red-shifted region than the WT, which may be attributed to a much lower energy level of red Chls in LHCA4 (E146Q) than in intact LHCA4. By contrast, substitutions at the N99 residue in LHCA4 had less effect on the FWHM values no matter the fluorescence emission spectra were detected with leaves or isolated PSI-LHCI samples (Table S4). In summary, the E146Q substitution in LHCA4 enhanced and broadened the far-red absorption window of plants, suggesting that changing the micro-environment around one of the red Chls, Chl *a*609, might increase far-red absorption.

To determine the effect of the E146Q substitution in LHCA4 on the far-red absorption at the level of the PSI-LHCI complex, we isolated PSI-LHCI complexes from lines *E146Q-1* and *E146Q-5* by sucrose density gradient ultracentrifugation. We observed the same three major bands in these transgenic lines as in the WT (Figure 6A).

10.3389/fpls.2022.1118189

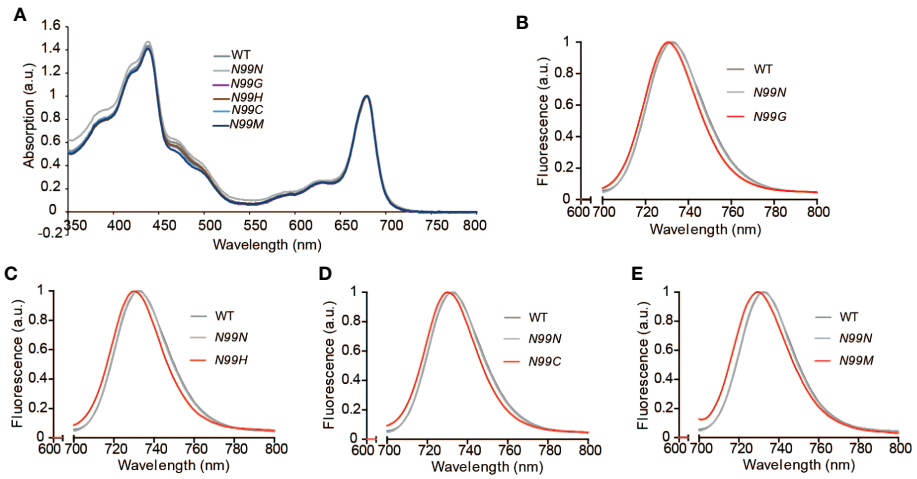

FIGURE 4
Spectroscopic properties of PSI-LHCI isolated from the WT and N99 point mutant lines. **(A)** Absorption spectra at room temperature of the WT and N99 point mutant lines. The spectra were normalized, with their maximal absorption in the Qy region set to 1. **(B-E)** Low-temperature (77K) fluorescence emission spectra of PSI-LHCI complexes (Band 3) isolated from the WT (dark grey solid line), the control line *35S:LHCA4*(*N99N*) (light gray solid line), and the N99 point mutant lines *35S:LHCA4*(*N99G*) **(B)**, *35S:LHCA4*(*N99H*) **(C)**, *35S:LHCA4*(*N99C*) **(D)**, and *35S:LHCA4*(*N99M*) **(E)**, shown as red solid lines. The excitation wavelength was 440 nm.

Band 3 in the two transgenic lines displayed the same full-size PSI-LHCI complex as the WT (Figures 6B, C), although the associated Chl differed, with Band 3 in line *E146Q-1* having less Chls than the WT or line *E146Q-5* (Figure 6A), which was consistent with the lower accumulation of LHCA4 in line *E146Q-1* (Figure 5B). These results suggest that LHCA4 with the E146Q substitution can bind to the PSI core and form a PSI-LHCI complex, with a yield of PSI-LHCI complex formation that depends on LHCA4 abundance.

We established that isolated PSI-LHCI complexes from the WT and lines *E146Q-1* and *E146Q-5* have similar absorption spectra, all with an absorption maximum at 679 nm in the red region (Figure 6D), indicating that the E146Q substitution did not affect the pigment composition of the PSI-LHCI complex. In terms of fluorescence emission spectra, the PSI-LHCI complexes from lines *E146Q-1* and *E146Q-5* showed peaks at 732.6 and 733.2 nm, respectively, which were close to those in the WT. We noticed an important difference in the FWHMs of the three genotypes: the FWHM from the WT was 31.0 nm, while the FWHMs from *E146Q-1* and *E146Q-5* were 32.4 and 32.2 nm, respectively, indicating that isolated PSI-LHCI complexes with the E146Q substitution have a 1- to 2-nm wider FWHM than the intact PSI-LHCI complex. To better illustrate this difference, we calculated the difference spectrum between *E146Q-1* and the WT and between *E146Q-5* and the WT as above. We observed a positive peak in the 733- to 800-nm range with a maximum at 748.8 nm, indicating that PSI-LHCI with the E146Q substitution in LHCA4 displays an increased fluorescence emission at longer wavelengths (Figure 6E). As the increased fluorescence emission came from the red absorption form only, we concluded that the E146Q substitution in LHCA4 enhances the far-red absorption of the PSI-LHCI complex, in agreement with the results obtained with leaves. Notably, the extent of FWHM broadening varied between plants and their isolated PSI-LHCI complexes, with a smaller broadening observed when PSI-LHCI was dissociated from the thylakoid membrane (Figures 5F and 6E). We conclude that the E146Q substitution in LHCA4 increases fluorescence emission into the red part of the spectrum, which was easier to detect in leaves than in isolated PSI-LHCI complexes, suggesting that changes in the micro-environment around red Chl may affect its far-red absorption properties.

Discussion

Because the red forms of LHCAs originated from the excitonically coupled Chl *a*603-*a*609 dimer mixed with a charge-transfer state (Romero et al., 2009), changes in the organization of the Chl dimer or in the protein environment might influence the energy level of red forms. In this work, we investigated the influence of single amino acid substitutions at amino acid positions 99 and 146 in LHCA4 on the energy levels of the red forms *in vivo* to clarify how the red forms are regulated.

The transgenic lines with the single substitutions N99G, N99C, N99H, or N99M in LHCA4 exhibited similar fluorescence emission spectra as the *lhca4-1* mutant generated by genome editing (Figure 1E), as well as the *LHCA4* antisense mutant previously reported (Zhang et al., 1997). Moreover, all transgenic lines (outside of the N99N control line) showed a blue shift of 5–6 nm when compared to the WT (Figures 2D-H). To ascertain that the blue-shifted emission of these transgenic lines harboring single substitutions at N99 was solely the reflection of an emission blue shift of the PSI-LHCI complex, we examined the extent of the shift from PSI-LHCI complexes isolated from the transgenic lines. We confirmed that the substitutions did not prevent the formation of a full-size PSI-LHCI complex (Figure 3), supporting the notion that any observed shift in emission can be attributed to the introduced mutations.

The fluorescence emission maximum of WT leaves was not identical to that of its corresponding purified PSI-LHCI complex. Indeed, the PSI-LHCI complex isolated from WT leaves had a fluorescence emission peak at 732.4 nm, which was blue-shifted by 3 nm relative to the peak measured in WT leaves (Figure 2D). This observation suggested that the embedding of PSI-LHCI particles into the thylakoid membrane may help the complex remain in its most red-shifted state, further raising the possibility that the

10.3389/fpls.2022.1118189

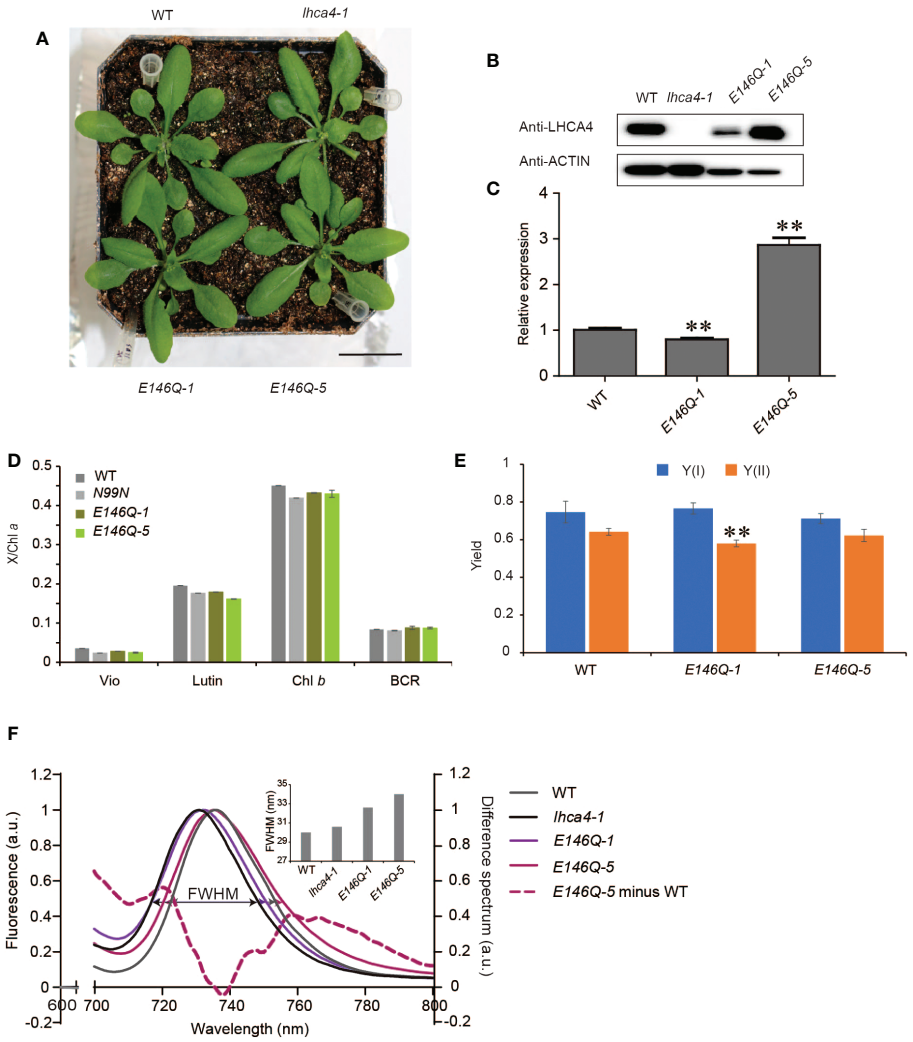

FIGURE 5
Characterization of LHCA4(E146Q) point mutant lines. **(A)** Phenotype of the WT, *lhca4-1*, and two LHCA4(E146Q) point mutant lines, *35S:LHCA4(E146Q)-1* and *35S:LHCA4(E146Q)-5* (scale bars = 2 cm). **(B-C)** LHCA4 abundance as detected by immunoblot analysis. Anti-ACTIN antibodies were used for the immunoblots assays. **(B)** and relative *LHCA4* expression levels as detected by RT-qPCR (using the two-tailed Student's t-test; **significant at $P < 0.05$) **(C)** in the WT, *lhca4-1*, and LHCA4(E146Q) point mutant lines. **(D-E)** Pigment composition **(D)** and chlorophyll fluorescence parameters Y(II) and Y(I) **(E)** of the WT and LHCA4(E146Q) point mutant lines (using the two-tailed Student's t-test; **significant at $P < 0.01$). **(F)** Low-temperature (77K) fluorescence emission spectra (excited at 440 nm) of the WT (gray), *lhca4-1* (black), *35S:LHCA4(E146Q)-1* (light purple), and *35S:LHCA4(E146Q)-5* (dark purple). The purple dotted line shows the difference between the spectra of *35S:LHCA4(E146Q)-5* and the WT (and multiplied by 5 to facilitate comparison). The FWHMs (full widths at half maximum) for each line are labeled and marked with double arrows in the same colors as the spectra.

red forms are sensitive to conformational or a surrounding micro-environmental change caused by dissociation from the thylakoid membrane. By contrast, the fluorescence emission peaks of PSI-LHCI complexes purified from the N99 substitution lines were around 730 nm (Figures 4B-E), which was almost identical to those from leaves for their respective plant materials (Figures 2E-H). All N99 substitutions in LHCA4 induced a 5-nm blue shift from 735 to 730 nm in leaves (Figures 2D-H) and a 2- to 3-nm blue shift from 732.4 to 730 nm in isolated PSI-LHCI complexes, relative to the WT (Figures 4B-E). Importantly, the transgenic line harboring the *N99N* construct showed no difference with the WT, indicating that the N99 residue is essential for maintaining the red form of the complex. This result is in agreement with the *in vitro* findings that substitutions of the N99 residue led to the loss of the red form (Morosinotto et al., 2003; Wientjes et al., 2012). These results suggest that none of the substitutions of the Chl *a*603 ligand in LHCA4 can maintain a proper geometry between Chl *a*603 and Chl *a*609 to allow for their strong interaction, thus leading to the observed red shift seen for the PSI-LHCI complex in its free from *in vitro* or embedded in the thylakoid membrane. The surrounding micro-environment of the Chl *a*603-*a*609 pair may affect the red forms. Indeed, fluctuations between conformations with and without red forms in LHCA were detected by single-molecule spectroscopy in a natural state of the isolated LHCA1-LHCA4 dimer (Kruger et al., 2011). The PSI-LHCI structure of pea revealed that many lipids can bind at the gap region between LHCA4 and the PSI core and that the interaction between LHCA4 and the core is the most vulnerable to the alkaline pH among interactions between LHCI and the core (Wang et al., 2021). Interestingly, amino acid 99 of LHCA4 is located at the interface between LHCA4 and the core and may therefore affect the interaction between LHCA4 and the core in response to changes in the local micro-environment.

The TMH region of LHCA4 contains five Glu residues, of which three form ion pairs with Arg residues to stabilize the protein structure, one

10.3389/fpls.2022.1118189

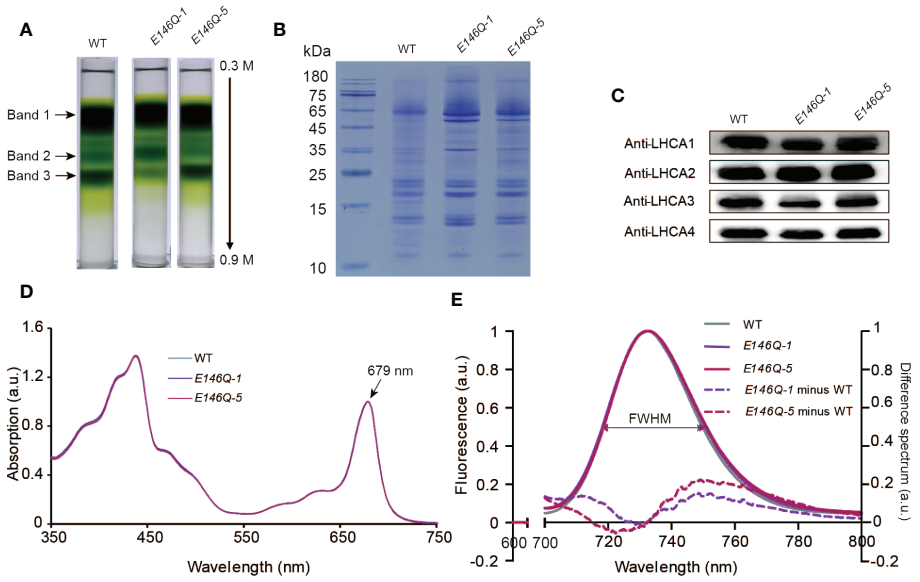

FIGURE 6
Isolation and characterization of PSI-LHCI from *35S:LHCA4*(*E146Q*) point mutant plants. **(A)** Sucrose density gradient (0.3–0.9 M) ultracentrifugation of thylakoid membranes isolated from WT and *35S:LHCA4*(*E146Q*) point mutant lines. Samples corresponding to 0.5 mg Chls were loaded onto each tube, and three major bands were separated. **(B-C)** Polypeptide composition of PSI-LHCI from the WT and *35S:LHCA4*(*E146Q*) lines analyzed by Coomassie staining following SDS-PAGE (samples corresponding to 2.5μg Chl were loaded per lane). **(B)** and immunoblot analysis **(C)** with antibodies against LHCA1, LHCA2, LHCA3, and LHCA4. **(D)** Absorption spectra of PSI-LHCI complexes isolated from the WT and *35S:LHCA4*(*E146Q*) lines. The spectra were normalized to their maximal absorption in the Qy region, which was set to 1. **(E)** Low-temperature (77K) fluorescence emission spectra (excited at 440 nm) of PSI-LHCI complexes isolated from the WT and *35S:LHCA4*(*E146Q*) lines. The spectra were normalized to their emission maxima (set to 1), with their FWHMs labeled and shown as double arrows in the same colors as the spectra. The dotted lines show the difference between the spectra from *35S:LHCA4*(*E146Q*)*-1* and the WT (light purple line) or *35S:LHCA4*(*E146Q*)*-5* and the WT (dark line) and multiplied by 5 to facilitate comparison.

binds on the lumenal side of helix B, and one in helix C (E146) is close to Chl *a*609 and interacts with Chl *b*607. We investigated the effect of the E146Q substitution on the absorption and emission properties of the red forms *in vivo* by isolating two transgenic lines expressing *LHCA4*(*E146Q*), lines *E146Q-1* and *E146Q-5*, with lower or higher relative *LHCA4* expression levels than the WT, respectively (Figures 5B, C). Although the emission peak of line *E146Q-5* was almost identical to that of the WT, around 735 nm, the transgenic lines showed a broader emission into the red part of the spectrum (Figure 5F). By contrast, line *E146Q-1* exhibited a blue-shifted emission similar to that of the *lhca4-1* mutant (Figure 5F). We propose that the blue shift in line *E146Q-1* was caused by the low LHCA4 abundance rather than by the substitution, as isolated PSI-LHCI complexes from both *E146Q* lines showed no blue shift in their emission spectra when compared to intact PSI-LHCI from the WT, with the mutant-isolated complexes even showing a slight red shift compared to the WT complexes (Figure 6E). Indeed, leaves from line *E146Q-5* had a broader absorption window in the red part of the spectrum than its corresponding isolated PSI-LHCI complexes, suggesting that the embedding PSI-LHCI complexes incorporating the LHCA4(E146Q) substitution into the thylakoid membrane contributed to maintaining the red form.

However, compared to the large red shift seen in rLHCA4 with E146Q (Wientjes et al., 2012), the red shift of PSI-LHCI isolated from leaves with the E146Q substitution in LHCA4 was not significant, likely reflecting the differential protein environment surrounding the red dimer of Chls *a*603–*a*609. We propose two hypotheses to explain the large red shift seen in rLHCA4 with the E146Q substitution: 1) the change in charge distribution caused by replacing negatively charged E with neutral Q and 2) one more Chl *b* binding into the protein, thus favoring a more red rLHCA4 conformation. In the context of the PSI-LHCI complex, LHCA4 with the E146Q substitution was not free but interacted with the PSI core and adjacent LHCAs, perhaps making it more difficult to insert additional Chl molecules due to steric hindrance. Importantly, both *in vitro* and *in vivo* experiments agreed that the E146Q substitution showed the same red shift in emission properties, although to a different extent. We thus speculate that the replacement of the negatively charged E in the surrounding environment of Chl *a*609 can change the local environment and enhance the red forms, offering a means to broadening absorption into the far-red region of the spectrum.

Improving energy utilization efficiency has been an important goal of photosynthetic research. Plants are much less effective at absorbing and utilizing far-red light than visible light, which can be a problem in a far-red light–enriched environment such as within or under canopies. Improving far-red light utilization could be an approach to increasing crop production under suboptimal conditions. Oxygenic photosynthetic organisms have two main strategies to use far-red light. In some cyanobacteria, Chl *d* and Chl *f* are produced to capture far-red light; most algae and land plants do not synthesize other Chls outside of Chl *a* and Chl *b*, so they capture far-red light by shifting the absorption spectrum of Chl *a* to a more red region (Wolf and Blankenship, 2019). While engineering a crop that can better utilize far-red light may borrow either of the two above strategies, the introduction of Chl *d* and Chl *f* might prove more difficult, as it would require the biosynthesis of new pigments. Conversely, while the second approach would be easier to implement, a serious limitation is the modest extent of red-shifted absorption compared to cyanobacterial Chl *d* and Chl *f*. The aim of this study was to determine how much the red forms can be shifted *in vivo* when changing amino acids surrounding the red Chls.

In this research, all N99 substitutions tested exhibited a blue shift in their fluorescence emission, suggesting that it might be difficult to engineer a more red-shifted absorbing form by replacing the N99 residue of LHCA4. However, targeting E146 in LHCA4 may be a promising method to expanding the absorption wavelength of LHCA4 and PSI-LHCA complexes into the far-red region. Evolutionarily, the amino acid coordinating with Chl *a*603 has changed from His in green algae such as *Chlamydomonas reinhardtii* (Su et al., 2019) and *Bryopsis corticulans* (Qin et al., 2019), and in the moss *Physcomitrium patens* (Yan et al., 2021), to Asn in angiosperms, concomitantly with a red shift in fluorescence emission maxima from 710 nm in green algae to 727 nm in the moss, and to 735 nm in angiosperms. This evolutionary pattern suggests that land plants have selected LHCA sequences to achieve a lower energy level for red Chls. It may therefore be easier to engineer crop plants with a blue shift in their absorption maxima relative to making red-shifted crops, as land plants appear to have evolved over billions of years to lower the energy level of their PSI-LHCs. In angiosperms, the function of the uphill energy transfer from low-energy Chls to bulk Chls with higher energy is still not well understood, but may be related to adaptation to the complex light environment on land. We speculate that engineering blue-shifted plants might provide a means to improving crop production under artificial light environments, as a weakened uphill energy transfer may lead to a faster EET. As the first exploration of the effects of amino acids surrounding Chl *a*603 and Chl *a*609 on their energy levels *in vivo*, this study provides new information on the relationship between structure and function of red Chls. Continued research on this topic is needed to clarify the mechanisms that tune the energy level of red forms and to design red-shifted or blue-shifted crops to make full use of limited light.

Data availability statement

The datasets presented in this study can be found in online repositories. The names of the repository/repositories and accession number(s) can be found in the article/Supplementary Material.

Author contributions

XQ planned and designed the research, analyzed the data and wrote the paper. XL and LZ performed the experiments, analyzed the data and wrote the manuscript. JS, GY and CH assisted in performing the experiments. TK and WW analyzed the data. All authors contributed to the article and approved the submitted version.

Funding

This work was funded by National Key R&D Program of China (2019YFA0906300, 2021YFA1300403); National Natural Science Foundation of China (32270260, 32070267); Taishan Scholars Project, Natural Science Foundation of Shandong Province, China (ZR2019ZD48, ZR2020MC106), and Higher Educational Science and Technology Program of Jinan City (2020GXRC058).

Acknowledgments

We thank Prof. Qijun Chen from China Agricultural University for providing plasmid (pHSE401).

Conflict of interest

The authors declare that the research was conducted in the absence of any commercial or financial relationships that could be construed as a potential conflict of interest.

Publisher's note

Supplementary material

The Supplementary Material for this article can be found online at: https://www.frontiersin.org/articles/10.3389/fpls.2022.1118189/full#supplementary-material

References

Angeler, D. G., and Schagerl, M. (1997). Distribution of the xanthophyll loroxanthin in selected members of the chlamydomonadales and volvocales (Chlorophyta). *Phyton-Ann. Rei. Bota* 37, 119–132.

Arnon, D. I. (1949). Copper enzymes in isolated chloroplasts. polyphenoloxidase in *beta vulgaris*. *Plant Physiol.* 24, 1–15.

Ballottari, M., Govoni, C., Caffarri, S., and Morosinotto, T. (2004). Stoichiometry of LHCI antenna polypeptides and characterization of gap and linker pigments in higher plants photosystem I. *Eur. J. Biochem.* 271, 4659–4665.

Bassi, R., and Simpson, D. (1987). Chlorophyll-protein complexes of barley photosystem I. *FEBS J.* 163, 221–230.

Ben-Shem, A., Frolow, F., and Nelson, N. (2003). Crystal structure of plant photosystem I. *Nature* 426, 630–635.

Buchel, C. (2015). Evolution and function of light harvesting proteins. *J. Plant Physiol.* 172, 62–75.

Castelletti, S., Morosinotto, T., Robert, B., Caffarri, S., Bassi, R., and Croce, R. (2003). Recombinant Lhca2 and Lhca3 subunits of the photosystem I antenna system. *Biochemistry* 42, 4226–4234.

Chen, M., and Blankenship, R. E. (2011). Expanding the solar spectrum used by photosynthesis. *Trends Plant Sci.* 16, 427–431.

Croce, R. (2015). Structural biology. a close view of photosystem I. *Science* 348, 970–971.

Croce, R., and van Amerongen, H. (2013). Light-harvesting in photosystem I. *Photosynth. Res.* 116, 153–166.

Croce, R., and van Amerongen, H. (2014). Natural strategies for photosynthetic light harvesting. *Nat. Chem. Biol.* 10, 492–501.

Croce, R., Zucchelli, G., Garlaschi, F. M., Bassi, R., and Jennings, R. C. (1996). Excited state equilibration in the photosystem I–Light-Harvesting I complex: P700 is almost isoenergetic with its antenna. *Biochemistry* 35, 8572–8579.

Klughammer, C., and Schreiber, U. (2008). Complementary PS II quantum yields calculated from simple fluorescence parameters measured by PAM fluorometry and the saturation pulse method. *PAM Appl. Notes* 1, 201–247.

Knoetzel, J., Svendsen, I., and Simpson, D. J. (1992). Identification of the photosystem I antenna polypeptides in barley : Isolation of three pigment-binding antenna complexes. *FEBS J.* 206, 209–215.

Kruger, T. P., Wientjes, E., Croce, R., and van Grondelle, R. (2011). Conformational switching explains the intrinsic multifunctionality of plant light-harvesting complexes. *Proc. Natl. Acad. Sci. U.S.A.* 108, 13516–13521.

Kuang, T. Y., Argyroudiakoyunoglou, J. H., Nakatani, H. Y., Watson, J., and Arntzen, C. J. (1984). The origin of the long-wavelength fluorescence emission band (77 K) from photosystem-I. *Arch. Biochem. Biophys.* 235, 618–627.

Kühlbrandt, W., Wang, D. N., and Fujiyoshi, Y. (1994). Atomic model of plant light-harvesting complex by electron crystallography. *Nature* 367, 614–621.

Li, T.-Y., Shi, Q., Sun, H., Yue, M., Zhang, S.-B., and Huang, W. (2021). Diurnal response of photosystem I to fluctuating light is affected by stomatal conductance. *Cells* 10, 3128.

Liu, Z., Yan, H., Wang, K., Kuang, T., and Chang, W. (2004). Crystal structure of spinach major light-harvesting complex at 2.72 a resolution. *Nature* 428, 287–292.

Li, X., Yang, G., Yuan, X., Wu, F., Wang, W., Shen, J.-R., et al. (2022). Structural elucidation of vascular plant photosystem I and its functional implications. *Funct. Plant Biol.* 49, 432–443.

Mazor, Y., Borovikova, A., and Nelson, N. (2015). The structure of plant photosystem I super-complex at 2.8 a resolution. *Elife* 4, e07433.

Morosinotto, T., Breton, J., Bassi, R., and Croce, R. (2003). The nature of a chlorophyll ligand in lhca proteins determines the far red fluorescence emission typical of photosystem I. *J. Biol. Chem.* 278, 49223–49229.

Morosinotto, T., Castelletti, S., Breton, J., Bassi, R., and Croce, R. (2002). Mutation analysis of Lhca1 antenna complex. low energy absorption forms originate from pigment-pigment interactions. *J. Biol. Chem.* 277, 36253–36261.

Nussberger, S., Dekker, J. P., Kuhlbrandt, W., van Bolhuis, B. M., van Grondelle, R., and van Amerongen, H. (1994). Spectroscopic characterization of three different monomeric forms of the main chlorophyll a/b binding protein from chloroplast membranes. *Biochemistry* 33, 14775–14783.

Qin, X., Pi, X., Wang, W., Han, G., Zhu, L., Liu, M., et al. (2019). Structure of a green algal photosystem I in complex with a large number of light-harvesting complex I subunits. *Nat. Plants* 5, 263–273.

Qin, X., Suga, M., Kuang, T., and Shen, J. R. (2015). Structural basis for energy transfer pathways in the plant PSI-LHCI supercomplex. *Science* 348, 989–995.

Qin, X., Wang, K., Chen, X., Qu, Y., Li, L., and Kuang, T. (2006). Rapid purification of photosystem I chlorophyll-binding proteins by differential centrifugation and vertical rotor. *Photosynth. Res.* 90, 195–204.

Rivadossi, A., Zucchelli, G., Garlaschi, F. M., and Jennings, R. C. (1999). The importance of PS I chlorophyll red forms in light-harvesting by leaves. *Photosynth. Res.* 60, 209–215.

Romero, E., Mozzo., M., van Stokkum, I. H. M., Dekker, J. P., van Grondelle., R., and Croce, R. (2009). The origin of the low-energy form of photosystem I light-harvesting complex Lhca4: mixing of the lowest exciton with a charge-transfer state. *Biophys. J.* 96, L35–L37.

Satoh, K. (1986). Chlorophyll-protein complexes. *Photosynth. Res.* 10, 181–187.

Schmid, V. H. R., Cammarata, K. V., and Schmidt, B. G. W. (1997). *In vitro* reconstitution of the photosystem I light-harvesting complex LHCI-730: Heterodimerization is required for antenna pigmentorganization. *Proc. Natl. Acad. Sci. U.S.A.* 94, 7667–7672.

Schmid, V., Paulsen, H., and Rupprecht, J. (2002). Identification of n- and c-terminal amino acids of Lhca1 and Lhca4 required for formation of the heterodimeric peripheral photosystem I antenna LHCI-730. *Biochemistry* 41, 9126–9131.

Su, X., Ma, J., Pan, X., Zhao, X., Chang, W., Liu, Z., et al. (2019). Antenna arrangement and energy transfer pathways of a green algal photosystem-I-LHCI supercomplex. *Nat. Plants* 5, 273–281.

Suzuki, K., Ohmori, Y., and Ratel, E. (2011). High root temperature blocks both linear and cyclic electron transport in the dark during chilling of the leaves of rice seedlings. *Plant Cell Physiol.* 52, 1697–1707.

Wang, J., Yu, L. J., Wang, W., Yan, Q., Kuang, T., Qin, X., et al. (2021). Structure of plant photosystem I-light harvesting complex I supercomplex at 2.4 a resolution. *J. Integr. Plant Biol.* 63, 1367–1381.

Wientjes, E., and Croce, R. (2011). The light-harvesting complexes of higher-plant photosystem I: Lhca1/4 and Lhca2/3 form two red-emitting heterodimers. *Biochem. J.* 433, 477–485.

Wientjes, E., Roest, G., and Croce, R. (2012). From red to blue to far-red in Lhca4: how does the protein modulate the spectral properties of the pigments? *Biochim. Biophys. Acta* 1817, 711–717.

Wolf, B. M., and Blankenship, R. E. (2019). Far-red light acclimation in diverse oxygenic photosynthetic organisms. *Photosynth. Res.* 142, 349–359.

Xing, H., Dong, L., Wang, Z., Zhang, H., Han, C., Liu, B., et al. (2014). A CRISPR/Cas9 toolkit for multiplex genome editing in plants. *BMC Plant Biol.* 14, 327.

Yan, Q., Zhao, L., Wang, W., Pi, X., Han, G., Wang, J., et al. (2021). Antenna arrangement and energy-transfer pathways of PSI-LHCI from the moss *Physcomitrella patens*. *Cell Discovery* 7, 10.

Zhang, H., Goodman, H. M., and Jansson, S. (1997). Antisense inhibition of the photosystem I antenna protein Lhca4 in *Arabidopsis thaliana*. *Plant Physiol.* 115, 1525–1531.

frontiers | Frontiers in Plant Science

TYPE Original Research
PUBLISHED 19 January 2023
DOI 10.3389/fpls.2023.1050483

OPEN ACCESS

EDITED BY
Agepati S Raghavendra,
University of Hyderabad, India

REVIEWED BY
Zhanguo Xin,
Agricultural Research Service, United States Department of Agriculture (USDA), United States
Rajagopal Subramanyam,
University of Hyderabad, India

*CORRESPONDENCE
Devin Coleman-Derr
devin.coleman-derr@usda.gov

SPECIALTY SECTION
This article was submitted to Photosynthesis and Photobiology, a section of the journal Frontiers in Plant Science

RECEIVED 21 September 2022
ACCEPTED 09 January 2023
PUBLISHED 19 January 2023

CITATION
Caddell D, Langenfeld NJ, Eckels MJH, Zhen S, Klaras R, Mishra L, Bugbee B and Coleman-Derr D (2023) Photosynthesis in rice is increased by CRISPR/Cas9-mediated transformation of two truncated light-harvesting antenna. *Front. Plant Sci.* 14:1050483. doi: 10.3389/fpls.2023.1050483

Photosynthesis in rice is increased by CRISPR/Cas9-mediated transformation of two truncated light-harvesting antenna

Daniel Caddell[1,2], Noah J. Langenfeld[3], Madigan JH. Eckels[3], Shuyang Zhen[4], Rachel Klaras[2], Laxmi Mishra[2], Bruce Bugbee[3] and Devin Coleman-Derr[1,2]*

[1]Plant Gene Expression Center, United States Department of Agriculture - Agricultural Research Service (USDA ARS), Albany, CA, United States, [2]Plant and Microbial Biology Department, University of California at Berkeley, Berkeley, CA, United States, [3]Department of Plants, Soils, and Climate, Utah State University, Logan, UT, United States, [4]Department of Horticultural Sciences, Texas A&M University, College Station, TX, United States

Plants compete for light partly by over-producing chlorophyll in leaves. The resulting high light absorption is an effective strategy for out competing neighbors in mixed communities, but it prevents light transmission to lower leaves and limits photosynthesis in dense agricultural canopies. We used a CRISPR/Cas9-mediated approach to engineer rice plants with truncated light-harvesting antenna (TLA) via knockout mutations to individual antenna assembly component genes CpSRP43, CpSRP54a, and its paralog, CpSRP54b. We compared the photosynthetic contributions of these components in rice by studying the growth rates of whole plants, quantum yield of photosynthesis, chlorophyll density and distribution, and phenotypic abnormalities. Additionally, we investigated a Poales-specific duplication of CpSRP54. The Poales are an important family that includes staple crops such as rice, wheat, corn, millet, and sorghum. Mutations in any of these three genes involved in antenna assembly decreased chlorophyll content and light absorption and increased photosynthesis per photon absorbed (quantum yield). These results have significant implications for the improvement of high leaf-area-index crop monocultures.

KEYWORDS

truncated light antenna, photosynthesis, chlorophyll, CRISPR/Cas9, rice

1 Introduction

In plants, pigments such as chlorophyll and carotenoids harvest light and transfer the energy toward reaction centers, where it is converted to chemical energy via photochemical charge separation, initiating photosynthesis. In full sunlight, plants absorb more light than can be used for photosynthesis. This overaccumulation enables a selective advantage in

natural communities, whereby plants with large light-harvesting antenna complexes can outcompete neighboring plants for sunlight, which is a major growth-limiting factor in most environments. Prevention of weed establishment in agricultural settings is often accomplished through herbicidal or management practices, such as planting in dense monocultures. The absorption of excess photons by upper leaves reduces the amount of light within the canopy that is used for photosynthesis, and can negatively impact plant yields (Bugbee, 1992). Recent studies have suggested that mutations that reduce the size of light-harvesting antenna complexes, producing mutants commonly referred to as truncated light antenna (TLA) mutants, may improve quantum yield of PSII by increasing light penetration deeper into the canopy, particularly under high density, high light conditions (Gu et al., 2017a; Gu et al., 2017b; Kirst et al., 2017; Kirst et al., 2018).

Chloroplast light-harvesting antenna assembly relies on cytosolic synthesis of nuclear-encoded light-harvesting chlorophyll a/b binding proteins (LHCPs). To function, LHCPs must be imported into the chloroplast, transported, and ultimately assembled into the thylakoid membrane. This process is mediated by the chloroplast signal recognition particle (CpSRP) pathway (Ziehe et al., 2017). In the stroma, CpSRP43 and CpSRP54 form a heterodimer that binds LHCPs, forming a transit complex (DeLille et al., 2000; Tu et al., 2000; Jonas-Straube et al., 2001; Hermkes et al., 2006). This complex is important for preventing aggregation of hydrophobic LHCPs prior to insertion into the thylakoid membrane (Payan and Cline, 1991; Li et al., 1995; Schuenemann et al., 1998; Klimyuk et al., 1999; Tu et al., 1999). At the thylakoid membrane, the CpSRP receptor, CpFTSY, binds the transit complex (Kogata et al., 1999; Tu et al., 1999; Stengel et al., 2007; Chandrasekar et al., 2008) and positions it such that LHCPs can be integrated into the thylakoid membrane by the insertase ALBINO3 (ALB3) (Moore et al., 2000; Yuan et al., 2002; Moore et al., 2003).

Reducing light harvesting pigment concentration has been shown to improve photosynthesis in microalgae (Nakajima and Ueda, 1997; Nakajima et al., 2001) and cyanobacteria (Kirst et al., 2014). In plants, mutants of the CpSRP pathway (TLA mutants) have been identified in genetic screens by pale green leaf phenotypes that correspond to higher chlorophyll a/b ratios (Liu et al., 2016; Kirst et al., 2017; Kirst et al., 2018). Multiple studies have demonstrated trait alterations in TLA mutant plants with the potential for agronomic benefit, with particular focus on plants with mutations in CpSRP43 (TLA3 mutants) and CpSRP54 (TLA4 mutants). For example, the Arabidopsis TLA3 mutant *chaos* showed significantly higher tolerance to photooxidative stress in lab and field conditions (Klenell et al., 2005), and CpSRP43 knockdown in *Nicotiana tobacum* was recently demonstrated to enhance leaf-to-stem ratio and plant biomass (Kirst et al., 2018). Similarly, a TLA3 mutation in rice reduced plant height and tillering with no loss of grain mass (Lv et al., 2015), and three distinct TLA4 mutant alleles have been identified in rice that cause reduced tillering with no loss of grain weight (Zhang et al., 2013; Liu et al., 2016). In the Poales family, mutations to paralogous proteins CpSRP54a and CpSRP54b (creating TLA4 and TLA4L mutants, respectively) also caused plants to display a pale-green phenotype, although TLA4L mutants died before reaching maturity (Shi et al., 2020). In contrast to potential benefits associated with TLA3 and TLA4 mutants, plants lacking CpFTSY (TLA2 mutants) or ALB3 have been shown to suffer significant pleiotropic effects on growth and development. For example, Arabidopsis *cpftsY* and *alb3* mutants (Durrett et al., 2006; Asakura et al., 2008), and a maize *cpftsY* null-mutant (Asakura et al., 2004) had pleiotropic defects associated with broad roles in thylakoid biogenesis in addition to a substantial reduction in chlorophyll.

Previous research has indirectly compared various molecular characteristics of TLA mutants in Arabidopsis (Amin et al., 1999; Asakura et al., 2008; Walter et al., 2015). However, direct comparisons of potential agronomic benefits between TLA mutants in crop plants have not been performed, in part because they have been independently identified and characterized in different genetic backgrounds, which can prevent the ability to distinguish phenotypic differences due to broad genotypic contributions from specific TLA mutations. Gene engineering mediated by CRISPR/Cas9 now provides the ability to compare gene function in near-isogenic backgrounds, allowing for a direct dissection of the contribution of each TLA mutation to photosynthesis and fitness phenotypes. In this study, we used CRISPR/Cas9 to create three independent mutant lines, each with a single null mutation in predicted components of the rice CpSRP pathway; *CpSRP43* (TLA3), *CpSRP54a* (TLA4), and *CpSRP54b* (TLA4L), and assessed their potential agronomic benefits.

2 Materials and methods

2.1 Plasmid construction

Assembly of CRISPR/Cas9 T-DNA vectors was performed as described previously (Lowder et al., 2015). In short, sgRNA oligo pairs targeting *CpSRP43* (LOC_Os03g03990), *CpSRP54a* (LOC_Os11g05552), and *CpSRP54b* (LOC_Os11g05556) were designed and annealed (Table 1). Annealed oligos with a single target near the N-terminal of CpSRP54a or CpSRP54b were cloned into the gateway entry vector pYPQ141C (Lowder et al., 2015) to create 1-TLA4 and 1-TLA4L. Annealed oligos for golden gate assembly were cloned into the golden gate recipient vectors: pYPQ131C, pYPQ132C, or pYPQ133C (Lowder et al., 2015). Proper ligation of oligos was confirmed at all stages by Sanger sequencing with either primer M13-F (for pYPQ141C) or pTC14-F2 (for pYPQ131C, pYPQ132C, and pYPQ133C). See Table 2 for the sequences of primers used in this study. The following golden gate assemblies were also performed: assembly of two sgRNAs targeting the N- and C-terminal regions of CpSRP43, CpSRP54a, or CpSRP54b into pYPQ142 (Lowder et al., 2015) to create 2-TLA3, 2-TLA4, and 2-TLA4L, respectively, and assembly of three sgRNAs targeting near the N- and C-terminal of CpSRP54a and the C-terminal of CpSRP54b into pYPQ143 (Lowder et al., 2015) to create TLA4/TLA4L. Gateway assembly of the sgRNA entry vectors, the Cas9 entry vector pYPQ167 (Lowder et al., 2015), and the gateway-compatible destination vector Ubi-CAMBIA-1300 (Chern et al., 2001) were performed using LR clonase II enzyme (Thermo Fisher Scientific, Waltham, MA), to generate the final CRISPR/Cas9 T-DNA vectors Ubi-2-TLA3, Ubi-1-TLA4, Ubi-2-TLA4, Ubi-1-TLA4L, Ubi-2-TLA4L, and Ubi-TLA4/TLA4L. Proper assembly was verified by restriction digestion and sequencing with Ubi-pro-F and Cas9-seq-R primers (Table 2).

10.3389/fpls.2023.1050483

TABLE 1 sgRNA oligo pairs designed to produce CRISPR/Cas9-based knockouts of *CpSRP43*, *CpSRP54a*, and *CpSRP54b*.

Construct name	sgRNA Oligo Pair Sequence 5′ – 3′	Target
1-TLA3	gtgtgCGAGCCTTCGTGGATCCCGG	*CpSRP43* N-terminal
	aaacCCGGGATCCACGAAGGCTCGc	
1-TLA4	gtgtgTCTTATAAGAGGAGTCCGAC	*CpSRP54a* N-terminal
	aaacGTCGGACTCCTCTTATAAGAc	
1-TLA4L	gtgtgGTAGGCACTGATGTGATTCG	*CpSRP54b* N-terminal
	aaacCGAATCACATCAGTGCCTACc	
2-TLA3	gtgtgCCACTCGACGAGGTACTCCG	*CpSRP43* N-terminal
	aaacCGGAGTACCTCGTCGAGTGGc	
	gtgtgTTCGGCGTCGACGTTCTCCG	*CpSRP43* C-terminal
	aaacCGGAGAACGTCGACGCCGAAc	
2-TLA4	gtgtgGCCACGCAGCTTGTTCCAGG	*CpSRP54a* N-terminal
	aaacCCTGGAACAAGCTGCGTGGCc	
	gtgtgGCATTTGTAGATATGATGGT	*CpSRP54a* C-terminal
	aaacACCATCATATCTACAAATGCc	
2-TLA4L	gtgtgTCCCCGCAGCTTGTTCCACG	*CpSRP54b* N-terminal
	aaacCGTGGAACAAGCTGCGGGGAc	
	gtgtgCCGCTGGTACTGGAAAGCGA	*CpSRP54b* C-terminal
	aaacTCGCTTTCCAGTACCAGCGGc	
TLA4/TLA4L	gtgtgTCTTATAAGAGGAGTCCGAC	*CpSRP54a* N-terminal
	aaacGTCGGACTCCTCTTATAAGAc	
	gtgtgGCTCTTCTGATATCCCGCAT	*CpSRP54a* C-terminal
	aaacATGCGGGATATCAGAAGAGCc	
	gtgtgCCGCTGGTACTGGAAAGCGA	*CpSRP54b* N-terminal
	aaacTCGCTTTCCAGTACCAGCGGc	
Systems designed to target one, two, or three loci can be differentiated by the number of sgRNA sequences listed under the construct name.		

TABLE 2 Primers used in this study. Both sequencing and RT-PCR primers are listed with corresponding purposes.

Primer Name	Sequence 5′ – 3′	Purpose
M13 F	TGTAAAACGACGGCCAGT	Sequencing of pYPQ141C vectors
pTC14-F2	CAAGCCTGATTGGGAGAAAA	Sequencing of pYPQ131C, pYPQ132C, and pYPQ133C vectors
Ubi-pro-F	TTGTCGATGCTCACCCTGTTGTTT	Forward sequencing of Ubi-CAMBIA-1300 vectors
Cas9-seq-R	ACCGTCAATGTAACCGGCGTAG	Reverse sequencing of Ubi-CAMBIA-1300 vectors
TLA4-F	AGAGGAGTCCGACCGGAACAGC	RT-PCR of *CpSRP54a*
TLA4-R	TTCCCAACACCTTGCAGGCCTG	
TLA4L-F	AGCCAATTGGTTGCGCAGCTCT	RT-PCR of *CpSRP54b*
TLA4L-R	CTTTCCAGTACCAGCGGCAGCC	
Actin-F	GTCCTCTTCCAGCCTTCCTT	RT-PCR of Actin-1 gene as internal control
Actin-R	GCGACCACCTTGATCTTCAT	

2.2 Rice transformation

Transformation of *Agrobacterium tumefaciens* strain EHA105 with plasmids Ubi-2-TLA3, Ubi-1-TLA4, Ubi-2-TLA4, Ubi-1-TLA4L, Ubi-2-TLA4L, or Ubi-TLA4/TLA4L was performed by electroporation using the Gene Pulser Xcell (Bio-Rad), per the manufacturer's instructions. Rice transformation was performed at the University of California, Davis Rice Transformation Facility using *A. tumefaciens* strain EHA105 to infect rice calli (*Oryza sativa* ssp. japonica L., cv. Kitaake). Selection of transformants carrying the transgenes was performed using hygromycin as a selectable marker and later confirmed by PCR with transgene specific primers Ubi-pro-F and Cas9-seq-R (Table 2). Identification of successful CRISPR/Cas9-mediated indels was determined by PCR using primers flanking the target cut site. Indels were further validated by Sanger sequencing. All plants used in this study were homozygous TLA mutants unless otherwise specified as null mutants (n).

2.3 Plant growing conditions and phenotyping

Rice plants were grown in the greenhouse with 16-h day and 8-h night cycle, 28°C day and 26°C night temperature, and 50-60% relative humidity. Plants were grown in a peat-based soilless media and watered daily with a complete nutrient solution (Zhen and Bugbee, 2020). The solution was supplemented with 20 ppm ethylenediamine-N,N′-bis(2-hydroxyphenylacetic acid) (EDDHA) chelated iron to minimize any possible iron chlorosis. Photosynthetic rate was measured using a portable photosynthesis system (model LI-6800, LICOR Biosciences, Lincoln, NE) with a fluorometer head attached (model LI-6800-01A, LICOR Biosciences). The chamber settings held constant across measurements were: 25°C air temperature, 150 μmol s^{-1} flow rate, 5000 rpm fan speed, 50% relative humidity, 90% red photon fraction, and 10% blue photon fraction. Light response curves (LRCs) were generated by measuring assimilation rates stepwise at 400, 100, 0, 50, 200, 400, 800, 1400, and 2000 μmol photons m^{-2} s^{-1} using the built-in light response curve program. A minimum chamber stabilization time of 10 minutes was set, and carbon dioxide and water infrared gas analyzers were matched following the logging of each measurement. LRCs were run first at 400 ppm CO_2 and then at 1200 ppm CO_2 without removing the leaf from the chamber. All photosynthetic rate measurements were collected on rice plants ranging from 33 to 35 d old.

Photon absorbance was calculated by subtraction from measurements of transmission and calculated reflectance. Photon transmission was measured after placing the leaf over quantum sensor (model LI-190R, LICOR Biosciences). The transmitted fraction of photons was multiplied by 2 to account for an equal number of reflected and transmitted photons (Jacquemoud and Ustin, 2019). Photosynthetic rates were then divided by the absorbed photon flux to calculate photosynthetic rate per photon absorbed. Chlorophyll content was measured using an optical chlorophyll meter (Model MC-100, Apogee Instruments, Logan, UT) using generic coefficients (Parry and Bugbee, 2017). Laboratory measurements were made on nine leaves and averaged. To confirm optical chlorophyll measurements, 0.05 g of tissue was cut from the newest fully expanded leaf of mature rice plants and ground to a fine powder in liquid N_2. Photosynthetic pigment was extracted using 80% acetone and incubated in the dark at room temperature for 24-h. Absorbance measurements at 663.2 nm, 646.8 nm, and 470 nm were recorded using a Shimadzu UV-1280 spectrophotometer. Estimates of chlorophyll and carotenoid content were calculated with the equations previously described by Wellburn (1994).

2.4 CpSRP54 alignments and phylogenetic tree

Protein blast was performed using Arabidopsis CpSRP54 (At5g03940) as an input in phytozome v12.1 against other genomes, retrieving 188 hits. Because plants have both an SRP54 and CpSRP54 system, we used ChloroP v1.1 (Emanuelsson et al., 1999) to predict which proteins were chloroplast localized, reducing our protein lists to 60 hits. Of those 60, 32 genes that were predicted to encode the SRP receptor (CpFTSY) were removed from the list, leaving 28 genes predicted to encode CpSRP54 across 21 species. CpSRP54 proteins were aligned using the MUSCLE alignment algorithm, with 100 iterations. The phylogenetic tree was built using the Jukes-cantor neighbor joining method, with 1,000 bootstraps. The CpSRP pathway functional gene network predictions were made using RiceNet v2 (Lee et al., 2015) with default parameters.

2.5 TLA gene expression

Leaf tissue from the youngest fully expanded leaves of three independent TLA4 mutant lines and Kitaake WT was collected from four-week-old plants (five plants per line) and RNA was extracted using a Qiagen Plant RNA extraction kit. RNA was converted to cDNA using a cDNA synthesis kit, and quantitative RT-PCR was performed using primers specific to *CpSRP54a* (TLA4-F/R) or *CpSRP54b* (TLA4L-F/R) (Table 2). Actin-1 (LOC_Os03g50885) gene expression was amplified as a control using the primers Actin-F/R (Table 2).

2.6 Statistical analyses

Statistical tests were performed using a one-way analysis of variance (ANOVA) test. Statistically significant results were followed up with a Tukey's honest significance *post-hoc* test using R (Version 3.6.1, R Core Team). Significance for all statistical tests was predetermined at $p < 0.05$, and significant differences are reported in figures using capital letters to differentiate between groups. Groups with the same letter are not significantly different from one another.

3 Results

3.1 The rice TLA3 mutant has altered chlorophyll accumulation in leaves

Rice TLA3 mutations have emerged as the cause of pale-green leaf phenotypes in multiple rice ethyl methane sulfonate (EMS) screens

(Lv et al., 2015; Wang et al., 2016; Ye et al., 2018). Likewise, previous EMS and T-DNA screens have also identified putative TLA4 mutations in rice (Zhang et al., 2013; Liu et al., 2016). However, direct comparisons between TLA mutants in rice have been difficult, as these studies were performed in different cultivars, and as EMS-generated mutants may not be complete loss-of-function mutants or may carry additional genetic mutations that contribute to phenotypic outcomes (Wang et al., 2016). To gain a better understanding of the agronomic potential of these TLA mutants, we utilized CRISPR/Cas9 to generate targeted TLA knock-out mutants in the rice cultivar Kitaake. Rice CpSRP43 is encoded by a single gene copy with a single exon. Using CRISPR/Cas9, we generated near-complete gene knockouts of *CpSRP43* in rice (Figure 1D) to create TLA3 mutants. In agreement with previous studies, TLA3 mutants had reduced plant height (Figure 1A, C). Likewise, these mutants displayed a pale green leaf phenotype and had reduced chlorophyll content (Figure 1B, C). These results demonstrate that CRISPR/Cas9 can be successfully implemented to generate targeted TLA-engineered rice plants with phenotypes consistent with the previous studies described above.

3.2 A *CpSRP54* duplication occurred in the Poales lineage

Two previous EMS and T-DNA screens have identified the putative *CpSRP54* gene in rice encoded by LOC Os11g05552

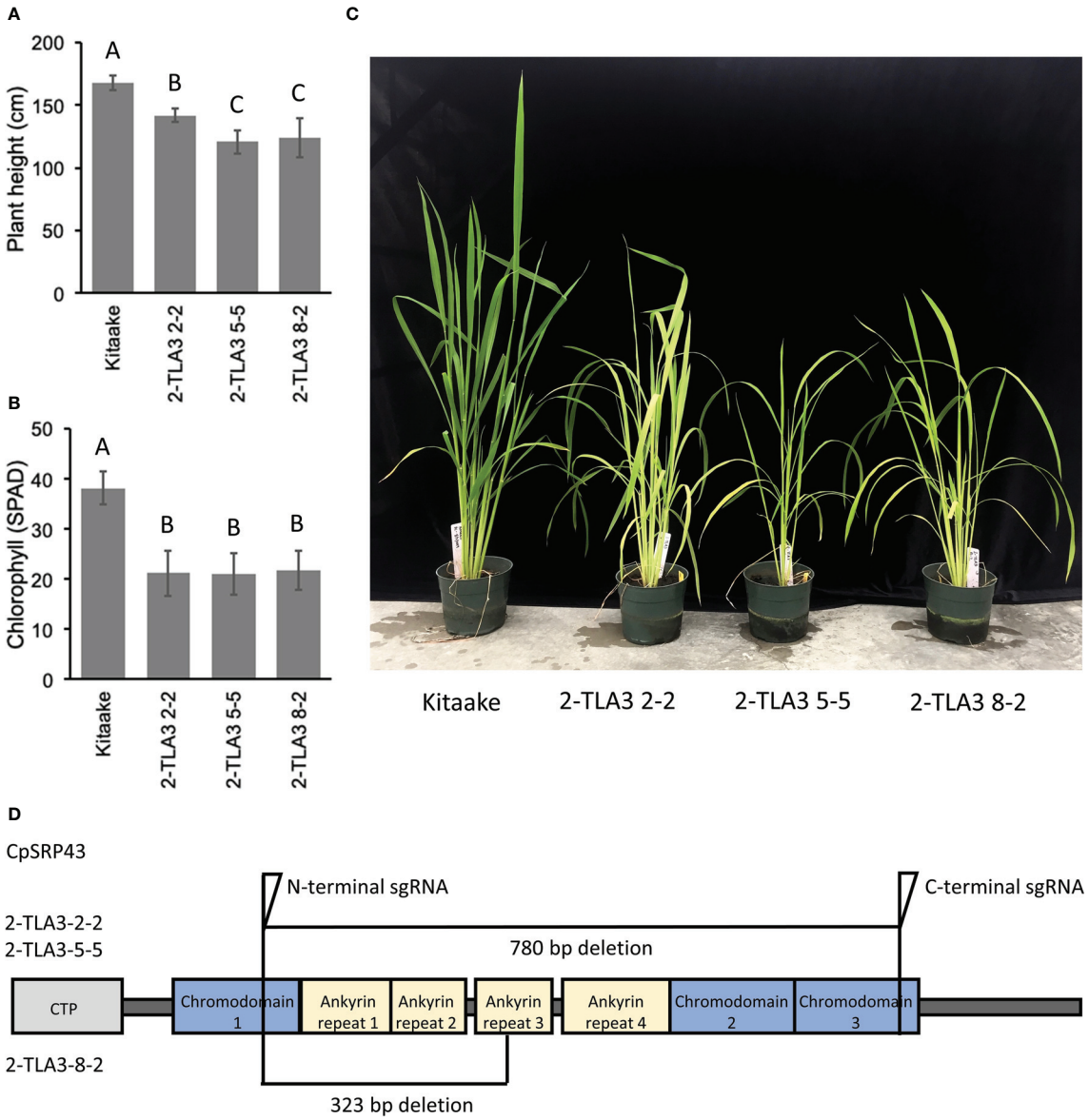

FIGURE 1
TLA3 mutants have reduced height and chlorophyll content. **(A)** Measurements of plant height for three independent CRISPR/Cas9-generated TLA3 mutant lines as compared to Kitaake wild type (WT). **(B)** Measurements of chlorophyll content for these three mutants, as measured using a SPAD meter. **(C)** Representative images of the homozygous parental line of each of the three mutant lineages characterized in **(A)** and **(B)**, demonstrating reduced stature and a pale green leaf phenotype. **(D)** Protein domain model of validated CRISPR/Cas9-mediated TLA3 mutations generated using two sgRNAs indicating the relative position and size in base pairs of large deletions within CpSRP43. Frameshift mutations occurred in the middle of chromodomain 1 in each line. CTP, Chloroplast targeting peptide.

(Zhang et al., 2013; Liu et al., 2016), here called *CpSRP54a*. The canonical CpSRP54a protein structure consists of conserved N, G, and M domains (Figure 2A). While CpSRP54 is predicted to be encoded by a single gene copy in algae, mosses, and dicots, a tandem duplication of *CpSRP54a* occurred in an ancestor of the Poales lineage of monocots (here referred to as *CpSRP54b*). This duplication is absent from non-Poales monocot species, such as duckweed and banana, and is present in all sequenced members of the Poales family (Figure 2B). To predict whether both genes are involved in the CpSRP pathway, we performed a computational functional gene network prediction using *CpSRP43*, *CpSRP54a*, and *CpSRP54b* as inputs using RiceNet v2 (Lee et al., 2015), which utilizes a large repository of published expression data for rice for its calculations. Network predictions demonstrated that the predicted rice *CpFTSY* was a node shared by all three genes, suggesting that they are all involved in the anticipated CpSRP pathway (Supplemental Figure 1). Likewise, CpSRP43 is predicted to functionally interact with the insertase ALB3 (Supplemental Figure 1), which has been previously characterized in Arabidopsis as part of the CpSRP pathway (Tzvetkova-Chevolleau et al., 2007). The most direct connections between inputs were shared between CpSRP54a and CpSRP54b, suggesting a strong level of functional overlap. Notably, CpSRP54b has more predicted connections with CpSRP43 than does CpSRP54a (Supplemental Figure 1), suggesting that it may play a more important role in CpSRP pathway function than its paralog. Collectively these data suggest that both putative CpSRP54 paralogs are expressed and are predicted to interact with other CpSRP pathway components.

3.3 Rice TLA4 and TLA4L mutants can be distinguished by plant height and phenotype

To allow for direct comparisons between mutations in CpSRP54a, CpSRP54b, and CpSRP43 in the context of photosynthetic and agronomic traits within the same genetic background, we used CRISPR/Cas9 to generate TLA4 and TLA4L single null mutants and TLA4/TLA4L double null mutants in the Kitaake cultivar (Figure 3F). In agreement with previous findings (Shi et al., 2020), we confirmed that TLA4 mutants had reduced plant height, and a demonstrable decrease in chlorophyll content (Figure 3A-E). Notably, unlike the findings of Shi et al. (2020), TLA4L rice plants were able to set seed and be propagated (Figure 3C). However, compared with the TLA4 mutants, the TLA4L mutants had a greater decrease in both plant height (Figure 3D) and chlorophyll content (Figure 3E), further suggesting that TLA4L and TLA4 do not perform identical roles within the CpSRP pathway. The inclusion of TLA4L null segregants with restored plant height and chlorophyll content demonstrate that observed phenotypes are due to specific mutations in the target gene and not the result of off-target cutting by CRISPR/Cas9.

Due to the close proximity of *CpSRP54a* and *CpSRP54b* in the rice genome, and the fact that TLA4 mutations reside upstream of the *CpSRP54b* promoter, we hypothesized that the loss of function mutation in TLA4 may have led to altered expression of CpSRP54b, making the dissection of CpSRP54a and CpSRP54b contributions to phenotype difficult in TLA4 mutant lines. To test this, we used quantitative RT-PCR to first confirm the reduced expression of

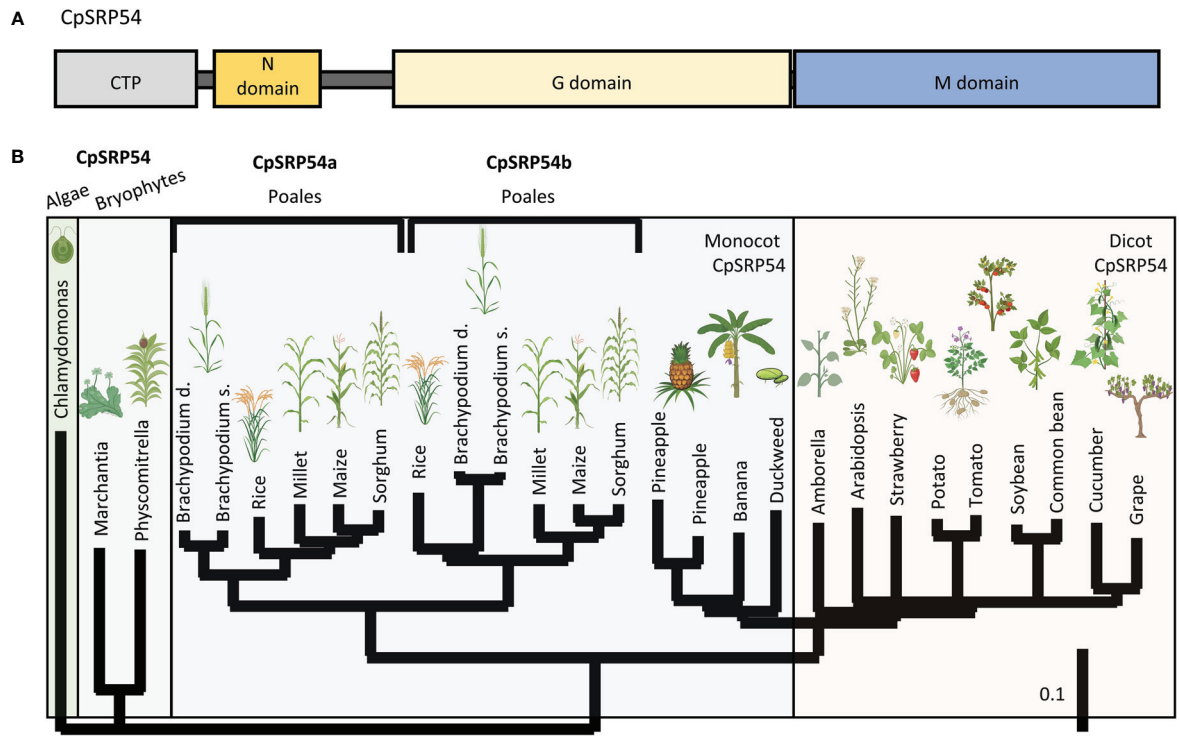

FIGURE 2
A duplication of CpSRP54 occurred in the Poales lineage. **(A)** Protein domain model of CpSRP54 with CTP (chloroplast targeting peptide). **(B)** Phylogenetic tree of CpSRP54 showing a duplication event in the Poales lineage to produce CpSRP54a and CpSRP54b Created with BioRender.com.

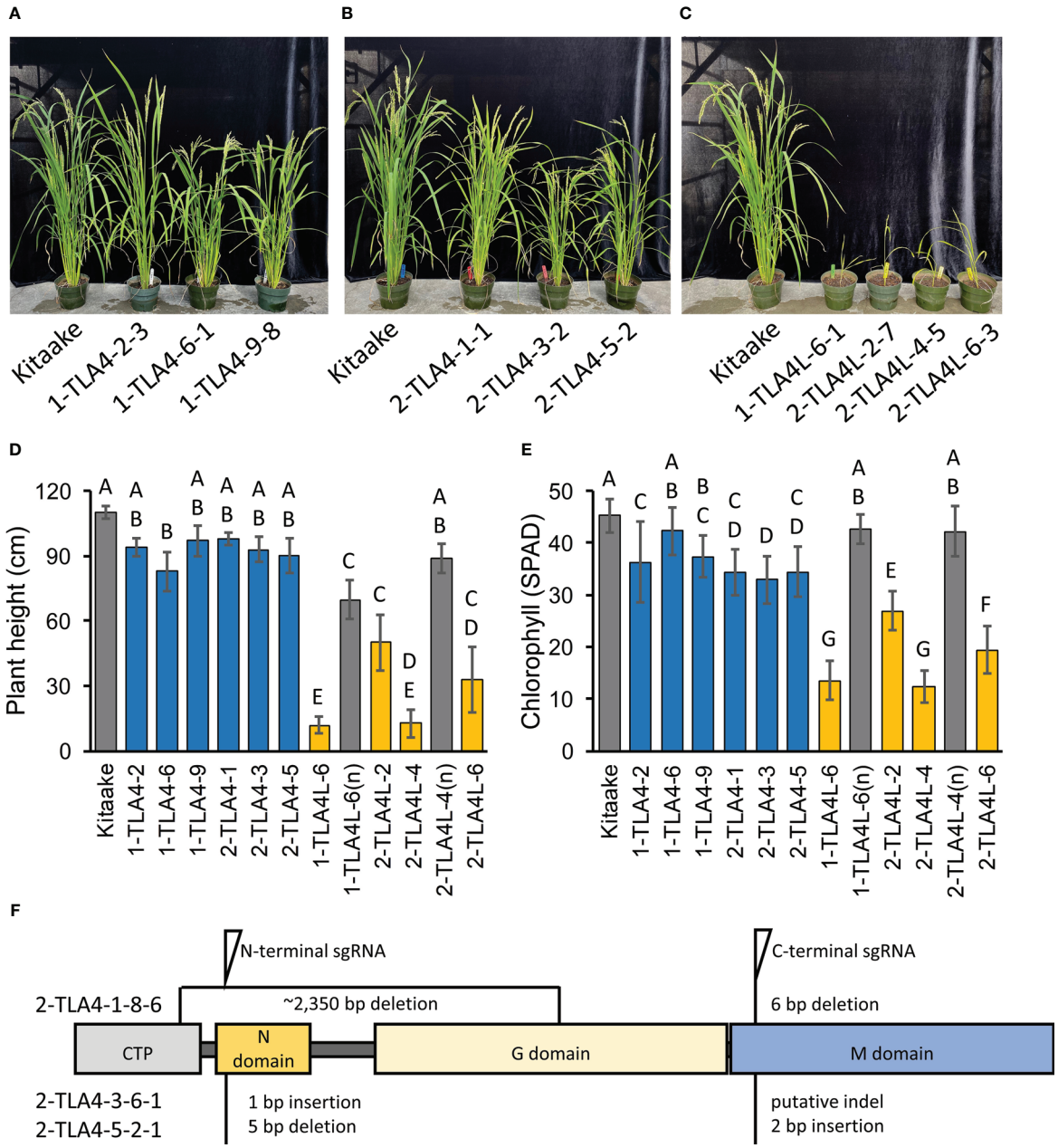

FIGURE 3
CpSRP54a and CpSRP54b both contribute to leaf chlorophyll accumulation. **(A, B, C)** Representative images of several mutant TLA4 **(A, B)** and TLA4L **(C)** lineages demonstrate reduced plant height and a pale green leaf phenotype as compared to WT. TLA4L mutants display a particularly severe phenotype. **(D)** Plant height of representative TLA4 and TLA4L mutant individuals from independently CRISPR/Cas9-generated lineages. Blue bars represent TLA4 mutants, yellow bars represent TLA4L mutants, and gray bars represent null-segregants (n). Null-segregants show restored WT phenotypes. **(E)** Measurements of chlorophyll content for TLA4, TLA4L, and TLA4L(n) individuals as measured using a SPAD meter. Blue bars represent TLA4 mutants, yellow bars represent TLA4L mutants, and gray bars represent null-segregants (n). **(F)** Protein domain model with CTP (Chloroplast targeting peptide) of validated CRISPR/Cas9-mediated TLA4 mutations generated using two sgRNAs indicating the relative position and size in base pairs of indels within CpSRP54a. All three mutant lines have multiple indels.

CpSRP54a in three independent TLA4 lines (2-TLA4-1-8-6, 2-TLA4-3-6, and 2-TLA4-5-2) compared with WT Kitaake (Supplemental Figure 2A). We observed significantly reduced *CpSRP54a* expression in TLA4 mutant lines 2-TLA4-3-6 and 2-TLA4-5-2, and a complete loss of *CpSRP54a* expression in 2-TLA4-1-8-6 (Supplemental Figure 2A). Contrary to our hypothesis, no significant reduction in *CpSRP54b* expression was observed in any of the three independent TLA4 mutant lines as compared with Kitaake (Supplemental Figure 2B). These results indicate that the phenotypes observed in TLA4 mutants are not due to reduced expression of *CpSRP54b*, but can be attributed to the knockout of *CpSRP54a* alone.

To evaluate the degree to which CpSRP54a and CpSRP54b perform similar functions in the CpSRP pathway, 30 rice plantlets were recovered from tissue culture containing the TLA4/TLA4L sgRNA designed to generate double knockout mutants. However, unlike either single mutant, all putative TLA4/TLA4L double mutant plantlets died shortly after transplanting to the greenhouse. While not definitive, this observation suggests that CpSRP54a and CpSRP54b

may contribute additively to chlorophyll accumulation in rice. Combined with the observation that TLA4 mutants do not have reduced expression of *CpSRP54b* yet display significant phenotypes, these results suggest that CpSRP54a and CpSRP54b are both functional proteins with overlapping but not identical roles in rice.

3.4 Photosynthetic rate per photon absorbed is increased in TLA mutants

To more precisely determine the relative contributions of CpSRP43 and CpSRP54a to photosynthesis and fitness, a series of experiments were performed to evaluate chlorophyll and carotenoid content, plant height, and photosynthetic rate across physiological development and a range of lighting conditions. TLA4L mutants were not included in this study due to the extremely severe phenotypes associated with the mutations, including dramatically smaller plant size.

First, the pigment content and plant height of three independent lines of TLA3 (2-TLA3-2-5, 2-TLA3-5-5-1-5, 2-TLA3-8-2-3) and TLA4 (2-TLA4-1-8-6, 2-TLA4-3-6, 2-TLA4-5-2) mutants were compared. At five weeks post germination, both the chlorophyll and carotenoid content were significantly reduced in TLA mutants compared to wild-type plants, with TLA3 having lower levels of each pigment than TLA4 (Supplemental Figure 3). Similarly, the plant heights of both TLA3 and TLA4 mutants were reduced two weeks after panicle emergence (Supplemental Figure 3A). In agreement with previous reports (Lv et al., 2015; Liu et al., 2016; Wang et al., 2016; Shi et al., 2020), chlorophyll a/b ratio was elevated and the ratio of chlorophyll to carotenoids was reduced in TLA mutants (Supplemental Figure 3F).

A further characterization of TLA phenotypes was performed using two independent mutant lines for both TLA3 (2-TLA3-5-5-1-5-1, 2-TLA3-8-2-3-4) and TLA4 (2-TLA4-1-8-6-1, 2-TLA4-3-6-1).We observed that while chlorophyll concentration increased over time for all lines, rates of accumulation differed between WT and TLA mutant lines (Figure 4A). Specifically, while the WT reached a steady chlorophyll concentration after 40 days, all the genetically altered lines continued to increase until heading at 78 days. As expected, plant height steadily increased over time for all lines, but the height of the mutant lines was less than the WT until 60 days after planting (Figure 4B). Additionally, we saw that optically measured chlorophyll content was positively correlated with leaf photon absorbance fraction across all lines (Figure 5). Collectively, these results confirm earlier observations of decreased height and chlorophyll content during early and mid-development.

As hypothesized, we also observed that mutant lines exhibited only minimally reduced photosynthetic rate compared to the wild type under standard conditions (Figure 6A). When considering the reduced chlorophyll content of all mutant lines, this formally demonstrates that photosynthetic rates per photons absorbed increased in most TLA mutants compared to WT (Figure 6B). Furthermore, we demonstrated that the photosynthetic rate across all lines increased at elevated CO_2, and there was no interaction between increased CO_2 and mutant lines (Figure 6C, D). Significant increases in photosynthesis per photon absorbed in TLA mutants are consistent with the theory that plants overproduce chlorophyll.

4 Discussion

Organisms need to safeguard the ability to capture light, which varies diurnally, changes with weather conditions, and can be blocked by shade produced by other plants (Kirst and Melis, 2018). As a genetically encoded strategy to ensure access to light even under suboptimal conditions, photosynthetic organisms often overproduce light-harvesting machinery. The net result is an overproduction of chlorophyll in leaves (Zhao et al., 2020), and at high light intensities there is wasteful absorption of photons by upper leaves, as they far exceed the capacity of the thylakoid membrane for electron transport and the biochemical rate of the carbon reactions of photosynthesis (Kirst et al., 2017; Kirst and Melis, 2018). The excess photons absorbed by upper leaves are used inefficiently for photosynthesis, with an increased fraction of the absorbed light being dissipated as heat (Demmig-Adams et al., 1996; Baker, 2008). By engineering TLA3 and TLA4 mutants with reduced light-harvesting antenna size and chlorophyll content (resulting in more uniform light distribution within the plant canopy) and higher quantum yield compared to WT

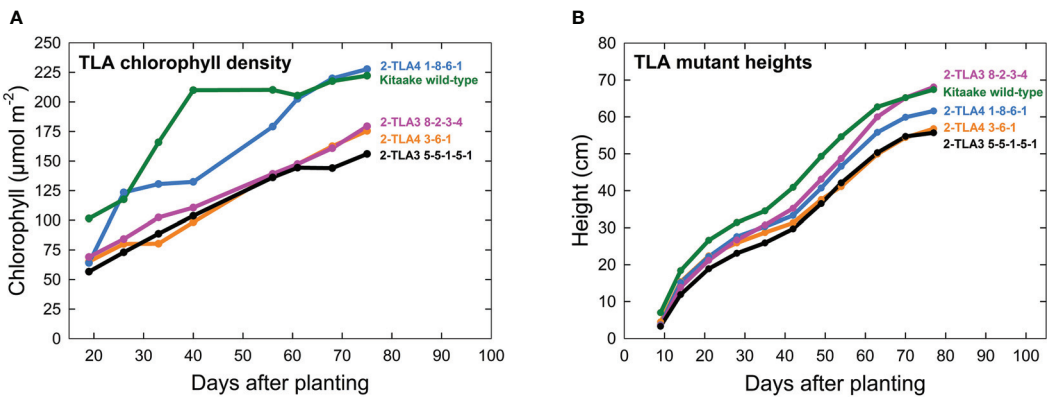

FIGURE 4
TLA mutants have reduced chlorophyll content and height. **(A)** Plots of chlorophyll content, (y-axis) across time (x-axis) for WT and all mutant lines demonstrate that chlorophyll content increases over time for all lines. **(B)** Most mutants are reduced in height compared to the wild-type.

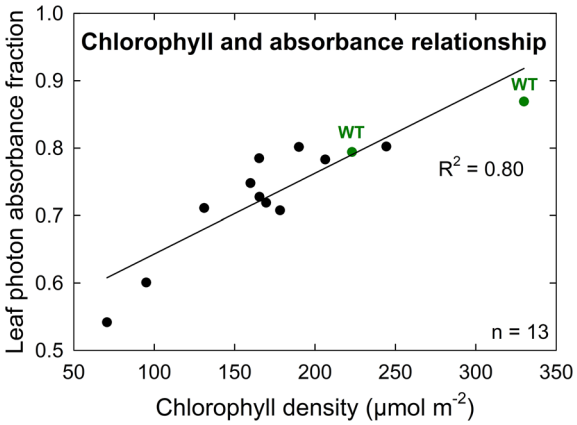

FIGURE 5
Chlorophyll density is positively correlated with leaf photon absorbance fraction among both wild-type (WT, green) and TLA mutant (black) lines. The high correlation (R^2 = 0.80) of this relationship implies similar chlorophyll structures and orientations between TLA mutant and WT lines.

lines, we show that reduced chlorophyll content is a valid method to improve photosynthetic solar energy conversion efficiency on a whole-plant level. This reduction in chlorophyll content helps to reduce the excess absorption of light by the upper canopy, which increases light transmission to lower leaves, improves photochemical efficiency, and reduces the ensuing wasteful non-photochemical dissipation of excitation energy (Kirst et al., 2018).

Reduced chlorophyll content in leaves can lead to an overall reduction in heat dissipation processes, such as nonphotochemical quenching (NPQ), by limiting the amount of excess energy that is received by the photosynthetic reaction center. A failure in these photoprotective processes can lead to overaccumulation of energy, generation of reactive oxygen species (ROS), and damage to the photosynthetic machinery. However, plants that are too deficient in chlorophyll will capture suboptimal amounts of light energy and suffer a growth penalty as a result. In the case of TLA3 and TLA4 mutants, we observed no detrimental effects in plant growth or appearance throughout the lifecycle of the rice, indicating that this potential reduction had a minimal impact on plant health. We also observed no signs of photoinhibition among the lines and therefore did not measure ROS. However, it is possible that the initial decrease in height observed in TLA3 and TLA4 mutants may be due in part to a decrease in NPQ and associated ROS, which has been shown to decrease leaf elongation in maize (Rodríguez et al., 2002).

Previous research indicates that the CpSRP pathway may behave differently among plant species. In Arabidopsis, single mutants in either *CpSRP43* (*chaos*) or *CpSRP54* (*ffc*) do not drastically reduce chlorophyll accumulation. The CpSRP54 mutant *ffc* first produces yellow leaves, but

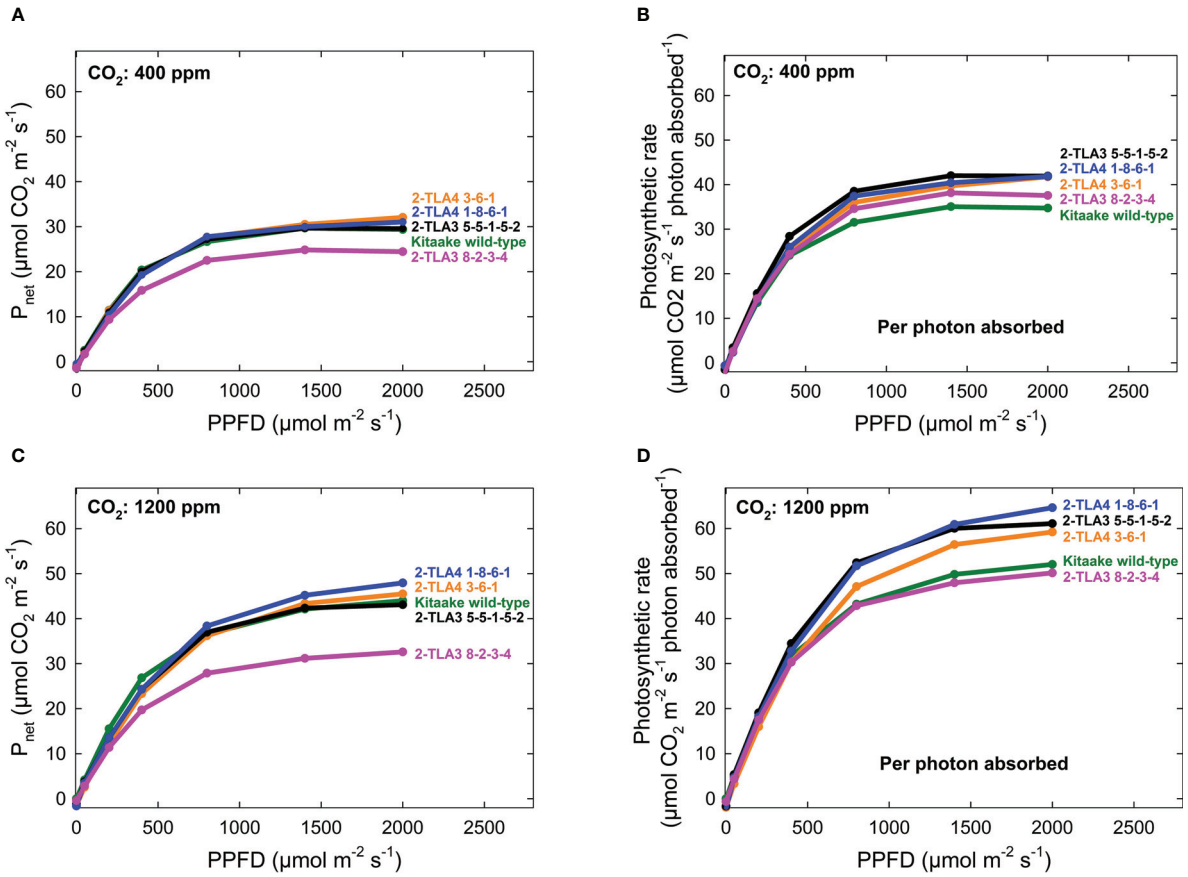

FIGURE 6
Photosynthetic rates in TLA mutants. The photosynthetic rates for mutant lines are increased compared to the Kitaake wild-type (WT) when accounting for the photosynthetic rate per photon absorbed at 400 ppm CO_2 **(A, B)**. The relationship is the same at 1200 ppm CO_2 **(C, D)**. The photosynthetic rate of 2-TLA3 8-2-3-4 (pink) is often less than the photosynthetic rate Kitaake WT (green).

these eventually recover and produce green leaves by maturity (Amin et al., 1999). A double mutant *chaos/ffc* was required to see a significant and lasting reduction of LCHPs (Hutin et al., 2002). In rice, we observed that TLA4 mutants follow this trend, but TLA4L mutants do not. We also observed that although the engineered TLA3 and TLA4 plants increased in chlorophyll content over time, levels did remain lower than WT until plants were 60 days old.

The potential redundancy between components of this pathway may allow for plants to compensate for the loss of individual components, and is alluded to by the apparent increase in *CpSRP54b* expression in plants with mutated *CpSRP54a* (Shi et al., 2020). This putatively-observed compensation may allow plants with reduced chlorophyll synthesis to reach WT levels given sufficient time, and may indicate that the greatest advantages of these mutants in terms of photosynthetic efficiency and light penetration would occur during early growth, when the most significant reductions in chlorophyll content are observed. Future work is needed to further characterize the change in CpSRP pathway function across developmental stages, which remains largely unexplained.

This study, and other recently published work, also suggests that a Poales-specific duplication of *CpSRP54* has allowed for further evolution of this ancient and essential pathway. In bacteria, the SRP pathway requires the conserved SRP54 protein and an SRP RNA component (Ziehe et al., 2017). In higher plants, the CpSRP pathway maintains the CpSRP54 protein, lacks bacterially-required RNA, and contains a novel, chloroplast-specific CpSRP43 (Ziehe et al., 2017). A recent study in rice found that CpSRP54a and CpSRP54b both independently interact with CpSRP43, though their specific functions in this regard are not yet known (Shi et al., 2020). Specifically, this research has shown that while both CpSRP54a and CpSRP54b appear to colocalize with CpSRP43 in the chloroplast, the phenotypes of the two mutants TLA4 and TLA4L and their impact on gene expression of the remaining members of the pathway are distinct. These observed differences in phenotype for TLA4 and TLA4L mutants suggest that the functions of the two proteins do not strictly overlap. Indeed, it has recently been proposed that these two closely related paralogs may be responsible for transporting different chloroplast proteins into the thylakoid (Shi et al., 2020). Our study confirms that mutations in these two proteins have distinct phenotypes when compared within a common genetic background. While initial heights of TLA4 mutants were reduced compared to WT, they approached normal heights during the grain-fill stage, which suggests that impact on grain yield should be minimal. However, TLA4L mutants showed a more drastic reduction in plant height and chlorophyll content than did TLA4 mutants and never recovered to the stature observed for WT individuals. The difference in severity of observed phenotypes is also consistent with the findings of our CpSRP network analysis, which shows a greater number of predicted connections between CpSRP54b and CpSRP43 than between CpSRP54a and CpSRP43, indicating a potentially more integral role for the former. Previous work also corroborates these findings to suggest that CpSRP54b might be more essential for chloroplast development, as single knockout mutants are significantly smaller and were previously thought to be seedling lethal (Shi et al., 2020). The TLA4L plants generated in this study, however, survived beyond the seedling stage, although they remained severely stunted, developmentally delayed, and had poor seed set.

The prior study conducted by Shi et al. (2020) compared an EMS mutation of TLA4 in the cultivar IR64 and a CRISPR mutation in TLA4L in the cultivar Kitaake, preventing a comparison of TLA4 and TLA4L function in an isogenic background, and making the development and analysis of a double mutant challenging. Finally, it is worth noting that our study utilizing CRISPR/Cas9 enabled a direct test of the viability of a TLA4/TLA4L double mutant, which is not feasible by genetic crossing, as the two genes are located at the same genetic locus. In our study, we failed to produce any double TLA4/TLA4L mutants, suggesting that CpSRP54a and CpSRP54b collectively contribute to an indispensable part of plant development. The large number of overlapping functions between these proteins as shown in our CpSRP network analysis substantiates that our lack of double mutants was likely not due to CRISPR/Cas9 methodological challenges but is instead indicative of plant lethality in double mutants. Collectively, the phenotypic differences among TLA mutants in both the present and prior studies suggest that CpSRP genes likely vary in suitability as targets for plant engineering, and that care must be taken in choosing the target to avoid detrimental phenotypes.

In the wild, plants maximize light absorption through synthesis of large light-harvesting antenna, which makes individual plants more competitive by capturing more photons than neighboring plants (Kirst and Melis, 2018). However, in monoculture agriculture this normally beneficial trait leads to decreased light use efficiency and reduced yield potential because the top leaves absorb about 95% of the photons and the remaining leaves are light-starved. In theory, increased light transmission to lower leaves means more equal light distribution among leaves, especially in plants with a planophile (horizontal) leaf architecture, where excessive light absorption by the top-most leaves results in non-uniform light distribution. More uniform distribution of light among leaves should lead to increased canopy photosynthesis and yield. This study demonstrates the potential for this novel yet counterintuitive approach toward crop improvement *via* the knockout of essential genes and paves the way for work in other crop species. Future investigations involve expanding this work to larger scale field studies under multiple planting densities to show community-level improvements.

Data availability statement

The original contributions presented in the study are included in the article/Supplementary Materials. Further inquiries can be directed to the corresponding author.

Author contributions

Conceptualization, DC-D, BB and DC; methodology, DC, NL, SZ, LM; formal analysis, DC, NL; data curation, RK; writing—original draft preparation, DC, DC-D, BB, NL, ME, RK; supervision, DC-D, BB; project administration, DC-D. All authors contributed to the article and approved the submitted version.

Funding

This research was funded by NASA, grant number NNX17AJ31G.

Conflict of interest

The authors declare that the research was conducted in the absence of any commercial or financial relationships that could be construed as a potential conflict of interest.

Publisher's note

All claims expressed in this article are solely those of the authors and do not necessarily represent those of their affiliated organizations, or those of the publisher, the editors and the reviewers. Any product that may be evaluated in this article, or claim that may be made by its manufacturer, is not guaranteed or endorsed by the publisher.

Supplementary material

The Supplementary Material for this article can be found online at: https://www.frontiersin.org/articles/10.3389/fpls.2023.1050483/full#supplementary-material

References

Amin, P., Sy, D. A. C., Pilgrim, M. L., Parry, D. H., Nussaume, L., and Hoffman, N. E. (1999). Arabidopsis mutants lacking the 43- and 54-kilodalton subunits of the chloroplast signal recognition particle have distinct phenotypes. *Plant Physiol.* 121, 61–70. doi: 10.1104/pp.121.1.61

Asakura, Y., Hirohashi, T., Kikuchi, S., Belcher, S., Osborne, E., Yano, S., et al. (2004). Maize mutants lacking chloroplast FtsY exhibit pleiotropic defects in the biogenesis of thylakoid membranes. *Plant Cell* 16, 201–214. doi: 10.1105/tpc.014787

Asakura, Y., Kikuchi, S., and Nakai, M. (2008). Non-identical contributions of two membrane-bound cpSRP components, cpFtsY and Alb3, to thylakoid biogenesis. *Plant J.* 56, 1007–1017. doi: 10.1111/j.1365-313X.2008.03659.x

Baker, N. R. (2008). Chlorophyll fluorescence: A probe of photosynthesis *in vivo*. *Annu. Rev. Plant Biol.* 59, 89–113. doi: 10.1146/annurev.arplant.59.032607.092759

Bugbee, B. (1992). Determining the potential productivity of food crops in controlled environments. *Adv. Space Res.* 12, 85–95. doi: 10.1016/0273-1177(92)90014-O

Chern, M. S., Fitzgerald, H. A., Yadav, R. C., Canlas, P. E., Dong, X., and Roland, P. C. (2001). Evidence for a disease-resistance pathway in rice similar to the *NPR1*-mediated signaling pathway in *Arabidopsis*. *Plant J.* 27(2), 101–113. doi: 10.1046/j.1365-313x.2001.01070.x

Chandrasekar, S., Chartron, J., Jaru-Ampornpan, P., and Shan, S. (2008). Structure of the chloroplast signal recognition particle (SRP) receptor: Domain arrangement modulates SRP–receptor interaction. *J. Mol. Biol.* 375, 425–436. doi: 10.1016/j.jmb.2007.09.061

DeLille, J., Peterson, E. C., Johnson, T., Moore, M., Kight, A., and Henry, R. (2000). A novel precursor recognition element facilitates posttranslational binding to the signal recognition particle in chloroplasts. *Proc. Natl. Acad. Sci.* 97, 1926–1931. doi: 10.1073/pnas.030395197

Demmig-Adams, B., Adams, W. W.III, Barker, D. H., Logan, B. A., Bowling, D. R., and Verhoeven, A. S. (1996). Using chlorophyll fluorescence to assess the fraction of absorbed light allocated to thermal dissipation of excess excitation. *Physiol. Plant* 98, 253–264. doi: 10.1034/j.1399-3054.1996.980206.x

Durrett, T. P., Connolly, E. L., and Rogers, E. E. (2006). Arabidopsis *cpFtsY* mutants exhibit pleiotropic defects including an inability to increase iron deficiency-inducible root Fe(III) chelate reductase activity. *Plant J.* 47, 467–479. doi: 10.1111/j.1365-313X.2006.02803.x

Emanuelsson, O., Nielsen, H., and Heijne, G. V. (1999). ChloroP, a neural network-based method for predicting chloroplast transit peptides and their cleavage sites. *Protein Sci.* 8, 978–984. doi: 10.1110/ps.8.5.978

Gu, J., Zhou, Z., Li, Z., Chen, Y., Wang, Z., and Zhang, H. (2017b). Rice (oryza sativa l.) with reduced chlorophyll content exhibit higher photosynthetic rate and efficiency, improved canopy light distribution, and greater yields than normally pigmented plants. *Field Crops Res.* 200, 58–70. doi: 10.1016/j.fcr.2016.10.008

Gu, J., Zhou, Z., Li, Z., Chen, Y., Wang, Z., Zhang, H., et al. (2017a). Photosynthetic properties and potentials for improvement of photosynthesis in pale green leaf rice under high light conditions. *Front. Plant Sci.* 8. doi: 10.3389/fpls.2017.01082

Hermkes, R., Funke, S., Richter, C., Kuhlmann, J., and Schünemann, D. (2006). The α-helix of the second chromodomain of the 43 kDa subunit of the chloroplast signal recognition particle facilitates binding to the 54 kDa subunit. *FEBS Lett.* 580, 3107–3111. doi: 10.1016/j.febslet.2006.04.055

Hutin, C., Havaux, M., Carde, J., Kloppstech, K., Meiherhoff, K., Hoffman, N., et al. (2002). Double mutation cpSRP43 $^{-}$ /cpSRP54 $^{-}$ is necessary to abolish the cpSRP pathway required for thylakoid targeting of the light-harvesting chlorophyll proteins. *Plant J.* 29, 531–543. doi: 10.1046/j.0960-7412.2001.01211.x

Jacquemoud, S., and Ustin, S. (2019). *Leaf optical properties. 1st ed* (Cambridge, United Kingdom:Cambridge University Press). . doi: 10.1017/9781108686457

Jonas-Straube, E., Hutin, C., Hoffman, N. E., and Schünemann, D. (2001). Functional analysis of the protein-interacting domains of chloroplast SRP43. *J. Biol. Chem.* 276, 24654–24660. doi: 10.1074/jbc.M100153200

Kirst, H., Formighieri, C., and Melis, A. (2014). Maximizing photosynthetic efficiency and culture productivity in cyanobacteria upon minimizing the phycobilisome light-harvesting antenna size. *Biochim. Biophys. Acta BBA - Bioenerg.* 1837, 1653–1664. doi: 10.1016/j.bbabio.2014.07.009

Kirst, H., Gabilly, S. T., Niyogi, K. K., Lemaux, P. G., and Melis, A. (2017). Photosynthetic antenna engineering to improve crop yields. *Planta* 245, 1009–1020. doi: 10.1007/s00425-017-2659-y

Kirst, H., and Melis, A. (2018). "Improving photosynthetic solar energy conversion efficiency: the truncated light-harvesting antenna (TLA) concept," in *Comprehensive series in photochemical & photobiological sciences*. Eds. M. Seibert and G. Torzillo (Cambridge: Royal Society of Chemistry), 335–354. doi: 10.1039/9781849737128-00335

Kirst, H., Shen, Y., Vamvaka, E., Betterle, N., Xu, D., Warek, U., et al. (2018). Downregulation of the CpSRP43 gene expression confers a truncated light-harvesting antenna (TLA) and enhances biomass and leaf-to-stem ratio in *Nicotiana tabacum* canopies. *Planta* 248, 139–154. doi: 10.1007/s00425-018-2889-7

Klenell, M., Morita, S., Tiemblo-Olmo, M., Mühlenbock, P., Karpinski, S., and Karpinska, B. (2005). Involvement of the chloroplast signal recognition particle cpSRP43 in acclimation to conditions promoting photooxidative stress in arabidopsis. *Plant Cell Physiol.* 46, 118–129. doi: 10.1093/pcp/pci010

Klimyuk, V. I., Persello-Cartieaux, F., Havaux, M., Contard-David, P., Schuenemann, D., Meiherhoff, K., et al. (1999). A chromodomain protein encoded by the arabidopsis *CAO* gene is a plant-specific component of the chloroplast signal recognition particle pathway that is involved in LHCP targeting. *Plant Cell* 11, 87–99. doi: 10.1105/tpc.11.1.87

Kogata, N., Nishio, K., Hirohashi, T., Kikuchi, S., and Nakai, M. (1999). Involvement of a chloroplast homologue of the signal recognition particle receptor protein, FtsY, in protein targeting to thylakoids. *FEBS Lett.* 447, 329–333. doi: 10.1016/s0014-5793(99)00305-1

Lee, T., Oh, T., Yang, S., Shin, J., Hwang, S., Kim, C. Y., et al. (2015). RiceNet v2: An improved network prioritization server for rice genes. *Nucleic Acids Res.* 43, W122–W127. doi: 10.1093/nar/gkv253

Li, X., Henry, R., Yuan, J., Cline, K., and Hoffman, N. E. (1995). A chloroplast homologue of the signal recognition particle subunit SRP54 is involved in the posttranslational integration of a protein into thylakoid membranes. *Proc. Natl. Acad. Sci. U. S. A.* 92, 3789–3793. doi: 10.1073/pnas.92.9.3789

Liu, S., Deng, L., Fu, Y., Hu, G., Liu, W., and Zhao, X. (2016). Identification and characterization of the yls mutation in rice (*Oryza sativa* l.) with lower photosynthetic pigment content. *Czech J. Genet. Plant Breed.* 52, 101–107. doi: 10.17221/42/2016-CJGPB

Lowder, L. G., Zhang, D., Baltes, N. J., Paul, J. W., Tang, X., Zheng, X., et al. (2015). A CRISPR/Cas9 toolbox for multiplexed plant genome editing and transcriptional regulation. *Plant Physiol.* 169, 971–985. doi: 10.1104/pp.15.00636

Lv, X., Shi, Y., Xu, X., Wei, Y., Wang, H., Zhang, X., et al. (2015). *Oryza sativa* chloroplast signal recognition particle 43 (OscpSRP43) is required for chloroplast development and photosynthesis. *PloS One* 10, e0143249. doi: 10.1371/journal.pone.0143249

Moore, M., Goforth, R. L., Mori, H., and Henry, R. (2003). Functional interaction of chloroplast SRP/FtsY with the ALB3 translocase in thylakoids. *J. Cell Biol.* 162, 1245–1254. doi: 10.1083/jcb.200307067

Moore, M., Harrison, M. S., Peterson, E. C., and Henry, R. (2000). Chloroplast Oxa1p homolog albino3 is required for post-translational integration of the light harvesting chlorophyll-binding protein into thylakoid membranes. *J. Biol. Chem.* 275, 1529–1532. doi: 10.1074/jbc.275.3.1529

Nakajima, Y., Tsuzuki, M., and Ueda, R. (2001). Improved productivity by reduction of the content of light-harvesting pigment in *Chlamydomonas perigranulata*. *J. Appl. Phycol.* 13, 95–101. doi: 10.1023/A:1011192832502

Nakajima, Y., and Ueda, R. (1997). Improvement of photosynthesis in dense microalgal suspension by reduction of light harvesting pigments. *Hydrobiologia* 9, 503–510. doi: 10.1023/A:1007920025419

Parry, C., and Bugbee, B. (2017). Reduced root-zone phosphorus concentration decreases iron chlorosis in maize in soilless substrates. *HortTechnology* 27, 490–493. doi: 10.21273/HORTTECH03735-17

Payan, L. A., and Cline, K. (1991). A stromal protein factor maintains the solubility and insertion competence of an imported thylakoid membrane protein. *J. Cell Biol.* 112, 603–613. doi: 10.1083/jcb.112.4.603

Rodríguez, A. A., Grunberg, K. A., and Taleisnik, E. L. (2002). Reactive oxygen species in the elongation zone of maize leaves are necessary for leaf extension. *Plant Physiol.* 129, 1627–1632. doi: 10.1104/pp.001222

Schuenemann, D., Gupta, S., Persello-Cartieaux, F., Klimyuk, V. I., Jones, J. D., Nussaume, L., et al. (1998). A novel signal recognition particle targets light-harvesting proteins to the thylakoid membranes. *Proc. Natl. Acad. Sci. U. S. A.* 95, 10312–10316. doi: 10.1073/pnas.95.17.10312

Shi, Y., He, Y., Lv, X., Wei, Y., Zhang, X., Xu, X., et al. (2020). Chloroplast SRP54s are essential for chloroplast development in rice. *Rice* 13, 54. doi: 10.1186/s12284-020-00415-2

Stengel, K. F., Holdermann, I., Wild, K., and Sinning, I. (2007). The structure of the chloroplast signal recognition particle (SRP) receptor reveals mechanistic details of SRP GTPase activation and a conserved membrane targeting site. *FEBS Lett.* 581, 5671–5676. doi: 10.1016/j.febslet.2007.11.024

Tu, C. J., Peterson, E. C., Henry, R., and Hoffman, N. E. (2000). The L18 domain of light-harvesting chlorophyll proteins binds to chloroplast signal recognition particle 43. *J. Biol. Chem.* 275, 13187–13190. doi: 10.1074/jbc.c000108200

Tu, C.-J., Schuenemann, D., and Hoffman, N. E. (1999). Chloroplast FtsY, chloroplast signal recognition particle, and GTP are required to reconstitute the soluble phase of light-harvesting chlorophyll protein transport into thylakoid membranes. *J. Biol. Chem.* 274, 27219–27224. doi: 10.1074/jbc.274.38.27219

Tzvetkova-Chevolleau, T., Hutin, C., Noël, L. D., Goforth, R., Carde, J.-P., Caffarri, S., et al. (2007). Canonical signal recognition particle components can be bypassed for posttranslational protein targeting in chloroplasts. *Plant Cell* 19, 1635–1648. doi: 10.1105/tpc.106.048959

Walter, B., Pieta, T., and Schünemann, D. (2015). *Arabidopsis thaliana* mutants lacking cpFtsY or cpSRP54 exhibit different defects in photosystem II repair. *Front. Plant Sci.* 6. doi: 10.3389/fpls.2015.00250

Wang, Z., Zhang, T., Xing, Y., Zeng, X., Wang, L., Liu, Z., et al. (2016). YGL9, encoding the putative chloroplast signal recognition particle 43 kDa protein in rice, is involved in chloroplast development. *J. Integr. Agric.* 15, 944–953. doi: 10.1016/S2095-3119(15)61310-7

Wellburn, A. R. (1994). The spectral determination of chlorophylls a and b, as well as total carotenoids, using various solvents with spectrophotometers of different resolution. *J. Plant Physiol.* 144, 307–313. doi: 10.1016/S0176-1617(11)81192-2

Ye, J., Yang, Y., Wei, X., Niu, X., Wang, S., Xu, Q., et al. (2018). PGL3 is required for chlorophyll synthesis and impacts leaf senescence in rice. *J. Zhejiang Univ.-Sci. B* 19, 263–273. doi: 10.1631/jzus.B1700337

Yuan, J., Kight, A., Goforth, R. L., Moore, M., Peterson, E. C., Sakon, J., et al. (2002). ATP stimulates signal recognition particle (SRP)/FtsY-supported protein integration in chloroplasts. *J. Biol. Chem.* 277, 32400–32404. doi: 10.1074/jbc.M206192200

Zhang, F., Luo, X., Hu, B., Wan, Y., and Xie, J. (2013). YGL138(t), encoding a putative signal recognition particle 54 kDa protein, is involved in chloroplast development of rice. *Rice* 6, 7. doi: 10.1186/1939-8433-6-7

Zhao, X., Jia, T., and Hu, X. (2020). HCAR is a limitation factor for chlorophyll cycle and chlorophyll b degradation in chlorophyll-b-overproducing plants. *Biomolecules* 10, 1639. doi: 10.3390/biom10121639

Zhen, S., and Bugbee, B. (2020). Substituting far-red for traditionally defined photosynthetic photons results in equal canopy quantum yield for CO2 fixation and increased photon capture during long-term studies: Implications for re-defining PAR. *Front. Plant Sci.* 11. doi: 10.3389/fpls.2020.581156

Ziehe, D., Dünschede, B., and Schünemann, D. (2017). From bacteria to chloroplasts: evolution of the chloroplast SRP system. *Biol. Chem.* 398, 653–661. doi: 10.1515/hsz-2016-0292

frontiers | Frontiers in Plant Science

TYPE Original Research
PUBLISHED 04 September 2023
DOI 10.3389/fpls.2023.1261174

OPEN ACCESS

EDITED BY
Jose R Peralta-Videa,
The University of Texas at El Paso,
United States

REVIEWED BY
Yuqing Ye,
Rice University, United States
Nubia Zuverza,
Connecticut Agricultural Experiment
Station, United States

*CORRESPONDENCE
Fabiano Guimarães Silva
fabiano.silva@ifgoiano.edu.br
Ana Helena Januário
ana.januario@unifran.edu.br

RECEIVED 19 July 2023
ACCEPTED 14 August 2023
PUBLISHED 04 September 2023

CITATION
Lima IHA, Rodrigues AA, Resende EC, da Silva FB, Farnese FS, Silva LJ, Rosa M, Reis MNO, Bessa LA, de Oliveira TC, Januário AH and Silva FG (2023) Light means power: harnessing light spectrum and UV-B to enhance photosynthesis and rutin levels in microtomato plants.
Front. Plant Sci. 14:1261174.
doi: 10.3389/fpls.2023.1261174

Light means power: harnessing light spectrum and UV-B to enhance photosynthesis and rutin levels in microtomato plants

Iury Henrique Almeida Lima[1], Arthur Almeida Rodrigues[1], Erika Crispim Resende[2], Fábia Barbosa da Silva[1], Fernanda dos Santos Farnese[3], Lucas de Jesus Silva[1], Márcio Rosa[4], Mateus Neri Oliveira Reis[5], Layara Alexandre Bessa[5], Thales Caetano de Oliveira[1], Ana Helena Januário[6]* and Fabiano Guimarães Silva[1]*

[1]Laboratory of Advanced Studies in Vertical Agriculture, Goiano Federal Institute of Education, Science and Technology, Rio Verde, Brazil, [2]Department of Biomolecules, Goiano Federal Institute of Education, Science and Technology, Iporá, Brazil, [3]Laboratory of Plant Physiology, Goiano Federal Institute of Education, Science and Technology, Rio Verde, Brazil, [4]PostGraduate Program in Plant Production, University of Rio Verde, Rio Verde, Brazil, [5]Biodiversity Metabolism and Genetics Laboratory, Goiano Federal Institute of Education, Science and Technology, Rio Verde, Brazil, [6]Research Center for Exact and Technological Sciences, Franca University, Franca, Brazil

Urban vertical agriculture with lighting system can be an alternative green infrastructure to increase local food production irrespective of environmental and soil conditions. In this system, light quality control can improve the plant physiological performance, well as induce metabolic pathways that contribute to producing phenolic compounds important to human health. Therefore, this study aimed to evaluate the influence of RBW (red, blue and white) and monochromatic (red and blue; R and B, respectively) light associated or not with UV-B on photosynthetic performance and phenolic compound production in microtomato fruits cultivated via vertical agriculture. The experimental design adopted was completely randomized, with six replicates illuminated with 300 $\mu mol \cdot m^{-2} \cdot s^{-1}$ light intensities (RBW, RBW + UV, B, B + UV, R, and R + UV), 12 h photoperiod, and 3.7 $W \cdot m^{-2}$ UV-B irradiation for 1 h daily for the physiological evaluations. Twenty-six days after the installation, gas exchange, chlorophyll a fluorescence and nocturnal breathing were evaluated. Fruits in different ripening stages (green, orange, and red) were collected from microtomato plants grown under with different light qualities, to evaluate the physiological performance. The identification and quantification of the phenolic compound rutin was also performed to investigate their metabolic response. This study identified that plants grown under B + UV had high photosynthetic rates (A=11.57 $\mu mol \cdot m^{-2} \cdot s^{-1}$) and the fruits at all maturation stages from plants grown under B and B + UV had high rutin content. Meanwhile, the activation of suppressive mechanisms was necessary in plants grown under R because of the high nocturnal respiration and

unregulated quantum yield of the non-photochemical dissipation of the photosystem II. These results highlight the importance of selecting light wavelength for vegetable cultivation to produce fruits with a high content of specialized metabolites that influence color, flavor, and health promotion, which is of special interest to farmers using sustainable cropping systems.

KEYWORDS

flavonoids, LEDs, tomato, rutin, vertical agriculture, *Solanum lycopersicum*

Introduction

Specialized metabolites, traditionally referred to as secondary metabolites, are compounds present in some natural sources that benefit both survival and reproduction in different environments. These molecules are derived from the primary metabolism, and plants synthesize approximately 200,000 to 1 million such compounds (Garagounis et al., 2021). Phenolic compounds, particularly phenolic acids and flavonoids are a class of compounds of interest due to their high antioxidant capacity that modulates and/or regulates oxidative stress (Ribeiro et al., 2019; Shih and Morgan, 2020). Rutin, a glycoside flavonoid widely distributed in the plant kingdom, is a natural molecule of great interest due to its pharmacological activities and used for treating varicose veins, internal bleeding, and hemorrhoids. It also has antioxidant, anti-inflammatory, antidiabetic, and cardioprotective activities (Semwal et al., 2021).

Elicitors have been a promising strategy to increase bioactive compound production. Light is one of the most studied factors; thus, information is available for several plant species grown under different wavelengths (Liu et al., 2019). Besides being a key factor in regulating growth and development, light also acts as an environmental signal that triggers the production of specific molecules in response to the environment and influences plant development stage (Silva et al., 2020). Wavelength differences are perceived due to the action of several photoreceptors, such as phytochromes (that absorb red and far-red light), cryptochromes, and phototropins (that absorb blue and UV-A light), and UVR8 (that absorbs UV-B light) (Wang et al., 2020). Light also strongly affects the biosynthesis and accumulation of several secondary metabolites in plants, which is related to both increased photosynthesis that generates more carbon skeletons for plant metabolism, including secondary metabolism, and the action of photoreceptors that can perceive photons and trigger signaling pathways, which in turn change gene expression levels. Thus, light condition modulation can stimulate both growth and production of specific compounds of interest (Silva et al., 2020; Thoma et al., 2020). Several studies confirm that photosynthesis can be modulated, and secondary metabolite synthesis is enhanced in species grown under light-emitting diodes (LEDs), particularly when monochromatic blue or red lights are used instead of white light. The individual effects of each wavelength vary depending on the species studied and their growing conditions (Wu et al., 2007; Li and Kubota, 2009; Johkan et al., 2010; Bian et al., 2015; Lobiuc et al., 2017).

Ultraviolet radiation also induces bioactive compound synthesis, since it induces the synthesis of flavonoids and phenolic compounds, which work both as antioxidants and defense molecules for plants (Neugart and Schreiner, 2018). UV-B doses can be manipulated to control secondary metabolite production and plant performance; for example, plants can initially be grown under optimal conditions until they reach a certain degree of development, and then be subjected to UV-B treatment to produce the compounds of interest, thus reducing the morphological impacts of UV-B (Mosadegh et al., 2018). Suzuki et al. (2005) observed a 122% increase in rutin content in UV-B irradiated buckwheat. Moreover, the rutin content also increased in lettuce grown under continuous blue light (Naoya Fukuda et al., 2022). However, high levels of UV-B can be deleterious to plants and are able to influence growth and development, as well as alter genetic, physiological and biochemical aspects, leading to damage to photosynthetic machinery and compromising the photosynthetic rate, triggering photoinhibition and photoprotection responses (Nocchi et al., 2020).

Controlled growing environments mainly circumvent the light-related issues since multiple factors can be controlled. Thus, LEDs can be used because they efficiently convert electrical energy into light energy in addition to having a narrow and specific emission band (Zou et al., 2020). Their use in plant cultivation and the number of studies on the most suitable wavelengths have increased (Thwe et al., 2014; Kim et al., 2015; Ko et al., 2015; Liu et al., 2016; Kim et al., 2018; Liu et al., 2018; Taulavuori et al., 2016; Nam et al., 2018; Taulavuori et al., 2018). Additionally, this protected cultivation environment also circumvents the effects of current climate change scenarios that are expected to worsen in the coming decades, considering that the frequency of natural disasters such as droughts and storms has increased (Fang et al., 2020). It is already well established that blue (425-490 nm) and red (610-700 nm) light are the best spectral qualities for promoting the photosynthetic process of plants (Shafiq et al., 2021). The light environment includes the intensity, quality, and direction of light, with light intensity being the key factor for plant growth (Pan et al., 2020). High light intensities can lead to increased thickness and reduction in leaf area to avoid damage caused by excess light (Matos et al., 2009). Yasar & Uzal (2023) investigated the effect of increased

light intensity on tomato plants grown under LED lights with a spectrum similar to the sun and concluded that high intensities can be beneficial, but only if they are within the tolerable limits of the species, since thus the antioxidant system is able to reduce or eliminate the harmful effects of reactive oxygen species (ROS) generated under stress conditions, like that of excess light. For the microtomato, Ke et al. (2022) and Ke et al. (2023) found that 300 $\mu mol.m^{-2}.s^{-1}$ is the appropriate intensity for both the vegetative and reproductive stages, favoring plant growth and increase in fruit biomass. High luminous intensity (700 $\mu mol.m^{-2}.s^{-1}$) led to reduced chlorophyll content and reduced photosynthetic capacity.

Tomato (*Solanum lycopersicum* L.), one of the most consumed vegetables worldwide (>180 million ton being produced yearly), is one of the many crops that can be favored by a controlled environment using LEDs. Its cultivation has become highly effective due to the development of new varieties from breeding programs initiated in the 20th century and the introduction of advanced cultivation technologies (Mata-Nicolás et al., 2020). The main agricultural challenge in the last 20 years has been to produce sufficient nutritious food for a growing population and, at the same time, meet the requirements of sustainable cultivation, thereby reducing environmental impacts (Ronga et al., 2020).

Although rutin is found in many species, few plants are known as major rutin sources (Kianersi et al., 2020). Its concentration increases in UVB-irradiated plants, which reinforces its protective role against UV-B (Chua, 2013). Thus, investigating strategies to increase the production of compounds of interest, such as rutin, is essential to produce nutraceutical foods that will contribute to human health.

In this scenario, we hypothesize that different light wavelengths promote contrasting responses in the production of secondary metabolites such as rutin, the associated use of UV-B light may enhance the secondary metabolite production by increasing plant stress, and using different light wavelengths and UV-B promotes different physiological responses in plants. Thus, this study aimed to evaluate the influence of RBW and monochromatic wavelengths associated with UV-B on the photosynthetic performance and phenolic compound production in microtomato fruits grown in vertical farming.

Materials and methods

Plant material and growing conditions

The experiment was conducted at the Plant Biotechnology Laboratory Complex of the Goiano Federal Institute/Rio Verde campus (17°48′10.9″S, 50°54′21.8″W, 755 m altitude). Initially, Micro-Tom (MT) wild type microtomato (MTwt) cultivar seeds were sown in trays containing Bioplant Plus® substrate (BioPlant Agrícola Ltd., Nova Ponte, Brazil) and germinated for 15 days. The seedlings were transplanted to 350 cm^3 pots containing the same substrate, supplemented with 0.5 g 4:14:8 NPK, and grown until 39 days in a greenhouse under controlled irradiance, temperature (approximately 25°C), and relative humidity (approximately 60%).

Then, the plants were transferred to an indoor vertical farming system at 50 ± 5% relative humidity and 25 ± 2°C (the room was cooled with air conditioning, to ensure constant temperature and humidity. In addition, the environments with the microtomato plants presented a thermohygrometer for constant monitoring of these variables) in insulated 1.00×0.75 m^2 vertical boxes with adjustable height and illuminated with LEDs (SG4 – SpectraGrow). Each booth was separated by an expanded polystyrene board (Styrofoam®). The plants were exposed to 300 $\mu mol \cdot m^{-2} \cdot s^{-1}$ broad spectrum control LEDs [RBW light (RBW) and RBW + UV-B (RBWUV)], 480 nm blue light (B), blue light + UV-B (BUV), 660 nm red light (R), and red light + UV-B (RUV) for 40 days at constant light intensity, creating approximately 12.96 $mol \cdot m^{-2} \cdot d^{-1}$ daily light integral (DLI) and 12 h photoperiod (7:00 AM to 7:00 PM). UV-B light (UV-B Broadband lamp – Philips) was administered daily from 11:00 AM to 12:00 PM (mean intensity: 3.7 $W \cdot m^{-2}$).

The experiment was conducted in an entirely randomized design, with six light qualities and six repetitions. The physiological parameters were evaluated using the leaves 26 days after exposure, considering that most fruits were at their full size. The fruits were collected for rutin content analysis at each growing condition, according to the ripeness level as green, orange, and red.

Gas exchange and chlorophyll a fluorescence

Gas exchanges were evaluated to record the photosynthesis rate (A, $\mu mol \cdot m^{-2} \cdot s^{-1}$), transpiration rate (E, $mmol \cdot m^{-2} \cdot s^{-1}$), stomatal conductance (gs, mol $H_2O \cdot m^{-2} \cdot s^{-1}$), internal CO_2 concentration (Ci), and nocturnal respiration rate (Rn, $\mu mol\ CO_2 \cdot m^{-2} \cdot s^{-1}$). These data were used to calculate the water use efficiency (WUE = A/E). Measurements were made using a LI-6800 XT portable gas exchange meter (IRGA, Li-Cor Inc., Nebraska, USA) between 08:00 AM and 11:00 AM on a fully expanded leaf at 25°C, 1000 $\mu mol \cdot m^{-2} \cdot s^{-1}$ artificial photosynthetically active radiation (PAR), approximately 400 $\mu mol \cdot mol^{-1}$ atmospheric CO_2 concentration (Ca), and approximately 65% relative humidity.

Chlorophyll a fluorescence was evaluated on the same leaf in which gas exchange was measured using an IRGA. The fluorescence obtained was the effective quantum yield of photochemical energy conversion in photosystem II (FSII) (YII = (Fm′–F)/Fm′). The quantum yields of regulated energy dissipation (YNPQ = (F/Fm′)–(F/Fm)), and unregulated energy dissipation (YNO = F/Fm), were calculated according to the protocols reported by Genty et al. (1989) and Hendrickson et al. (2004), respectively. The ΔF/Fm′ was further used to estimate the apparent electron transport rate (ETR = ΔF/Fm′ $PAR.Leaf_{ABS}$.0.5) (Bilger et al., 1995), where PAR is the photon flux density ($\mu mol \cdot m^{-2} \cdot s^{-1}$) incident on the leaf; $Leaf_{ABS}$ corresponds to the incident light fraction absorbed by the leaves; and 0.5 is the excitation energy fraction distributed to the FSII (Laisk and Loreto, 1996). The apparent electron transport rate to CO_2 assimilation (ETR/A) rate was calculated to estimate photosynthesis at risk of oxidative stress (Geissler et al., 2015).

Chloroplast pigment index

Chlorophyll a, b, and total indices were obtained using a CLOROFILOG chlorophyll meter (CFL; Falker 1030, Porto

Alegre, Brazil) on a fully expanded leaf, in triplicate. Rutin content analysis

Chromatographic conditions

Chromatographic analyses were performed on a Shimadzu® high efficiency liquid chromatograph with SPD-M20A photodiode detector and Zorbax Eclipse Plus C18 analytical column (250×4.6 mm², 5 µm; Agilent®) coupled to Zorbax Eclipse Plus C18 pre-column (12.5×4.6 mm², 5 µm; Agilent®). The chromatographic conditions were: 10 µL injection volume, 30°C oven temperature, 200–400 nm scanning range, and monitored readings at 254 nm. The mobile phase was eluted at 1.0 mL·min^{-1} flow rate, with phase A comprising 0.1% acetic acid UV/HPLC/spectroscopic grade (Proquimios®) and mobile phase B comprising HPLC-grade methanol (J.T. Baker®). The elution gradient of mobile phase B increased from 10 to 66% over 32 min, decreased from 66 to 10% in 3 min, and remained isocratic at 10% for 5 min; thus, the total run time was 40 min. The mobile phase with acidified water was filtered using a vacuum mobile filtration system (Restek) with a cellulose filter membrane (47 mm × 0.45 µm, Whatman®). The HPLC-grade methanol was filtered through a polytetrafluoroethylene (PTFE) membrane (47 mm × 0.45 µm, Whatman®).

Analytical curves and sample preparation

The rutin standard (standard bank of the Natural Products Group of the Franca University) was serially diluted to 100, 50, 25, 12.5, 6.25, and 3.125 µg·mL^{-1} using HPLC-grade methanol to construct calibration curves. The resulting solutions were injected in triplicate into the chromatograph. Calibration curves were constructed by plotting the standard chromatographic peak areas versus concentrations in the Microsoft® Excel® software for Microsoft 365 version 2010 for Windows®. Linearity was verified by the coefficient of determination (R^2) and the correlation coefficient (r), which should be above 0.99 according to RDC No. 166/2017 (BRASIL, 2017), with relative standard deviation (RSD) lower than 5%. The resulting equations for each curve were estimated by the least squares method (LSM).

Methanolic extracts were prepared by suspending approximately 0.1 g freeze-dried microtomato in 2 mL HPLC-grade methanol in an ultrasonic bath (Saners Medical, Sonic Clean 2PS) for 30 min. The supernatant was transferred to a 3.0 mL syringe and directly filtered using a syringe containing a Nylon filter (13 mm diameter; 0.45 µm pore diameter; Analítica®). Then, 10 µL sample extracts were injected in duplicate in the high-performance liquid chromatograph. The compounds were detected by comparing with the standard retention peak periods and the resulting spectra and quantified through the peak areas and equations obtained from respective analytical curves.

Statistical analyses

The data obtained were analyzed by the Shapiro–Wilk and Komolgorov–Smirnov tests for normality, and then the homogeneity of variance was verified by the Levene test. These were the necessary assumptions for analysis of variance. These tests showed that the assumptions were not met. Thus, the non-parametric Kruskal–Wallis test was followed by the Dunn (1964) test for multiple comparisons, with methods to control a false discovery rate (FDR) (Benjamini & Hochberg, 1995). The test considered a significance level α equal to 5%. The R statistical software version 4.3.0 (R Core Team, 2023) was used for statistical analyses using the "FSA" (Ogle et al., 2020), "PMCMRplus" (Pohlert, 2018), and "ggplot2" (Wickham, 2011) packages.

Results

The MT life cycle is accelerated compared to that of conventional tomatoes, since the fruits begin to develop at 39 days and many fruits begin to ripen at 65 days. MT plants were sensitive to R, which was intensified under RUV; thus, evaluating their physiological characteristics were difficult.

Different wavelength lights with and without UV-B modify the chloroplast pigment index

Microtomato plants grown under RBW had higher chlorophyll a, b, and total chlorophyll index (Figures 1A–C), compared to plants grown under B.

Different wavelength lights with and without UV-B change the light energy used for photosynthesis

Chlorophyll a fluorescence was measured to estimate the proportion of light used in photosynthetic processes and its regulatory mechanisms. The maximum FSII quantum yield (Fv/Fm) was low in plants grown under R (Figure 2A), indicating sensitivity to light source. However, the plants exposed to BUV and R had lower YII (Figure 2B), photochemical quenching (qP, Figure 2C), and ETR (Figure 2D) than those grown under RBWUV. No difference was observed in quantum yield of regulated energy dissipation (Figure 2E). In response to a low YII, qP, and ETR, plants mainly grown under R showed non-regulated energy dissipation (Figure 2F), while the lowest values were evident under B.

Different wavelength lights with and without UV-B affect gas exchange

Gas exchange variables showed that plants grown under BUV maintained gs (Figure 3A), resulting in high A (Figure 3B) and E (Figure 3C). Plants grown under RBWUV showed lower Ci than plants grown under BUV (Figure 3D). In turn, the increased ETR/A (Figure 3E) in plants grown under RBWUV may indicate oxidative stress risk.

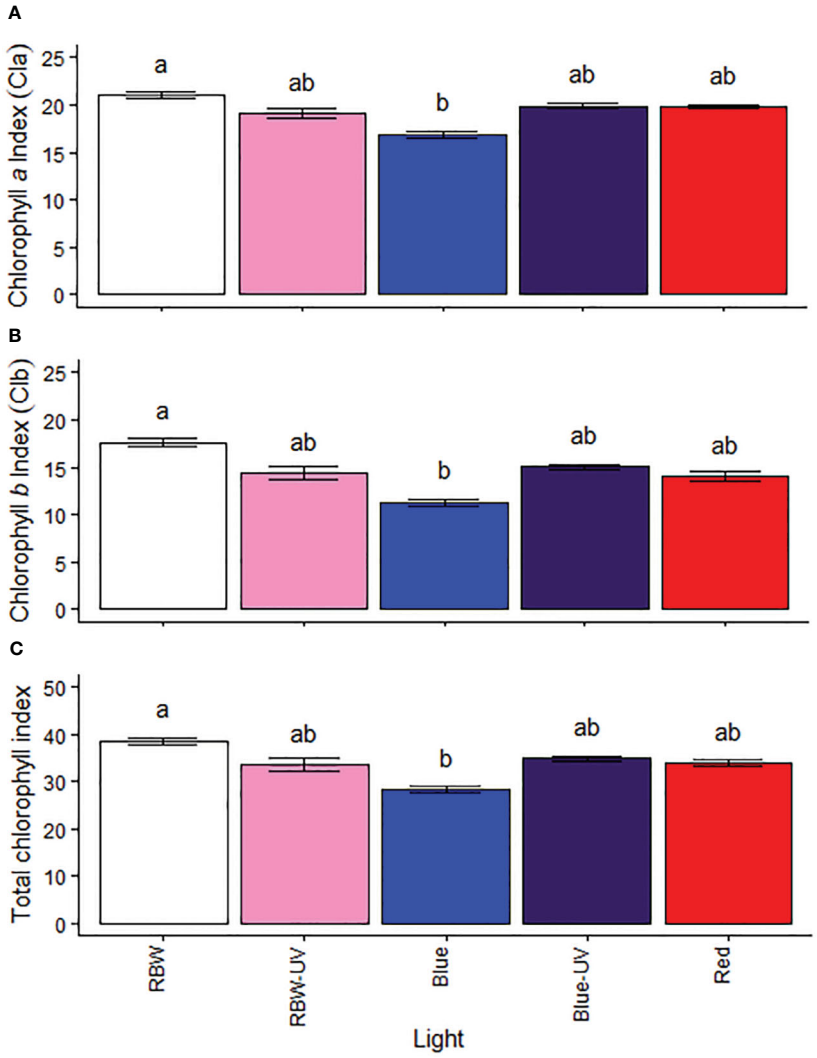

FIGURE 1
(A) Chlorophyll a, **(B)** chlorophyll b, and **(C)** total chlorophyll indexes of microtomato plants after cultivating for 26 days under different light sources with or without UV-B radiation. Means followed by the same letter do not differ by the Dunn's test at 5% probability.

Nocturnal respiration rate changes under monochromatic red light

Rn and Rn/A were higher in the plants grown under R, while they were the lowest in the plants grown under BUV (Figures 4A, B).

Principal component analysis of the physiological variables evaluated

The first two dimensions of the principal components (DIM1 and DIM2) together explained 80.3% (DIM1 47.9% and DIM2 32.4%) data variation (Figures 5A, B). DIM1 variation was mainly explained by the high influence of BUV on the variables A, gs, and E. W influenced chloroplast pigments (Chla, Chlb, and total chlorophyll). B had the greatest influence on the variables F0, ETR, qP, and YII with DIM2. R directly influenced unregulated energy dissipation and negatively influenced Rn (Figure 4A). No variables were influenced by RBWUV. The representation quality of the variable performance (cos^2, Figure 5B) show that A, gs, E, YII, ETR, qP, Ci, F0, and Chla were well-represented in DIM1 and DIM2. B and BUV were the most dominant contributors (Figure 5C). A high percentage of contribution (Figure 5D) was observed, while Chla, total chlorophyll, YNO, Chlb, YNPQ, and Rn had a low representation (Figure 5B).

Monochromatic blue light and UV-B radiation improve rutin levels in MT fruit

Rutin content was evaluated in green, orange, and red (ripe) MT fruits, except those grown under RUV, due to plant death. In the chromatographic analyzes for the quantification of rutin (RT = 26.9 min e λ_{Max} = 255 e 355 nm), the response of the UV detector at 255 nm was linear from 3,125-100 μg,mL^{-1}. The obtained regression

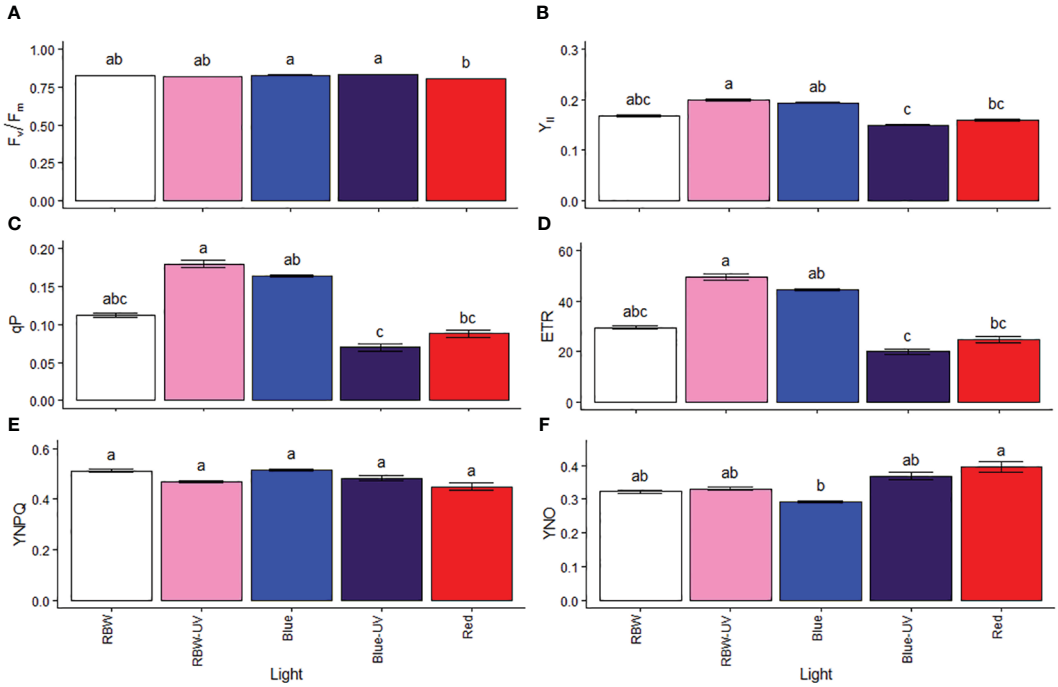

FIGURE 2
(A) Potential quantum yield of photosystem II (Fv/Fm), **(B)** effective quantum yield of photosystem II (YII), **(C)** photochemical quenching (qP), electron transport rate (ETR), quantum yield of regulated energy dissipation (YNPQ), and quantum yield of non-regulated energy dissipation (YNO) in microtomato plants after cultivating for 26 days under different light sources with or without UV-B radiation. Means followed by the same letter do not differ by Dunn's test at 5% probability.

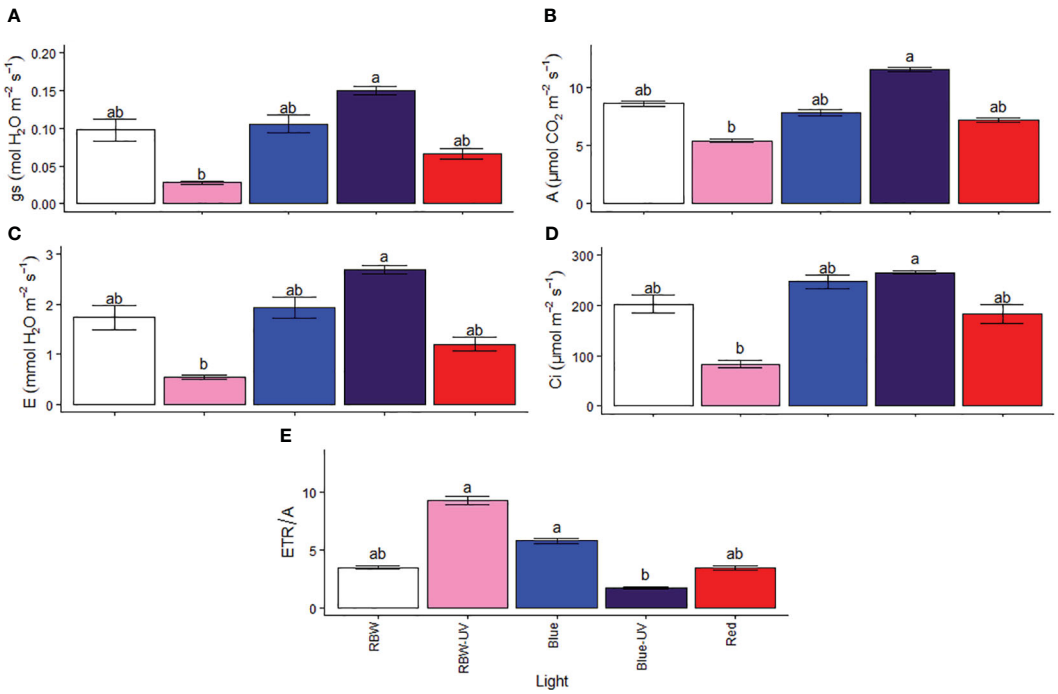

FIGURE 3
(A) Stomatal conductance (gs), **(B)** photosynthetic rate **(A)**, **(C)** transpiration rate **(E)**, **(D)** internal CO_2 concentration (Ci), and **(E)** electron transport to photosynthetic ratio (ETR/A) for microtomato plants after cultivating for 26 days under different light sources with or without UV-B radiation. Means followed by the same letter do not differ by the Dunn's test at 5% probability.

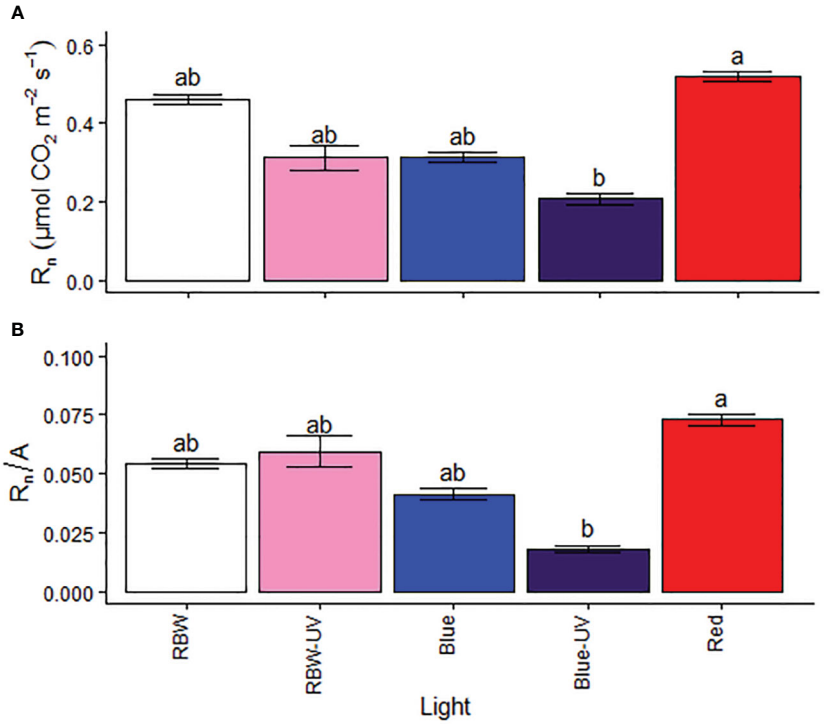

FIGURE 4
(A) Respiration rate (Rn) and **(B)** respiration to photosynthetic ratio (Rn/A) of microtomato plants after cultivating for 26 days under different light sources with or without UV-B radiation. Means followed by the same letter do not differ by the Dunn's test at 5% probability.

equation was y = 21183x – 9983.1 with a correlation coefficient (R2) of 0.9999 (Supplementary Figures S1–S3). Higher content of rutin was found in fruits at all maturation stages, both in plants under B and BUV lights, highlighting the green fruits grown under B and orange fruits grown under BUV had the highest rutin concentrations (853.141 ± 37.5 and 882.059 ± 62.2 $mg.kg^{-1}$, respectively) (Figure 6).

The response surface graphs for rutin content ($mg.kg^{-1}$) as function of collection stages and light treatments combined or not with UV show that blue light (represented in the graph by the number 2) was the quality of light that most contributed to production of rutin in the three stages of maturation (Figures S4, S5). Therefore, they corroborate the results shown in figure 6. Moreover, the green fruits grown under R and RUV had the lowest rutin concentrations (68.234 ± 0.352 and 27.357 ± 1.43 $mg.kg^{-1}$, respectively). Furthermore, the green fruits grown under RBW and RBWUV also had low rutin concentrations (Figure 6 and Supplementary Figures S4, S5).

Discussion

Various studies have focused on the effects of light spectral quality on the physiological and biochemical performance of plants. Improving the production of bioactive compounds, such as rutin, in fruits is a key step toward healthy food production. This study indicated that despite the positive effects of light wavelength and UV-B radiation on rutin concentration in microtomato fruits, the blue light alone and/or associated with UV-B considerably increased its content. This is probably because monochromatic lights affect photosynthetic parameters, morphology, and stomatal opening rates (Liu et al., 2011; XiaoYing et al., 2011; Wang et al., 2016). Lanoue et al. (2017) have reported high E and Ci in tomatoes grown under monochromatic lights, corroborating the results of this study, in which plants grown under BUV had the highest E (Figure 3). Photoreceptors play a fundamental role in plant responses to the environment. Cryptochromes are primarily responsible for mediating blue light-induced changes in gene expression, phenolic compound accumulation, and flowering regulation. Phototropins mediate chloroplast movement and phototropism, both responsible for mediating stoma opening and inhibiting hypocotyl growth. In addition, UVR8 mediates UV-B-induced responses, also changing gene expression and favoring the biosynthesis and accumulation of flavonoids such as rutin (Rai et al., 2021). Blue light-stimulated stomatal opening increases the efficiency of photosynthesis, which are associated with the high absorption capacity of this wavelength by photosynthetic pigments (chlorophylls and carotenoids), leading to decreased chlorophyll content for many species and reduced FSII efficiency (Landi et al., 2020), without affecting CO_2 fixation efficiency, as observed in this study. The results indicate that pigment and FSII efficiency reductions were adjustments made by the plants to maintain their high photosynthetic efficiency due to high stoma regulation. In contrast, the plants grown under RBWUV light had low gs and A and high FSII efficiency, ETR, and ETR/A, demonstrating that many electrons are transported for energy and NADPH

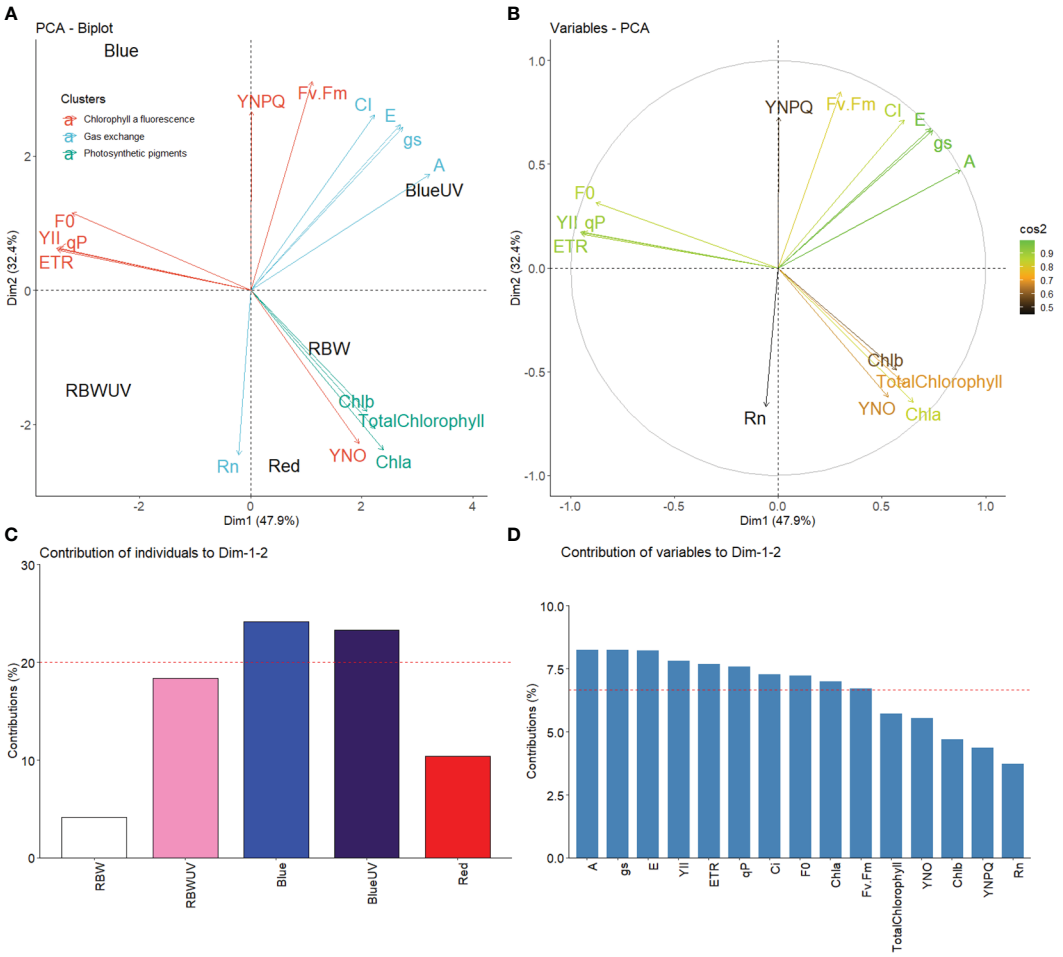

FIGURE 5
(A) Principal component analysis of microtomato chloroplast pigments, chlorophyll a fluorescence, and gas exchange under different light sources with or without UV-B radiation; **(B)** representation quality (cos^2) of the variables DIM1 and DM2. The color gradient indicates the quality of variable representations; **(C)** plot of contribution of spectral qualities of light with or without UV-B radiation; **(D)** plot of the contribution of the variables DIM1 and DIM2. The dashed line indicates the expected measured contribution.

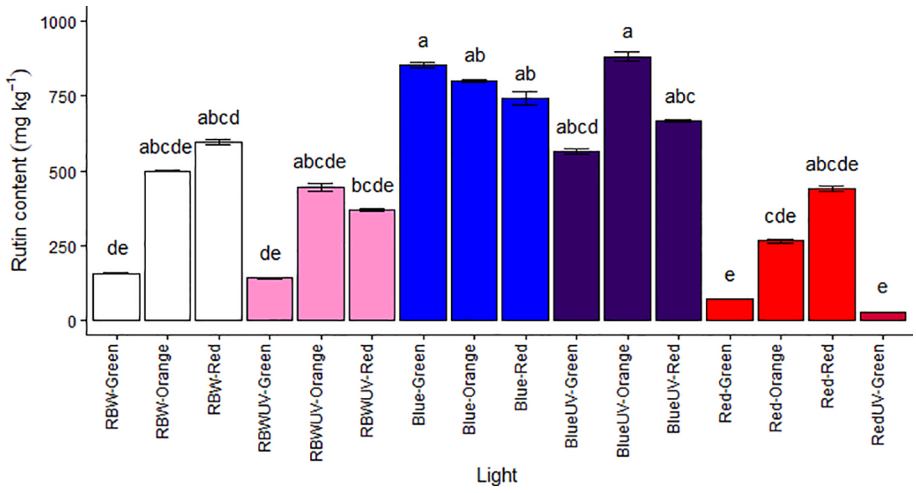

FIGURE 6
Rutin content (mg·kg^{-1}) in the fruits of microtomato plants subjected to six light treatments [RBW light (RBW), RBW + ultraviolet light (RBWUV), blue light (B), blue light + ultraviolet light (BUV), red light (R), and red light + ultraviolet light (RUV)] at different harvesting stages: green tomato (G), orange tomato (O), and red tomato (R). Means followed by the same letter do not differ by the Dunn's test at 5% probability.

production, not being used for CO_2 fixation. Shadow avoidance syndrome is often observed in plants grown under R and the negative effects attributed to high phytochrome stimulation are observed in plants whose development have been affected by the absence of far-red light (Izzo et al., 2020).

Hoffmann et al. (2015) have reported that high blue light intensity improved the photosynthetic performance of pepper. MT plants grown under BUV showed similar behavior, with higher gs and, consequently, higher A and E than those grown under other wavelengths (Figure 3). This behavior may be related to low photosynthetic pigment degradation and increased production of ultraviolet light-absorbing compounds, which are usually expressed in greater amounts in the presence of both blue light and UV-B light (Nascimento et al., 2013; Ouzounis et al., 2014; Hoffmann et al., 2015). In this study, BUV favored both photosynthetic process and rutin accumulation.

Although the photosynthetic pigments observed in this study (chlorophyll a, b, and total chlorophyll; Figure 4) were not the highest in the plants grown under B, they probably induced the production of other pigments, such as carotenoids, which are accessory pigments that invariably increase in response to UV-B because they are associated with light absorption in this spectrum (Kurinjimalar et al., 2019). Palma et al. (2021) have reported that the chlorophyll content variation in peppers treated with associated UV-B and white light is similar to those reported in this study, as the plants grown under RBW had the highest chlorophyll content (Figure 4). Although contrary results have been reported in several previous studies, they focus on the use of different UV-B dosages, and the different light to UV-B ratio can lead to different results.

Yang et al. (2018) reported that YII decreased and YNO increased in tomato plants grown under blue and purple light with increasing light intensity compared to those grown under white light. Moreover, the authors reported increased non-photochemically dissipated YNPQ in plants grown under blue and purple light, which indicates photoprotection induction. The results obtained in this study showed similar behavior in microtomato plants grown under BUV with reduced YII and increased YNO, suggesting that the photoprotective capacity of plants grown under BUV improved their development and the accumulation of rutin, a photoprotective metabolite.

According to Igamberdiev et al. (2014), respiration and photorespiration are regulated by gene expression, oxidation state changes, metabolites produced by the photosynthetic process, and photorespiration. Phytochromes mediate the expression of these genes, proving that light perception plays a crucial role in these steps. The high respiration rates in plants grown under R reported in this study indicate high energy demand to handle the stress imposed by this wavelength.

Phenolic compounds are influenced by genetic factors, being associated with the ripening process and phenolic compound metabolism (Scalzo et al., 2005; Atkinson et al., 2006; Paula et al., 2015). Several factors, such as pest attacks, weather stress, ultraviolet radiation, cultivation site, agricultural practices, harvest and storage, processing and preparation conditions and methods, analytical variability, can cause the quantitative variation of a specific flavonoid in a plant; moreover, location and cultivar accounts for 25% and 33% variability, respectively (Haytowitz et al., 2013; Verma et al., 2019). This study confirmed and quantified high rutin contents, particularly in plants grown under B and BUV. Several studies reported similar results, with rutin being the main phenolic compound quantified (Blasa et al., 2010; Vallverdú-Queralt et al., 2012; Flores et al., 2021). Durán et al. (2018) reported higher phenolic compound accumulation in tomato peel than those in seeds and pulp. The whole fruit was analyzed in this study.

Rutin is a compound found in asparagus, buckwheat, Fava d'anta fruit, blackberry, rue, apple, passion fruit flower, grape, and citrus fruits such as orange, lime, lemon, grapefruit. Buckwheat is considered the main rutin source, which despite being present in most plants, is rarely found in the edible parts (Patel & Patel, 2019). Polyphenolic compounds are poorly absorbed or metabolized before reaching their sites of action, due to their low water solubility. Its bioavailability is low in the gastrointestinal tract; thus, approximately 500 mg rutin should be consumed daily, distributed twice a day, to provide its beneficial effects (Remanan & Zhu, 2021). The extraction of bioactive compounds such as rutin requires care, and a series of steps, such as efficiency, cost-effectiveness, and molecule integrity, must be considered for its preservation in the plant (Gullón et al., 2017). Thus, producing fruits with high rutin content is an excellent advantage since it provides health benefits without the need to be extracted. Naoya Fukuda et al. (2022) observed increased expression of genes regulated by blue light. Cryptochromes can induce reactive oxygen species (ROS) synthesis to adapt to stressful environments. Under stress conditions, they can produce phenolic compounds through flavonoid activation and phenylpropanoid biosynthesis. This defense mechanism corroborates the results observed in this study, because the plants grown under B and BUV had high rutin content.

The results of this study show that MT cultivation under blue light with or without UV increases the photosynthetic rate and bioactive compound production. Derived from primary metabolism, compounds that are part of a specialized metabolism use the carbon skeletons generated mainly by the photosynthetic process to be produced. Furthermore, light is an effective elicitor for the increased production of these molecules, as demonstrated in this study and corroborated by many others. The results shown here are fundamental to understanding the influence of different light wavelengths on different crops. In addition, producing bioactive compound-rich foods is important to improve the quality of life of the population that will consume these foods. These results provide a theoretical basis to further elucidate the mechanism behind rutin synthesis regulation by blue light and associated UV-B in tomatoes and establish a new generation of technological innovations for enhancing specialized metabolite production in crops. This work opens the opportunity to improve the nutraceutical quality of fruits, working with the manipulation of phytochromes and with plants more responsive to UVR8 receptors. Furthermore, in future studies it would be possible to verify the effects of increased light intensity, as well as to vary the time of exposure to UV-B to obtain new responses, in addition to those observed in this study. Thus, the tolerable limit for the microtomato plant could be identified, without observing deleterious effects on plants.

Data availability statement

The original contributions presented in the study are included in the article/Supplementary Material. Further inquiries can be directed to the corresponding authors.

Author contributions

IL: Formal Analysis, Investigation, Methodology, Writing – original draft. AA: Investigation, Methodology, Writing – original draft. ER: Investigation, Methodology, Writing – review & editing. FBS: Investigation, Writing – review & editing. FF: Investigation, Writing – review & editing, Formal Analysis. LS: Investigation, Resources, Writing – original draft. MRo: Writing – original draft, Conceptualization, Methodology. MRe: Writing – original draft, Data curation, Formal Analysis. LB: Data curation, Formal Analysis, Writing – original draft. TO: Resources, Writing – original draft, Investigation. AJ: Conceptualization, Supervision, Visualization, Writing – review & editing. FGS: Conceptualization, Supervision, Writing – review & editing, Funding acquisition.

Funding

The author(s) declare financial support was received for the research, authorship, and/or publication of this article. The project was funded by the Coordination for the Improvement of Higher Education Personnel (CAPES, Finance Code 001), The National Council for Scientific and Technological Development (CNPq, Grant # 408285/2021-4), and by the Financier of Studies and Projects/ the Research Support Foundation of the State of Goiás (FINEP/FAPEG Tecnova II Grant # 202010267000346).

Acknowledgments

The authors thank the Goiano Federal Institute of Education, Science and Technology - Rio Verde CAMPUS, the Coordination for the Improvement of Higher Education Personnel (CAPES), The National Council for Scientific and Technological Development (CNPq), and the Financier of Studies and Projects (FINEP), the Research Support Foundation of the State of Goiás (FAPEG) for the funding, and SpectraGrow Inc. represented by Audax Electronics for the partnership in the supply of LEDs lights.

Conflict of interest

The authors declare that the research was conducted in the absence of any commercial or financial relationships that could be construed as a potential conflict of interest.

Publisher's note

All claims expressed in this article are solely those of the authors and do not necessarily represent those of their affiliated organizations, or those of the publisher, the editors and the reviewers. Any product that may be evaluated in this article, or claim that may be made by its manufacturer, is not guaranteed or endorsed by the publisher.

Supplementary material

The Supplementary Material for this article can be found online at: https://www.frontiersin.org/articles/10.3389/fpls.2023.1261174/full#supplementary-material

References

Atkinson, C. J., Dodds, P. A., Ford, Y. Y., Le Mière, J., Taylor, J. M., Blake, P. S., et al. (2006). Effects of cultivar, fruit number and reflected photosynthetically active radiation on Fragaria x ananassa productivity and fruit ellagic acid and ascorbic acid concentrations. *Ann. Bot.* 97, 429–441. doi: 10.1093/aob/mcj046

Benjamini, Y., and Hochberg, Y. (1995). Controlling the false discovery rate: a practical and powerful approach to multiple testing. *J. R. Stat. Soc Ser. B Stat. Methodol.* 57, 289–300. doi: 10.2307/2346101

Bian, Z. H., Yang, Q. C., and Liu, W. K. (2015). Effects of light quality on the accumulation of phytochemicals in vegetables produced in controlled environments: A review. *J. Sci. Food Agric.* 95, 869–877. doi: 10.1002/jsfa.6789

Bilger, W., Schreiber, U., and Bock, M. (1995). Determina,on of the quantum efficiency of photosystem II and of non-photochemical quenching of chlorophyll fluorescence in the field. *Oecologia* 102, 425–432. doi: 10.1007/BF00341354

Blasa, M., Gennari, L., Angelino, D., and Ninfali, P. (2010). "Fruit and vegetable antioxidants in health," in *Bioactive foods in promoting health*. Eds. R. R. Watson and V. R. Preedy (Amsterdam: Academic Press), 37–58. doi: 10.1016/B978-0-12-374628-3.00003-7

Chua, L. S. (2013). A review on plant-based rutin extraction methods and its pharmacological activities. *J. Ethnopharmacol.* 150, 805–817. doi: 10.1016/j.jep.2013.10.036

Dunn, O. J. (1964). Multiple comparisons using rank sums. *Technometrics.* 6, 241–252. doi: 10.2307/1266041

Durán, D. I. R., Cárdenas, S. A., Martinez, P. R., Ochoa, F. G., and del Socorro López Cortez, M. (2018). Antioxidant content in skin and seeds of three tomato varieties grown in two regions of Mexico. *Int. J. Food Nutr. Sci.* 7, 1–14.

Fang, M.-H., De Guzman, G. N. A., Bao, Z., Majewska, N., Mahlik, S., Grinberg, M., et al. (2020). Ultra-high-efficiency near-infrared Ga_2O_3:Cr^{3+}phosphor and controlling of phytochrome. *J. Mater. Chem. C.* 8, 11013–11017. doi: 10.1039/d0tc02705g

Flores, I. R., Vásquez-Murrieta, M. S., Franco-Hernández, M. O., Márquez-Herrera, C. E., Ponce-Mendoza, A., and del Socorro López-Cortéz, M. (2021). Bioactive compounds in tomato (*Solanum lycopersicum*) variety saladette and their relationship with soil mineral content. *Food Chem.* 344, 128608. doi: 10.1016/j.foodchem.2020.128608

Garagounis, C., Delkis, N., and Papadopoulou, K. K. (2021). Unraveling the roles of plant specialized metabolites: using synthetic biology to design molecular biosensors. *New Phytol.* 231 (4), 1338–1352. doi: 10.1111/nph.17470

Geissler, N., Hussin, S., El-Far, M. M. M., and Koyro, H. W. (2015). Elevated atmospheric CO2 concentra,on leads to different salt resistance mechanisms in a C3 (*Chenopodium quinoa*) and a C4 (*Atriplex nummularia*) halophyte. *Environ Exp Bot* 118, 67–77. doi: 10.1016/j.envexpbot.2015.06.003

Genty, B., Briantais, J. M., and Baker, N. R. (1989). The relationship between the quantum yield of photosynthetic electron transport and quenching of chlorophyll fluorescence. *Biochim Biophys Acta Gen Subj* 990, 87–92. doi: 10.1016/S0304-4165(89)80016-9

Gullón, B., Lú-Chau, T. A., Moreira, M. T., Lema, J. M., and Eibes, G. (2017). Rutin: A review on extraction, identification and purification methods, biological activities and approaches to enhance its bioavailability. *Trends Food Sci. Technol.* 67, 220–235. doi: 10.1016/j.tifs.2017.07.008

Haytowitz, D. B., Bhagwat, S., and Holden, J. M. (2013). Sources of variability in the flavonoid content of foods. *Proc. Food Sci.* 2, 46–51. doi: 10.1016/j.profoo.2013.04.008

Hendrickson, L., Furbank, R. T., and Chow, W. S. (2004). A simple alternative approach to assessing the fate of absorbed light energy using chlorophyll fluorescencee. *Photosynth Res* 82, 73–81. doi: 10.1023/B:PRES.0000040446.87305.f4

Hoffmann, A. M., Noga, G., and Hunsche, M. (2015). High blue light improves acclimation and photosynthetic recovery of pepper plants exposed to UV stress. *Environ. Exp. Bot.* 109, 254–263. doi: 10.1016/j.envexpbot.2014.06.017

Igamberdiev, A. U., Eprintsev, A. T., Fedorin, D. N., and Popov, V. N. (2014). Phytochrome-mediated regulation of plant respiration and photorespiration. *Plant Cell Environ.* 37, 290–299. doi: 10.1111/pce.12155

Izzo, L. G., Mele, B. H., Vitale, L., Vitale, E., and Arena, C. (2020). The role of monochromatic red and blue light in tomato early photomorphogenesis and photosynthetic traits. *Environ. Exp. Bot.* 179, 104195. doi: 10.1016/j.envexpbot.2020.104195

Johkan, M., Shoji, K., Goto, F., Hashida, S.-N., and Yoshihara, T. (2010). Blue light-emitting diode light irradiation of seedlings improves seedling quality and growth after transplanting in red leaf lettuce. *HortScience* 45, 1809–1814. doi: 10.21273/hortsci.45.12.1809

Ke, X., Yoshida, H., Hikosaka, S., and Goto, E. (2022). Optimization of photosynthetic photon flux density and light quality for increasing radiation-use efficiency in dwarf tomato under led light at the vegetative growth stage. *Plants* 11, 121. doi: 10.3390/plants11010121

Ke, X., Yoshida, H., Hikosaka, S., and Goto, E. (2023). Photosynthetic photon flux density affects fruit biomass radiation-use efficiency of dwarf tomatoes under LED light at the reproductive growth stage. *Front. Plant Sci.* 14. doi: 10.3389/fpls.2023.1076423

Kianersi, F., Abdollahi, M. R., Mirzaie-Asl, A., Dastan, D., and Rasheed, F. (2020). Identification and tissue-specific expression of rutin biosynthetic pathway genes in Capparis spinosa elicited with salicylic acid and methyl jasmonate. *Sci. Rep.* 10, 1–15. doi: 10.1038/s41598-020-65815-2

Kim, Y. J., Kim, H. M., Kim, H. M., Jeong, B. R., Lee, H.-J., Kim, H.-J., et al. (2018). Ice plant growth and phytochemical concentrations are affected by light quality and intensity of monochromatic light-emitting diodes. *Hortic. Environ. Biotechnol.* 59, 529–536. doi: 10.1007/s13580-018-0058-3

Kim, Y. J., Kim, Y. B., Li, X., Choi, S. R., Park, S., Park, J. S., et al. (2015). Accumulation of phenylpropanoids by white, blue, and red light irradiation and their organ-specific distribution in Chinese cabbage (*Brassica rapa* ssp. *pekinensis*). *J. Agric. Food Chem.* 63, 6772–6778. doi: 10.1021/acs.jafc.5b02086

Ko, E. Y., Nile, S. H., Sharma, K., Li, G. H., and Parka, S. W. (2015). Effect of different exposed lights on quercetin and quercetin glucoside content in onion (*Allium cepa* L.). *Saudi J. Biol. Sci.* 22, 398–403. doi: 10.1016/j.sjbs.2014.11.012

Kurinjimalar, C., Ganapathy, K., Rangaraja, T., Govindaswamy, K., and Ramasamy, R. (2019). Impact of ultraviolet-B radiation on growth and biochemical composition of *Botryococcus braunii* Kutz. *Curr. Sci.* 116, 89–95. doi: 10.18520/cs/v116/i1/89-95

Laisk, A., and Loreto, F. (1996). Determining photosynthetic parameters from leaf CO_2 exchange and chlorophyll fluorescence (Ribulose-1,5-Bisphosphate Carboxylase/Oxygenase Specificity Factor, Dark Respiration in the Light, Excitation Distribution between Photosystems, Alternative Electron Transport Rate, and Mesophyll Diffusion Resistance). *Plant Physiol.* 110, 903–912. doi: 10.1104/pp.110.3.903

Landi, M., Zivcak, M., Sytar, O., Brestic, M., and Allakhverdiev, S. I. (2020). Plasticity of photosynthetic processes and the accumulation of secondary metabolites in plants in response to monochromatic light environments: A review. *Biochimica et Biophysica Acta - BioenergeBcs*. 1861, 148131. doi: 10.1016/j.bbabio.2019.148131

Lanoue, J., Leonardos, E. D., Ma, X., and Grodzinski, B. (2017). The effect of spectral quality on daily patterns of gas exchange, biomass gain, and water-use-efficiency in tomatoes and lisianthus: An assessment of whole plant measurements. *Front. Plant Sci.* 8. doi: 10.3389/fpls.2017.01076

Li, Q., and Kubota, C. (2009). Effects of supplemental light quality on growth and phytochemicals of baby leaf lettuce. *Environ. Exp. Bot.* 67, 59–64. doi: 10.1016/j.envexpbot.2009.06.011

Liu, X. Y., Chang, T. T., Guo, S. R., Xu, Z. G., and Li, J. (2011). Effect of different light quality of LED on growth and photosynthetic character in cherry tomato seedling. *Acta Hortic.* 907, 325–330. doi: 10.17660/ActaHortic.2011.907.53

Liu, H. K., Chen, Y. Y., Hu, T. T., Zhang, S. J., Zhang, Y. H., Zhao, T. Y., et al. (2016). The influence of light-emitting diodes on the phenolic compounds and antioxidant activities in pea sprouts. *J. Funct. Foods.* 25, 459–465. doi: 10.1016/j.jff.2016.06.028

Liu, Y., Fang, S., Yang, W., Shang, X., and Fu, X. (2018). Light quality affects flavonoid production and related gene expression in *Cyclocarya paliurus*. *J. Photochem. Photobiol. B.* 179, 66–73. doi: 10.1016/j.jphotobiol.2018.01.002

Liu, H. K., Kang, Y. F., Zhao, X. Y., Liu, Y. P., Zhang, X. W., and Zhang, S. (2019). Effects of elicitation on bioactive compounds and biological activities of sprouts. *J. Funct. Foods.* 53, 136–145. doi: 10.1016/j.jff.2018.12.019

Lobiuc, A., Vasilache, V., Pintilie, O., Stoleru, T., Burducea, M., Oroian, M., et al. (2017). Blue and red LED illumination improves growth and bioactive compounds contents in acyanic and cyanic *Ocimum basilicum* L. Microgreens. *Molecules* 22, 2111. doi: 10.3390/molecules22122111

Mata-Nicolás, E., Montero-Pau, J., Gimeno-Paez, E., Garcia-Carpintero, V., Ziarsolo, P., Menda, N., et al. (2020). Exploiting the diversity of tomato: the development of a phenotypically and genetically detailed germplasm collection. *Hortic. Res.* 7, 66. doi: 10.1038/s41438-020-0291-7

Matos, F. S., Wolfgramm, R., Gonçalves, F. V., Cavatte, P. C., Ventrella, M. C., and DaMatta, F. M. (2009). Phenotypic plasticity in response to light in the coffee tree. *Environ. Exp. Bot.* 67, 421–427. doi: 10.1016/j.envexpbot.2009.06.018

Mosadegh, H., Trivellini, A., Ferrante, A., Lucchesini, M., Vernieri, P., and Mensuali, A. (2018). Applications of UV-B lighting to enhance phenolic accumulation of sweet basil. *Sci. Hortic.* 229, 107–116. doi: 10.1016/j.scienta.2017.10.043

Nam, T. G., Kim, D. O., and Eom, S. H. (2018). Effects of light sources on major flavonoids and antioxidant activity in common buckwheat sprouts. *Food Sci. Biotechnol.* 27, 169–176. doi: 10.1007/s10068-017-0204-1

Naoya Fukuda, M. E., Yoshida, H., and Kusano, M. (2022). Effects of light quality, photoperiod, CO_2 concentration, and air temperature on chlorogenic acid and rutin accumulation in young lettuce plants. *Plant Physiol. Biochem.* 186, 290–298. doi: 10.1016/j.plaphy.2022.07.010

Nascimento, L. B. S., Leal-Costa, M. V., Coutinho, M. A., Moreira, N., Lage, C. L., dosS., N., et al. (2013). Increased antioxidant activity and changes in phenolic profile of *Kalanchoe pinnata* (Lamarck) Persoon (Crassulaceae) specimens grown under supplemental blue light. *Photochem. Photobiol.* 89, 391–399. doi: 10.1111/php.12006

Neugart, S., and Schreiner, M. (2018). UVB and UVA as eustressors in horticultural and agricultural crops. *Sci. Hortic.* 234, 370–381. doi: 10.1016/j.scienta.2018.02.021

Nocchi, N., Duarte, H. M., Pereira, R. C., Konno, T. U. P., and Soares, A. R. (2020). Effects of UV-B radiation on secondary metabolite production, antioxidant activity, photosynthesis and herbivory interactions in Nymphoides humboldtiana (Menyanthaceae). *J. Photochem. Photobiol. B* 212, 112021. doi: 10.1016/J.JPHOTOBIOL.2020.112021

Ogle, D., Wheeler, P., and Dinno, A. (2020) *FSA: Simple fisheries stock assessment methods*. Available at: https://cran.r-project.org/web/packages/FSA/index.html (Accessed February 2, 2023).

Ouzounis, T., Fretté, X., Rosenqvist, E., and Ottosen, C. O. (2014). Spectral effects of supplementary lighting on the secondary metabolites in roses, chrysanthemums, and campanulas. *J. Plant Physiol.* 171, 1491–1499. doi: 10.1016/j.jplph.2014.06.012

Palma, C. F. F., Castro-Alves, V., Morales, L. O., Rosenqvist, E., Ottosen, C. O., and Strid, Å. (2021). Spectral composition of light affects sensitivity to UV-B and photoinhibition in cucumber. *Front. Plant Sci.* 11. doi: 10.3389/fpls.2020.610011

Pan, T., Wang, Y., Wang, L., Ding, J., Cao, Y., Qin, G., et al. (2020). Increased CO2 and light intensity regulate growth and leaf gas exchange in tomato. *Physiologia Plantarum* 168 (3), 694–708. doi: 10.1111/ppl.13015

Patel, K., and Patel, D. K. (2019). "The beneficial role of rutin, a naturally occurring flavonoid in health promotion and disease prevention: A systematic review and update," in *Bioactive food as dietary interventions for arthritis and related inflammatory diseases*. Eds. R. R. Watson and V. R. Preedy (Amsterdam: Elsevier Inc), 457–479. doi: 10.1016/B978-0-12-813820-5.00026-X

Paula, J. T., Resende, J. T. V., Faria, M. V., Figueiredo, A. S. T., Schwarz, K., and Neumann, E. R. (2015). Características físico-químicas e compostos bioativos em frutos de tomateiro colhidos em diferentes estádios de maturação (Physicochemical characteristics and bioactive compounds in tomato fruits harvested at different ripeness stages). *Hortic. Bras.* 33, 434–440. doi: 10.1590/s0102-053620150000400005

Pohlert, T. (2018) *PMCMRplus: calculate pairwise multiple comparisons of mean rank sums extended*. Available at: https://CRAN.Rproject.org/package=PMCMRplus (Accessed February 2, 2023).

R Core Team (2023) *The R project for statistical computing*. Available at: https://www.R-project.org/ (Accessed February 2, 2023).

Rai, N., Morales, L. O., and Aphalo, P. J. (2021). Perception of solar UV radiation by plants: photoreceptors and mechanisms. *Plant Physiol.* 186, 1382–1396. doi: 10.1093/PLPHYS/KIAB162

Remanan, M. K., and Zhu, F. (2021). Encapsulation of rutin using quinoa and maize starch nanoparticles. *Food Chem.* 353, 128534. doi: 10.1016/j.foodchem.2020.128534

Ribeiro, V. R., Mari, I. P., Stafussa, A. P., Rossetto, R., and Maciel, G. M. (2019). Bringing together *Saccharomyces cerevisiae* and bioactive compounds from plants: A new function for a well-known biosorbent. *J. Funct. Foods.* 60, 103433. doi: 10.1016/j.jff.2019.103433

Ronga, D., Caradonia, F., Parisi, M., Bezzi, G., Parisi, B., Allesina, G., et al. (2020). Using digestate and biochar as fertilizers to improve processing tomato production sustainability. *Agronomy* 10, 138. doi: 10.3390/agronomy10010138

Scalzo, J., Politi, A., Pellegrini, N., Mezzetti, B., and Battino, M. (2005). Plant genotype affects total antioxidant capacity and phenolic contents in fruit. *Nutrition.* 21, 207–213. doi: 10.1016/j.nut.2004.03.025

Semwal, R., Joshi, S. K., Semwal, R. B., and Semwal, D. K. (2021). Health benefits and limitations of rutin - A natural flavonoid with high nutraceutical value. *Phytochem. Lett.* 46, 119–128. doi: 10.1016/j.phytol.2021.10.006

Shafiq, I., Hussain, S., Raza, M. A., Iqbal, N., Asghar, M. A., Raza, A., et al. (2021). 'Crop photosynthetic response to light quality and light intensity'. *J. Integr. Agric.* 20 (1), 4–23. doi: 10.1016/S2095-3119(20)63227-0

Shih, M. L., and Morgan, J. A. (2020). Metabolic flux analysis of secondary metabolism in plants. *Metab. Eng. Commun.* 10, e00123. doi: 10.1016/j.mec.2020.e00123

Silva, T. D., Batista, D. S., Fortini, E. A., Castro, K. M., Felipe, S. H. S., Fernandes, A. M., et al. (2020). Blue and red light affects morphogenesis and 20-hydroxyecdisone

content of in *vitro Pfaffia glomerata* accessions. *J. Photochem. Photobiol. B.* 203, 111761. doi: 10.1016/j.jphotobiol.2019.111761

Suzuki, T., Honda, Y., and Mukasa, Y. (2005). Effects of UV-B radiation, cold and desiccation stress on rutin concentration and rutin glucosidase activity in tartary buckwheat (*Fagopyrum tataricum*) leaves. *Plant Sci.* 168, 1303–1307. doi: 10.1016/j.plantsci.2005.01.007

Taulavuori, K., Hyöky, V., Oksanen, J., Taulavuori, E., and Julkunen-Tiitto, R. (2016). Species-specific differences in synthesis of flavonoids and phenolic acids under increasing periods of enhanced blue light. *Environ. Exp. Bot.* 121, 145–150. doi: 10.1016/j.envexpbot.2015.04.002

Taulavuori, K., Pyysalo, A., Taulavuori, E., and Julkunen-Tiitto, R. (2018). Responses of phenolic acid and flavonoid synthesis to blue and blue-violet light depend on plant species. *Environ. Exp. Bot.* 150, 183–187. doi: 10.1016/j.envexpbot.2018.03.016

Thoma, F., Somborn-Schulz, A., Schlehuber, D., Keuter, V., and Deerberg, G. (2020). Effects of light on secondary metabolites in selected leafy greens: A review. *Front. Plant Sci.* 11. doi: 10.3389/fpls.2020.00497

Thwe, A. A., Kim, Y. B., Li, X., Seo, J. M., Kim, S. J., Suzuki, T., et al. (2014). Effects of light-emitting diodes on expression of phenylpropanoid biosynthetic genes and accumulation of phenylpropanoids in *Fagopyrum tataricum* sprouts. *J. Agric. Food Chem.* 62, 4839–4845. doi: 10.1021/jf501335q

Vallverdú-Queralt, A., Jáuregui, O., Medina-Remón, A., and Lamuela-Raventós, R. M. (2012). Evaluation of a method to characterize the phenolic profile of organic and conventional tomatoes. *J. Agric. Food Chem.* 60, 3373–3380. doi: 10.1021/jf204702f

Verma, M. L., Sharma, S., Saini, R., Rani, V., and Kushwaha, R. (2019). "Bioflavonoids: Synthesis, functions and biotechnological applications," in *Biotechnological production of bioactive compounds*. Eds. M. L. Verma and A. K. Chandel (Amsterdam: Elsevier), 69–105. doi: 10.1016/B978-0-444-64323-0.00003-5

Wang, P., Chen, S., Gu, M., Chen, X., Chen, X., Yang, J., et al. (2020). Exploration of the effects of different blue led light intensities on flavonoid and lipid metabolism in tea plants via transcriptomics and metabolomics. *Int. J. Mol. Sci.* 21, 1–18. doi: 10.3390/ijms21134606

Wang, J., Lu, W., Tong, Y., and Yang, Q. (2016). Leaf morphology, photosynthetic performance, chlorophyll fluorescence, stomatal development of lettuce (*Lactuca sativa* L.) exposed to different ratios of red light to blue light. *Front. Plant Sci.* 7. doi: 10.3389/fpls.2016.00250

Wickham, H. (2011). ggplot2. Wiley interdiscip. *Rev. Comput. Stat.* 3, 180–185. doi: 10.1002/wics.147

Wu, M.-C., Hou, C.-Y., Jiang, C.-M., Wang, Y.-T., Wang, C.-Y., Chen, H.-H., et al. (2007). A novel approach of LED light radiation improves the antioxidant activity of pea seedlings. *Food Chem.* 101, 1753–1758. doi: 10.1016/j.foodchem.2006.02.010

XiaoYing, L., ShiRong, G., ZhiGang, X., XueLei, J., and Tezuka, T. (2011). Regulation of chloroplast ultrastructure, cross-section anatomy of leaves, and morphology of stomata of cherry tomato by different light irradiations of light-emitting diodes. *HortScience* 46, 217–221. doi: 10.21273/hortsci.46.2.217

Yang, X., Hui, X. H., Shao, L., Li, T., Wang, Y., and Wang, R. (2018). Response of photosynthetic capacity of tomato leaves to different LED light wavelength. *Environ. Exp. Bot.* 150, 161–171. doi: 10.1016/j.envexpbot.2018.03.013

Yasar, F., and Uzal, O. (2023). Oxidative Stress and Antioxidant Enzyme Activities in Tomato (Solanum lycopersicum) Plants Grown at Two Different Light Intensities. *Gesunde Pflanzen* 75 (3), 479–485. doi: 10.1007/s10343-022-00716-0

Zou, J., Zhou, C.-B., Xu, H., Cheng, R.-F., Yang, Q.-C., and Li, T. (2020). The effect of artificial solar spectrum on growth of cucumber and lettuce under controlled environment. *J. Integr. Agric.* 19, 2027–2034. doi: 10.1016/S2095-3119(20)63209-9

frontiers | Frontiers in Plant Science

TYPE Original Research
PUBLISHED 21 June 2024
DOI 10.3389/fpls.2024.1393918

OPEN ACCESS

EDITED BY
Meijian Yang,
Cornell University, United States

REVIEWED BY
Yaniv Shlosberg,
Technion Israel Institute of Technology, Israel
Jung Eek Son,
Seoul National University, Republic of Korea

*CORRESPONDENCE
Eiji Goto
goto@faculty.chiba-u.jp

RECEIVED 29 February 2024
ACCEPTED 04 June 2024
PUBLISHED 21 June 2024

CITATION
Ke X, Yoshida H, Hikosaka S and Goto E (2024) Effect of red and blue light versus white light on fruit biomass radiation-use efficiency in dwarf tomatoes. *Front. Plant Sci.* 15:1393918. doi: 10.3389/fpls.2024.1393918

Effect of red and blue light versus white light on fruit biomass radiation-use efficiency in dwarf tomatoes

Xinglin Ke[1], Hideo Yoshida[1], Shoko Hikosaka[1] and Eiji Goto[1,2]*

[1]Graduate School of Horticulture, Chiba University, Matsudo, Chiba, Japan, [2]Research Center for Space Agriculture and Horticulture, Chiba University, Chiba, Matsudo, Japan

The effect of the ratio of red and blue light on fruit biomass radiation-use efficiency (FBRUE) in dwarf tomatoes has not been well studied. Additionally, whether white light offers a greater advantage in improving radiation-use efficiency (RUE) and FBRUE over red and blue light under LED light remains unknown. In this study, two dwarf tomato cultivars ('Micro-Tom' and 'Rejina') were cultivated in three red-blue light treatments (monochromatic red light, red/blue light ratio = 9, and red/blue light ratio = 3) and a white light treatment at the same photosynthetic photon flux density of 300 μmol m^{-2} s^{-1}. The results evidently demonstrated that the red and blue light had an effect on FBRUE by affecting RUE rather than the fraction of dry mass partitioned into fruits (F_{fruits}). The monochromatic red light increased specific leaf area, reflectance, and transmittance of leaves but decreased the absorptance and photosynthetic rate, ultimately resulting in the lowest RUE, which induced the lowest FBRUE among all treatments. A higher proportion of blue light (up to 25%) led to a higher photosynthetic rate, resulting in a higher RUE and FBRUE in the three red-blue light treatments. Compared with red and blue light, white light increased RUE by 0.09–0.38 g mol^{-1} and FBRUE by 0.14–0.25 g mol^{-1}. Moreover, white light improved the F_{fruits} in 'Rejina' and Brix of fruits in 'Micro-Tom' and both effects were cultivar-specific. In conclusion, white light may have greater potential than mixed red and blue light for enhancing the dwarf tomato FBRUE during their reproductive growth stage.

KEYWORDS

blue light, indoor farming, micro-tom, plant factory, red light, vertical farming

1 Introduction

Cultivation of dwarf tomatoes in a plant factory with artificial light (PFAL), also known as a vertical farm, offers numerous advantages (Kato et al., 2011; Ke et al., 2021). In comparison with general tomato cultivars, the plant density (Meissner et al., 1997) and space-use efficiency of the dwarf tomato are higher, and its growth cycle is shorter

(Sun et al., 2006). However, half of the energy cost in a PFAL is used for lighting (Ohyama et al., 2002; Graamans et al., 2018). Hence, cultivating dwarf tomatoes sustainably in a PFAL to improve radiation-use efficiency (RUE) is crucial. Additionally, particular attention should be given to improving fruit biomass radiation-use efficiency (FBRUE) in commercial PFALs producing tomato fruits. FBRUE is defined as the ratio of the dry mass of a plant's fruits to the number of photosynthetic photons captured by the plant (Wheeler et al., 2008; Li et al., 2019; Ke et al., 2023) and calculated as the product of RUE and the fraction of dry mass partitioned into fruits (Ke et al., 2023). In a PFAL, light quality can be manipulated and regulated to not only improve biomass yield and quality (Goto, 2003; Ilić and Fallik, 2017; Ji et al., 2020) but also potentially upgrade FBRUE by enhancing RUE and/or the fraction of dry mass partitioned into fruits in tomatoes.

According to McCree (1972a), many plants exhibit the highest quantum efficiency of absorption in the red and blue wavelength ranges, making red and blue light highly efficient in PFALs. Red and blue light can also affect the morphology and photosynthesis of tomatoes. Red light can increase plant height (Liu et al., 2011; Nanya et al., 2012), increase leaf area (Bugbee, 2016), and reduce specific leaf area (SLA), while blue light can reduce plant height and increase SLA (Snowden et al., 2016; Ke et al., 2021; Kong and Nemali, 2021). However, the effect of blue light on photosynthesis varies with cultivars in tomatoes (Ouzounis et al., 2016). The ratio of red and blue light may affect the RUE of the canopy by affecting the photosynthetic quantum yield of the canopy and leaf (Ke et al., 2021), as well as the dry matter distribution, such as increasing the shoot/root ratio (Goto, 2003; Nanya et al., 2012). Therefore, this ratio may have an effect on FBRUE by affecting RUE and the fraction of dry mass partitioned into fruits. However, to date, no study has investigated the effect of the ratio of red and blue light on the FBRUE of dwarf tomatoes.

Recently, white LEDs are increasingly being utilized in PFALs owing to their advantages, which include low price, wide spectrum range, and creating a more comfortable working environment. More than 60% of horticultural lighting devices use white LEDs (Kusuma et al., 2020). Moreover, white light not only contains red and blue light but also green light and far-red light. The transmittance of green light is high, allowing leaves in the lower canopy to absorb light, which enhances the uniformity of light distribution in the canopy. Additionally, far-red light can increase the photosynthetic rate (Pn) (Zhen and van Iersel, 2017; Kalaitzoglou et al., 2019), and a previous study demonstrated that it could increase the allocation of dry matter to fruits (Ji et al., 2019); therefore, compared with red and blue light, white light may increase FBRUE. However, to the best of our knowledge, there is not much information on the comparison of FBRUE in dwarf tomatoes grown under white light and red-blue light.

This study aimed to investigate the effect of the ratio of red and blue light on FBRUE in dwarf tomatoes. Additionally, we aimed to verify whether FBRUE under white light is higher than that under red and blue light and to determine an appropriate light quality to improve FBRUE at the reproductive growth stage. In this study, we quantified the effects of light quality on FBRUE, RUE, and dry matter partitioning of fruits by using white light and blue and red light with three different red/blue light ratios.

2 Materials and methods

2.1 Plant materials and growth conditions

Two dwarf tomato cultivars, 'Micro-Tom' and 'Rejina' (*Lycopersicon esculentum*), were used as the test materials. After 3-day germination, at a photosynthetic photon flux density (PPFD) of 200 μmol m^{-2} s^{-1}, we cultivated tomato seeds using white light (LDL40S-N19/21, Panasonic Corporation, Osaka, Japan) in a cultivation room with the following environmental conditions: 1000 μmol mol^{-1} CO_2 concentration, 25/20°C (day/night) air temperature, 70% relative humidity, and 16/8 h (day/night) photoperiod.

At 24 days after sowing (DAS), all seedlings were transplanted under red and blue LED lamps (CIVILIGHT, DPT2RB120Q33 40 type, Showa Denko K.K., Tokyo, Japan; red:blue = 9:1), and PPFD above the top of the canopy was set as 300 μmol m^{-2} s^{-1}. As the growth rate and anthesis time of the first flower in the two cultivars were distinct, the plant density management between the two cultivars was different. The number of days, plant density, used lamps, and PPFD on the top of the canopy during growth periods are shown in Supplementary Table 1. The first flowers of half of the plants in 'Micro-Tom' and 'Rejina' bloomed at 36 and 50 DAS, respectively. Finally, when the experiments started, the values of leaf area (LA) / projected leaf area (PLA) in 'Micro-Tom' at 36 DAS and in 'Rejina' at 50 DAS were modulated at 1.5 and 1.6, respectively (Supplementary Figure 1).

Following 36 DAS in 'Micro-Tom' and 50 DAS in 'Rejina', the plants were placed in four treatments with different light qualities (Supplementary Figure 2): red light (R), white light (WH, the same lamps as previously described white LED), and the mixture of red and blue lights: red/blue light ratio = 3 (R3B1) and red/blue light ratio = 9 (R9B1). The PPFD above the top of all canopies was set at 300 μmol m^{-2} s^{-1}. Apart from the light condition, other environmental conditions remained unchanged. As soon as visible side shoots and axillary buds appeared, all plants were pruned. Final harvests were conducted when half of the fruits turned red at 82 DAS in 'Micro-Tom' and at 100 DAS in 'Rejina', respectively. The spectral photon flux distributions of the LED lamps are shown in Supplementary Figure 3 and calculations were performed for the blue, green, and red wavelength fractions (Supplementary Table 2).

2.2 Growth measurement, Brix, and acidity of fruits

In each treatment, three to four plants were sampled for fresh and dry biomass analysis at 36, 43, 50, 57, 64, 71, and 82 DAS for 'Micro-Tom' and at 50, 60, 70, 80, 90, and 100 DAS for 'Rejina'. A leaf area meter (LI-3000C, Li-Cor Inc., Lincoln, NE, USA) was utilized to measure LA in 'Micro-Tom' and 'Rejina' at 82 and 100

DAS, respectively, with the results taken from two replicates. Specific leaf area (SLA, $cm^2\ g^{-1}$) was calculated by dividing the LA (cm^2) by the leaf dry weight (g). Additionally, the number of fruits was recorded and plant height was measured.

At 82 DAS in 'Micro-Tom' and 100 DAS in 'Rejina', two parameters of fruit quality (Brix and acidity level) were determined using a pocket Brix-Acidity Meter (PAL-BX|ACID3; Atago Co. Ltd.) in 6–9 ripe tomatoes from three or four plants for each treatment.

2.3 Reflectance, transmittance, absorptance, Pn and chlorophyll concentration of leaves

The reflection and transmission spectra of leaves at 50, 71, and 82 DAS for 'Micro-Tom' and 50, 60, 70, and 80 DAS for 'Rejina' were measured with three plants sampled per treatment using the same method reported by Ke et al. (2023). The absorptance was then computed by subtracting the reflectance and transmittance from 100%.

At 53, 67, and 81 DAS, the Pn of the topmost, fully expanded, and unshaded leaf of three randomly selected plants in each treatment was determined using a portable photosynthesis measurement system (LI-6400XT, LI-COR Inc., Lincoln, NE, USA) under the same environmental conditions shown in the article (Ke et al., 2023).

The chlorophyll concentration was determined on a dry weight basis using an ultraviolet-visible spectrophotometer (V-750, JASCO Corporation, Tokyo, Japan) and was extracted from the first leaf from the top of the main stem with N,N-dimethylformamide at 50, 71 and 82 DAS in 'Micro-Tom' and at 50, 70, 80, and 100 DAS in 'Rejina', according to the protocol and method of Porra et al. (1989). Three or four plants (one leaf per plant) in each treatment were sampled.

2.4 Radiation-use efficiency (RUE) and fruit biomass radiation-use efficiency (FBRUE)

RUE ($g\ mol^{-1}$) is the proportion of the accumulated dry mass (ΔW, g) to the integrated PPFD received by a plant during a given period (ΔI_{PPFD}, mol) using projected leaf area (Ke et al., 2023). In this study, the RUE remained constant through the reproductive growth stage. Thus, the gradient of the fitted linear regression expressing the connection between ΔW and ΔI_{PPFD} was the value of RUE. FBRUE is defined as RUE ($g\ mol^{-1}$) multiplied by the fraction of dry mass partitioned into fruits (F_{fruits}, $g\ g^{-1}$) on a given day (Ke et al., 2023).

2.5 Statistical analysis

Data analysis was performed using SPSS for Windows (Version 24.0; SPSS Inc., Chicago, IL, USA). The Tukey–Kramer test at $p < 0.05$ was conducted to investigate significant differences among treatments after performing one-way analysis of variance (ANOVA) on the data. The mean values of measured data were compared, and the measurements related to FBRUE in each treatment were repeated three times.

3 Results

3.1 Growth condition

Light quality significantly affected the plant height of 'Rejina' but not 'Micro-Tom' (Table 1). The plant height in R was significantly higher than that in WH. Additionally, light quality affected the SLA in the two cultivars. The SLA of the two cultivars in R without blue light was the highest and significantly higher than those in R3B1, which had the highest blue light ratio. Light quality also had significant effects on the total dry weight ratio in 'Micro-Tom'. However, total fresh and dry weights in the two cultivars were not significantly affected by light quality.

3.2 Reflectance, transmittance, and absorptance of leaves

Photosynthetically active radiation was most reflected and least absorbed by the top leaves in R in the two cultivars (Tables 2, 3). In 'Micro-Tom', the reflectance values to green and red light in R were significantly higher than those in WH (Table 2). Moreover, the absorptance values to green and red light in R were significantly lower than those in other treatments. In 'Rejina', the transmittance of leaves in R was significantly higher than those in other treatments (Table 3).

3.3 Pn and chlorophyll concentration

The values of Pn in R at 53, 67, and 82 DAS were the lowest among all treatments in 'Micro-Tom' (Figure 1A). At 67 DAS, the Pn in R was significantly lower than that in other treatments. Similar to 'Micro-Tom', the values of Pn in 'Rejina' under red light were significantly lower than those in WH at 53 and 67 DAS (Figure 1B).

Light quality significantly affected the concentration of chlorophyll a+b in the two cultivars (Figure 2). The chlorophyll concentration of leaves in 'Micro-Tom' in WH was significantly lower than that in other treatments at 71 DAS (Figure 2A). At 82 DAS, it was significantly higher in R than in WH and R3B1. Similar to 'Micro-Tom', the chlorophyll concentration of leaves in 'Rejina' in WH at 80 DAS was significantly lower than that in other treatments (Figure 2B). Additionally, at 100 DAS, the chlorophyll concentration of leaves in R was significantly higher than WH.

3.4 RUE and FBRUE

The RUE in Figure 3 was calculated using the data in Supplementary Figures 4, 5. In 'Micro-Tom', the values of RUE

TABLE 1 Effect of light quality on the growth in 'Micro-Tom' 82 days after sowing (DAS) and in 'Rejina' 100 DAS.

Cultivar	Initial value or treatment	Plant height (cm)	Specific leaf area ($cm^2\ g^{-1}$ DW)	Total fresh weight (g)	Total dry weight (g)	Total dry matter ratio (%)
Micro-Tom	Initial value at 36 DAS	10.3 ± 0.4	288.5 ± 13.7	10.2 ± 0.7	0.9 ± 0.1	8.9 ± 0.3
	R	12.7 ± 0.7	157.2 ± 17.4 a	118.8 ± 12.7	10.4 ± 1.6	8.6 ± 0.5 b
	R9B1	12.1 ± 0.3	133.0 ± 8.5 ab	115.0 ± 9.8	10.9 ± 0.9	9.5 ± 0.4 ab
	WH	11.3 ± 0.3	115.7 ± 4.8 ab	104.6 ± 17.4	10.9 ± 1.8	10.5 ± 0.1 a
	R3B1	13.2 ± 0.2	109.0 ± 1.6 b	133.9 ± 5.8	13.1 ± 0.5	9.8 ± 0.2 ab
Rejina	Initial value at 50 DAS	13.7 ± 0.4	186.9 ± 11.9	69.4 ± 2.0	6.5 ± 0.2	9.3 ± 0.2
	R	21.7 ± 1.7 a	136.4 ± 6.8 a	382.2 ± 67.0	31.2 ± 4.5	8.3 ± 0.6
	R9B1	18.5 ± 0.8 ab	113.6 ± 1.3 b	416.8 ± 85.3	34.7 ± 5.7	8.5 ± 0.3
	WH	16.5 ± 0.3 b	102.0 ± 3.4 b	435.7 ± 57.7	35.4 ± 5.1	8.1 ± 0.1
	R3B1	19.0 ± 0.8 ab	110.3 ± 4.2 b	452.4 ± 91.1	37.0 ± 6.0	8.4 ± 0.4

DW is dry weight (g). Each value represents the mean ± standard error. Different letters in a column in a cultivar indicate significant differences among the treatments based on Tukey–Kramer's test at $p < 0.05$ (n = 6–8). R, red light; R9B1, red/blue light ratio = 9; WH, white light; R3B1, red/blue light ratio = 3.

in WH and R3B1 were significantly higher than those in R and R9B1 (Figure 3A). The highest RUE in WH was 0.38 g mol^{-1} higher than the lowest RUE in R. Similarly, in 'Rejina', the RUE value in WH was the highest, and that in R was the lowest among all treatments (Figure 3B). The blue light proportions of R, R9B1, and R3B1 were 0%, 10%, and 25%, respectively (Supplementary Table 2). The RUE increased with an increase in the blue light proportion from 0% to 25% under red and blue light in both cultivars (Figure 3).

In 'Micro-Tom', F_{fruits} increased from 36 to 71 DAS in all treatments and did not change until 82 DAS (Figure 4A). At 64 DAS, the F_{fruits} values in WH and R3B1 were significantly higher than F_{fruits} in R and R9B1, temporarily. Finally, no significant difference was observed in F_{fruits} at 82 DAS (harvest time) among treatments. In 'Rejina', F_{fruits} increased from 50 to 90 DAS in all treatments and decreased until 100 DAS except in WH (Figure 4B). The F_{fruits} values in WH and R3B1 were significantly higher than those in R9B1 at 90 DAS. Moreover, the F_{fruits} in WH were significantly higher than those in other treatments at 100 DAS.

In 'Micro-Tom', FBRUE was significantly affected by light quality at 43, 57, 64, 71, and 82 DAS (Figure 5A). The FBRUE values in WH and R3B1 were significantly higher than those in R and R9B1 from 64 DAS. In 'Rejina', FBRUE was affected by light quality from 70 DAS; specifically, the FBRUE in WH was significantly greater than that observed in other treatments (Figure 5B).

3.5 Yield, Brix and acidity of fruits

In 'Micro-Tom', there were no significant differences in fruit fresh and dry weights among the treatments at 71 and 82 DAS (Supplementary Tables 3, 4). At 82 DAS, the fruit dry matter ratio in WH was significantly higher than that in R. Additionally, Brix in WH was significantly higher than that in R3B1 (Table 4). In 'Rejina', at 70 DAS, fruit fresh and dry weights in WH were the highest among all treatments and significantly higher than those in R (Supplementary Table 3). However, at 100 DAS, no significant differences were observed in all items among treatments (Table 4; Supplementary Table 4).

TABLE 2 Effects of light quality on the reflectance and absorptance of leaves in 'Micro-Tom' at the green and red wavelengths 82 DAS.

Treatment	Reflectance (%)		Absorptance (%)	
	500–599 nm (Green)	600–700 nm (Red)	500–599 nm (Green)	600–700 nm (Red)
R	9.3 ± 0.0 a	7.2 ± 0.0 a	86.1 ± 1.2 b	90.9 ± 0.6 b
R9B1	6.3 ± 0.0 ab	5.0 ± 0.1 ab	90.8 ± 0.8 a	94.0 ± 0.3 a
WH	5.2 ± 1.4 b	3.8 ± 1.4 b	89.4 ± 0.4 a	94.0 ± 0.9 a
R3B1	6.1 ± 0.4 ab	4.8 ± 0.0 ab	91.8 ± 0.7 a	93.1 ± 0.0 a

The range of measured light spectrum was 400–700 nm. Each value represents the mean ± standard error. Different letters in a column in a cultivar indicate significant differences among the treatments based on Tukey–Kramer's test at $p < 0.05$ (n = 3–4). R, red light; R9B1, red/blue light ratio = 9; WH, white light; R3B1, red/blue light ratio = 3.

TABLE 3 Effects of light quality on the reflectance, transmittance and absorptance of leaves in 'Rejina' at the blue, green and red wavelengths 100 DAS.

Treatment	Reflectance (%)			Transmittance (%)			Absorptance (%)		
	400–499 nm (Blue)	500–599 nm (Green)	600–700 nm (Red)	400–499 nm (Blue)	500–599 nm (Green)	600–700 nm (Red)	400–499 nm (Blue)	500–599 nm (Green)	600–700 nm (Red)
R	5.6 ± 0.1	8.9 ± 0.4 a	7.7 ± 0.5 a	0.5 ± 0.1 a	5.7 ± 0.7 a	3.3 ± 0.4 a	94.1 ± 0.1 b	85.7 ± 0.6 b	88.7 ± 0.2 b
R9B1	5.5 ± 0.0	6.5 ± 0.1 b	6.2 ± 0.1 ab	0.1 ± 0.0 b	1.8 ± 0.4 b	0.9 ± 0.2 b	94.5 ± 0.0 ab	91.7 ± 0.5 a	92.9 ± 0.3 a
WH	5.0 ± 0.3	5.9 ± 0.1 b	5.3 ± 0.5 b	0.1 ± 0.0 b	2.5 ± 0.6 b	1.3 ± 0.2 b	94.9 ± 0.3 ab	91.6 ± 0.6 a	93.4 ± 0.5 a
R3B1	4.7 ± 0.3	5.8 ± 0.5 b	5.1 ± 0.0 b	0.1 ± 0.0 b	1.7 ± 0.1 b	1.6 ± 0.0 b	95.3 ± 0.3 a	92.5 ± 0.4 a	93.3 ± 0.0 a

The range of measured light spectrum was 400–700 nm. Each value represents the mean ± standard error. Different letters in a column in a cultivar indicate significant differences among the treatments based on Tukey–Kramer's test at $p < 0.05$ (n = 3–4). R, red light; R9B1, red/blue light ratio = 9; WH, white light; R3B1, red/blue light ratio = 3.

4 Discussion

4.1 Influence of the proportion of red and blue light on RUE due to alterations in leaf optical characteristics and photosynthesis

In the present study, monochromatic red light increased SLA (Table 1) and chlorophyll concentration (Figure 2) compared with combined red-blue light and white light. In corn, there is an inverse correlation between chlorophyll concentrations and the reflectance of green and red light (Daughtry et al., 2000). Moreover, higher SLA leads to thinner leaves with the same dry matter ratio and higher transmittance of leaves. Consequently, the monochromatic red light increased the reflectance and transmittance but decreased the absorptance (Tables 2, 3) and may ultimately cause the over-valuation of the ΔI_{PPFD} and the under-valuation of RUE. Additionally, there were no significant differences in leaf optical properties among all treatments at 50 and 71 DAS in 'Micro-Tom' and 50, 70, and 80 DAS in 'Rejina' (data not shown). Therefore, the effects of light quality on leaf optical properties appeared significantly in the late period of the reproductive growth stage.

RUE is affected by the ratio of red and blue light not only because of its effect on optical properties but also its effect on photosynthesis. For optimal plant growth, the addition of at least a low percentage of blue light to supplement red light is necessary (Hoenecke et al., 1992; Cope and Bugbee, 2013). Monochromatic red light decreased the RUE (Figure 3) by decreasing the Pn (Figure 1). Several crop plants have demonstrated a decreased photosynthesis rate when grown solely under red light, such as rice (Matsuda et al., 2004), wheat (Goins et al., 1997), cucumber (Hogewoning et al., 2010), and radish (Yorio et al., 2001). This may be because the disruption to the photosynthetic machinery is caused by the presence of red light only or the lack of blue light (Hogewoning et al., 2010). Additionally, monochromatic red light results in low F_v/F_m in cucumber (Hogewoning et al., 2010) and the inhibition of PSI and PSII development in wheat (Sood et al., 2004).

Under the combined red and blue light, a higher blue light proportion, up to 25%, resulted in a higher Pn at 67 DAS in 'Rejina' (Figure 1B). This may be associated with the decreasing SLA (Table 1) and stomatal conductance and an increase in photosynthetic electron transport capacity (Miao et al., 2016; Izzo et al., 2020). However, there were no significant differences in total dry weights between the two

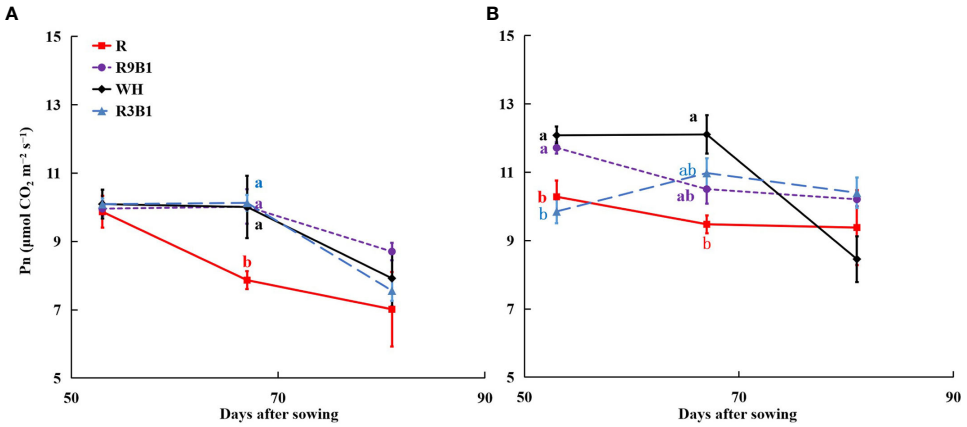

FIGURE 1
Effects of light quality on net photosynthetic rate (Pn) in 'Micro-Tom' **(A)** and 'Rejina' **(B)** at 53, 67, and 81 DAS. Solid points represent the average Pn of three or four plants in each treatment. Error bars represent ± standard error. Different letters indicate significant differences among the treatments based on Tukey–Kramer's test at $p < 0.05$ (n = 3–4). R, red light; R9B1, red/blue light ratio = 9; WH, white light; R3B1, red/blue light ratio = 3; DAS, days after sowing.

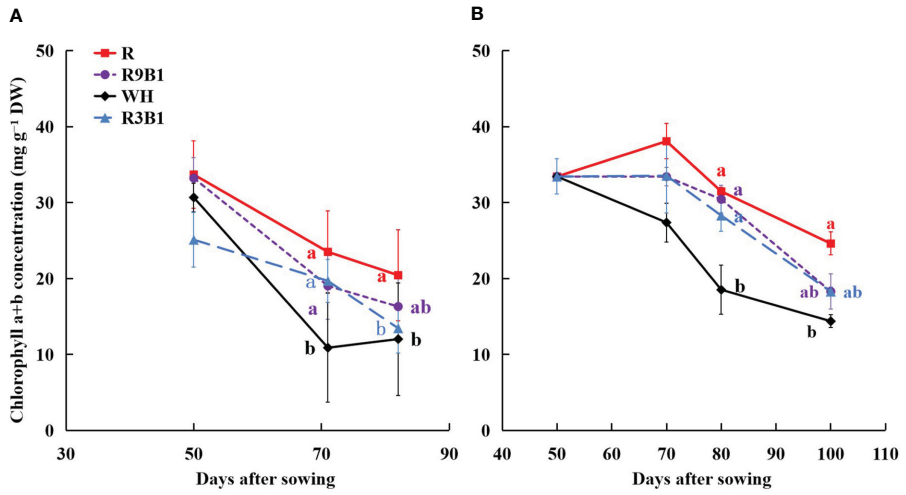

FIGURE 2
Effects of light quality on chlorophyll concentration of leaves in 'Micro-Tom' **(A)** at 50, 71, and 82 DAS, and in 'Rejina' **(B)** at 50, 70, 80, and 100 DAS. DW **(g)** is dry weight. Solid points represent the average value of three plants in each treatment. Error bars represent ± standard error. Different letters indicate significant differences among the treatments based on Tukey–Kramer's test at $p < 0.05$ (n = 3). R, red light; R9B1, red/blue light ratio = 9; WH, white light; R3B1, red/blue light ratio = 3; DAS, days after sowing.

cultivars (Table 1). This result contrasts with the finding that a large proportion of blue light has the potential to hinder the production of biomass in tomato seedlings (cv. Early girl) at PPFDs of 200 and 500 µmol m^{-2} s^{-1} (Snowden et al., 2016). However, in the same study, there were no significant differences in dry mass among different light qualities in cucumber at a PPFD of 200 µmol m^{-2} s^{-1} as well as in radish, soybean, lettuce (cv. Waldmann's Green), and wheat at PPFDs of 200 and 500 µmol m^{-2} s^{-1}. The dry mass of lettuce plants "Gentilina" (cv. Rebelina) decreased and then increased with an improved proportion of blue light at a PPFD of 215 µmol m^{-2} s^{-1} (Pennisi et al., 2019). This may be attributed to the highly cultivar-specific effects of the ratio of red and blue light on stomatal conductance and Pn in tomatoes (Ouzounis et al., 2016). Therefore, at 67 DAS, there was a significant difference in Pn between monochromatic red light and mixed red and blue light in 'Micro-Tom' (Figure 1A) but no significant difference in 'Rejina' (Figure 1B). Additionally, the values of Pn in the two cultivars decreased with time. This may be attributed to leaf senescence (Quirino et al., 2000). Thus, a higher blue light proportion led to higher Pn and further led to higher RUE (Figure 3) under the combination of red and blue light.

4.2 Blue light improves FBRUE by improving RUE rather than F_{fruits}

Except for two temporary periods around 64 DAS in 'Micro-Tom' and 90 DAS in 'Rejina', there was no significant difference in F_{fruits} among the three treatments under the combination of red and

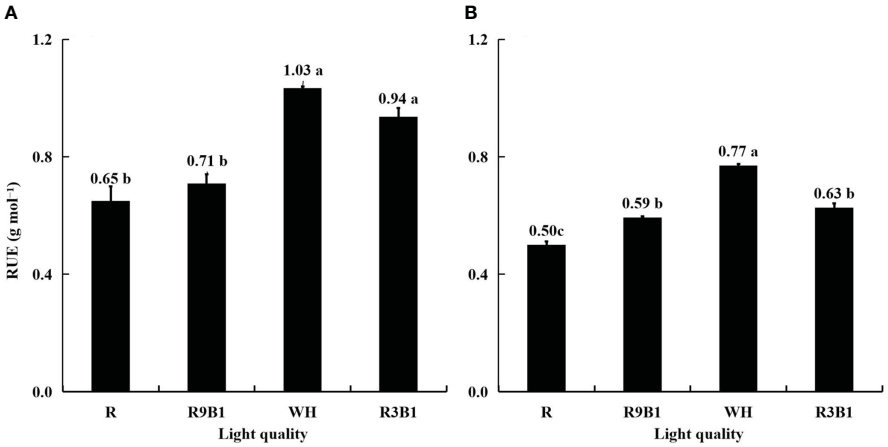

FIGURE 3
Effects of light quality on RUE in 'Micro-Tom' **(A)** and 'Rejina' **(B)** during the reproductive growth stage. The RUE was calculated using the data in Supplementary Figures 4, 5. Error bars represent ± standard error. Different letters indicate significant differences among the treatments based on Tukey–Kramer's test at $p < 0.05$ (n = 3). R, red light; R9B1, red/blue light ratio = 9; WH, white light; R3B1, red/blue light ratio = 3.

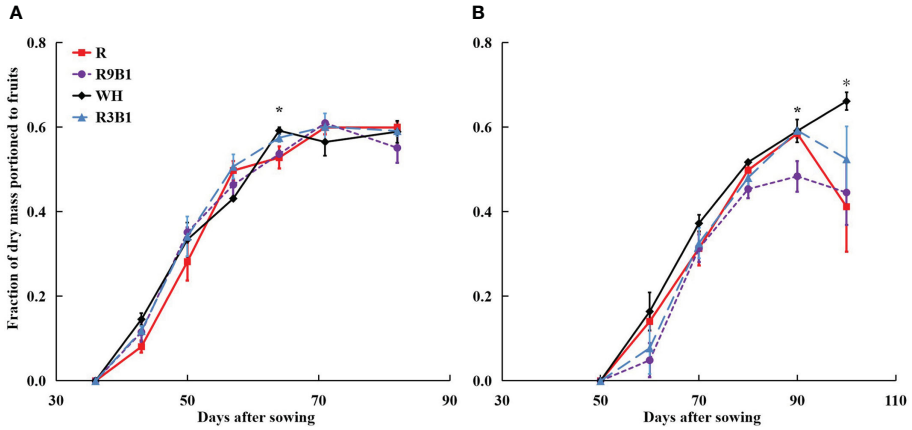

FIGURE 4
Effects of light quality on the fraction of dry mass portioned to fruits (F_{fruits}) over time in 'Micro-Tom' **(A)** and 'Rejina' **(B)**. Error bars represent ± standard error. * indicates significant differences among the treatments based on Tukey–Kramer's test at $p < 0.05$ (n = 3–6). R, red light; R9B1, red/blue light ratio = 9; WH, white light; R3B1, red/blue light ratio = 3.

blue light (Figure 4). Until 71 DAS in 'Micro-Tom' and 70 DAS in 'Rejina', a higher blue light proportion resulted in higher fruit fresh and dry weights among the three treatments (Supplementary Table 3). However, both cultivars are determinate tomatoes, and no new fruits emerged from the main stem during the late reproductive growth stage. Hence, there were no significant differences in the number of fruits and fruit fresh and dry weights among the three treatments until the harvest (Supplementary Table 4). Consequently, blue light improved FBRUE by mainly increasing RUE rather than F_{fruits}.

The range of FBRUE in 'Micro-Tom' was 0.39–0.61 g mol^{-1}, which was higher than 0.21–0.33 g mol^{-1} in 'Rejina' (Figure 5). Previous studies have demonstrated that the FBRUE values of tomatoes cultivated in a controlled environment ranged from 0.20–0.36 g mol^{-1} (Goto, 2011; Li et al., 2019), which was almost the same as for 'Rejina' in the present study. The F_{fruits} values in 'Micro-Tom' and 'Rejina' were 0.55–0.60 and 0.41–0.66 g mol^{-1}, respectively (Figure 4) which were similar to the values reported perviously (Cockshull et al., 1992; De Koning, 1993; Cavero et al., 1998; Scholberg et al., 2000). The range of RUE in 'Micro-Tom' was 0.65–1.03 g mol^{-1}, which was higher than the RUE of 0.50–0.77 g mol^{-1} in 'Rejina' (Figure 3). Therefore, the difference in FBRUE between the two cultivars was mainly due to the distinction in RUE rather than F_{fruits}.

Although the two cultivars could not be compared statistically because of the inconsistency in plant density and light environment, the RUE of 'Micro-Tom' was higher than that of 'Rejina', although the Pn of 'Rejina' was higher than that of 'Micro-Tom' (Figure 1). This discrepancy may be attributed to two reasons. Firstly, the respiration rate of 'Rejina' was higher than that of 'Micro-Tom' (Supplementary Figure 6), leading to more dry mass being consumed during the dark period. Secondly, there were about ten true leaves in 'Rejina' and six true leaves in 'Micro-Tom' on the main stem. The fifth true leaf from the bottom in 'Rejina' and the

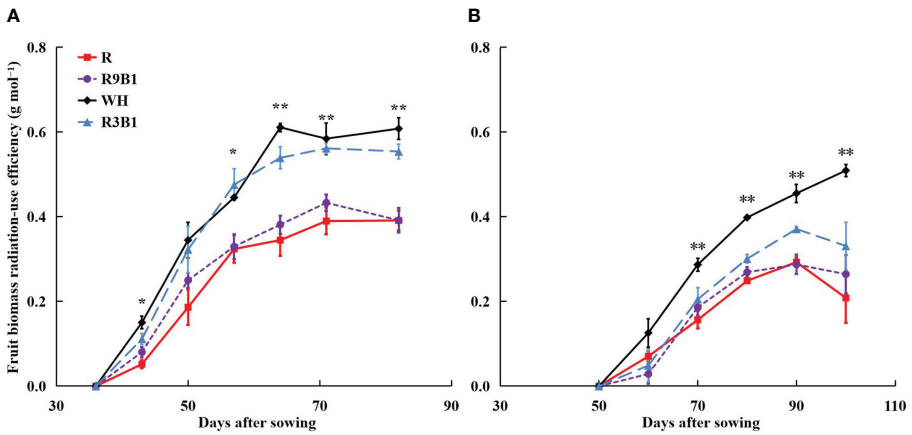

FIGURE 5
Effects of light quality on fruit biomass radiation-use efficiency (FBRUE) over time in 'Micro-Tom' **(A)** and 'Rejina' **(B)**. Error bars represent ± standard error. * and ** indicates significant difference among the treatments based on Tukey–Kramer's test at $p < 0.05$ and $p < 0.01$ (n = 3), respectively. R, red light; R9B1, red/blue light ratio = 9; WH, white light; R3B1, red/blue light ratio = 3.

10.3389/fpls.2024.1393918

TABLE 4 Effects of light quality on the fruit dry matter ratio and fruit quality in 'Micro-Tom' 82 DAS and in 'Rejina' 100 DAS.

Cultivar	Treatment	Fruit dry matter ratio (%)	Brix (%)	Acidity (%)	Brix/acidity
Micro-Tom	R	7.7 ± 0.4 b	5.4 ± 0.1 ab	1.2 ± 0.1	4.7 ± 0.3
	R9B1	8.3 ± 0.4 ab	5.3 ± 0.2 ab	1.2 ± 0.1	4.5 ± 0.4
	WH	9.6 ± 0.1 a	5.7 ± 0.4 a	1.3 ± 0.1	4.5 ± 0.3
	R3B1	8.5 ± 0.2 ab	4.8 ± 0.2 b	1.3 ± 0.1	4.1 ± 0.6
Rejina	R	6.5 ± 0.4	5.5 ± 0.1	0.7 ± 0.1	8.5 ± 0.8
	R9B1	6.5 ± 0.1	5.5 ± 0.2	0.7 ± 0.1	7.9 ± 0.6
	WH	5.8 ± 0.2	5.9 ± 0.2	0.6 ± 0.0	10.6 ± 0.8
	R3B1	6.8 ± 0.1	5.8 ± 0.1	0.7 ± 0.0	8.1 ± 0.5

Each value represents the mean ± standard error. Different letters indicate significant differences at the $p < 0.05$ level among light-quality treatments with Tukey–Kramer's test. Each value of the fruit dry matter ratio represents a mean of three values. There were 6–9 fruits sampled in each treatment for fruit quality. R, red light; R9B1, red/blue light ratio = 9; WH, white light; R3B1, red/blue light ratio = 3.

sixth true leaf in 'Micro-Tom' were expanded at 36 DAS (Supplementary Figure 7A). The age of the top leaf in 'Rejina' was younger than that in 'Micro-Tom' at the same DAS. In addition, until harvest, the age of the bottom leaf in 'Micro-Tom' was younger than that in 'Rejina'. Furthermore, the top leaves (2–3 leaves) in 'Rejina' occupied 20–30% and in 'Micro-Tom' occupied 30–50%. Therefore, the Pn of the whole canopy in 'Rejina' may be less than that in 'Micro-Tom'. In the future, the Pn of the whole canopy should be measured and used for the investigation of the RUE of the canopy. Moreover, the growth speed was also different between the two cultivars. Until 36 DAS, when the first flower in 'Micro-Tom' bloomed, the 'Micro-Tom' plant was taller and larger than the 'Rejina' plant (Supplementary Figure 7A). However, the 'Rejina' plant was taller and larger than the 'Micro-Tom' plant at 50 DAS (Supplementary Figure 7B). Therefore, it is also important to consider choosing tomato cultivars with high RUE in the commercial PFAL.

4.3 White light may have a greater capacity for enhancing FBRUE than red and blue light in a PFAL

LED fixtures for horticulture generally comprise a combination of LEDs emitting red (approx. 660 nm), blue (approx. 450 nm), white, and/or far-red (approx. 730 nm) light because of their high efficiency and efficacy (Kusuma et al., 2020). Theoretically, the photon efficacy (μmol J^{-1}) of blue LEDs is less than that of red LEDs (Tsao et al., 2010). Additionally, the photosynthetic efficiency of blue photons is at most 20% lower than that of photons from a typical red LED (660 nm) (McCree, 1971). Therefore, more red light usually leads to higher energy use efficiency. However, a blue light percentage of 5–22 or 30% is typically employed to prevent excessive stem elongation and shade-avoidance characteristics (Hogewoning et al., 2010; Kusuma et al., 2020). Therefore, in the present study, the proportion of blue light we selected did not exceed 25% (Supplementary Table 2). Moreover, a luminescent material coating that absorbs blue photons and luminesces at longer wavelengths is used to construct white LEDs. Hence, the photon efficacy of white LEDs is less than that of blue and red LEDs. However, the advantages of white LEDs, such as affordability, wide spectrum range, and enhanced comfort in the workplace, have made them increasingly popular in PFALs.

In the present study, white light increased FBRUE (Figure 5) by increasing RUE (Figure 3) and F_{fruits} (Figure 4). There may be two possible reasons why RUE in WH was the highest. First, the changing trend of RUE under different light qualities was associated with Pn changes in the two cultivars. The Pn in WH was high until 67 DAS in both cultivars (Figure 1). In this study, the white LED light had 3.3% far-red photons (Supplementary Table 2) that may increase Pn. Zhen and van Iersel (2017) and Murakami et al. (2018) reported that supplementing far-red photons (peaking at 735 nm) to existing red+blue or white LED light synergistically enhanced the quantum yield of PSII and the Pn of leaves in a broad range of light intensities. Second, the white light in WH in this study had 46.7 % green light, while other light treatments had less than 1% green light (Supplementary Table 2). Green light is able to penetrate into the leaves more deeply than both red and blue lights, thus enabling leaves in the lower canopy to absorb more of the green light (Terashima et al., 2009). Additionally, the efficiency of photosynthesis is known to be highly driven by the absorption of green light in leaves (Björkman, 1968; McCree, 1972b). More green light in WH might enhance the canopy RUE by improving the uniformity of light distribution throughout the canopy.

The F_{fruits} in WH was significantly higher than those in other treatments at 100 DAS in 'Rejina' (Figure 4B). A higher red/blue light ratio led to higher dry mass partitioning to leaves in tomatoes under red and blue LED light (Liang et al., 2021). The shoot-root ratio in tomatoes (cv. Sida) was higher under high red-to-blue ratio light, which was in agreement with Thwe et al. (2020). In the present study, the dry mass partitioning to leaves in both R and R9B1 was higher than that in WH and R3B1 in 'Micro-Tom' at 64 DAS (data not shown). In addition, far-red light promotes fruit growth by increasing dry mass partitioning to fruits (Ji et al., 2019). This may be one reason why F_{fruits} was the highest at 90 and 100 DAS in 'Rejina' (Figure 4B).

In 'Micro-Tom', the lowest Pn in R (Figure 1A) led to the lowest fruit dry weight, which resulted in the lowest fruit dry matter ratio (Table 4). However, red light may improve the content of soluble sugars in tomatoes (Erdberga et al., 2020). This aligns with a previous study indicating that an increased red-to-blue ratio enhanced tomato glucose and fructose contents and sugar/acid ratio (Thwe et al., 2020). Therefore, the fruit Brix in R3B1 rather than R was the lowest (Table 4). In addition, the fruit dry matter ratio and Brix in WH were the highest among all treatments at 82 DAS. This may be attributed to white light containing far-red radiation that can increase fruit sugar concentration (Ji et al., 2020). The expression of genes related to both sugar transportation and metabolism, such as *HY5* (van Gelderen et al., 2018), *SWEET11*, and *SWEET12* (Chen et al., 2016), were increased by far-red light. In summary, white light is suitable for enhancing RUE, FBRUE, and fruit quality.

This study has certain limitations. It is important to note that white light is a mixture of light. In this study, we used just one kind of white light. Therefore, other kinds of white light with different spectra emitted by white LEDs with different color temperatures should be investigated in the future to determine whether white light has a greater capacity for enhancing the FBRUE of tomatoes than red and blue light in a PFAL. In addition, the cool-type white LED with a lower R/B light ratio may improve RUE and FBRUE of dwarf tomatoes at the reproductive growth stage. In *Arabidopsis*, a blue light (470 nm) threshold intensity of 5 μmol m^{-2} s^{-1} was found to activate *psbD*, a PSII core protein D2-encoding gene through cryptochromes (Mochizuki et al., 2004). In addition, there may be a qualitative or threshold effect of blue photons on leaf photosynthesis in cucumbers (Hogewoning et al., 2010). However, the relationship between blue light and RUE/FBRUE is still unclear, in terms of whether there is a qualitative threshold and/or quantitative progressive effect.

5 Conclusions

Our study showed that the decrease in RUE was ultimately caused by the monochromatic red light, which increased SLA, reflectance, and transmittance but decreased absorptance and Pn. Additionally, a higher blue light proportion, up to 25%, led to higher Pn, which further caused higher RUE under the combined red and blue light. Moreover, blue light improved FBRUE by enhancing RUE rather than F_{fruits}. We also found that FBRUE is cultivar-specific and was higher in 'Micro-Tom' than in 'Rejina'. This distinction was attributed to RUE rather than F_{fruits}.

Compared with red and blue light, white light increased FBRUE by 0.14–0.25 g mol^{-1}. In both cultivars, white light improved RUE. However, F_{fruits} was increased by the white light only in 'Rejina'. Moreover, white light improved fruit dry matter ratio and Brix in 'Micro-Tom', and this effect was also cultivar-specific. In summary, white light has more potential to enhance FBRUE than red and blue light by improving RUE and F_{fruits}; hence, it is recommended for improving RUE, FBRUE, and fruit quality at the reproductive growth stage. Our study results will be helpful in comprehending how light quality affects the RUE and FBRUE of dwarf tomatoes in PFALs. Further studies are essential to determine what kinds of white light have more potential to boost the FBRUE of tomatoes than blue and red light, and whether blue light intensity has a qualitative threshold effect on FBRUE in tomatoes.

Data availability statement

The original contributions presented in the study are included in the article/Supplementary Material. Further inquiries can be directed to the corresponding author.

Author contributions

EG: Conceptualization, Funding acquisition, Methodology, Supervision, Writing – review & editing. XK: Conceptualization, Formal analysis, Investigation, Methodology, Validation, Visualization, Writing – original draft. HY: Writing – review & editing. SH: Writing – review & editing.

Funding

The author(s) declare financial support was received for the research, authorship, and/or publication of this article. This research was funded by the Program on Open Innovation Platform with Enterprises, Research Institute, and Academia, Japan Science and Technology Agency (JST-OPERA, JPMJOP1851). The tomato seed (TOMJPF00001(1)) was provided by the University of Tsukuba, Tsukuba Plant Innovation Research Center, through the National Bio-Resource Project (NBRP) of the AMED, Japan.

Conflict of interest

The authors declare that the research was conducted in the absence of any commercial or financial relationships that could be construed as a potential conflict of interest.

The author(s) declared that they were an editorial board member of Frontiers, at the time of submission. This had no impact on the peer review process and the final decision.

Publisher's note

Supplementary material

The Supplementary Material for this article can be found online at: https://www.frontiersin.org/articles/10.3389/fpls.2024.1393918/full#supplementary-material

References

Björkman, O. (1968). Carboxydismutase activity in shade-adapted and sun-adapted species of higher plants. *Physiol. Plant* 21, 1–10. doi: 10.1111/j.1399–3054.1968.tb07225.x

Bugbee, B. (2016). Toward an optimal spectral quality for plant growth and development: the importance of radiation capture. *Acta Hortic.* 1134, 1–12. doi: 10.17660/ActaHortic.2016.1134.1

Cavero, J., Plant, R. E., Shennan, C., Williams, J. R., Kiniry, J. R., and Benson, V. W. (1998). Application of epic model to nitrogen cycling in irrigated processing tomatoes under different management systems. *Agric. Syst.* 56, 391–414. doi: 10.1016/S0308-521X(96)00100-X

Chen, X., Yao, Q., Gao, X., Jiang, C., Harberd, N. P., and Fu, X. (2016). Shoot-to-root mobile transcription factor HY5 coordinates plant carbon and nitrogen acquisition. *Curr. Biol.* 26, 640–646. doi: 10.1016/j.cub.2015.12.066

Cockshull, K. E., Graves, C. J., and Cave, C. R. J. (1992). The influence of shading on yield of glasshouse tomatoes. *J. Hortic. Sci.* 67, 11–24. doi: 10.1080/00221589.1992.11516215

Cope, K. R., and Bugbee, B. (2013). Spectral effects of three types of white light-emitting diodes on plant growth and development: absolute versus relative amounts of blue light. *Hortscience.* 48, 504–509. doi: 10.21273/HORTSCI.48.4.504

Daughtry, C. S. T., Walthall, C. L., Kim, M. S., de Colstoun, E. B., and McMurtrey, J. E. (2000). Estimating corn leaf chlorophyll concentration from leaf and canopy reflectance. *Remote Sens. Environ.* 74, 229–239. doi: 10.1016/S0034-4257(00)00113-9

De Koning, A. N. M. (1993). Growth of a tomato crop. *Acta Hortic.* 328, 141–146. doi: 10.17660/ActaHortic.1993.328.11

Erdberga, I., Alsina, I., Dubova, L., Dūma, M., Sergejeva, D., Augšpole, I., et al. (2020). Changes in the biochemical composition of tomato fruit under the influence of illumination quality. *Key Eng. Mater.* 850, 172–178. doi: 10.4028/www.scientific.net/KEM.850.172

Goins, G. D., Yorio, N. C., Sanwo, M. M., and Brown, C. S. (1997). Photomorphogenesis, photosynthesis, and seed yield of wheat plants grown under red light-emitting diodes (LEDs) with and without supplemental blue lighting. *J. Exp. Bot.* 48, 1407–1413. doi: 10.1093/jxb/48.7.1407

Goto, E. (2003). Effects of light quality on growth of crop plants under artificial lighting. *Environ. Control Biol.* 41, 121–132. doi: 10.2525/ecb1963.41.121

Goto, E. (2011). Production of pharmaceutical materials using genetically modified plants grown under artificial lighting. *Acta Hortic.* 907, 45–52. doi: 10.17660/ActaHortic.2011.907.3

Graamans, L., Baeza, E., Van Den Dobbelsteen, A., Tsafaras, I., and Stanghellini, C. (2018). Plant factories versus greenhouses: comparison of resource use efficiency. *Agric. Syst.* 160, 31–43. doi: 10.1016/j.agsy.2017.11.003

Hoenecke, M., Bula, R., and Tibbitts, T. (1992). Importance of blue photon levels for lettuce seedlings grown under red-light-emitting diodes. *Hortic. Sci.* 27, 427–430. doi: 10.21273/HORTSCI.27.5.427

Hogewoning, S. W., Trouwborst, G., Maljaars, H., Poorter, H., Van Ieperen, W., and Harbinson, J. (2010). Blue light dose–responses of leaf photosynthesis, morphology, and chemical composition of Cucumis sativus grown under different combinations of red and blue light. *J. Exp. Bot.* 61, 3107–3117. doi: 10.1093/jxb/erq132

Ilić, Z. S., and Fallik, E. (2017). Light quality manipulation improves vegetabl quality at harvest and postharvest: a review. *Environ. Exp. Bot.* 139, 79–90. doi: 10.1016/j.envexpbot.2017.04.006

Izzo, L. G., Hay Mele, B. H., Vitale, L., Vitale, E., and Arena, C. (2020). The role of monochromatic red and blue light in tomato early photomorphogenesis and photosynthetic traits. *Environ. Exp. Bot.* 179, 104195. doi: 10.1016/j.envexpbot.2020.104195

Ji, Y., Nuñez Ocaña, D., Choe, D., Larsen, D. H., Marcelis, L. F. M., and Heuvelink, E. (2020). Far-red radiation stimulates dry mass partitioning to fruits by increasing fruit sink strength in tomato. *New Phytol.* 228, 1914–1925. doi: 10.1111/nph.16805

Ji, Y., Ouzounis, T., Courbier, S., Kaiser, E., Nguyen, P. T., Schouten, H. J., et al. (2019). Far-red radiation increases dry mass partitioning to fruits but reduces Botrytis cinerea resistance in tomato. *Environ. Exp. Bot.* 168, 103889. doi: 10.1016/j.envexpbot.2019.103889

Kalaitzoglou, P., Van Ieperen, W., Harbinson, J., van der Meer, M., Martinakos, S., Weerheim, K., et al. (2019). Effects of continuous or end-of-day far-red light on tomato plant growth, morphology, light absorption, and fruit production. *Front. Plant Sci.* 10. doi: 10.3389/fpls.2019.00322

Kato, K., Maruyama, S., Hirai, T., Hiwasa-Tanase, K., Mizoguchi, T., Goto, E., et al. (2011). A trial of production of the plant-derived high-value protein in a plant factory: photosynthetic photon fluxes affect the accumulation of recombinant miraculin in transgenic tomato fruits. *Plant Signal. Behav.* 6, 1172–1179. doi: 10.4161/psb.6.8.16373

Ke, X., Yoshida, H., Hikosaka, S., and Goto, E. (2021). Optimization of photosynthetic photon flux density and light quality for increasing radiation-use efficiency in dwarf tomato under LED light at the vegetative growth stage. *Plants (Basel).* 11, 121. doi: 10.3390/plants11010121

Ke, X., Yoshida, H., Hikosaka, S., and Goto, E. (2023). Photosynthetic photon flux density affects fruit biomass radiation-use efficiency of dwarf tomatoes under LED light at the reproductive growth stage. *Front. Plant Sci.* 14. doi: 10.3389/fpls.2023.1076423

Kong, Y., and Nemali, K. (2021). Blue and far-red light affect area and number of individual leaves to influence vegetative growth and pigment synthesis in lettuce. *Front. Plant Sci.* 12. doi: 10.3389/fpls.2021.667407

Kusuma, P., Pattison, P. M., and Bugbee, B. (2020). From physics to fixtures to food: current and potential LED efficacy. *Hortic. Res.* 7, 56. doi: 10.1038/s41438-020-0283-7

Li, J., Zhang, N., Luo, J., Yu, Q., Ai, W., Zhang, L., et al. (2019). Growth and biomass yield of 25 crops in the 4-subject 180-day integrated experiment. *Acta Astronaut.* 162, 336–343. doi: 10.1016/j.actaastro.2019.06.028

Liang, Y., Kang, C. Q., Kaiser, E., Kuang, Y., Yang, Q. C., and Li, T. (2021). Red/blue light ratios induce morphology and physiology alterations differently in cucumber and tomato. *Sci. Hortic.* 281, 109995. doi: 10.1016/j.scienta.2021.109995

Liu, X. Y., Chang, T. T., Guo, S. R., Xu, Z. G., and Li, J. (2011). Effect of different light quality of LED on growth and photosynthetic character in cherry tomato seedling. *Acta Hortic.* 907, 325–330. doi: 10.17660/ActaHortic.2011.907.53

Matsuda, R., Ohashi-Kaneko, K., Fujiwara, K., Goto, E., and Kurata, K. (2004). Photosynthetic characteristics of rice leaves grown under red light with or without supplemental blue light. *Plant Cell Physiol.* 45, 1870–1874. doi: 10.1093/pcp/pch203

McCree, K. J. (1971). The action spectrum, absorptance and quantum yield of photosynthesis in crop plants. *Agric. Meteorol.* 9, 191–216. doi: 10.1016/0002-1571(71)90022-7

McCree, K. J. (1972a). Test of current definitions of photosynthetically active radiation against leaf photosynthesis data. *Agric. Meteorol.* 10, 443–453. doi: 10.1016/0002-1571(72)90045-3

McCree, K. J. (1972b). Significance of enhancement for calculations based on the action spectrum for photosynthesis. *Plant Physiol.* 49, 704–706. doi: 10.1104/pp.49.5.704

Meissner, R., Jacobson, Y., Melamed, S., Levyatuv, S., Shalev, G., Ashri, A., et al. (1997). A new model system for tomato genetics. *Plant J.* 12, 1465–1472. doi: 10.1046/j.1365-313x.1997.12061465.x

Miao, Y. X., Wang, X. Z., Gao, L. H., Chen, Q. Y., and Qu, M. (2016). Blue light is more essential than red light for maintaining the activities of photosystem II and I and photosynthetic electron transport capacity in cucumber leaves. *J. Integr. Agric.* 15, 87–100. doi: 10.1016/S2095-3119(15)61202-3

Mochizuki, T., Onda, Y., Fujiwara, E., Wada, M., and Toyoshima, Y. (2004). Two independent light signals cooperate in the activation of the plastid psbD blue light-responsive promoter in Arabidopsis. *FEBS Lett.* 571, 26–30. doi: 10.1016/j.febslet.2004.06.052

Murakami, K., Matsuda, R., and Fujiwara, K. (2018). A mathematical model of photosynthetic electron transport in response to the light spectrum based on excitation energy distributed to photosystems. *Plant Cell Physiol.* 59, 1643–1651. doi: 10.1093/pcp/pcy085

Nanya, K., Ishigami, Y., Hikosaka, S., and Goto, E. (2012). Effects of blue and red light on stem elongation and flowering of tomato seedlings. *Acta Hortic.* 956, 261–266. doi: 10.17660/ActaHortic.2012.956.29

Ohyama, K., Kozai, T., Kubota, C., Chun, C., Hasegawa, T., Yokoi, S., et al. (2002). Coefficient of performance for cooling of a home-use air conditioner installed in a closed-type transplant production system. *J. Soc High Technol. Agric.* 14, 141–146. doi: 10.2525/jshita.14.141

Ouzounis, T., Heuvelink, E., Ji, Y., Schouten, H. J., Visser, R. G. F., and Marcelis, L. F. M. (2016). Blue and red LED lighting effects on plant biomass, stomatal conductance, and metabolite content in nine tomato genotypes. *Acta Hortic.* 1134, 251–258. doi: 10.17660/ActaHortic.2016.1134.34

Pennisi, G., Orsini, F., Blasioli, S., Cellini, A., Crepaldi, A., Braschi, I., et al. (2019). Resource use efficiency of indoor lettuce (Lactuca sativa L.) cultivation as affected by red:blue ratio provided by LED lighting. *Sci. Rep.* 9, 14127. doi: 10.1038/s41598–019-50783-z

Porra, R. J., Thompson, W. A., and Kriedemann, P. E. (1989). Determination of accurate extinction coefficients and simultaneous equations for assaying chlorophylls a and b extracted with four different solvents: verification of the concentration of chlorophyll standards by atomic absorption spectroscopy. *Bioenergetics.* 975, 384–394. doi: 10.1016/S0005-2728(89)80347-0

Quirino, B. F., Noh, Y. S., Himelblau, E., and Amasino, R. M. (2000). Molecular aspects of leaf senescence. *Trends Plant Sci.* 5, 278–282. doi: 10.1016/S1360-1385(00)01655-1

Scholberg, J., McNeal, B. L., Jones, J. W., Boote, K. J., Stanley, C. D., and Obreza, T. A. (2000). Growth and canopy characteristics of field-grown tomato. *Agron. J.* 92, 152–159. doi: 10.2134/agronj2000.921152x

Snowden, M. C., Cope, K. R., and Bugbee, B. (2016). Sensitivity of seven diverse species to blue and green light: interactions with photon flux. *PloS One* 11, e0163121. doi: 10.1371/journal.pone.0163121

Sood, S., Tyagi, A. K., and Tripathy, B. C. (2004). Inhibition of photosystem I and photosystem II in wheat seedlings with their root–shoot transition zones exposed to red light. *Photosynth. Res.* 81, 31–40. doi: 10.1023/B:PRES.0000028337.72340.3a

Sun, H. J., Uchii, S., Watanabe, S., and Ezura, H. (2006). A highly efficient transformation protocol for Micro-Tom, a model cultivar for tomato functional genomics. *Plant Cell Physiol.* 47, 426–431. doi: 10.1093/pcp/pci251

Terashima, I., Fujita, T., Inoue, T., Chow, W. S., and Oguchi, R. (2009). Green light drives leaf photosynthesis more efficiently than red light in strong white light: revisiting the enigmatic question of why leaves are green. *Plant Cell Physiol.* 50, 684–697. doi: 10.1093/pcp/pcp034

Thwe, A. A., Kasemsap, P., Vercambre, G., Gay, F., Phattaralerphong, J., and Gautier, H. (2020). Impact of red and blue nets on physiological and morphological traits, fruit yield and quality of tomato (Solanum lycopersicum Mill.). *Sci. Hortic.* 264, 109185. doi: 10.1016/j.scienta.2020.109185

Tsao, J. Y., Coltrin, M. E., Crawford, M. H., and Simmons, J. A. (2010). Solid-state lighting: an integrated human factors, technology, and economic perspective. *Proc. IEEE.* 98, 1162–1179. doi: 10.1109/JPROC.2009.2031669

van Gelderen, K., Kang, C., Paalman, R., Keuskamp, D., Hayes, S., and Pierik, R. (2018). Far-red light detection in the shoot regulates lateral root development through the HY5 transcription factor. *Plant Cell.* 30, 101–116. doi: 10.1105/tpc.17.00771

Wheeler, R. M., Mackowiak, C. L., Stutte, G. W., Yorio, N. C., Ruffe, L. M., Sager, J. C., et al. (2008). Crop productivities and radiation use efficiencies for bioregenerative life support. *Adv. Space Res.* 41, 706–713. doi: 10.1016/j.asr.2007.06.059

Yorio, N. C., Goins, G. D., Kagie, H. R., Wheeler, R. M., and Sager, J. C. (2001). Improving spinach, radish, and lettuce growth under red light-emitting diodes (LEDs) with blue light supplementation. *Hortscience.* 36, 380–383. doi: 10.21273/HORTSCI.36.2.380

Zhen, S., and van Iersel, M. W. (2017). Far-red light is needed for efficient photochemistry and photosynthesis. *J. Plant Physiol.* 209, 115–122. doi: 10.1016/j.jplph.2016.12.004

frontiers | Frontiers in Plant Science

TYPE Original Research
PUBLISHED 01 August 2024
DOI 10.3389/fpls.2024.1397948

OPEN ACCESS

EDITED BY
Meijian Yang,
Cornell University, United States

REVIEWED BY
Ningbo Cui,
Sichuan University, China
Jiameng Lai,
Cornell University, United States

*CORRESPONDENCE
Yuping Lv
lvyuping@yzu.edu.cn

RECEIVED 08 March 2024
ACCEPTED 08 July 2024
PUBLISHED 01 August 2024

CITATION
Lv Y, Gu L, Man R, Liu X and Xu J (2024) Response of stomatal conductance, transpiration, and photosynthesis to light and CO_2 for rice leaves with different appearance days. *Front. Plant Sci.* 15:1397948. doi: 10.3389/fpls.2024.1397948

Response of stomatal conductance, transpiration, and photosynthesis to light and CO_2 for rice leaves with different appearance days

Yuping Lv [1*], Linhui Gu [1], Runze Man [1], Xiaoyin Liu [2] and Junzeng Xu [2]

[1]College of Hydraulic Science and Engineering, Yangzhou University, Yangzhou, Jiangsu, China, [2]College of Agricultural Science and Engineering, Hohai University, Nanjing, Jiangsu, China

To investigate the dynamics of stomata, transpiration, and photosynthesis under varying light intensities and CO_2 conditions during leaf development, the light response and CO_2 response of stomatal conductance (g_{sw}), transpiration rate (T_r), and net photosynthetic rate (P_n) were observed for rice leaves at different days after leaf emergence (DAE). The results showed that (1) as photosynthetically active radiation (PAR) increased, leaf g_{sw}, T_r, and P_n initially increased rapidly and linearly, followed by a more gradual rise to maximum values, and then either stabilized or showed a declining trend. The maximum g_{sw}, T_r, and P_n were smaller and occurred earlier for old leaves than for young leaves. The g_{sw}, T_r, and P_n all exhibited a linear decreasing trend with increasing DAE, and the rate of decrease slowed down with the reduction in PAR; (2) as the CO_2 concentration (C_a) increased, g_{sw} and T_r decreased gradually to a stable minimum value, while P_n increased linearly and slowly up to the maximum and then kept stable or decreased. The g_{sw}, T_r, and P_n values initially kept high and then decreased with the increase of DAE. These results contribute to understanding the dynamics in g_{sw}, T_r, and P_n during rice leaf growth and their response to varied light and CO_2 concentration conditions and provide mechanistic support to estimate dynamic evapotranspiration and net ecosystem productivity at field-scale and a larger scale in paddy field ecosystems through the upscaling of leaf-level stomatal conductance, transpiration, and photosynthesis.

KEYWORDS

photosynthetic rate, transpiration rate, stomatal conductance, light response, CO_2 response, leaf with different appearance days

1 Introduction

Stomata play a crucial role in regulating water loss through transpiration and carbon dioxide (CO_2) uptake for photosynthesis, significantly influencing water use efficiency and plant productivity (Lawson and Vialet-Chabrand, 2019). Understanding the responses of stomatal conductance (g_{sw}), transpiration rate (T_r), and net photosynthetic rates (P_n) to environmental factors is essential to assess evapotranspiration and net ecosystem productivity in agroecosystems (Bellasio, 2023; Konieczna et al., 2023; Lv et al., 2024). Research into the intricate dynamics of g_{sw}, T_r, and P_n across different environments improves predictive abilities and refines strategies for water utilization and agricultural optimization, which contributes to developing sustainable agricultural strategies aimed at maximizing productivity while minimizing water consumption (Elfadl and Luukkanen, 2006; Katul, 2023; Wu et al., 2023).

Several factors, including crop canopy structure (leaf area index, leaf tilt angle, etc.), leaf nutrient elements (nitrogen, chlorophyll, etc.), soil water-thermal conditions, and meteorological factors (solar radiation, CO_2 concentration, temperature, atmospheric humidity, etc.), have been widely studied for their influence on leaf g_{sw}, T_r, and P_n (Chen et al., 2011; Xu et al., 2015; Liu et al., 2019). The impact of light and CO_2, as the primary energy source and substrate for plant photosynthesis, on leaf g_{sw}, T_r, and P_n have been extensively studied (Baroli et al., 2008, Li F, et al., 2023, Yi et al., 2023). With increased light intensity and CO_2 concentration, leaf P_n initially increase rapidly and then slowly up to the maximum, followed by a declining trend or a stable state, which have been universally acknowledged on various crops (Kabir et al., 2023). Yu et al. (2004) reported that winter wheat g_{sw} decreases with increased CO_2 concentration and increases with increased light intensity, Marín et al. (2014) stated that tobacco T_r is higher at high than at low light intensities, and Kirschbaum and McMillan (2018) showed that increasing atmospheric CO_2 concentrations reduce canopy transpiration. Additionally, the duration (such as cumulative time, thermal time accumulation, or radiant heat accumulation) after leaf emergence also leads to changes in leaf g_{sw}, T_r, and P_n due to changes in both leaf traits (Legner et al., 2014; Scoffoni et al., 2016; Hirooka et al., 2018) and biomass sink–source relations (Kitajima et al., 2002; Xie and Luo, 2003) along with leaf aging from leaf appearance to senescence—for example, Vos and Oyarzun (1987) reported that potato P_n and g_{sw} decreased at near-saturating irradiance with leaf age, Echer and Rosolem (2015) stated that cotton P_n and g_{sw} decreased in the order of 15-, 30-, 45-, and 60-day-old leaves. Locke and Ort (2014) showed that soybean P_n decreased at a specific light intensity. However, the response of g_{sw}, T_r, and P_n to light and CO_2, respectively, are rarely reported for rice leaves with different durations after emergence.

As the most important staple food crop in the world, the three-dimensional canopy structure of rice, describing the elongation process and spatial distribution of various organs (leaves, leaf sheaths, stems, and panicles), has been widely studied (Watanabe et al., 2005; Song et al., 2013). Temporal leaf evapotranspiration and photosynthesis with detailed 3D representation of canopy architecture are necessary to estimate seasonal variation in evapotranspiration and ecosystem productivity at field-scale and a larger scale in paddy field ecosystems, which are often achieved through the upscaling of leaf-level stomatal conductance, transpiration, or photosynthesis (Van der Zande et al., 2009; Chang et al., 2019; Shi et al., 2019). Measured light-saturated rice P_n reaches a maximum at the fully developed stage and then declines gradually as leaves senesce (Wang et al., 2009) or decreases from the top (young leaves) to the base (old leaves) within the rice canopy (Murchie et al., 2002; Jin et al., 2004). The response of P_n to light and CO_2 also changes as rice leaves age (Xu et al., 2019). Thus, it is well known that g_{sw} and T_r, under different light density and CO_2 concentration conditions, also vary among leaves with various durations after leaf emergence. However, the response of g_{sw} and T_r to light and CO_2 is rarely reported for rice leaves with different durations after leaf emergence.

The southern regions of the Yangtze River constitute the primary rice cultivation area in China (You et al., 2011). Understanding how the duration after leaf emergence affects P_n, g_{sw}, and T_r under different light density and CO_2 concentration conditions is essential to unravel the physiological mechanisms of crop transpiration and photosynthesis and to assess seasonal changes in evapotranspiration and ecosystem productivity under different environmental conditions. Therefore, this study aimed to elucidate and analyze the influence of different days after leaf emergence (DAE) on P_n, g_{sw}, and T_r as well as their quantitative relationships with DAE. This will help to understand the dynamic changes in P_n, g_{sw}, and T_r and provide a reference to clarify the mechanism of transpiration and photosynthesis during the growth process of rice leaves.

2 Materials and methods

The Japonica Rice NJ46 was transplanted with 13 cm × 25 cm hill spacing on July 1, 2017 and harvested on October 26, 2017 in Kunshan, East China (31°15′50″ N, 120°57′43″ E) under field conditions. The rice field extended approximately 200 m in all directions. The region has a subtropical monsoon climate, with average temperature, mean relative humidity, and seasonal precipitation of 25.9°C, 76.9%, and 450.8 mm during the 2017 rice season. Irrigation, fertilizer, and pesticides were applied according to local farming practice (Guo et al., 2017; Li JP, et al., 2023; Lv et al., 2024). To record DAE for subsequent data collection, three latest-emerged leaves on approximately 20 rice plants were tagged at 2-day intervals during tillering, jointing, and booting stages. Using a photosynthesis system (LI- 6800; LI-COR, Lincoln, NE, USA) equipped with a red/blue LED light source (LI-6800–02B) and a charged CO_2 cartridge (CO_2 source), the response of leaf stomatal conductance (g_{sw}), transpiration rate (T_r), and net photosynthetic rate (P_n) to photosynthetically active radiation (PAR) and atmospheric CO_2 concentration (C_a) were measured for tagged leaves at various DAE values at booting and heading stages. The chamber temperature and relative humidity were set as 30°C and 70%, and the measurements were conducted under saturated soil moisture conditions at 8:00–12:00 a.m. on randomly selected sunny days during jointing and heading stages. For the response of g_{sw}, T_r, and

P_n to PAR, the C_a and PAR were set at 400 μmol mol^{-1} (approximate atmospheric CO_2 concentration) and 2,000 μmol m^{-2} s^{-1}, and such a condition was maintained for 15 min for adaptation and stabilization of leaf photosynthesis prior to measurement. Then, leaf g_{sw}, T_r, and P_n were recorded automatically at 120-s intervals at 19 PAR levels (in decreasing order of 2,000, 1,950, 1,900, 1,800, 1,600, 1,400, 1,200, 1,000, 800, 600, 400, 300, 200, 150, 100, 70, 50, 30, and 0 μmol m^{-2} s^{-1}). For the response of g_{sw}, T_r, and P_n to C_a, the C_a and PAR were set at 400 μmol mol^{-1} and 1,600 μmol m^{-2} s^{-1} [slightly lower than saturation light intensity (Xu et al., 2019) to prevent photo inhibition], and leaf g_{sw}, T_r, and P_n were recorded automatically at 120-s intervals at 14 C_a levels (in the order of 400, 300, 200, 100, 50, 400, 400, 500, 600, 800, 1,000, 1,300, 1,500, and 1,800 μmol mol^{-1}) after a 15-min pre-treatment. Totally, 37 response curves to PAR and 24 curves to C_a were measured, evenly distributed across DAE values ranging from 3 to 55.

3 Results

3.1 Light response of stomatal conductance, transpiration, and photosynthesis for rice leaves with different days after leaf emergence

The g_{sw}, T_r, and P_n values were influenced by both the DAE and PAR (Figure 1). Under dark conditions (PAR = 0 μmol m^{-2} s^{-1}), leaves at different DAE maintained relatively low g_{sw} and T_r and negative P_n. As PAR increased, g_{sw}, T_r, and P_n initially exhibited a linear and rapid increase, and then the increase rate (indicated by dg_{sw}/dPAR, dT_r/dPAR, and dP_n/dPAR) gradually slowed down. When PAR reached a certain light intensity (referred to the saturation light intensity for g_{sw}, T_r, and P_n, respectively), g_{sw}, T_r, and P_n reached their maximum values. Subsequently, with further increases in PAR, there was a declining trend (for leaves at DAE lower than approximately 40 days) or a stable state (for leaves at *DAE* higher than approximately 40 days). The g_{sw}, T_r, and P_n, as well as their increase rates with increasing PAR among leaves at different DAE, exhibited similar values under low PAR conditions and showed more pronounced differences as PAR increased.

Both the maximum g_{sw} and its corresponding saturation light intensity decreased with increasing DAE, with older leaves reaching maximum g_{sw} at lower PAR conditions (Figure 1A). The maximum g_{sw} were 0.517, 0.456, 0.394, 0.364, 0.275, and 0.221 mol m^{-2} s^{-1} for leaves at *DAE* of 1–10, 11–20, 21–30, 31–40, 41–50, and 51–60 days. Young leaves (low DAE) maintained high g_{sw}, facilitating photosynthesis and transpiration under high PAR conditions. The light response curves of leaf T_r were distinctly influenced by DAE (Figure 1B). The T_r at specific PAR values, as well as the saturation light intensity when T_r reached the maximum, considerably decreased with increasing DAE. The average P_n values, respectively, were -1.173, -1.141, -0.990, -0.720, -0.519, and -0.462 μmol m^{-2} s^{-1} for leaves at DAE of 1–10, 11–20, 21–30, 31–40, 41–50, and 51–60 days under PAR = 0 μmol m^{-2} s^{-1} conditions (Figure 1C). The negative P_n observed under no-light conditions represented leaf respiration capacity. The decreased absolute value of P_n with increasing DAE implied that the leaf respiration rate attenuated with an increase in DAE, attributable to the exuberant leaf respiration for young leaves. The maximum P_n values were 32.263, 31.959, 27.645, 22.164, 15.676, and 12.582 μmol m^{-2} s^{-1}, respectively, for leaves at DAE of 1–10, 11–20, 21–30, 31–40, 41–50, and 51–60 days. Young leaves sustained high P_n under high PAR conditions and exhibited vigorous physiological growth.

In any PAR condition, leaf g_{sw} linearly decreased with an increase in DAE, and the decrease rate (indicated by the absolute value of the slope of the linear regression line) increased with enhanced PAR (Figure 2). Under PAR of 0 and 100 μmol m^{-2} s^{-1} conditions, DAE had a negligible impact on leaf g_{sw}, and the leaves consistently maintained a lower g_{sw} value. Under PAR of 200, 400, and 800 μmol m^{-2} s^{-1} conditions, the slopes of g_{sw} against DAE were -0.0018, -0.0038, and -0.0057, respectively; the leaf g_{sw} significantly decreased with increasing DAE, and there are noticeable differences in both leaf g_{sw} and the decrease rate among different PAR intensities. Under conditions of PAR higher than 1,200 μmol m^{-2} s^{-1}, the decrease rate in leaf g_{sw} with DAE was approximately 0.007, and leaf g_{sw} ranged from 0.127 to 0.659 mmol m^{-2} s^{-1}. Leaf g_{sw} significantly decreased with increasing DAE, but the differences in both leaf g_{sw} and the decrease rate were less pronounced among different *PAR* intensities.

Consistent with the variation in leaf g_{sw}, leaf T_r linearly decreased with an increase in DAE under any PAR condition, and the decrease rate increased with enhanced PAR (Figure 3). Under PAR conditions lower than 200 μmol m^{-2} s^{-1}, leaf T_r external environmental demand for leaf evaporation is weak, and leaf T_r remains consistently low, with no significant decrease in leaf T_r with increasing DAE. Under PAR intensities of 400, 800, 1,200, 1,600, and 2,000 μmol m^{-2} s^{-1}, leaf T_r respectively ranged from 1.015 to 4.265, 1.724 to 5.359, 1.938 to 7.790, 2.221 to 7.677, and 2.819 to 9.072 mmol m^{-2} s^{-1}, and the slopes of leaf T_r against DAE, respectively, were -0.0325, -0.0464, -0.0666, -0.0771, and -0.0988. Under high PAR conditions (exceeding 400 μmol m^{-2} s^{-1}), leaf T_r significantly decreased, and the decrease rate becomes more pronounced with increasing PAR. Younger leaves can maintain higher T_r under high light conditions to expedite transpirational cooling, enabling the leaves to remain within the optimal temperature range for physiological activities. As the leaves aged, physiological activity decreased, and leaf adaptability to light intensity decreased, resulting in lower T_r under high light conditions.

Under no-light conditions (PAR = 0 μmol m^{-2} s^{-1}), leaf P_n was negative, and P_n linearly increased with DAE (Figure 4). The leaves were unable to perform photosynthesis under zero light intensity, and leaves with low DAE exhibited a stronger metabolic activity, reflected in a higher respiration rate (manifested as negative values). Under a PAR of 100 μmol m^{-2} s^{-1}, leaf P_n remained at approximately 3.6 μmol m^{-2} s^{-1}, with no significant change in leaf P_n with increasing DAE. Under PAR conditions higher than 200 μmol m^{-2} s^{-1}, leaf P_n significantly decreased with increasing DAE, and the magnitude of decrease became more pronounced with enhanced PAR.

10.3389/fpls.2024.1397948

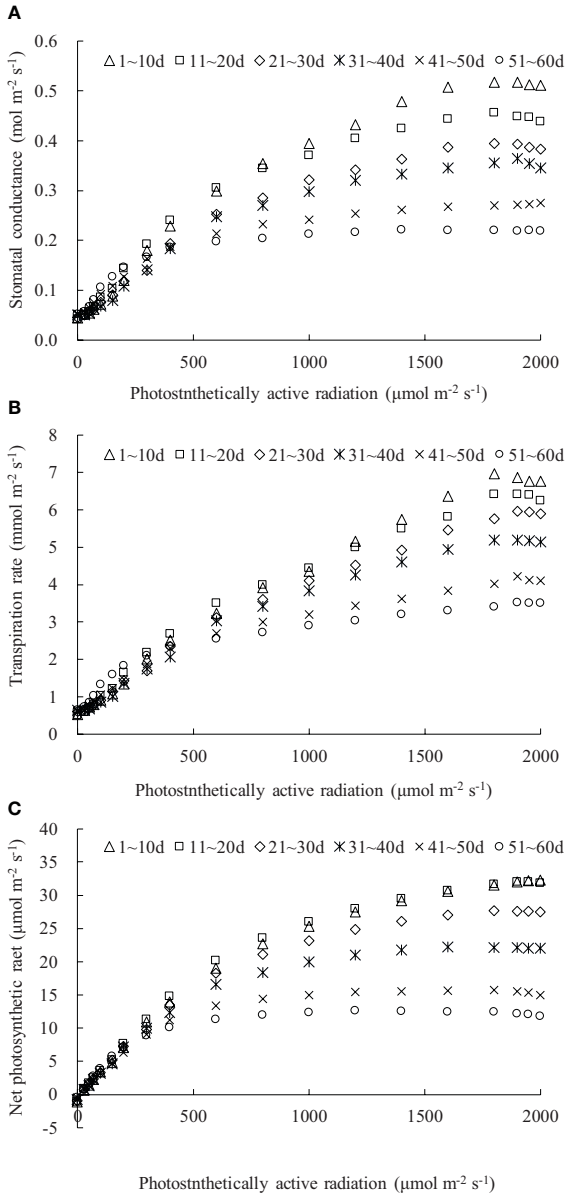

FIGURE 1
(A–C) The light response of stomatal conductance, transpiration rate, and net photosynthetic rate for rice leaves with different ranges of days after leaf emergence ("*m*~*n* d" in the legend indicates the days after leaf emergence; ranges from *m* to *n*).

3.2 CO_2 response of stomatal conductance, transpiration and photosynthesis for rice leaves with different days after emergence

The C_a considerably influenced g_{sw}, T_r, and P_n in rice leaves (Figure 5). The diffusion of CO_2 from the outside to the inside of the leaf primarily relied on stomata; an increase in C_a led to a reduction in leaf g_{sw}, followed by a decrease in leaf T_r (Figures 5A, B). Leaf g_{sw} and T_r gradually decreased with increasing C_a and DAE, and their decreasing rate slowed down as C_a increased. When C_a increased to approximately 1,500 μmol mol^{-1}, leaf g_{sw} and T_r stabilized at the minimum values. Under the C_a range of 0 to 1,800 μmol mol^{-1}, leaf g_{sw} respectively ranged from 0.103 to 0.693, 0.171 to 0.411, 0.139 to 0.458, 0.133 to 0.404, 0.135 to 0.247, and 0.104 to 0.165 mol m^{-2} s^{-1}, and leaf T_r respectively ranged from 1.426 to 7.895, 2.694 to 5.622, 2.431 to 6.401, 2.423 to 5.912, 2.326 to 3.872, and 1.615 to 2.514 mmol m^{-2} s^{-1} for DAE of 1–10, 11–20, 21–30, 31–40, 41–50, and 51–60 days. Both leaf g_{sw} and T_r decreased with increasing DAE under specific C_a conditions. Leaves at smaller DAE maintained higher g_{sw} and T_r at low C_a, indicating that vigorously growing leaves sustained higher g_{sw} for physiological processes (such as transpiration and photosynthesis) and exhibited robust physiological activity even under low C_a conditions. There was a relatively small difference in leaf g_{sw} and T_r among leaves at different DAE at high C_a concentrations. Leaves with larger DAE (41–50 and 51–60 days) showed limited sensitivity of g_{sw} and T_r to changes in C_a concentration, maintaining consistently lower values regardless of the variations in C_a concentration.

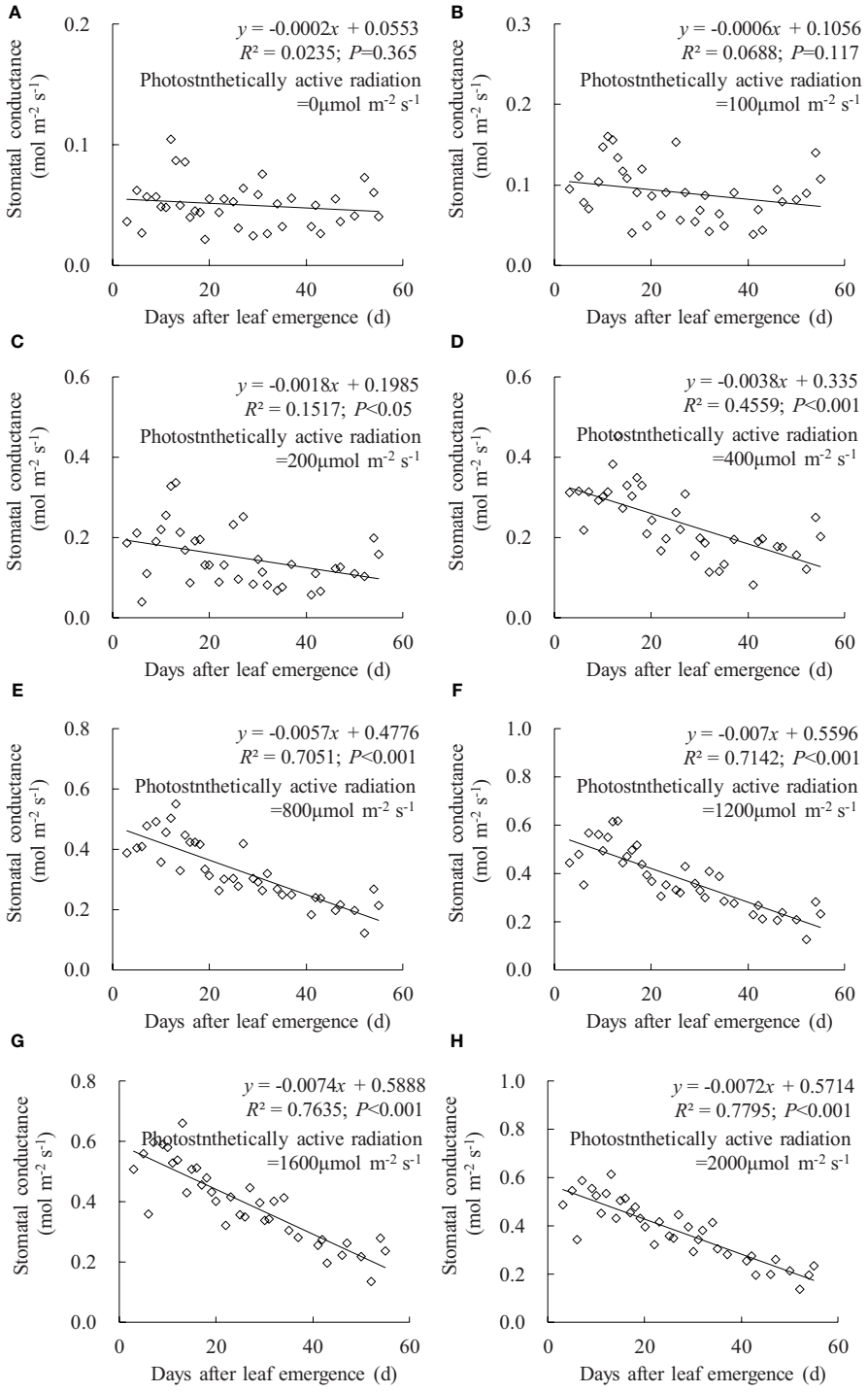

FIGURE 2
(A–H) Impact of days after leaf emergence on stomatal conductance under different photosynthetically active radiation conditions.

The leaf P_n at different DAE exhibited a similar trend with changing atmospheric C_a (Figure 5C). The increase rate of leaf P_n (indicated by dP_n/dC_a) gradually slowed down with increasing DAE. As C_a increased, rice leaf P_n initially increased rapidly in a linear fashion, and the increase rate subsequently decreased, and leaf P_n gradually reached its maximum value, resulting in either a stable or a declining P_n. Under CO_2 concentrations lower than 50 μmol mol^{-1}, leaf photosynthesis was constrained by the available CO_2 concentration; larger stomatal conductance could not compensate for the impact of low CO_2 concentration, resulting in lower leaf photosynthesis than respiration, leading to CO_2 emission (negative P_n values). Within the C_a range of 0 to 1,800 μmol mol^{-1}, leaf P_n ranged from -0.437 to 41.866, -0.419 to 39.614, -0.491 to 40.345, -0.639 to 29.344, -0.485 to 19.135, and -0.504 to 10.657 μmol m^{-2} s^{-1} for DAE of 1–10, 11–20, 21–30, 31–40, 41–50, and 51–60 days, respectively. As DAE decreases, both the peak value of P_n

10.3389/fpls.2024.1397948

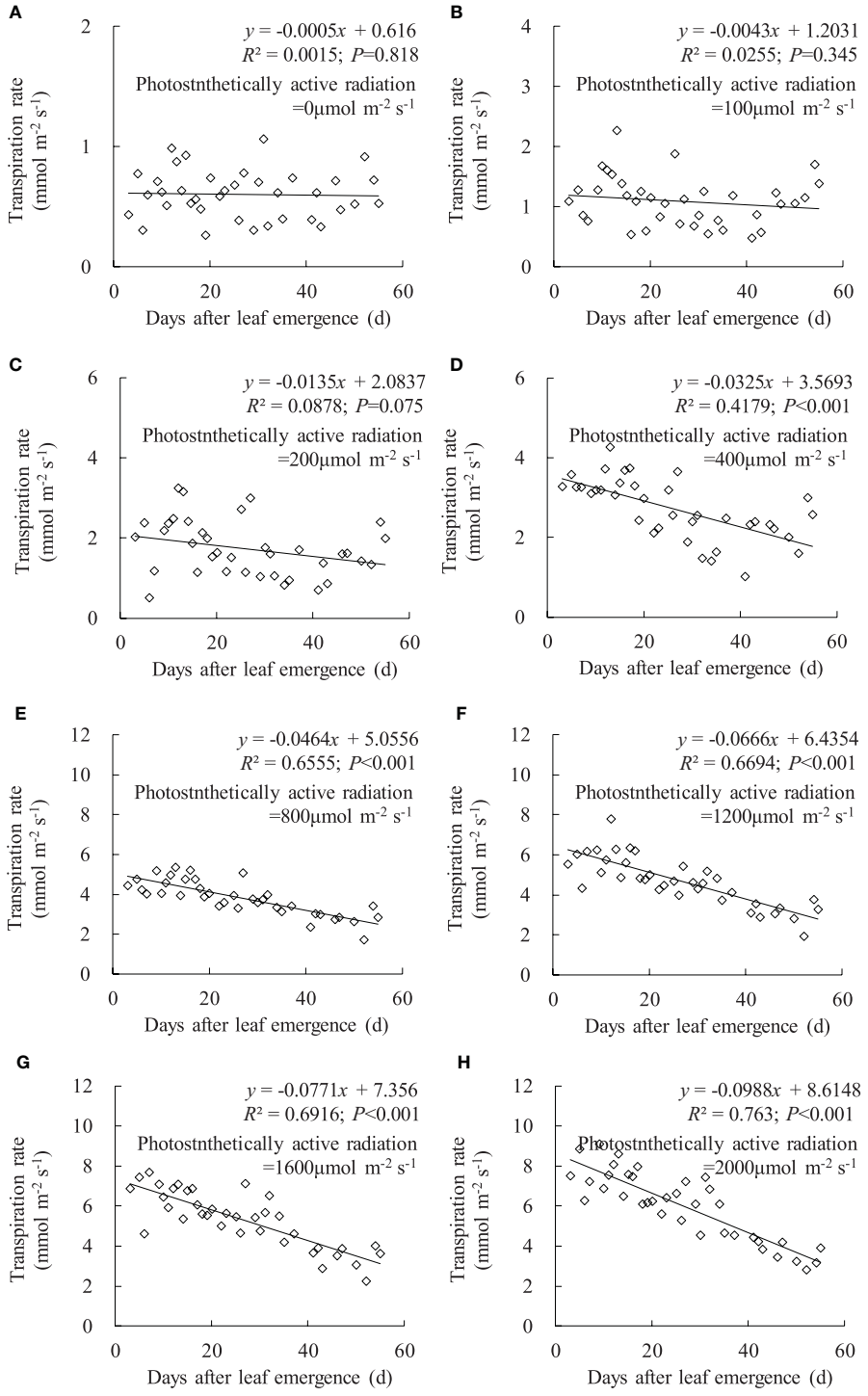

FIGURE 3
(A–H) Impact of days after leaf emergence on transpiration rate under different photosynthetically active radiation conditions.

and the carboxylation rate (the slope of the linear segment) increased, indicating that leaves with smaller DAE possessed a stronger photosynthetic capability.

The relationships between g_{sw}, T_r, and P_n and DAE could be fitted using quadratic regression equations (Figures 6–8). Under C_a of 50, 200, 400, 600, 1,000, and 1,800 μmol mol^{-1}, leaf g_{sw} respectively ranged from 0.132 to 0.535, 0.122 to 0.474, 0.134 to 0.478, 0.129 to 0.390, 0.111 to 0.316, and 0.046 to 0.224 mmol m^{-2} s^{-1}. Leaf g_{sw} decreased along with increasing C_a. As DAE increased, leaf g_{sw} initially remained at higher values and subsequently

10.3389/fpls.2024.1397948

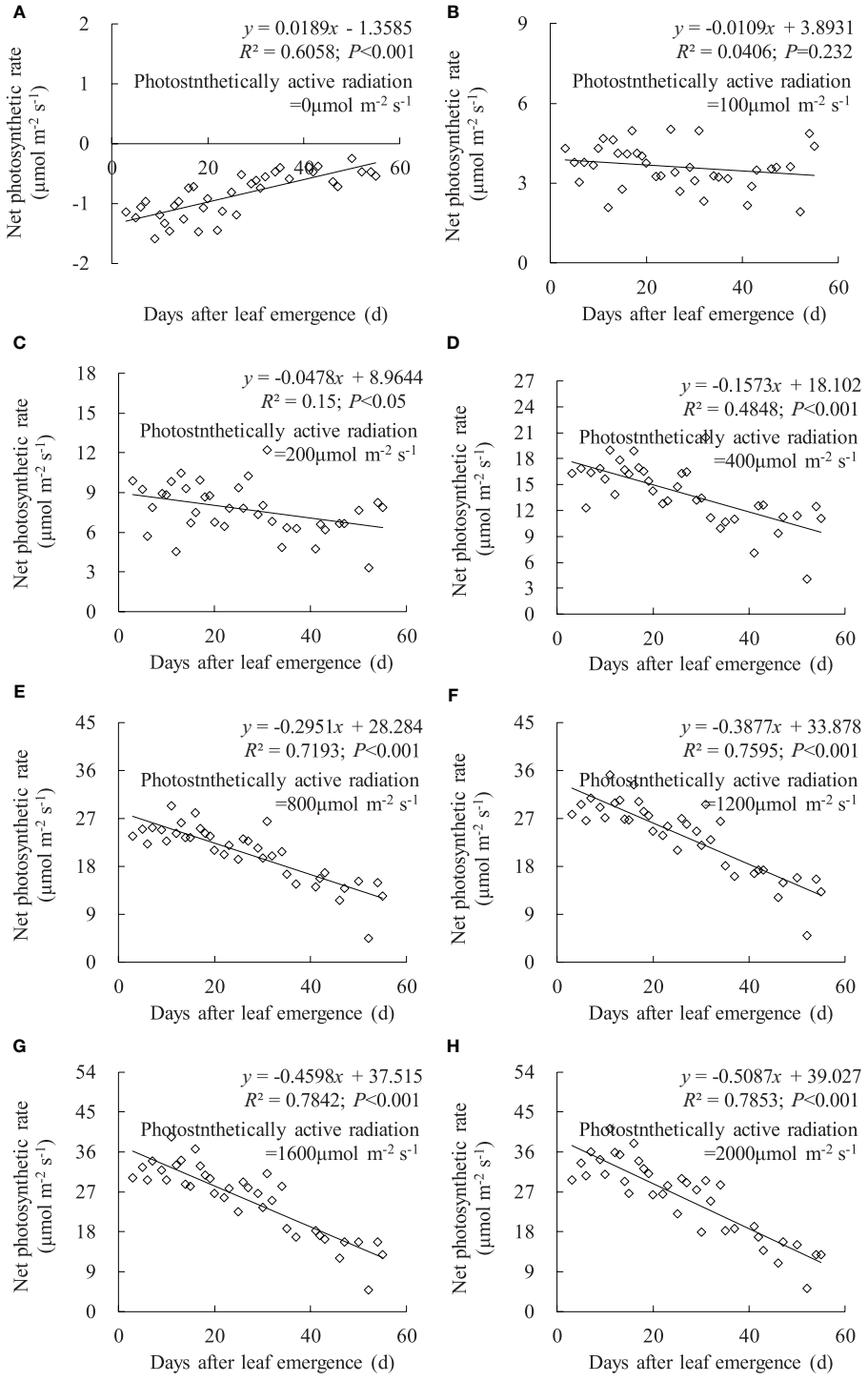

FIGURE 4
(A–H) Impact of days after leaf emergence on net photosynthetic rate under different photosynthetically active radiation conditions.

gradually decreased. Young leaves (small DAE) maintained higher g_{sw} to facilitate physiological activities at low C_a conditions. High CO_2 concentrations (especially at a C_a of 1,800 μmol mol^{-1}) inhibited stomatal aperture, and the leaf g_{sw} at different DAE consistently remained at lower values.

Leaf T_r exhibited a similar trend to leaf g_{sw} (Figure 7). Under C_a of 50, 200, 400, and 600 μmol mol^{-1}, leaf T_r for different DAE respectively ranged from 1.876 to 7.007, 1.743 to 7.810, 1.905 to 6.467, and 1.815 to 6.202 mmol m^{-2} s^{-1}. Leaf T_r decreased with increasing C_a, and rice leaves at small DAE maintained a higher T_r at low C_a. As DAE increased, leaf T_r initially remained at higher values and then gradually decreased. At C_a of 1,000 and 1,800 μmol mol^{-1}, the impact of DAE on T_r diminished, and high CO_2 concentration inhibited stomatal aperture and transpiration.

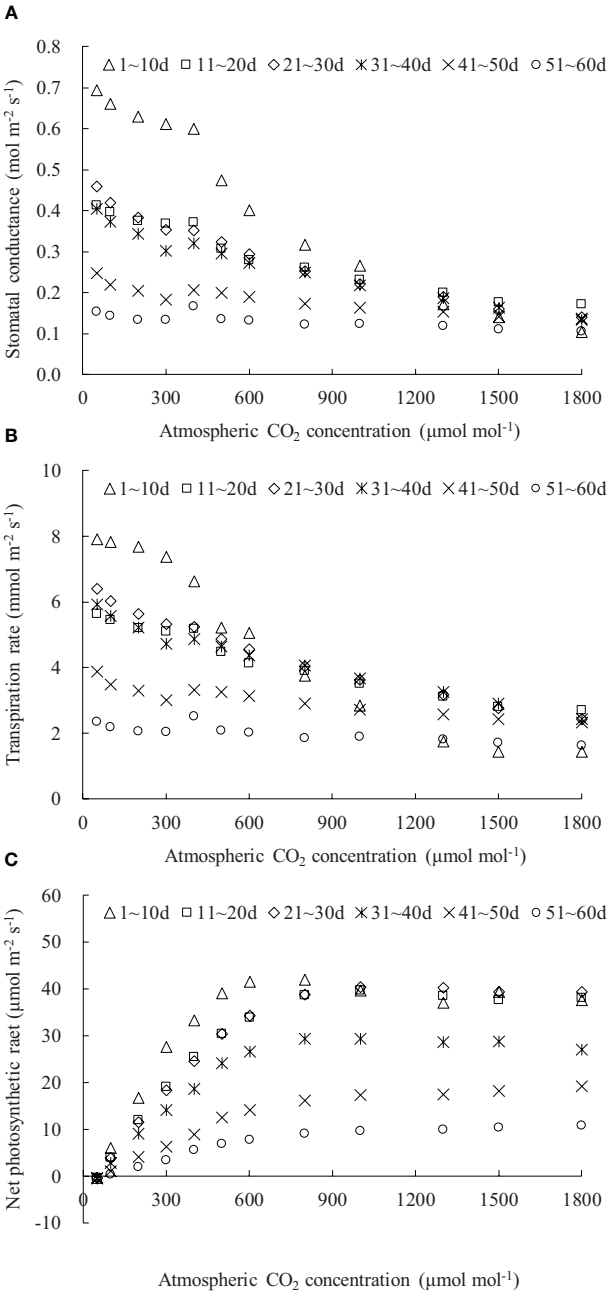

FIGURE 5
(A–C) CO_2 response of stomatal conductance, transpiration rate, and net photosynthetic rate of rice leaves with different ranges of days after leaf emergence ("*m*~*n* d" in the legend indicates the days after leaf emergence; ranges from *m* to *n*).

The variation in leaf P_n with DAE under different C_a is depicted in Figure 8. At C_a of 50 μmol mol^{-1}, the leaf P_n at different DAE consistently remained at approximately -0.5 μmol m^{-1} s^{-1}. This is primarily attributed to the limitation of photosynthetic capacity by low CO_2 concentrations, where leaf respiration exceeded photosynthesis, resulting in CO_2 release. At C_a of 200, 400, 600, 1,000, and 1,800 μmol mol^{-1}, leaf P_n respectively ranged from 1.690 to 13.114, 5.484 to 27.375, 6.694 to 41.858, 8.576 to 47.116, and 9.304 to 47.137. Leaf P_n rapidly increased with rising C_a, reaching its peak at approximately 1,000 μmol mol^{-1} C_a, with no considerable difference between 1,000 and 1,800 μmol mol^{-1} C_a. When C_a exceeded 200 μmol mol^{-1}, leaf P_n remained relatively high at smaller DAE and gradually decreased with further increases in DAE. This indicated that vigorously growing leaves exhibited higher P_n, and leaf photosynthetic capacity decreased as leaves age, leading to a decline in carbon assimilation.

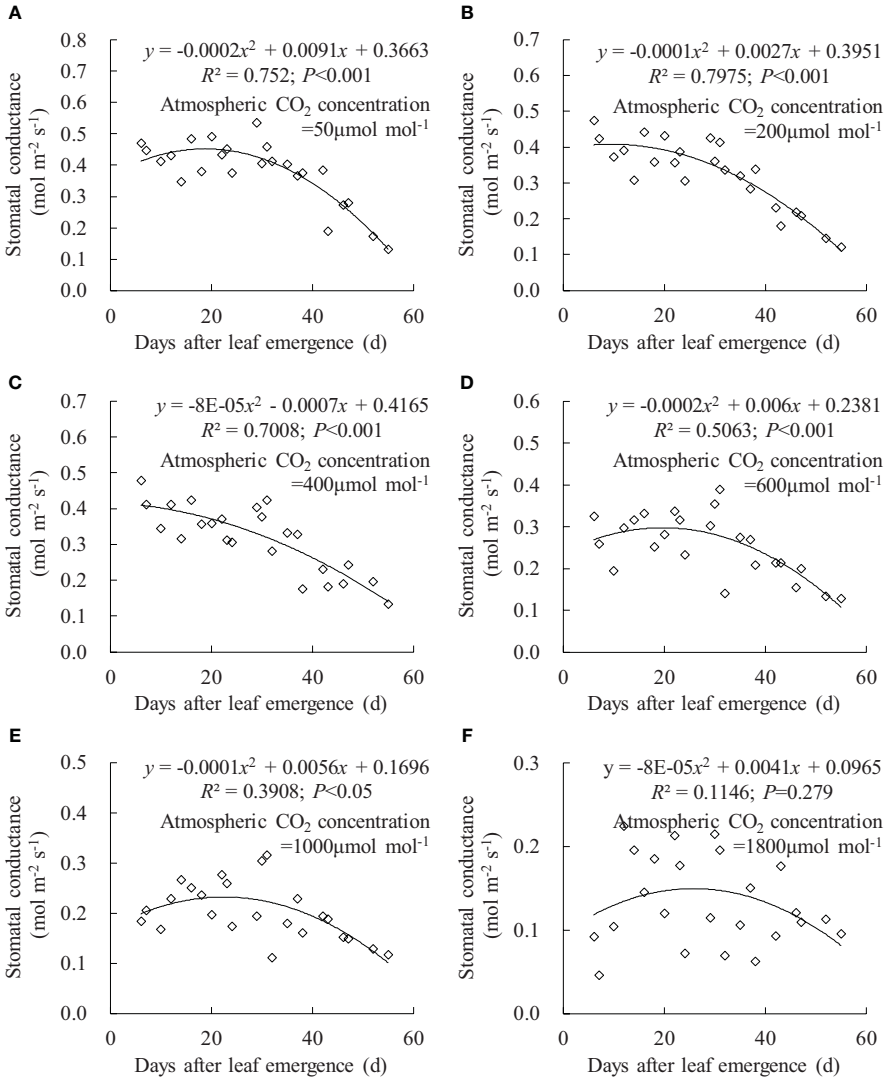

FIGURE 6
(A–F) Impact of days after leaf emergence on stomatal conductance under different atmospheric CO_2 concentration conditions.

4 Discussion

4.1 Effect of days after leaf emergence on the light response

As PAR was enhanced, leaf g_{sw}, T_r, and P_n initially exhibited a linear and rapid increase, followed by a gradual slowdown in the increase rate, eventually reaching a maximum value and then stabilizing or slightly decreasing thereafter (Figure 1). Similar trends have been observed in the flag leaves of winter wheat (Inoue et al., 2004; Carmo-Silva et al., 2017). Under no-light conditions *(PAR* = 0 μmol m^{-2} s^{-1}), the leaves were unable to undergo photosynthesis, resulting in metabolic CO_2 emission (with leaf P_n showing as a negative value). Leaves at smaller DAE released more CO_2 due to their vigorous metabolic activity (Pantin et al., 2012). Under low-light conditions, limited atmospheric evaporative capacity and insufficient PAR for photosynthesis led to lower g_{sw}, T_r, and P_n regardless of the variations in DAE. As PAR intensified, leaf stomatal opening widened, leading to an increase in g_{sw}. Larger stomatal apertures allowed a greater influx of CO_2 (providing an ample supply for leaf photosynthesis) and output of water vapor through the stomata; thus, leaf P_n and T_r increased. Simultaneously, the increased atmospheric evaporative capacity caused by enhanced PAR also resulted in higher T_r. Leaves with larger DAE reached the light saturation point earlier, and g_{sw}, T_r, and P_n, under saturated light conditions, decreased with increasing DAE, suggesting that young leaves could maintain larger stomatal apertures for efficient transpiration and photosynthesis under high light intensity (high T_r and P_n). As the leaves aged, their adaptation to high light weakened, and leaves with larger DAE could not fully utilize high light intensity for photosynthesis.

Under a specific PAR condition, g_{sw}, T_r, and P_n showed a consistent linear decrement with the increase in DAE (Figures 2–4). This finding was congruent with the decline in g_{sw} and P_n with potato leaf senesced (Vos and Oyarzun, 1987). Echer and Rosolem (2015) also asserted that cotton leaf DAE had nominal impact on leaf P_n under low PAR, while P_n was notably higher in 15- and 30-day-old

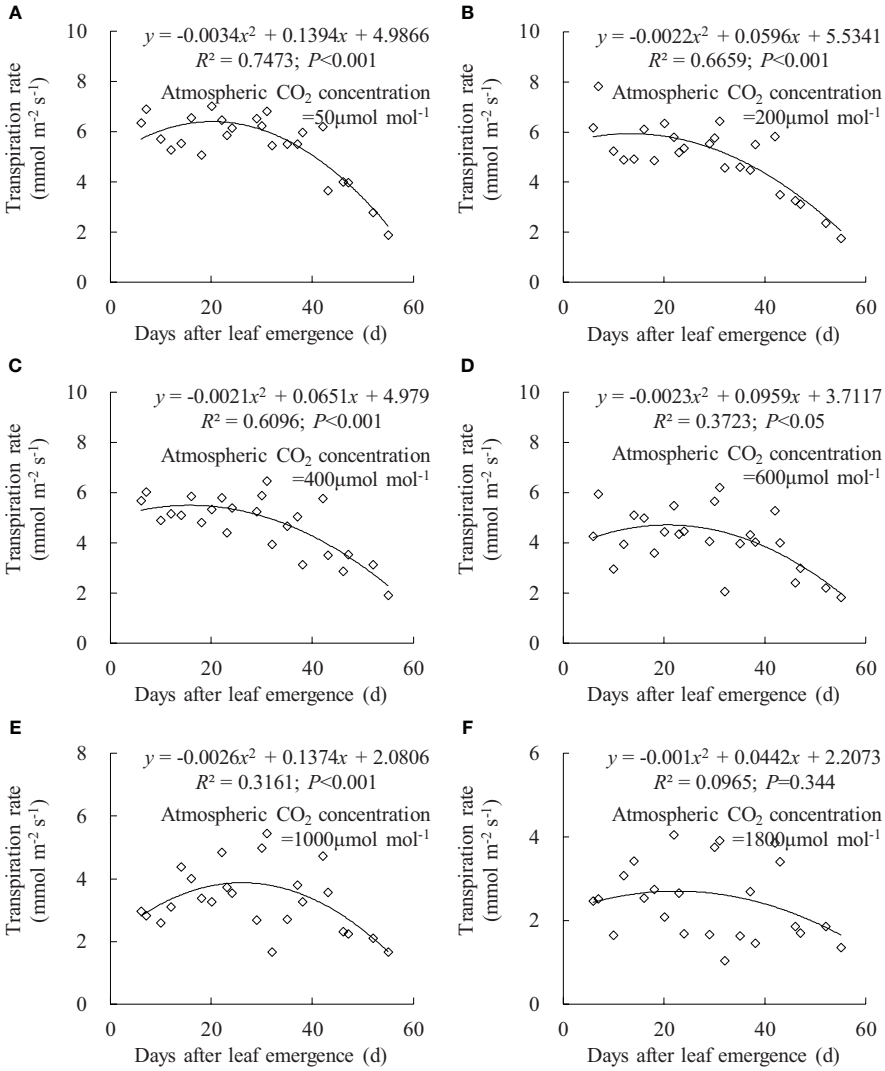

FIGURE 7
(A–F) Impact of days after leaf emergence on transpiration rate under different atmospheric CO_2 concentration conditions.

leaves compared to 45- and 60-day-old leaves when PAR exceeded a threshold, with both T_r and g_{sw} reduced as the leaves aged and the light intensity waned. Hossain et al. (2007) and Jin et al. (2004) reported that rice g_{sw}, T_r, and P_n, at particular PAR, decreased significantly with lowering leaf position, which was consistent with the current research, as newly emerged rice leaves appeared in the upper canopy, implicating a reduction in leaf DAE as leaf position decreased. Generally, rice leaf photosynthesis was highly related to leaf nitrogen level, efficiencies of radiant energy utilization, electron transport, and photophosphorylation, and these values decreased with leaf aging (or downward leaves) (Murchie et al., 2002; Suzuki et al., 2009; Okami et al., 2016; Yang et al., 2016), which also agreed with the decreased P_n. In contrast, Wang et al. (2009) reported that the measured light-saturated rice g_{sw}, T_r, and P_n reached the maximum at the last second fully developed leaf and then declined gradually in downward leaves at nine-leaf age (an indicator representing the developmental progress of plants) stage (tillering stage correspondingly). Xu et al. (2019) also stated that light-saturated rice P_n peaked at around 10 days after leaf emergence and then decreased as leaves aged. The discrepancy with the current study might be attributed to low-frequency measurement for photosynthetic characteristics under smaller DAE, as the measurement was inconvenient due to the small leaf area before they were fully expanded. Additionally, the measurement in the current study began at DAE of 3 days, at which time the leaves had a large leaf area. Consequently, the study did not monitor the increase in leaf g_{sw}, T_r, and P_n during the leaf expansion process.

4.2 Effect of days after leaf emergence on the CO_2 response

As C_a increased, leaf g_{sw} and T_r gradually decreased, while P_n increased linearly and rapidly, and the amplitude of variations in g_{sw}, T_r, and P_n decelerated, eventually leading to a stabilization of minimal g_{sw} and T_r and an elevation of P_n to its peak, subsequently maintaining

stability or experiencing a slight decline (Figure 5). Yasutake et al. (2016) found that 1,000 µmol mol^{-1} C_a significantly increased sweet pepper P_n but decreased g_{sw} and T_r compared with 400 C_a. Ahmed et al. (2022) reported that P_n increased and g_{sw} and T_r decreased in the order of 500, 1,000, and 1,500 µmol mol^{-1} C_a. This was consistent with the decreased g_{sw} and T_r and increased P_n with leaf aging observed in the current study. Inamoto et al. (2022) showed that the increase in Oriental Hybrid Lily P_n was greater in the low C_a range (380 to 1,000 µmol mol^{-1}) and lower in the high C_a range (1,000 to 2,000 µmol mol^{-1}), which agreed with the amplitude of variations in P_n.

Under specific C_a, the leaf g_{sw}, T_r, and P_n remained at a relatively high level when DAE was less than approximately 25 days and then gradually decreased with the further increase in DAE (Figures 6, 7, 8). Chlorophyll activity, Rubisco activity, RuBP regeneration capacity, and nitrogen content (positively correlated with the photosynthetic potential of leaves) generally exhibited an increasing trend during the leaf expansion phase, followed by the maintenance of relatively high values, and then decreased as the leaves aged (Murchie et al., 2002; Suzuki et al., 2009; Gunasekera et al., 2013), which might be the primary reasons for the variation in g_{sw}, T_r, and P_n. At lower C_a concentrations, leaves at a smaller DAE maintained higher g_{sw} to facilitate atmospheric CO_2 entering for transpiration and photosynthesis. Leaves at a greater DAE had weaker adaptability to external environments, maintaining lower levels of g_{sw}, T_r, and P_n regardless of C_a level. When C_a exceeded a certain level, C_a exerted a suppressive effect on stomatal conductance to reduce transpiration, but the photosynthetic rate did not decrease.

5 Conclusions

This study investigated the dynamics of stomatal conductance g_{sw}, transpiration rate T_r, and net photosynthetic rate P_n in rice leaves across

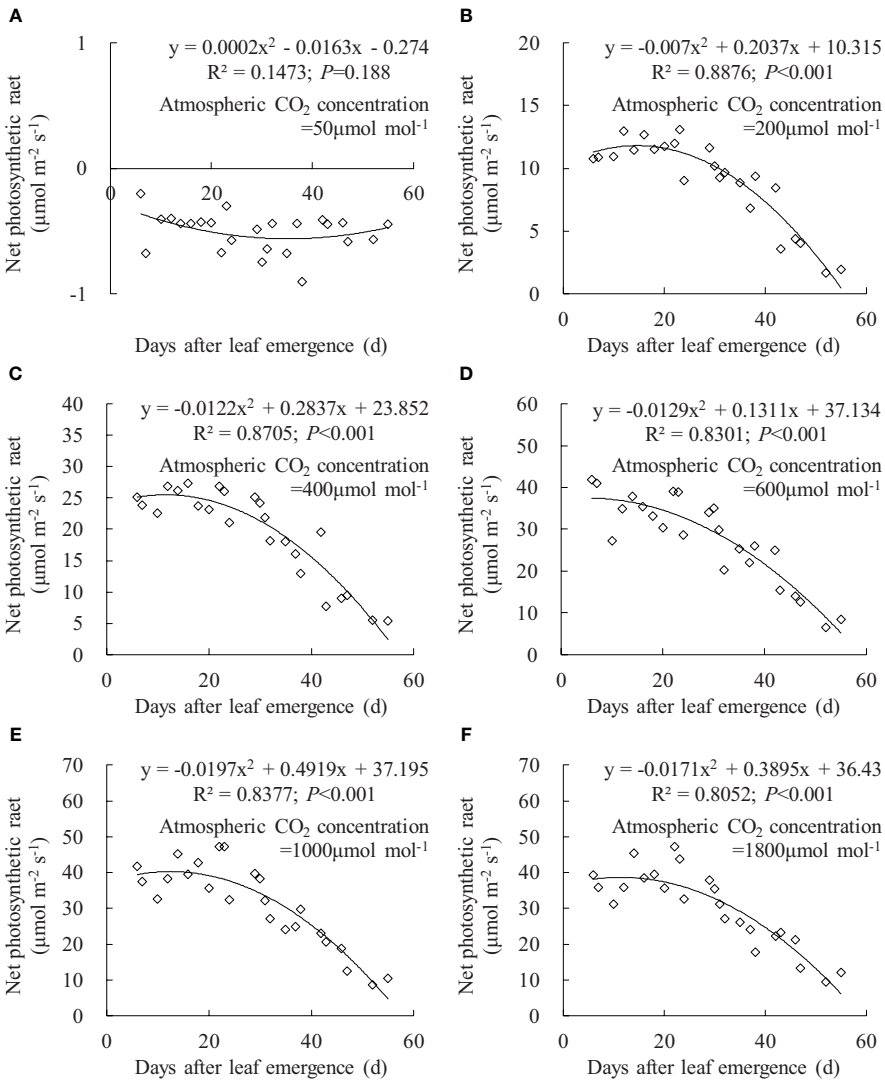

FIGURE 8
(A–F) Impact of days after leaf emergence on net photosynthetic rate under different atmospheric CO_2 concentration conditions.

varying light intensities and CO_2 conditions during leaf development. The key conclusions drawn from the findings are as follows:

(1) Response to photosynthetically active radiation PAR: Increasing PAR led to an initial rapid and linear increase in g_{sw}, T_r, and P_n, followed by a more gradual rise to maximum values, with subsequent stabilization or decline. Notably, old leaves reached their maximum g_{sw}, T_r, and P_n earlier and at smaller magnitudes compared to young leaves. Additionally, a linear decreasing trend in g_{sw}, T_r, and P_n with increasing DAE was observed, with the decrease rate slowing down with reduced PAR.

(2) Response to atmospheric CO_2 concentrations C_a: With increasing C_a, g_{sw} and T_r decreased gradually to a stable minimum value, while P_n exhibited a linear and slow increase up to a maximum before stabilizing or decreasing. Under specific C_a conditions, rice leaf g_{sw}, T_r, and P_n initially remain at higher values and then gradually decrease with increasing DAE.

These conclusions provided crucial mechanistic insights to estimate dynamic evapotranspiration and net ecosystem productivity at both field-scale and larger scales in paddy field ecosystems by upscaling leaf-level physiological processes. This knowledge can inform more accurate predictions and management strategies to optimize agricultural practices and enhance the sustainability of rice cultivation amidst changing environmental conditions.

Data availability statement

The datasets presented in this article are not readily available because the authors do not have permission to share data. Requests to access the datasets should be directed to YL, lvyuping@yzu.edu.cn.

Author contributions

YL: Conceptualization, Funding acquisition, Writing – original draft. LG: Investigation, Writing – original draft. RM: Formal analysis, Validation, Writing – review & editing. XL: Writing – review & editing. JX: Writing – review & editing.

Funding

The author(s) declare financial support was received for the research, authorship, and/or publication of this article. This project was supported financially by the National Science Foundation of China (NO. 52309064).

Conflict of interest

The authors declare that the research was conducted in the absence of any commercial or financial relationships that could be construed as a potential conflict of interest.

Publisher's note

All claims expressed in this article are solely those of the authors and do not necessarily represent those of their affiliated organizations, or those of the publisher, the editors and the reviewers. Any product that may be evaluated in this article, or claim that may be made by its manufacturer, is not guaranteed or endorsed by the publisher.

References

Ahmed, H. A., Tong, Y. X., Li, L., Sahari, S. Q., Almogahed, A. M., and Cheng, R. F. (2022). Integrative effects of CO_2 concentration, illumination intensity and air speed on the growth, gas exchange and light use efficiency of lettuce plants grown under artificial lighting. *Horticulturae.* 8, 270. doi: 10.3390/horticulturae8030270

Baroli, I., Price, G. D., Badger, M. R., and von Caemmerer, S. (2008). The contribution of photosynthesis to the red light response of stomatal conductance. *Plant Physiolology.* 146, 737–737. doi: 10.1104/pp.107.110924

Bellasio, C. (2023). The slope of assimilation rate against stomatal conductance should not be used as a measure of water use efficiency or stomatal control over assimilation. *Photosynthesis Res.* 158, 195 199. doi: 10.1007/s11120-023-01054-6

Carmo-Silva, E., Andralojc, P. J., Scales, J. C., Driever, S. M., Mead, A., Lawson, T., et al. (2017). Phenotyping of field-grown wheat in the UK highlights contribution of light response of photosynthesis and flag leaf longevity to grain yield. *J. Exp. Botany.* 68, 3473–3486. doi: 10.1093/jxb/erx169

Chang, T. G., Zhao, H. L., Wang, N., Song, Q. F., Xiao, Y., Qu, M. N., et al. (2019). A three-dimensional canopy photosynthesis model in rice with a complete description of the canopy architecture, leaf physiology, and mechanical properties. *J. Exp. Botany.* 70, 2479–2490. doi: 10.1093/jxb/ery430

Chen, Z. Y., Peng, Z. S., Yang, J., Chen, W. Y., and Ou-Yang, Z. M. (2011). A mathematical model for describing light-response curves in Nicotiana tabacum L. *Photosynthetica* 49, 467–471. doi: 10.1007/s11099-011-0056-5

Echer, F. R., and Rosolem, C. A. (2015). Cotton leaf gas exchange responses to irradiance and leaf aging. *Biol. Plantarum.* 59, 366–372. doi: 10.1007/s10535-015-0484-3

Elfadl, M. A., and Luukkanen, O. (2006). Field studies on the ecological strategies of *Prosopis juliflora* in a dryland ecosystem: 1. A leaf gas exchange approach. *J. Arid Environments.* 66, 1–15. doi: 10.1016/j.jaridenv.2005.09.006

Gunasekera, H., Costa, W. D., and Nugawela, A. (2013). Canopy photosynthetic capacity and light response parameters of rubber *hevea brasiliensis* with reference to exploitation. *Curr. Agric. Res. J.* 1, 1–12. doi: 10.12944/CARJ

Guo, J. X., Hu, X. Y., Gao, L. M., Xie, K. L., Ling, N., Shen, Q. R., et al. (2017). The rice production practices of high yield and high nitrogen use efficiency in Jiangsu, China. *Sci. Rep.* 7, 2101. doi: 10.1038/s41598-017-02338-3

Hirooka, Y., Homma, K., and Shiraiwa, T. (2018). Parameterization of the vertical distribution of leaf area index (LAI) in rice (*Oryza sativa* L.) using a plant canopy analyzer. *Sci. Rep.* 8, 6387. doi: 10.1038/s41598-018-24369-0

Hossain, S. T., Sugimoto, H., and Yamashita, J. (2007). Effect of topdressing on individual leaf photosynthesis at different position in direct-sown rice with non-woven fabric mulch system. *Photosynthetica.* 45, 576–581. doi: 10.1007/s11099-007-0099-9

Inamoto, K., Nagasuga, K., and Yano, T. (2022). Effect of CO2 enrichment on the photosynthesis and dry matter accumulation in the oriental hybrid lily 'Siberia'. *Horticulture J.* 91, 541–550. doi: 10.2503/hortj.UTD-372

Inoue, T., Inanaga, S., Sugimoto, Y., An, P., and Eneji, A. E. (2004). Effect of drought on ear and flag leaf photosynthesis of two wheat cultivars differing in drought resistance. *Photosynthetica* 42, 559–565. doi: 10.1007/S11099-005-0013-2

Jin, S. H., Wang, P. M., Zhao, K., Yang, Y. Q., Yao, S., and Jiang, D. A. (2004). Characteristic of gas exchange and chlorophyll fluorscence in different position leaves at booting stage in rice plants. *Rice Science.* 11, 283–289.

Kabir, M. Y., Nambeesan, S. U., and Díaz-Pérez, J. C. (2023). Carbon dioxide and light curves and leaf gas exchange responses to shade levels in bell pepper (Capsicum annuum L.). *Plant Sci.* 326, 111532. doi: 10.1016/j.plantsci.2022.111532

Katul, G. G. (2023). Agrivoltaics in color: going from light spectra to biomass. *Earth's Future.* 11, e2023EF003512. doi: 10.1029/2023EF003512

Kirschbaum, M. U. F., and McMillan, A. M. S. (2018). Warming and elevated CO_2 have opposing influences on transpiration. Which is more important? *Curr. Forestry Rep.* 4, 51–71. doi: 10.1007/s40725-018-0073-8

Kitajima, K., Mulkey, S. S., Samaniego, M., and Wright, S. J. (2002). Decline of photosynthetic capacity with leaf age and position in two tropical pioneer tree species. *Am. J. Botany.* 89, 1925–1932. doi: 10.3732/ajb.89.12.1925

Konieczna, W., Warchol, M., Mierek-Adamska, A., Skrzypek, E., Waligórski, P., Piernik, A., et al. (2023). Changes in physio-biochemical parameters and expression of metallothioneins in Avena sativa L. @ in response to drought. *Sci. Rep.* 13, 2486. doi: 10.1038/s41598-023-29394-2

Lawson, T., and Vialet-Chabrand, S. (2019). Speedy stomata, photosynthesis and plant water use efficiency. *New Phytologist.* 221, 93–98. doi: 10.1111/nph.15330

Legner, N., Fleck, S., and Leuschner, C. (2014). Within-canopy variation in photosynthetic capacity, SLA and foliar N in temperate broad-leaved trees with contrasting shade tolerance. *Trees-Structure Funct.* 28, 263–280. doi: 10.1007/s00468-013-0947-0

Li, F., Gao, X. D., Li, C. J., He, H. H., Siddique, K. H. M., and Zhao, X. N. (2023). Elevated CO_2 concentration regulate the stomatal traits of oilseed rape to alleviate the impact of water deficit on physiological properties. *Environ. Exp. Botany.* 211, 105355. doi: 10.1016/j.envexpbot.2023.105355

Li, J. P., Vatsa, P., and Ma, W. L. (2023). Can mechanized pesticide application help reduce pesticide use and increase crop yield? Evidence from rice farmers in Jiangsu province, China. *Int. J. Agric. Sustainability.* 21, 2227809. doi: 10.1080/14735903.2023.2227809

Liu, Q., Dong, L. H., and Li, F. R. (2019). Modification of a photosynthetic light-response (PLR) model for modeling the vertical gradient in the response of crown PLR curves. *Can. J. For. Res.* 49, 949–959. doi: 10.1139/cjfr-2018-0438

Locke, A. M., and Ort, D. R. (2014). Leaf hydraulic conductance declines in coordination with photosynthesis, transpiration and leaf water status as soybean leaves age regardless of soil moisture. *J. Exp. Botany.* 65, 6617–6627. doi: 10.1093/jxb/eru380

Lv, Y. P., Gu, L. H., Liu, X. Y., and Xu, J. Z. (2024). A coupled hourly water-carbon flux model at plot and field scales for water-saving irrigated rice paddy. *Agric. Water Management.* 293, 108706. doi: 10.1016/j.agwat.2024.108706

Marín, D., Martín, M., Serrot, P. H., and Sabater, B. (2014). Thermodynamic balance of photosynthesis and transpiration at increasing CO2 concentrations and rapid light fluctuations. *Biosystems.* 116, 21–26. doi: 10.1016/j.biosystems.2013.12.003

Murchie, E. H., Hubbart, S., Chen, Y. Z., Peng, S. B., and Horton, P. (2002). Acclimation of rice photosynthesis to irradiance under field conditions. *Plant Physiol.* 130, 1999–2010. doi: 10.1104/pp.011098

Okami, M., Kato, Y., and Yamagishi, J. (2016). Canopy Architecture and Leaf Nitrogen Distribution of Rice (*Oryza sativa* L.) under Chronic Soil Water Deficit. *J. Agron. Crop Sci.* 202, 464–471. doi: 10.1111/jac.12179

Pantin, F., Simonneau, T., and Muller, B. (2012). Coming of leaf age: control of growth by hydraulics and metabolics during leaf ontogeny. *New Phytologist.* 196, 349–366. doi: 10.1111/j.1469-8137.2012.04273.x

Scoffoni, C., Chatelet, D. S., Pasquet-kok, J., Rawls, M., Donoghue, M. J., Edwards, E. J., et al. (2016). Hydraulic basis for the evolution of photosynthetic productivity. *Nat. Plants.* 2, 16072. doi: 10.1038/nplants.2016.72

Shi, Z., Chang, T. G., Chen, G. Y., Song, Q. F., Wang, Y. J., Zhou, Z. W., et al. (2019). Dissection of mechanisms for high yield in two elite rice cultivars. *Field Crops Res.* 241, 107563. doi: 10.1016/j.fcr.2019.107563

Song, Q. F., Zhang, G. L., and Zhu, X. G. (2013). Optimal crop canopy architecture to maximize canopy photosynthetic CO_2 uptake under elevated CO_2 – a theoretical study using a mechanistic model of canopy photosynthesis. *Funct. Plant Biol.* 40, 109–124. doi: 10.1071/FP12056

Suzuki, Y., Miyamoto, T., Yoshizawa, R., Mae, T., and Makino, A. (2009). Rubisco content and photosynthesis of leaves at different positions in transgenic rice with an overexpression of RBCS. *Plant Cell Environ.* 32, 417–427. doi: 10.1111/j.1365-3040.2009.01937.x

Van der Zande, D., Mereu, S., Nadezhdina, N., Cermak, J., Muys, B., Coppin, P., et al. (2009). 3D upscaling of transpiration from leaf to tree using ground-based LiDAR: Application on a Mediterranean Holm oak (Quercus ilex L. *) tree. Agric. Water Manage.* 149, 1573–1583. doi: 10.1016/j.agrformet.2009.04.010

Vos, J., and Oyarzun, P. J. (1987). Photosynthesis and stomatal conductance of potato leaves- effects of leaf age, irradiance, and leaf water potential. *Photosynthesis Res.* 11, 253–264. doi: 10.1007/BF00055065

Wang, D., Lu, Q., Li, X. F., Jiang, Q. S., Wu, J. X., and Jiang, D. A. (2009). Relationship between Rubisco activase isoform levels and photosynthetic rate in different leaf positions of rice plant. *Photosynthetica.* 47, 621–629. doi: 10.1007/s11099-009-0089-1

Watanabe, T., Hanan, J. S., Room, P. M., Hasegawa, T., Nakagawa, H., and Takahashi, W. (2005). Rice morphogenesis and plant architecture: measurement, specification and the reconstruction of structural development by 3D architectural modelling. *Ann. Botany.* 95, 1131–1143. doi: 10.1093/aob/mci136

Wu, C. Y., Chen, D. S., Xia, G. W., Sun, X. M., and Zhang, S. G. (2023). Response characteristics of photosynthetic productivity to the canopy spatial distribution pattern of *larix kaempferi. Forests.* 14, 1171. doi: 10.3390/f14061171

Xie, S. X., and Luo, X. S. (2003). Effect of leaf position and age on anatomical structure, photosynthesis, stomatal conductance and transpiration of Asian pear. *Botanical Bull. Academia Sinica.* 44, 297–303.

Xu, J. Z., Lv, Y. P., Liu, X. Y., Wei, Q., Qi, Z. M., Yang, S. H., et al. (2019). A general non-rectangular hyperbola equation for photosynthetic light response curve of rice at various leaf ages. *Sci. Rep.* 9, 9909. doi: 10.1038/s41598-019-46248-y

Xu, J. Z., Wang, Y. H., Yang, S. H., Peng, S. Z., and Kong, W. L. (2015). Improved perfermance of photosynthetic light response equations with unified parameters for rice leaves with SPAD Values. *Pakistan J. Botany.* 47, 877–882.

Yang, J., Gong, W., Shi, S., Du, L., Sun, J., and Song, S. L. (2016). Estimation of nitrogen content based on fluorescence spectrum and principal component analysis in paddy rice. *Plant Cell Environment.* 62, 178–183. doi: 10.17221/802/2015-PSE

Yasutake, D., Miyauchi, K., Mori, M., Kitano, M., Ino, A., and Takahashi, A. (2016). Multiple effects of CO_2 concentration and humidity on leaf gas exchanges of sweet pepper in the morning and afternoon. *Environ. Control Biol.* 54, 177–181. doi: 10.2525/ecb.54.177

Yi, Y., Yano,, and Yano, K. (2023). Nocturnal versus diurnal transpiration in rice plants: Analysis of five genotypes grown under different atmospheric CO2 and soil moisture conditions. *Agric. Water Management.* 286, 108397. doi: 10.1016/j.agwat.2023.108397

You, L. Z., Spoor, M., Ulimwengu, J., and Zhang, S. M. (2011). Land use change and environmental stress of wheat, rice and corn production in China. *China Economic Review.* 22, 461–473. doi: 10.1016/j.chieco.2010.12.001

Yu, Q., Zhang, Y. G., Liu, Y. F., and Shi, P. L. (2004). Simulation of the stomatal conductance of winter wheat in response to light, temperature and CO2 changes. *Ann. Botany.* 93, 435–441. doi: 10.1093/aob/mch023

frontiers | Frontiers in Plant Science

TYPE Original Research
PUBLISHED 10 September 2024
DOI 10.3389/fpls.2024.1430241

OPEN ACCESS

EDITED BY
Meijian Yang,
Cornell University, United States

REVIEWED BY
Jun Liu,
Texas A&M AgriLife Research, Texas A and M University, United States
Ki-Ho Son,
Gyeongsang National University, Republic of Korea

*CORRESPONDENCE
Bingfu Lei
tleibf@scau.edu.cn

RECEIVED 09 May 2024
ACCEPTED 20 August 2024
PUBLISHED 10 September 2024

CITATION
Bi X, Xu H, Yang C, Zhang H, Li W, Su W, Zheng M and Lei B (2024) Investigating the influence of varied ratios of red and far-red light on lettuce (*Lactuca sativa*): effects on growth, photosynthetic characteristics and chlorophyll fluorescence.
Front. Plant Sci. 15:1430241.
doi: 10.3389/fpls.2024.1430241

Investigating the influence of varied ratios of red and far-red light on lettuce (*Lactuca sativa*): effects on growth, photosynthetic characteristics and chlorophyll fluorescence

Xueting Bi[1,2], Hong Xu[1,2], Chaowei Yang[1,2], Haoran Zhang[1], Wei Li[1], Wei Su[2], Mingtao Zheng[1,3] and Bingfu Lei[1,2,3]*

[1]Key laboratory for Biobased Materials and Energy of Ministry of Education, College Materials and Energy, South China Agricultural University, Guangzhou, China, [2]College of Horticulture, South China Agricultural University, Guangzhou, China, [3]Maoming Branch, Guangdong Laboratory for Lingnan Modern Agriculture, Maoming, China

Far red photon flux accelerates photosynthetic electron transfer rates through photosynthetic pigments, influencing various biological processes. In this study, we investigated the impact of differing red and far-red light ratios on plant growth using LED lamps with different wavelengths and $Ca_{1.8}Mg_{1.2}Al_2Ge_3O_{12}$:0.03$Cr^{3+}$ phosphor materials. The control group (CK) consisted of a plant growth special lamp with 450 nm blue light + 650 nm red light. Four treatments were established: F1 (650 nm red light), F2 (CK + 730 nm far-red light in a 3:2 ratio), F3 (650 nm red light + 730 nm far-red light in a 3:2 ratio), and F4 (CK + phosphor-converted far-red LED in a 3:2 ratio). The study assessed changes in red and far-red light ratios and their impact on the growth morphology, photosynthetic characteristics, fluorescence characteristics, stomatal status, and nutritional quality of cream lettuce. The results revealed that the F3 light treatment exhibited superior growth characteristics and quality compared to the CK treatment. Notably, leaf area, aboveground fresh weight, vitamin C content, and total soluble sugar significantly increased. Additionally, the addition of far-red light resulted in an increase in stomatal density and size, and the F3 treatments were accompanied by increases in net photosynthetic rate (Pn), transpiration rate (Tr), intercellular CO_2 concentration (Ci), and stomatal conductance (Gs). The results demonstrated that the F3 treatment, with its optimal red-to-far-red light ratio, promoted plant growth and photosynthetic characteristics. This indicates its suitability for supplementing artificial light sources in plant factories and greenhouses.

KEYWORDS

far-red light, phosphor converted LED, lettuce, stomata, photosynthetic characteristics

1 Introduction

In recent years, facility gardening has gained attention for enhancing horticultural productivity (Van Gerrewey et al., 2022), offering higher and more predictable yields per unit area while optimizing resource usage (Van Delden et al., 2021). Greenhouses, a popular choice for protected cultivation, often necessitate artificial lighting with specific intensity and spectral composition. The increasing use of energy-efficient LEDs in protected cultivation systems has rekindled interest in understanding light quality's impact on crop productivity (Wassenaar et al., 2022).

Photosynthesis is the process through which plants utilize light energy to convert carbon dioxide (CO_2) and water (H_2O) into organic matter, releasing oxygen (O_2) in the process (Wang et al., 2020). Light quality significantly influences photosynthesis (Parys et al., 2021). Given that light in the 400-700 nm wavelength range is most efficient for photosynthesis (Bautista-Saraiva et al., 2018), many studies have focused on this range (Matsuda et al., 2004; Baba et al., 2012). White light, comprising integrated wavelengths, is recognized as crucial for promoting normal plant growth as it provides ample energy for photosynthesis. However, recent research highlights the significance of red light in plant growth. Red light (600-700 nm), commonly used in plant factories with artificial lighting (PFAL), has been found to enhance biomass, leaf area, leaf length, leaf height, and soluble sugars, while reducing nitrate levels in green leafy vegetables (Baba et al., 2012).

Far-red light supplementation, which is adding far-red light to white light in combined light qualities, significantly enhances quantum yield and net photosynthesis of photosystem II while reducing non-photochemical fluorescence quenching (Zou et al., 2019; Zhen and Bugbee, 2020) This supplementation results in increased light use efficiency and plant biomass. Additionally, when combined with light of shorter wavelength, far-red photons (701-750 nm) have been demonstrated to drive photosynthesis as effectively as photons in the photosynthetically active radiation (PAR) region (400-700 nm) (Wong et al., 2020; Zhen et al., 2021). Moreover, far-red light exhibits a synergistic effect when combined with photons in the 400-700 nm range, enhancing the efficiency of PS II in lettuce. This was observed by Emerson (Emerson et al., 1957) and confirmed by recent studies (Zhen and van Iersel, 2017; Zhen et al., 2021). Zhen demonstrated that supplementing 110 μmol $m^{-2}·s^{-1}$ of far-red light (700-770 nm) with increasing intensities of red and blue or white light (ranging from 50-750 μmol $m^{-2}·s^{-1}$) enhances photochemical efficiency and carbohydrate synthesis. Far-red light preferentially excites photosystem I, which tends to be under-excited without it, thus restoring the balance between the two photosystems and ultimately improving overall photosynthetic efficiency (Zhen and Bugbee, 2020).

Far-red light (701-750 nm) can modulate plant morphology, including adjustments to leaf angle, increased plant height, and expanded leaf area to optimize light absorption and boost crop biomass (Park and Runkle, 2018; Tan et al., 2022). Far-red light-induced shade avoidance syndromes, including promoted shoot elongation and enlarged leaves, as documented by (Franklin and Quail, 2010; Park and Runkle, 2018; Meng et al., 2019), may facilitate better light interception and lead to a substantial biomass increase in PFAL. To investigate plant responses to various light qualities, the researchers conducted a red + far-red light study in addition to natural light. The findings from lettuce light treatments demonstrated that red light + far-red light could enhance soluble sugars in lettuce and reduce nitrate content, thereby improving lettuce quality (Chen et al., 2016). In recent years, phosphors can absorb light and re-emit it in a different color (fluorescence or phosphorescence) and these phosphors emit specific light wavelengths, providing plants with light of broad spectral distribution (Yang et al., 2023). By manipulating the combination of phosphor wavelengths, precise control over plant growth can be achieved. Phosphors absorb incident light and convert it into different wavelengths, enhancing the light received by plants. This promotes photosynthesis and efficiency (Wu et al., 2022). Different phosphor types possess varying properties regarding absorbed and emitted light wavelengths, complementing the specific spectrum needed by plants. For instance, some phosphors can increase the proportion of red or blue light, crucial for plant growth and photosynthesis. Through spectrum modulation, phosphors create a more suitable light environment for plant photosynthesis and growth (Fang et al., 2022).

Various light qualities exert unique influences on the photosynthesis and growth of plants. A thorough understanding of these mechanisms can assist in optimizing the plant growth environment and enhancing crop yields to address the escalating challenges of food security. In this study, lettuce was the research subject. We investigated the selection of different far-red light ratios and the introduction of a new luminescent material. The objective was to assess the impact of diverse light conditions on plant growth and photosynthesis by measuring growth indices (e.g., plant height, leaf area, biomass) and photosynthetic parameters (e.g., chlorophyll content, photosynthesis rate, and respiration rate). The aim of this study was to explore the effects of different ratios of red light and far-red light on plant growth and photosynthesis, and to explore the application effect of phosphor, to provide a scientific basis for the optimization of plant cultivation and photosynthesis.

2 Article types

Original Research

3 Materials and methods

3.1 Plant materials and experimental setup

The experiment spanned from November 10 to December 30, 2023, within a Venlo-type glass greenhouse at the College of Materials and Energy (South China Agricultural University, Guangzhou, China). The greenhouse climate conditions are shown in Figure 1. Cream Lettuce (Hebei Nanjixing Seed Co. Ltd., Guangzhou, China) was chosen as the lettuce variety (*Lactuca sativa*) for the study. The conditions for seedling cultivation are as follows: natural light conditions supplemented with LED lighting to maintain a consistent light intensity of 200 μmol/m^2/s during daylight hours, temperature of 20°C ± 2°C, light cycle of 12 hours per day, and

10.3389/fpls.2024.1430241

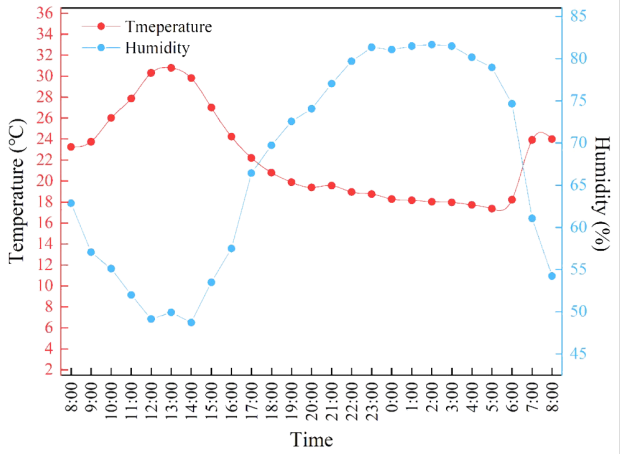

FIGURE 1
Average daily temperature and humidity in greenhouses from November to December.

relative humidity controlled between 70% and 90%. After soaking and cleaning the lettuce seeds, they are sown on seedling sponges. When the second true leaf of the seedlings is fully expanded, uniform seedlings in terms of shape and growth are selected and transplanted into hydroponic troughs using the Deep Flow Technique (The dimensions of the DFT device:120*400*150 cm) The planting density in the DFT system was set at 30 plants per square meter. The nutrient solution prepared using the Hogland formula. The pH of the Hogland solution is adjusted to 6.0, and the electrical conductivity (EC) is set to 2 mS/cm. A supplemental light mode was employed at night, with a 12-hour photoperiod (20:00 p.m. to 8:00 a.m.), daytime average temperature at 25 ± 5°C, nighttime temperature at 18°C, and controlled relative humidity at 75 ± 5%. Obvious growth phenotypes emerged 7 days post-transplanting. Each light treatment involved planting 50 lettuce plants, replicated three times. To ensure the rigor of the experimental design, each replication was re-randomized across different plots to mitigate location-specific environmental influences. This approach ensured that no single treatment was consistently applied to the same plot, thus reducing potential biases.

3.2 Lighting treatment

Various LED light processing techniques were applied to the split tube from Yueqing City, Jia Cheng Lighting Co., Ltd. For the F4 processing, phosphor-converted far-red light was generated using$Ca_{1.8}Mg_{1.2}Al_2Ge_3O_{12}$:0.03$Cr^{3+}$ phosphor under 450 nm chipexcitation (Yang et al., 2024). The distribution of spectral settings of different treatments and the production process of excitation phosphor are shown in Table 1; Figure 2. Light quality measurements for each treatment were conducted using the Aurora4000 Series High-Resolution Spectrometer (Changchun Institute of Optics, Fine Mechanics and Physics, Chinese Academy of Sciences, Changchun, China), and light intensity measurements were conducted using the photosynthetically Active Radiation sensor (LI-190R, Lincoln, NE, USA).

TABLE 1 Different light formulations and light quantum densities.

Treatments	Light quality formulations	Light intensity [μmol/(m^2·s)]
CK	450 nm Blue light + 650 nm Red light (1:1)	300
F1	650 nm Red light	300
F2	CK + 730 nm Far-red light (3:2)	300
F3	650 nm Red light + 730 nm Far-red light (3:2)	300
F4	CK + Phosphor Stimulated Far-red LED (3:2)	300

3.3 Stomata observation

After 45 days of growth, lettuce plants were sampled, and leaf slices were collected from five plants. To prepare leaf epidermal sections, 1 cm^2 leaf slices were uniformly coated with colorless transparent nail polish. After complete drying, the polish-coated slices were gently removed and placed on slides to create water-sealed plant slices (Li et al., 2010).

For leaf longitudinal sections, a hand sectioning method was employed. These prepared sections were then examined and photographed using the Nikon inverted fluorescence microscope imaging system (Ts2, Nikon Corporation, Japan) with a 10x eyepiece and a 40x objective. Stomatal status in the epidermal sections was observed at the same magnification.

3.4 Photosynthetic properties and chlorophyll fluorescence

The Li-6400XT Portable Photosynthesis Measurement System (LI-COR Biosciences, Lincoln, NE, USA) from Li-Cor was employed to assess plant photosynthetic parameters 45 days after planting. Three plants exhibiting consistent and uniform growth

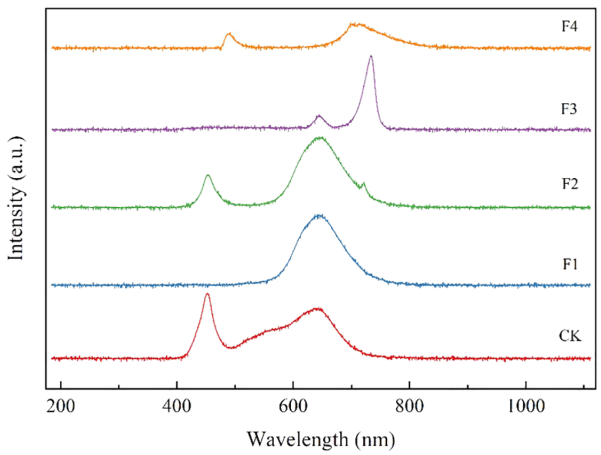

FIGURE 2
Emission spectra of different treatment.

were selected for each treatment. Functional leaves from the third position from the bottom of the plants were chosen to determine photosynthetic parameters., including leaf net photosynthetic rate (*Pn*), transpiration rate (*Tr*), stomatal conductance (*Gs*), and intercellular CO_2 concentration (*Ci*). Water utilization efficiency (WUE), calculated as *Pn*/*Tr*, was determined for each leaf, with the process repeated three times (The settings for the measurements were as follows: the light intensity was set to 800 μmol m^{-2} s^{-1} using the LI6800-01A light source with a light quality of 20R80B, the leaf temperature was maintained at 25°C, and the relative humidity inside the leaf chamber was kept at 70%, and the CO_2 concentration was set to 800 ppm. The airflow rate through the chamber was set to 1000 μmol s^{-1}. The leaf area used for measurements was 8 cm^2).

Using the Imaging-PAM chlorophyll fluorometer (IMAGMAX1, Heinz Walz, Effeltrich, Germany), three plants were measured for each treatment, selecting the first fully expanded functional leaf for measurement. The instrument was set with a leaf chamber area of 8 cm^2 and a light intensity of 1000 μmol·m^{-2}·s^{-1} (chlorophyll fluorescence was measured under saturation light conditions.). To construct the light response curve in photosynthetically active radiation (PAR) levels were incrementally adjusted, and measurements were taken at each level after a stabilization period of 2 minutes. The specific PAR levels used were 0, 50, 100, 200, 400, 600, 800, and 1000 μmol·m^{-2}·s^{-1}. Each measurement was performed with a wait time of 2 minutes between adjustments to ensure accurate readings. Measurements included the relative electron transport rate (rETR), maximum fluorescence (F'm), steady-state fluorescence (Fs), and minimum fluorescence (F'o).

The relative electron transport rate (rETR):

$$rETR = \Phi_{PSII} \times PPFD \quad (1)$$

The effective quantum yield of PSII (ΦPSII):

$$\Phi_{PSII} = \frac{F'm - Fs}{F'm} \quad (2)$$

Subsequently, the same leaf area was dark-adapted for 20 minutes to measure the initial fluorescence (Fo) and maximum fluorescence (Fm). Based on these chlorophyll fluorescence parameters, the variable fluorescence Fv = Fm - Fo, the maximum photochemical efficiency of photosystem II (Fv/Fm) = (Fm - Fo)/Fm, the potential photochemical efficiency of PSII (Fv/Fo) = (Fm - Fo)/Fo, the photochemical quenching coefficient (qP) = (F'm - Fs)/(F'm – F'o), and the non-photochemical quenching coefficient (NPQ) = (Fm – F'm)/F'm were calculated.

3.5 Growth parameters

Five plants with consistent growth under different light treatments were randomly selected for growth analysis. The leaf length and leaf width were measured using a tape measure and a vernier scale. Vernier calipers were used to measure stem thickness and petiole thickness; the number of leaves was calculated by the direct method (Use a plant marking pen to gently mark each leaf of the lettuce, and directly count each leaf); root data measurement is performed using a root scanner (WINRHIZO, Chengyi Imp & Exp Co., Ltd, Guangzhou, China). the aboveground and belowground fresh mass of lettuce was determined using an electronic balance (FA1004E, Sanlitech, China), and the aboveground and belowground dry masses of lettuce were determined using an electronic balance after lettuce was dried in an oven at 80°C for 72h to a constant mass; the strong seedling index was calculated by the formula, i.e., the strong seedling index was calculated as strong seedling index = (stem thickness/plant height + belowground dry mass/aboveground dry mass) × the whole dry mass. Mass per unit of leaf area (LMA) = dry mass/single leaf area. (Teklehaimanot, 2004).

For each treatment, 5 lettuce leaves were collected and processed with liquid nitrogen to grind into powder (stored in a -80°C freezer). The photosynthetic pigment content was determined by acetone ethanol mixing method (Wellburn, 1994). The leaf soluble protein content was determined by colorimetric method (Bradford, 1976). The leaf total soluble sugar content was determined by anthrone sulfate method (Irigoyen et al., 1992). The leaf Vitamin C content was determined by molybdenum blue colorimetric method (Omaye et al., 1979), and leaf nitrate content was measured by the salicylic acid-sulfuric acid colorimetric method (Miranda et al., 2001).

3.6 Statistical analysis

All the statistical analyses were performed using IBM SPSS 20.0 software (IBM SPSS Statistics, IBM Corporation, Armonk, NY, USA). Principal Component Analysis (PCA) was conducted to reduce the dimensionality of the dataset and to identify the principal components that explain the most variance. The data were first standardized to have mean zero and unit variance. The covariance matrix was then computed, and eigenvalues and eigenvectors were extracted to determine the principal components. The number of components retained was based on the eigenvalues greater than 1 criterion and a scree plot examination. Different lowercase letters represent significant differences between the treatments according to Duncan's multiple range test (one-way ANOVA, $p < 0.05$). Means separation was determined using the Tukey-Kramer HSD method ($p = 0.05$). The figures were plotted using Origin 2021.

4 Results

4.1 Impact of different light treatments on plant growth

The growth indices, including stem thickness, leaf length, leaf width, total area, and the number of leaves, were measured and fitted for lettuce plants subjected to different light quality treatments (Figure 3B). The results indicated variations in lettuce growth among the different light quality treatments (Figure 3A). On the 28th day of lettuce growth, the growth indices revealed notable differences. Stem thickness for F3 increased by 27.6% and 15.1% compared to CK and F2, respectively. Leaf length exhibited increases of 13.6%, 22.9% and 25.3% compared to CK, F1 and F2, respectively. Leaf width surpassed CK, F1, F2, and F4 by 24.6%, 30.1%, 25.1%, and 14.68%, respectively. Leaf area increased by

10.3389/fpls.2024.1430241

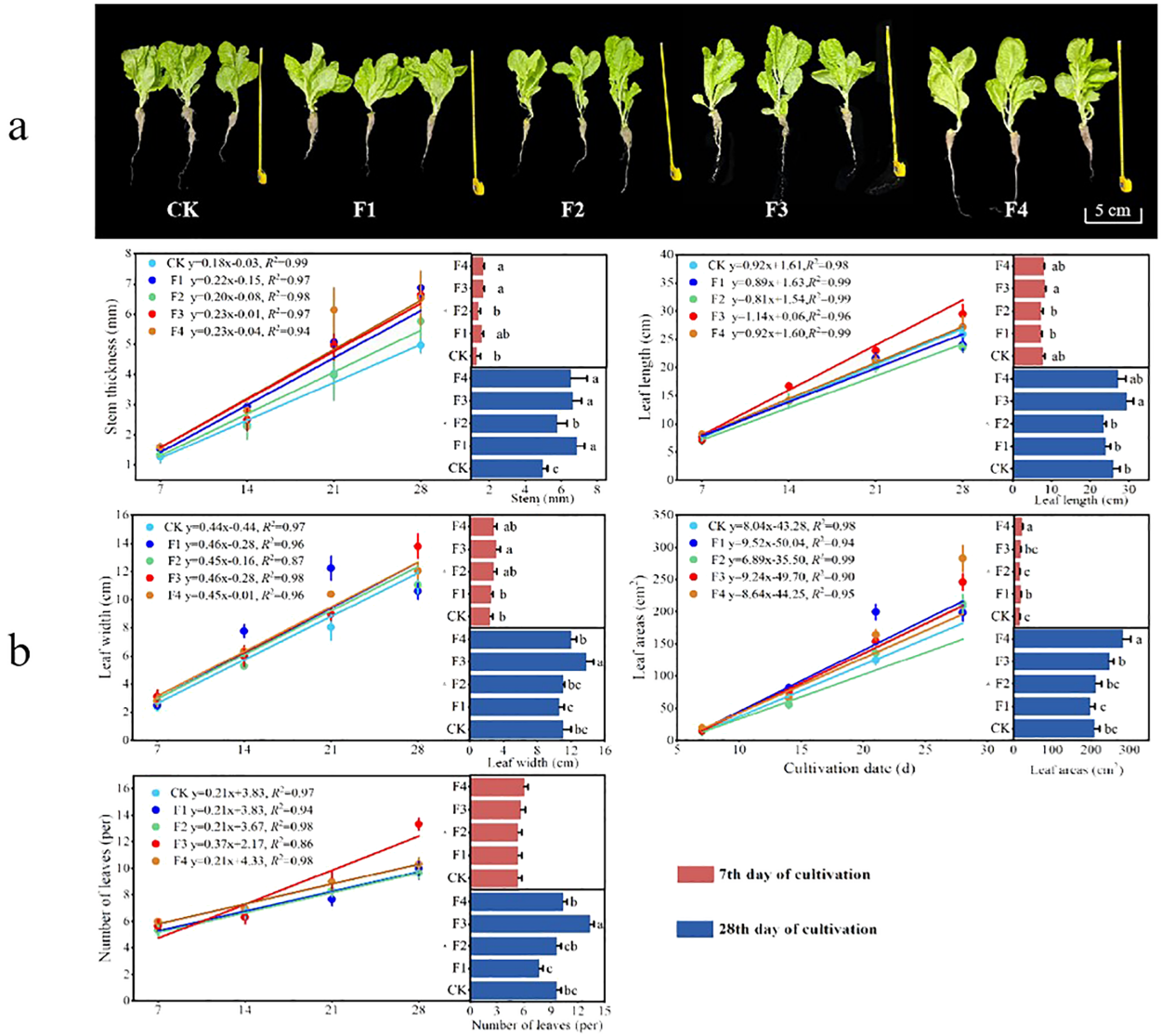

FIGURE 3
Fit curves and comparative analysis of lettuce growth during different light treatments: **(A)** Lettuce plant control, **(B)** lettuce growth fitting curve. Different lowercase letters in the same column in the Figure indicate that the difference between different treatments reaches a significant level of $p< 0.05$. The data fitting was performed using linear regression, with $R^2 > 0.80$ and $P > 0.75$, indicating a high level of fitting accuracy.

17.3%, 24.1%, and 15.7% compared to CK, F1, and F2, and was 12.9% less than F4. The number of leaf blades saw a significant increase by 37.9%, 73.9%, 37.9%, and 29.1%. The optimal lighting condition was found to be a 3:2 ratio of CK + Phosphor Stimulated Far-red LED (3:2) (F4), effectively regulating plant growth.

4.2 Impact of different light qualities on the biomass and root of lettuce

Significant differences were observed among various light treatments concerning lettuce biomass and root, as illustrated in Figure 4B. Regarding aboveground fresh mass, the F3 treatment outperformed others, showing a noteworthy increase of 25.6% compared to the control (CK) and a significant difference of 57.5% compared to the F2 treatment. Concerning belowground fresh weight mass, both the F3 and F4 treatments exhibited a substantial increase of 48.3% and 43.9%, respectively, compared to the control (CK). However, the difference between F3 and F4 was not statistically significant. In terms of aboveground dry mass, direct differences among treatments were not found to be significant. However, for underground dry mass, both F3 and F4 demonstrated a significant increase of 103% and 80.7% over the control (CK), with no significant differences between F3 and F4 (Figure 4A).

The total root length and area of lettuce under different light treatments followed this order (Table 2): F3 > F1 > F4 > F2 > CK. These results suggest that optimal values for aboveground fresh mass, dry mass, belowground fresh mass, dry mass, root length, and area of lettuce were achieved under the light conditions of the F1, F3, and F4 treatments, with the F3 treatment being superior to the others. This indicates that the F1, F3, and F4 treatments significantly enhance both biomass and root length, with F3 being the most effective.

10.3389/fpls.2024.1430241

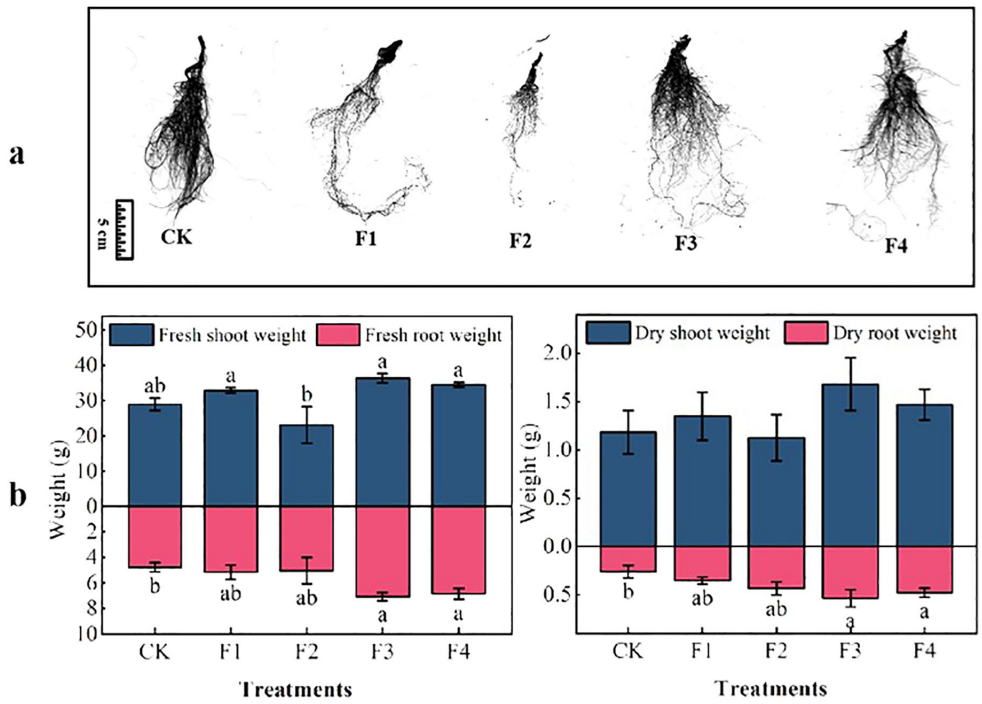

FIGURE 4
Effect of different light treatments on lettuce biomass: **(A)** root morphology, **(B)** lettuce plant biomass. Different lowercase letters in the same column in the figure indicate that the difference between different treatments reaches a significant level of $p< 0.05$.

4.3 Impact of different light qualities on the nutritional quality of lettuce

Figure 5 illustrates distinct trends in the quality indexes of lettuce leaves under various light treatments. Notably, the vitamin C content of F3 exhibited a significant increase of 38.1% compared to F2, while no significant differences were observed between CK, F1, and F4 treatments. In terms of nitrate content, F3 demonstrated a substantial increase of 110.7% compared to CK, whereas F2 showed a significant decrease of 39.8% compared to F3. No significant differences were found between F1, F3, and F4 treatments. Additionally, the soluble sugar content of both F3 and F4 significantly increased by 11.9% and 12.2%, respectively, compared to CK. However, the difference between F3 and F4 was not statistically significant, and F2 exhibited a significant decrease of 7.3% compared to CK. Furthermore, the soluble protein content of F4 displayed a significant increase of 27.5% compared to CK. These findings indicate that, among the different light treatments, F3 consistently showed higher Vitamin C content and soluble sugar content in lettuce leaf quality compared to other treatments.

4.4 Effects of different light treatments on stomatal structure of lettuce leaves

The experimental data reveal significant variations in the morphology and arrangement of the lower epidermis of lettuce leaves across different light treatments (Figure 6). Notably, compared to F2, F3 and F4 treatments exhibited the largest stomatal openings with tightly arranged stomata. The pore openings were larger, and the single area was greater in these treatments. In contrast, F2 treatment, on the other hand, featured the smallest stomatal openings, narrow and long stomata, and a small single area The individual stomatal opening of the lower-surface in lettuce leaves followed the order (Figure 7): F1 = F4 = F3 > CK > F2. Additionally, the order of stomatal density of the lower-surface in lettuce leaves was F3 > F4 > F1 > CK > F2.

4.5 Effects of different light treatments on photosynthetic pigments and photosynthetic properties of lettuce

As depicted in Figure 8, the photosynthetic characteristics of lettuce leaves varied significantly under different light treatments. The photosynthetic rate reached its peak in the F1 treatment, significantly surpassing that of other light treatments. Specifically, F1 However, the difference between F2 and CK was not significant. The trend of stomatal conductance (*Gs*) in lettuce leaves mirrored that of photosynthesis (*Pn*), with F3 and F4 experiencing significant increases of 32.9% and 24.6%, respectively, compared to CK. The Ci revealed that F3 and F4 exhibited significant increases of 21.2% and 16.6% compared to CK, with a significant difference between F3 and F4, while F2 decreased significantly by 8.1% compared to CK. In terms of transpiration rate (*Tr*) in lettuce leaves, there were significant differences among treatments. F1, F3, and F4

10.3389/fpls.2024.1430241

TABLE 2 Impact of varied light treatments on lettuce root development.

Treatments	Total Length (cm)	Total Surface Area (cm^2)	Average Diameter (mm)	Root Volume (cm^3)
CK	144.15 ± 19.71b	18.8 ± 1.03b	0.56 ± 0.05	1.24 ± 0.22ab
F1	332.92 ± 41.38a	24.54 ± 0.93a	0.49 ± 0.04	2.11 ± 0.45a
F2	206.99 ± 65.67ab	21.03 ± 1.87ab	0.41 ± 0.03	0.51 ± 0.16b
F3	347.37 ± 18.52a	24.55 ± 1.59a	0.48 ± 0.05	2.32 ± 0.33a
F4	298.37 ± 53.84a	25.16 ± 1.22a	0.5 ± 0.08	2.23 ± 0.45a

Data are means ± standard error, analysis of differences in different treatments, different letters in the same column indicate significant differences ($p< 0.05$).

demonstrated significant increases of 35.4%, 185.4%, and 123.9%, respectively, compared to CK, whereas F2 exhibited a significant decrease of 98.3% compared to CK.

Different light treatments exerted a noteworthy impact on the pigment content of lettuce leaves (Table 3). The effects of all light treatments on the chlorophyll a content in lettuce leaves were not significant. Light treatments F1, F2, and F3 increased the chlorophyll b content. Among these, the F4 light treatment resulted in the highest chlorophyll b content, with increases of 31.5% and 32.4% compared to CK and F3, respectively. Additionally, light treatments F1, F2, and F3 also increased the total chlorophyll (a+b) content, with F1 having the highest total chlorophyll (a+b) content, significantly increasing by 8.7% and 6.0% compared to CK and F3, respectively. The F3 treatment had the highest chlorophyll a/b ratio, significantly increasing by 29.1%, 31.9%, and 32.2% compared to F1, F2, and F4, respectively. Compared to CK, although F1, F2, F3, and F4 light treatments increased the carotenoid content to varying degrees, only F1 and F3 showed significant differences in carotenoid content compared to CK.

4.6 Effect of different light treatments on chlorophyll fluorescence parameters

Figure 9 illustrates that the relative electron transport rate (rETR), derived from Equation 1, under the F3 treatment surpasses that of other treatments. This increase in rETR is beneficial for enhancing photosynthetic efficiency and CO_2 fixation efficiency. Additionally, the rETR of lettuce in the F3 treatment rises concomitantly with the enhancement of photosynthetic capacity.

The chlorophyll fluorescence parameters of lettuce leaves were measured under each treatment, and the corresponding data are presented in Table 4. Specifically, the Fv/Fm values of the F3 and F4 treatments decreased by 6.25% and 6.38% compared to the control

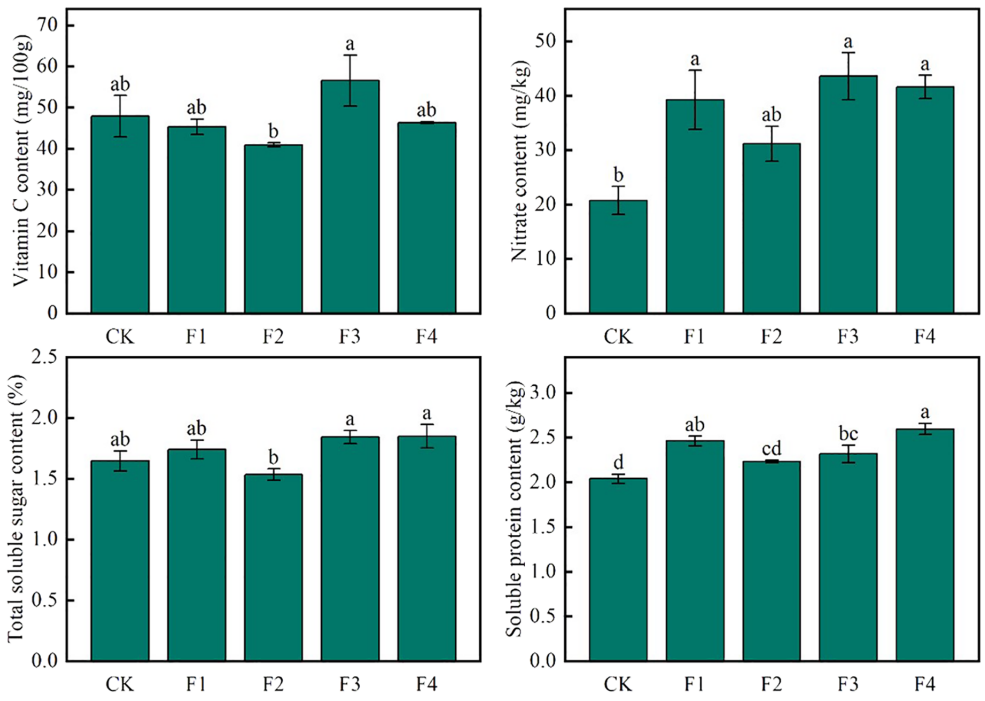

FIGURE 5
Effect of various light qualities on lettuce nutritional quality. Different lowercase letters in the same column in the figure indicate that the difference between different treatments reaches a significant level of $p< 0.05$.

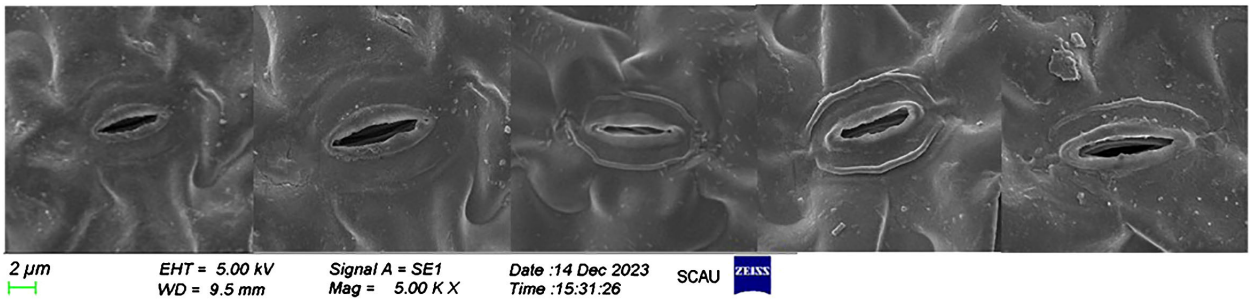

FIGURE 6
Scanning electron microscope photographs show the effects of different light treatments on the lower surface of lettuce leaves.

(CK), respectively. Notably, there were no significant differences among the treatments, except for CK. The non-photochemical quenching coefficients (NPQ) for the F3 and F4 treatments were 11.9% and 3.3% lower than those of CK. Conversely, the actual photochemical quantum yield (ΦPSII), derived from Equation 2, displayed an opposite trend to Fv/Fm, with the order being F1>F3>F4>F2>CK.

4.7 Photosynthetic characteristics, chlorophyll heat chart signs and growth correlation analysis of lettuce leaves

To comprehensively explore the interrelation among photosynthetic properties, chlorophyll fluorescence, and growth indicators in lettuce leaves and Pearson correlation heat map (Figure 10) were performed. Pearson correlation heat map analysis indicated significant positive correlations between *Tr*, *Pn*, *Gs*, *Ci*, and aboveground and belowground fresh weight, dry mass, ksoluble sugar, vitamin C content, nitrate content, and soluble protein content. This suggests that improved photosynthetic indexes positively influenced lettuce growth morphology and quality indices. Conversely, Fv/Fm, qL, and NPQ exhibited negative correlations with growth, quality, and biomass, emphasizing that chlorophyll content alone cannot entirely determine photosynthetic capacity, directly impacting growth and quality traits. The complex correlations among the measured photosynthetic quality indicators highlight diverse information interactions and overlaps. Singular indicators cannot serve as exclusive influencing factors for evaluating lettuce growth and

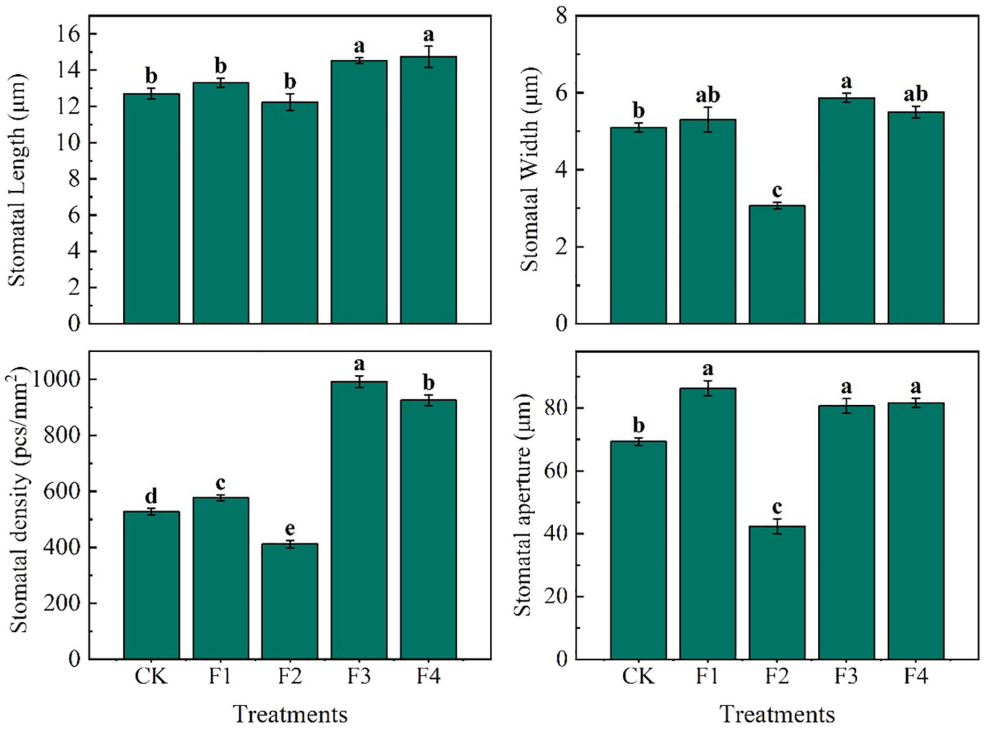

FIGURE 7
Data statistics of leaf lower-surface stomata in lettuce leaves under different light treatment. Different lowercase letters in the same column in the figure indicate that the difference between different treatments reaches a significant level of $p < 0.05$.

10.3389/fpls.2024.1430241

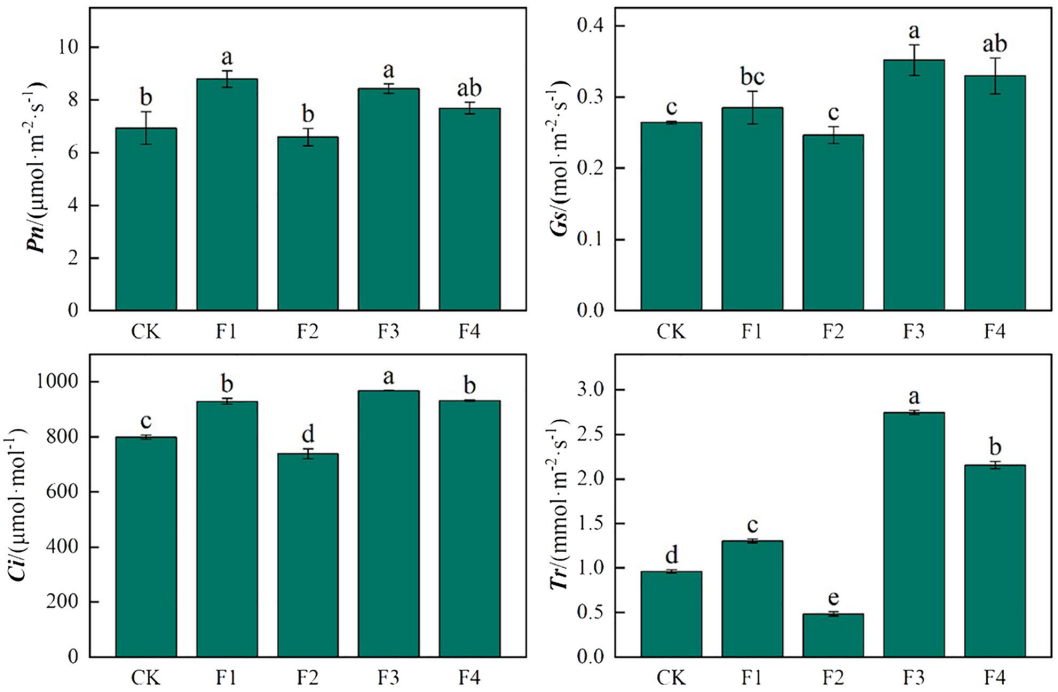

FIGURE 8
Effects of different light treatments on the photosynthetic characteristics of lettuce. Different lowercase letters in the same column in the figure indicate that the difference between different treatments reaches a significant level of $p< 0.05$.

quality in each treatment. Therefore, for a comprehensive assessment, the shortcomings of single indexes should be overcome. Utilizing principal component analysis, it becomes necessary to consider multiple growth and quality indicators to thoroughly evaluate lettuce growth and quality across different treatments.

4.8 Scores and evaluation analysis of comprehensive indicators of different light treatments

Evident separations among the treatments were observed after conducting a principal component analysis (PCA) of growth quality, biomass, photosynthetic indexes, and chlorophyll fluorescence (Figure 11). PC1 explained 40.5% of the variability, highlighting its substantial role in differentiating the main trends within the data. Conversely, PC2 accounted for an additional 17.2% of the variation, although its impact was less pronounced compared to PC1. In the variable loading plot, attributes such as chlorophyll a+b (BA), chlorophyll a (CA), and stem thickness (ST) demonstrated strong positive loadings on PC1, suggesting these variables are crucial in defining the primary distinctions across the dataset. Their minimal association with PC2 implies a lesser influence on the variation explained by this component.

The sample score plot revealed clear distinctions among the treatment groups, identified by different colors (CK, F1, F2, F3, F4). The CK and F1 were significantly separated along the PC1 axis, indicating pronounced differences in principal variables between these groups. In contrast, the F3 and F4 were clustered more closely, suggesting these treatments shared similarities in the variables considered. Overall, this PCA effectively highlighted the influential roles of principal variables across different experimental treatments, delineating clear distinctions among the groups. By uncovering the most significant sources of variation, the analysis

TABLE 3 Effects of different light treatments on photosynthetic pigments in lettuce (mg/L).

Treatments	Chlorophyll a content	Chlorophyll b content	Chlorophyll a +b content	Chlorophyll a/b	Carotenoid
CK	15.47 ± 1.21	3.01 ± 0.56b	18.43 ± 0.13b	5.22 ± 0.79a	3.21 ± 0.41b
F1	16.04 ± 0.41	3.92 ± 0.2a	19.95 ± 0.22a	4.13 ± 0.31b	3.96 ± 0.83a
F2	15.76 ± 0.54	3.93 ± 0.18a	19.68 ± 0.37a	4.04 ± 0.33b	3.4 ± 0.68ab
F3	15.82 ± 0.11	2.99 ± 0.16b	18.81 ± 0.16b	5.33 ± 0.31a	3.67 ± 0.03a
F4	15.82 ± 0.24	3.96 ± 0.23a	19.79 ± 0.1a	4.03 ± 0.3b	3.55 ± 0.03ab

Data are means ± standard error, analysis of differences in different treatments, different letters in the same column indicate significant differences ($p< 0.05$).

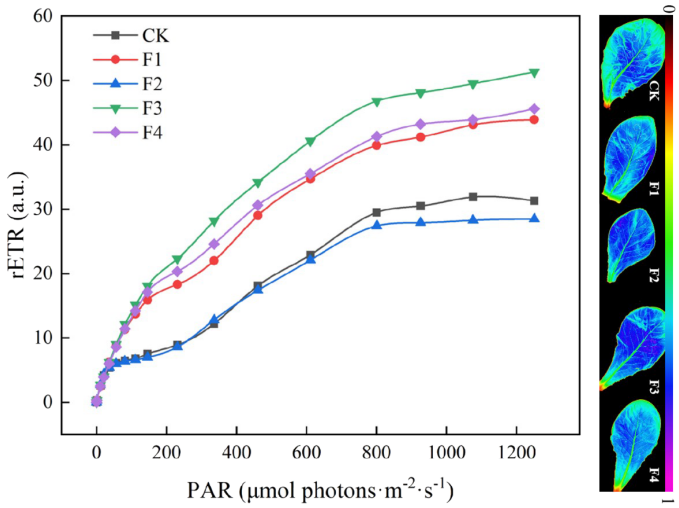

FIGURE 9
Effect of different light treatments on chlorophyll fluorescence parameters.

offers a detailed insight into how different conditions affect the dataset, providing a valuable foundation for further exploration of treatment effects.

By employing principal component analysis and calculating the scores for each index (Table 5), the comprehensive evaluation D value was derived from the membership functions u(X1), u(X2), u(X3), u (X4), and u(X5), in conjunction with weight processing. The results were ranked and presented in Table 5. Following a thorough analysis of comprehensive performance, considering growth quality, biomass, photosynthetic index, and chlorophyll fluorescence, the F3 treatment demonstrated the highest comprehensive evaluation D value, followed by F4 and F1. In contrast, the D values for F2 and CK treatments were the lowest. This discrepancy in evaluations could be attributed to the lower root index, chlorophyll content, and overall quality of lettuce in these treatments.

5 Discussion

Light, acting as both a signal and energy source for plant growth, plays a crucial role in regulating various aspects of plant development, morphogenesis, and physiological quality. Plants possess photoreceptors, known as phytochromes, that sense both red and far-red light, consisting of chromophores and apoproteins. In this experiment, the varied ratios of red and far-red light had significant effects on plant phenology. Far-red light creates a shading effect, giving plants the perception of reduced light. Consequently, plants respond by increasing height and leaf area, engaging in a competitive struggle for more light to ensure normal growth and enhance photosynthesis in the expanded leaf area (Hu et al., 2021; Mérai et al., 2023; Hu et al., 2024) The combination of red and far-red light can further regulate plant height, causing the above-ground portion to develop faster than the underground root system (Holalu et al., 2021). In our study, we observed that a red light to far-red light ratio of 3:2 significantly increased the dry/fresh weight of lettuce plants and promoted overall plant growth (Figure 4). This finding aligns with LI (Li and Kubota, 2009), who concluded that supplementing far-red light significantly enhances dry/fresh weight, leaf length, and leaf width in crops.

Various light qualities exert regulatory effects on physiological processes, including gas exchange and chlorophyll formation in plant leaves (Ramalho et al., 2002). The photoreceptors (such as phytochromes and cryptochromes) and chloroplasts within leaf cells play a role in regulating stomatal volume size and stomatal number in response to different light qualities. Notably, far-red light has a pronounced impact on the morphology of plant cells (Khattak

TABLE 4 Effects of different light treatments on chlorophyll fluorescence parameters in lettuce leaves.

Treatments	Fv/Fm	ΦPSII	qL	qP	NPQ
CK	0.833 ± 0.005a	0.069 ± 0.033c	0.183 ± 0.08a	0.129 ± 0.036b	0.93 ± 0.033ab
F1	0.779 ± 0.012b	0.303 ± 0.039a	0.056 ± 0.017b	0.46 ± 0.051a	0.789 ± 0.073b
F2	0.804 ± 0.008b	0.078 ± 0.022c	0.227 ± 0.029a	0.172 ± 0.042b	0.959 ± 0.04a
F3	0.784 ± 0.016b	0.198 ± 0.086ab	0.053 ± 0.026b	0.338 ± 0.137a	0.831 ± 0.026ab
F4	0.783 ± 0.017b	0.097 ± 0.024bc	0.083 ± 0.022b	0.118 ± 0.056b	0.9 ± 0.04ab

Fv/Fm is the maximum photometric quantum efficiency of PSII; ΦPSII is the actual photochemical quantum yield of PSII; qL and qP is photochemical quenching; NPQ is non-photochemical quenching. Data are means ± standard error, analysis of differences in different treatments, different letters in the same column indicate significant differences ($p < 0.05$).

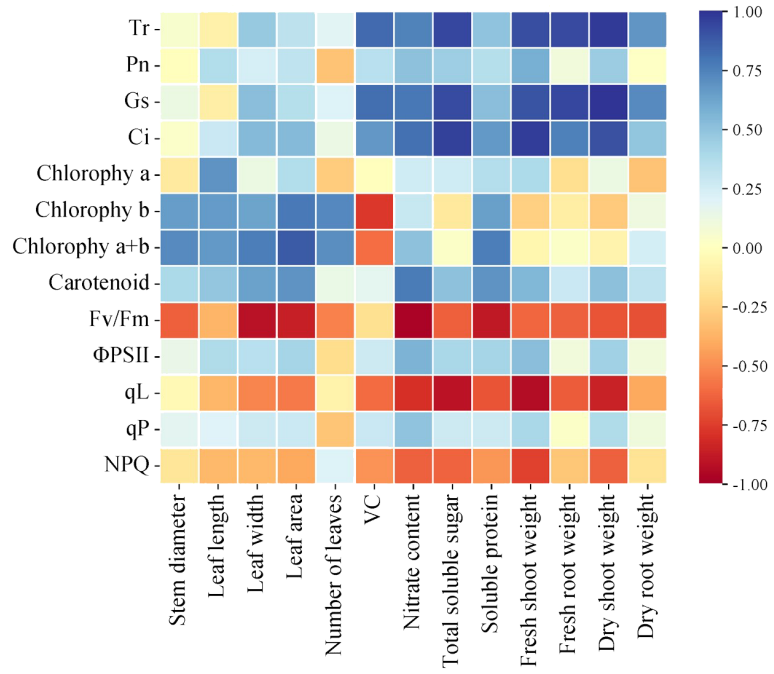

FIGURE 10
Correlation between photosynthetic characteristics and chlorophyll fluorescence components and growth parameters of lettuce leaves under different light treatments.

and Pearson, 2006; Yonghua et al., 2005). In our experiment, it was observed that the addition of far-red light led to an increase in stomatal density (Figure 7). Stomata exhibited well-defined elliptical shapes, resulting in a significant increase in stomatal conductance and facilitated gas exchange. This finding aligns with previous studies that demonstrated an elevated far-red light ratio contributing to increased stomatal density in Chrysanthemum (Momokawa et al., 2011) and plants within the Chrysanthemum family (Kim et al., 2004).

The photosynthetic pigments in plant leaves play crucial roles in light energy absorption, transmission, and conversion, forming the foundation of photosynthesis. The composition and content of these pigments significantly influence the photosynthetic process (Lee et al., 2016). In our experiment, we observed a decrease in the

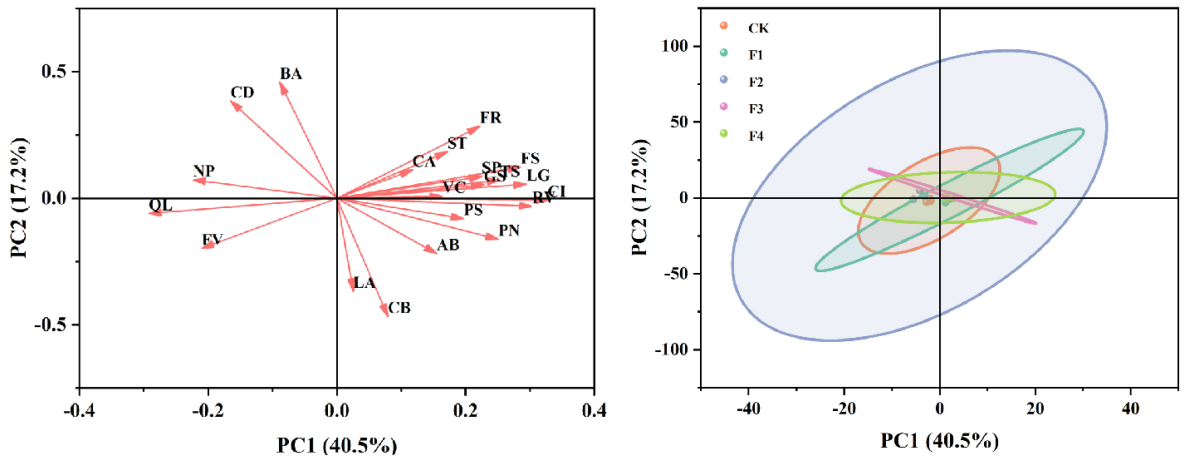

FIGURE 11
Principal component analysis (PCA) of the relationships among growth quality, biomass, photosynthetic indexes, and chlorophyll fluorescence. The direction and length of arrows indicate the correlations and their strengths, respectively. ST, stem thickness; LA, leaf area; FS, fresh shoot weight; FR, fresh root weight; VC, vitamin C; TS, total soluble sugar; SP, soluble protein; PN, photosynthesis; GS, stomatal conductance; CI, intercellular CO_2 concentration; CA, chlorophyll a; CB, chlorophyll b; AB, chlorophyll a+b; BA, chlorophyll a/b; CD, carotenoid; LG, root length; RV, root volume; FV, Fv/Fm; PS, ΦPSII; QL, Ql; NP, NPQ.

TABLE 5 Principal components, membership functions, comprehensive evaluation values(D) and rankings for different treatments.

Treatments	F1	F2	F3	F4	F5	u (X_1)	u (X_2)	u (X_3)	u (X_4)	u (X_5)	D value	Sort
CK	-55.66	-12.25	1.06	2.45	-1.19	0.40	0.17	0.62	0.91	0.34	1.64	5
F1	50.84	-8.17	1.99	-4.06	0.38	0.92	0.28	0.62	0.40	0.73	1.89	3
F2	-105.22	10.50	-0.23	-1.20	0.51	0.11	0.60	0.35	0.49	0.61	1.77	4
F3	43.57	2.05	-0.29	2.33	1.94	0.82	0.40	0.45	0.82	0.91	2.48	1
F4	66.47	7.86	-2.53	0.47	-1.65	0.95	0.53	0.41	0.70	0.25	2.19	2

content of photosynthetic pigments in lettuce leaves with the addition of far-red light. Notably, red light proved more favorable for the augmentation of chlorophyll b. Different light treatments had a significant impact on the pigment content of lettuce leaves. While there were no significant effects on chlorophyll a content, treatments F1, F2, and F3 increased the chlorophyll b content, with F4 showing the highest increase. Additionally, F1, F2, and F3 increased the total chlorophyll (a+b) content, with F1 being the most effective. The F3 treatment had the highest chlorophyll a/b ratio among all treatments. Although all light treatments increased carotenoid content compared to CK, only F1 and F3 showed significant differences (Table 3). The introduction of far-red light resulted in subsequent increases in the transpiration rate, intercellular CO_2 concentration, and stomatal conductance. This response may be attributed to the pronounced shade avoidance effect induced by far-red light in lettuce. The plant perceives the shading of its leaves and senses reduced light, prompting an adaptive increase in transpiration and stomatal conductance (Naznin et al., 2019). Photosynthetic pigments serve as the material basis for photosynthesis and the foundation for nutrient synthesis. The supplementation of far-red light can influence quality by regulating the Red/Far-Red (R/FR) ratio. Far-red light treatment demonstrated an increase in the content of soluble sugars and soluble proteins in lettuce. This effect is likely due to the impact of varying R/FR values on the synthesis and absorption of carbohydrates and various amino acids in plants following increased far-red light exposure, consequently altering the content of soluble sugars and soluble proteins (Meng and Runkle, 2019).

The Fv/Fm ratio serves as an indicator of the efficiency of Photosystem II (PSII) in utilizing absorbed light energy to reduce the main quinone acceptor (QA) of PSII (Baker, 2008). Typically, an Fv/Fm value lower than 0.83 suggests plant stress, signifying a reduction in photosynthetic capacity (Björkman and Demmig, 1987). In this study, the Fv/Fm value exhibited a declining trend with the addition of far-red light. Notably, the F3 and F4 treatment groups recorded values below 0.83, However, it is important to note that 'shade avoidance' stress, which typically involves morphological adaptations such as stem elongation and does not directly influence Fv/Fm, may not be the correct terminology to describe our observations. Instead, the decline in Fv/Fm may be more likely associated with other stress factors such as high light intensity or environmental stresses (e.g., temperature, drought), which could exacerbate the production of reactive oxygen species (ROS) under these lighting conditions. In the F2 treatment, blue light was added, and the presence of blue light might alter the overall light quality balance perceived by the plants. This could affect the plants' sensitivity to the increased ratio of far-red light, The observed changes in Fv/Fm and ΦPSII responses suggest an interaction of light quality with environmental factors, which could have been confounded by high plant density. Additionally, the signaling between blue light receptors and far-red light receptors (such as phytochrome) might interact, influencing the initiation of shade avoidance responses. (Forster and Bonser, 2009) ΦPSII represents the actual photosynthetic capacity of PSII, while ETR denotes the photosynthetic electron transfer rate. Our findings revealed a significant increase in ΦPSII with higher levels of red light. This increase is attributed to the enhanced activity of Photosystem I (PSI) induced by red light. Red light maximizes the absorption in chlorophylls, primarily benefiting PSII. Thus, a significant increase in ΦPSII might typically be expected with higher levels of red light rather than far-red light (Table 4). However, Zhen demonstrated that far-red light preferentially excites PSI over PSII, which can also increase ΦPSII. It is likely that under far-red light conditions, sufficient excitation of PSI helps balance the charges between PSII and PSI, leading to a reduced number of PSI centers. This reduction in PSI centers can limit the rate of electron transfer down the electron transport chain, causing PSII to relax slower than in other treatments. If the plants were dark-adapted for a longer period, the Fv/Fm values might be similar. The observed differences could also be influenced by high plant density and self-shading effects (Zhen et al., 2019).

Based on our principal component analysis (PCA) results, the study has significantly revealed the effects of different spectral treatments on plant growth and physiological characteristics (Figure 11). Specifically, the impacts of far-red light and red light on growth quality, biomass, photosynthetic indices, and chlorophyll fluorescence show distinct differences, providing an important basis for optimizing spectral treatments. The variable loading plot shows that chlorophyll a+b (BA), chlorophyll a (CA), and stem thickness (ST) exhibit strong positive loadings on PC1, indicating that these variables play a dominant role in distinguishing between far-red light and red light treatments. These results suggest that far-red and red light may regulate plant growth by affecting chlorophyll content and stem structure. Additionally, the F3 and F4 treatment groups are closely clustered in the sample score plot, indicating similarities in the considered variables. This finding provides a reference for optimizing light conditions in practical applications in the future. Overall, this study effectively highlights the different impacts of far-red and red light on plant growth and physiological characteristics through PCA, revealing the potential application value of spectral treatments in agriculture and horticulture. Future research can

further explore the effects of different spectral combinations and intensities on various plant species and growth stages, aiming to achieve precise light environment control, thereby improving crop yield and quality.

6 Conclusion

In this study, we investigated the regulatory mechanism of far-red light on plant growth and physiology, specifically focusing on photosynthetic characteristics. Under the irradiation condition of the F3 treatment (with a red-to-far-red light ratio of 3:2), there was a significant increase in photosynthetic characteristics. Additionally, both stomatal conductance and quantity increased, resulting in enhanced gas exchange and improved light utilization and capacity in plants. The improved photosynthetic performance significantly enhanced the utilization of light energy by lettuce. This enhancement, in turn, promoted the growth, quality, and biomass accumulation of lettuce. The F4 treatment demonstrates promising application prospects. However, further adjustments in the red-to-far-red light ratio are necessary for optimal results. This research aims to provide a reference basis for the application of phosphor in horticultural plants.

Data availability statement

The datasets presented in this study can be found in online repositories. The names of the repository/repositories and accession number(s) can be found in the article/supplementary material.

Author contributions

XB: Writing – original draft, Writing – review & editing, Conceptualization, Investigation, Methodology, Software, Validation. HX: Conceptualization, Investigation, Writing – original draft, Writing – review & editing. CY: Methodology, Software, Writing – original draft, Writing – review & editing. HZ: Writing – review & editing, Formal analysis, Project administration, Writing – original draft. WL: Investigation, Methodology, Writing – original draft, Writing – review & editing. WS: Formal analysis, Investigation, Writing – review & editing, Writing – original draft. MZ: Conceptualization, Resources, Visualization, Writing – review & editing, Writing – original draft. BL: Funding acquisition, Resources, Writing – review & editing, Supervision, Writing – original draft.

Funding

The author(s) declare financial support was received for the research, authorship, and/or publication of this article. The National Natural Science Foundations of China (No. 12274144), the Guangdong Provincial Special Fund for Modern Agriculture Industry Technology Innovation Teams (No. 2023KJ122), the Key Realm R&D Program of Guangdong Province (No. 2021B0707010003), the Guangdong Provincial Science and Technology Project (No. 2022A1515010229), and the Project of GDUPS (2018) for BL.

Conflict of interest

The authors declare that the research was conducted in the absence of any commercial or financial relationships that could be construed as a potential conflict of interest.

Publisher's note

References

Baba, M., Kikuta, F., Suzuki, I., Watanabe, M. M., and Shiraiwa, Y. (2012). Wave length specificity of growth, photosynthesis, and hydrocarbon production in the oil-producing green alga Botryococcus braunii. *Biores. Technol.* 109, 266–270. doi: 10.1016/j.biortech.2011.05.059

Baker, N. R. (2008). Chlorophyll fluorescence: a probe of photosynthesis. *vivo. Annu. Rev. Plant Biol.* 59, 89–113. doi: 10.1146/annurev.arplant.59.032607.092759

Bautista-Saraiva, A. I. N., Bonomi-Barufi, J., Figueroa, F. L., and Necchi, O. (2018). UV-radiation effects on photosynthesis and photoprotection in gametophytic and sporophytic stages of the freshwater red alga Kumanoa ambigua (*Rhodophyta, Batrachospermales*). *Phycol. Res.* 66, 108–116. doi: 10.1111/pre.12209

Björkman, O., and Demmig, B. (1987). Photon yield of O_2 evolution and chlorophyll fluorescence characteristics at 77 K among vascular plants of diverse origins. *Planta* 170, 489–504. doi: 10.1007/BF00402983

Bradford, M. M. (1976). A rapid and sensitive method for the quantitation of microgram quantities of protein utilizing the principle of protein-dye binding. *Anal. Biochem.* 72, 248–254. doi: 10.1016/0003-2697(76)90527-3

Chen, X., Xue, X., Guo, W., Wang, L., and Qiao, X. (2016). Growth and nutritional properties of lettuce affected by mixed irradiation of white and supplemental light provided by light-emitting diode. *Sci. Hortic.* 200, 111–118. doi: 10.1016/j.scienta.2016.01.007

Emerson, R., Chalmers, R., and Cederstrand, C. (1957). Some factors influencing the long-wave limit of photosynthesis. *Proc. Natl. Acad. Sci.* 43, 133–143. doi: 10.1073/pnas.43.1.133

Fang, S. Q., Lang, T. C., Cai, M. S., and Han, T. (2022). Light keys open locks of plant photoresponses: A review of phosphors for plant cultivation LEDs. *J. Alloys Compd* 902, 163825. doi: 10.1016/j.jallcom.2022.163825

Forster, M. A., and Bonser, S. P. (2009). Heteroblastic development and shade-avoidance in response to blue and redlight signals in Acacia implexa. *Photochem. Photobiol.* 85, 1375–1383. doi: 10.1111/j.1751-1097.2009.00605.x

Franklin, K. A., and Quail, P. H. (2010). Phytochrome functions in Arabidopsis development. *J. Exp. Bot.* 61, 11–24. doi: 10.1093/jxb/erp304

Holalu, S. V., Reddy, S. K., and Finlayson, S. A. (2021). Low red light: Far red light inhibits branching by promoting auxin signaling. *J. Plant Growth Regul.* 40, 2028–2036. doi: 10.1007/s00344-020-10253-7

Hu, H., Cheng, W., Wang, X., Yang, Y., Yu, X., Ding, J., et al. (2024). Enhancing plant photosynthesis using carbon dots as light converter and photosensitizer. *bioRxiv* 2024, 02. 06.579025. doi: 10.1101/2024.02.06.579025

Hu, C., Nawrocki, W. J., and Croce, R. (2021). Long-term adaptation of Arabidopsis thaliana to far-red light. *Plant Cell Environ.* 44, 3002–3014. doi: 10.1111/pce.14032

Irigoyen, J. J., Einerich, D. W., and Sánchez-Díaz, M. (1992). Water stress induced changes in concentrations of proline and total soluble sugars in nodulated alfalfa (Medicago sativa) plants. *Physiol. plant.* 84, 55–60. doi: 10.1111/j.1399-3054.1992.tb08764.x

Khattak, A. M., and Pearson, S. (2006). Spectral filters and temperature effects on the growth and development of chrysanthemums under low light integral. *J. Plant Growth Regul.* 49, 61–68. doi: 10.1007/s10725-006-0020-8

Kim, S. J., Hahn, E. J., Heo, J. W., and Paek, K. Y. (2004). Effects of LEDs on net photosynthetic rate, growth and leaf stomata of chrysanthemum plantlets. *vitro. Sci. Hortic.* 101, 143–151. doi: 10.1016/j.scienta.2003.10.003

Lee, M. J., Son, K. H., and Oh, M. M. (2016). Increase in biomass and bioactive compounds in lettuce under various ratios of red to far-red LED light supplemented with blue LED light. *Hortic. Environ. Biotechnol.* 57, 139–147. doi: 10.1007/s13580-016-0133-6

Li, Q., and Kubota, C. (2009). Effects of supplemental light quality on growth and phytochemicals of baby leaf lettuce. *Environ. Exp. Bot.* 67, 59–64. doi: 10.1016/j.envexpbot.2009.06.011

Li, H., Xu, Z., and Tang, C. (2010). Effect of light-emitting diodes on growth and morphogenesis of upland cotton (Gossypium hirsutum L.) plantlets *in vitro*. *Plant Cell Tiss. Organ Cult.* 103, 155–163. doi: 10.1007/s11240-010-9763-z

Matsuda, R., Ohashi-Kaneko, O., Fujiwara, K., Goto, E., and Kurata, K. (2004). Photosynthetic characteristics of rice leaves grown under red light with or without supplemental blue light. *Plant Cell Physiol.* 45, 1870–1874. doi: 10.1093/pcp/pch203

Meng, Q., Kelly, N., and Runkle, E. S. (2019). Substituting green or far-red radiation for blue radiation induces shade avoidance and promotes growth in lettuce and kale. *Environ. Exp. Bot.* 162, 383–391. doi: 10.1016/j.envexpbot.2019.03.016

Meng, Q., and Runkle, E. S. (2019). Far-red radiation interacts with relative and absolute blue and red photon flux densities to regulate growth, morphology, and pigmentation of lettuce and basil seedlings. *Sci. Hortic.* 255, 269–280. doi: 10.1016/j.scienta.2019.05.030

Mérai, Z., Xu, F., Musilek, A., Ackerl, F., Khalil, S., Soto-Jiménez, L. M., et al. (2023). Phytochromes mediate germination inhibition under red, far-red, and white light in Aethionema arabicum. *Plant Physiol.* 192, 1584–1602. doi: 10.1093/plphys/kiad138

Miranda, K. M., Espey, M. G., and Wink, D. A. A. (2001). rapid, simple spectrophotometric method for simultaneous detection of nitrate and nitrite. *Nitric. Oxide* 5, 62–71. doi: 10.1006/niox.2000.0319

Momokawa, N., Kadono, Y., and Kudoh, H. (2011). Effects of light quality on leaf morphogenesis of a heterophyllous amphibious plant, Rotala hippuris. *Ann. Bot.* 108, 1299–1306. doi: 10.1093/aob/mcr236

Naznin, M. T., Lefsrud, M., Gravel, V., and Azad, M. O. K. (2019). Blue light added with red LEDs enhance growth characteristics, pigments content, and antioxidant capacity in lettuce, spinach, kale, basil, and sweet pepper in a controlled environment. *Plants* 8, 93. doi: 10.3390/plants8040093

Omaye, S. T., Turnbull, J. D., and Sauberlich, H. E. (1979). Selected methods for the determination of ascorbic acid in animal cells, tissues, and fluids. *Acad. Press* 62, 3–11. doi: 10.1016/0076-6879(79)62181-X

Park, Y., and Runkle, E. S. (2018). Far-red radiation and photosynthetic photon flux density independently regulate seedling growth but interactively regulate flowering. *Environ. Exp. Bot.* 155, 206–216. doi: 10.1016/j.envexpbot.2018.06.033

Parys, E., Krupnik, T., Kułak, I., Kania, K., and Romanowska, E. (2021). Photosynthesis of the Cyanidioschyzon merolae cells in blue, red, and white light. *Photosynth. Res.* 147, 61–73. doi: 10.1007/s11120-020-00796-x

Ramalho, J. C., Marques, N. C., Semedo, J. N., Matos, M. C., and Quartin, V. L. (2002). Photosynthetic performance and pigment composition of leaves from two tropical species is determined by light quality. *Plant Biol.* 4, 112–120. doi: 10.1055/s-2002-20443

Tan, T., Li, S., Fan, Y., Wang, Z., Ali Raza, M., Shafiq, I., et al. (2022). Far-red light: A regulator of plant morphology and photosynthetic capacity. *Crop J.* 10, 300–309. doi: 10.1016/j.cj.2021.06.007

Teklehaimanot, Z. (2004). Review: Physiological plant ecology: Ecophysiology and stress physiology of functional groups, 4th edn. *Forestry: An International Journal of Forest Research.* 77 (4), 365–366. doi: 10.1093/forestry/77.4.365-a

Van Delden, S. H., SharathKumar, M., Butturini, M., Graamans, L. J. A., Heuvelink, E., Kacira, M., et al. (2021). Current status and future challenges in implementing and upscaling vertical farming systems. *Nat. Food.* 2.12, 944–956. doi: 10.1038/s43016-021-00402-w

Van Gerrewey, T., Boon, N., and Geelen, D. (2022). Vertical farming: The only way is up Agronomy 12, 1–15. doi: 10.3390/agronomy12010002

Wang, Y., Burgess, S. J., de Becker, E. M., and Long, S. P. (2020). Photosynthesis in the fleeting shadows: an overlooked opportunity for increasing crop productivity. *Plant J.* 101, 874–884. doi: 10.1111/tpj.14663

Wassenaar, M. L. J., van Ieperen, W., and Driever, S. M. (2022). Low red to far-red ratio increases resistance to CO2 diffusion and reduces photosynthetic efficiency in low light grown tomato plants. *Environmental and Experimental Botany.* 200, 104918. doi: 10.1016/j.envexpbot.2022.104918

Wellburn, A. R. (1994). The spectral determination of chlorophylls a and b, as well as total carotenoids, using various solvents with spectrophotometers of different resolution. *J. Plant Physiol.* 144, 307–313. doi: 10.1016/S0176-1617(11)81192-2

Wong, C. E., Teo, Z. W. N., Shen, L., and Yu, H. (2020). Seeing the lights for leafy greens in indoor vertical farming. *Trends Food Sci. Technol.* 106, 48–63. doi: 10.1016/j.tifs.2020.09.031

Wu, D., Wu, H., Xiao, Y., Dong, X. L., Wang, Y., Zhou, W. P., et al. (2022). Highly efficient and thermally stable far-red-emitting phosphors for plant-growth lighting. *J. Lumin* 244, 118750. doi: 10.1016/j.jlumin.2022.118750

Yang, C., Liu, W., You, Q., Zhao, X., Liu, S., Xue, L., et al. (2023). Recent advances in light-conversion phosphors for plant growth and strategies for the modulation of photoluminescence properties. *Nanomaterials* 13, 1715. doi: 10.3390/nano13111715

Yang, C., Zheng, D., Zou, X., Dai, X., Tang, B., Molokeev, M. S., et al. (2024). Highly-efficiency far-red emission in cr^{3+} Activated $ca_{1.8}Mg_{1.2}Al_2Ge_3O_{12}$ toward plant precise lighting. *Adv. Opt. Mater.* 12 (17), 2303235. doi: 10.1002/adom.202303235

Yonghua, Q., Shanglong, Z., Asghar, S., Lingxiao, Z., Qiaoping, Q., Kunsong, C., et al. (2005). Regeneration mechanism of Toyonoka strawberry under different color plastic films. *Plant Sci.* 168, 1425–1431. doi: 10.1016/j.plantsci.2004.11.016

Zhen, S., and Bugbee, B. (2020). Far-red photons have equivalent efficiency to traditional photosynthetic photons: Implications for redefining photosynthetically active radiation. *Plant Cell Environ.* 43, 1259–1272. doi: 10.1111/pce.13730

Zhen, S., Haidekker, M., and van Iersel., M. W. (2019). Far-red light enhances photochemical efficiency in a wavelength-dependent manner. *Physiol. Plant* 167, 21–33. doi: 10.1111/ppl.12834

Zhen, S., and van Iersel, M. W. (2017). Far-red light is needed for efficient photochemistry and photosynthesis. *J. Plant Physiol.* 209, 115–122. doi: 10.1016/j.jplph.2016.12.004

Zhen, S., van Iersel, M., and Bugbee, B. (2021). Why far-red photons should be included in the definition of photosynthetic photons and the measurement of horticultural fixture efficacy. *Front. Plant Sci.* 12. doi: 10.3389/fpls.2021.693445

Zou, J., Zhang, Y. T., Zhang, Y. Q., Bian, Z. H., Fanourakis, D., Yang, Q. C., et al. (2019). Morphological and physiological properties ofindoor cultivated lettuce in response to additional far-red light. *Sci. Hortic.* 257, 108725. doi: 10.1016/j.scienta.2019.108725

frontiers | Frontiers in Plant Science

TYPE Original Research
PUBLISHED 11 September 2024
DOI 10.3389/fpls.2024.1422814

OPEN ACCESS

EDITED BY
Sina Fallah,
Shahrekord University, Iran

REVIEWED BY
Yuqing Ye,
Rice University, United States
Idupulapati Madhusudana Rao,
International Center for Tropical Agriculture (CIAT), Colombia

*CORRESPONDENCE
Kevin Begcy
kbegcy.padilla@ufl.edu

RECEIVED 24 April 2024
ACCEPTED 20 August 2024
PUBLISHED 11 September 2024

CITATION
Egesa AO, Vallejos CE and Begcy K (2024) Cell size differences affect photosynthetic capacity in a Mesoamerican and an Andean genotype of *Phaseolus vulgaris* L. *Front. Plant Sci.* 15:1422814. doi: 10.3389/fpls.2024.1422814

Cell size differences affect photosynthetic capacity in a Mesoamerican and an Andean genotype of *Phaseolus vulgaris* L.

Andrew Ogolla Egesa [1], C. Eduardo Vallejos [2,3] and Kevin Begcy [1,3*]

[1]Environmental Horticulture Department, University of Florida, Gainesville, FL, United States, [2]Horticultural Sciences Department, University of Florida, Gainesville, FL, United States, [3]Plant Molecular and Cellular Biology Graduate Program, University of Florida, Gainesville, FL, United States

The efficiency of CO_2 flux in the leaf is hindered by a several structural and biochemical barriers which affect the overall net photosynthesis. However, the dearth of information about the genetic control of these features is limiting our ability for genetic manipulation. We performed a comparative analysis between three-week-old plants of a Mesoamerican and an Andean cultivar of *Phaseolus vulgaris* at variable light and CO_2 levels. The Mesoamerican bean had higher photosynthetic rate, maximum rate of rubisco carboxylase activity and maximum rate of photosynthetic electron transport at light saturation conditions than its Andean counterpart. Leaf anatomy comparison between genotypes showed that the Mesoamerican bean had smaller cell sizes than the Andean bean. Smaller epidermal cells in the Mesoamerican bean resulted in higher stomata density and consequently higher stomatal conductance for water vapor and CO_2 than in the Andean bean. Likewise, smaller palisade and spongy mesophyll cells in the Mesoamerican than in the Andean bean increased the cell surface area per unit of volume and consequently increased mesophyll conductance. Finally, smaller cells in the Mesoamerican also increased chlorophyll and protein content per unit of leaf area. In summary, we show that different cell sizes controls the overall net photosynthesis and could be used as a target for genetic manipulation to improve photosynthesis.

KEYWORDS

carboxylation, common bean, gene pools, leaf anatomy, photosynthetic efficiency

Abbreviations: A (µmol m^{-2} s^{-1}), Assimilation rate; A_n/A_{net} (µmol m^{-2} s^{-1}), Net photosynthesis/Net assimilation; C_i (µmol mol^{-1}), Intercellular CO_2; C_a (µmol mol^{-1}), CO_2 in the external environment; E (mol m^{-2} s^{-1}), Transpiration rate; g_{sw} (mol m^{-2} s^{-1}), Stomatal conductance to water vapor; g_{tc} (mol m^{-2} s^{-1}), Total conductance to CO_2; g_s (mol m^{-2} s^{-1}), Stomata conductance to CO_2/g_c CO_2 conductance into the leaf; V_{lmax} (µmol m^{-2} s^{-1}), Maximum photosynthetic rate at light-saturating conditions; l_{50} (µmol m^{-2} s^{-1}), PPFDs needed to attain 0.5 V_{lmax}; V_{cmax} (µmol m^{-2} s^{-1}), Maximum rate of Rubisco carboxylase activity; J_{max} (µEq m^{-2} sec^{-1}), Maximum rate of photosynthetic electron transport; R_d (µmol m^{-2} s^{-1}), Rate of dark respiration.

Highlights

- Leaf photosynthetic performance comparison between a Mesoamerican (Jamapa) genotype and an Andean (Calima) genotype showed that smaller cell size and higher stomatal density found in Jamapa contributed to higher photosynthetic performance.

Introduction

Enhancing photosynthetic efficiency can improve plant performance and productivity (Baker et al., 2007; Cardona et al., 2018; Lin et al., 2022; Keller et al., 2024). We have a limited understanding of the impact of anatomical, biochemical, and physiological architectures of the photosynthetic gas exchange apparatus on net photosynthesis (A_{net}) (Baker et al., 2007; Sakoda et al., 2022). Nevertheless, recent studies have identified inter- and intra-specific phenotypic variation in photosynthetic gas exchange structures associated with adaptation to different environments (Tanaka et al., 2019; Müller and Munné-Bosch, 2021; Cackett et al., 2022; Sakoda et al., 2022). For instance, adaptation to a wide range of hydrological environments by species of *Banksia* are related to changes in morphological and anatomical characteristics that impact net assimilation (Drake et al., 2013).

Leaf traits impact plant photosynthesis by regulating the ability to use CO_2 and light (Drake et al., 2013, 2019; Harrison et al., 2020; Elferjani et al., 2021). Manipulating stomatal characteristics can improve photosynthetic capacity (Tanaka et al., 2013; Ren et al., 2019; Harrison et al., 2020). For instance, size, shape, and density of the stomata as well as the architecture of the cellular and intercellular leaf layers, control CO_2 diffusion through the intracellular space into the chloroplasts (Büssis et al., 2006; Drake et al., 2013; Kollist et al., 2014; McAusland et al., 2016; Peguero-Pina et al., 2017). Particularly, the mesophyll cell size and wall thickness are inversely associated with the CO_2 diffusion path into the chloroplasts (see review by Ren et al., 2019). These traits are critical in C3 plants due to their higher susceptibility to limited CO_2 in the chloroplasts which promotes photorespiration.

The common bean (*Phaseolus vulgaris*, L.) is the most cultivated legume used for direct human consumption (Gepts, 2001), and it represents a significant component of the protein and carbohydrate caloric intake for over half a billion people worldwide (Siddiq et al., 2011; OECD, 2019; Uebersax et al., 2022). Therefore, improving the productivity of common bean will have a significant global impact on food security. The potential for improvement is based on the extent of variation in this species. DNA sequence analysis revealed that Mesoamerica is the primary center of diversity of *P. vulgaris*, from which it radiated to the Andean region (Gaut, 2014). Furthermore, allele frequency analysis also indicated that beans were domesticated independently in each gene pool (Schmutz et al., 2014). More recently, associations of certain DNA variants of beans with ecological niches independent of geographical distributions have been reported (Rodriguez et al., 2016).

Several groups have matched the extent of genotypic diversity between the gene pools and wild and cultivated beans with the phenotypic diversity of variable traits. For instance, significant phenotypic differences in seed size and yields among common beans between Mesoamerican and Andean cultivars were reported (Sexton et al., 1997). These findings pointed out that there were also some contrasting relative growth rates between the two groups under variable environmental conditions. On the other hand, Lynch et al. (1992) and González et al. (1995) reported extensive variation in leaf morphology, anatomy, biochemistry, and assimilation rates among a relatively large set of wild accessions from both gene pools. However, there is still very limited information on the extent and impact of the diversity of the anatomical traits on domesticated common bean genotypes. Early studies established that Mesoamerican beans have smaller organ (i.e. leaves and seeds), and cell sizes than the Andean genotypes (Singh, 1981; Singh et al., 1991; Sexton et al., 1997). These peculiar distinctions have been the basis of the selection of Jamapa as a representative cultivar for the Mesoamerican gene pool and Calima as its Andean counterpart. These two genotypes have been used as parental lines for QTL analysis to understand the inheritance of variable traits of common beans (Bhakta et al., 2015, 2017; Cichy et al., 2015). Therefore, we selected these two common bean genotypes to understand photosynthetic efficiency, particularly in the era of rapid climate change. We hypothesized that some of the existing anatomical differences could explain differences in photosynthetic characteristics between the two common bean genotypes from Andean and Mesoamerican gene pools.

Genetic characterization of the existing variation in photosynthesis-associated traits between Mesoamerican and Andean beans could enable genetic manipulations of the photosynthetic apparatus. The main aim of this study was to use two distinctly variable common bean genotypes that originated from separate domestication events to investigate the extent of the influence of anatomical and morphological traits on their photosynthetic gas exchange sites and how they impact photosynthesis in variable conditions of light and CO_2. Therefore, we used Calima, domesticated in the Andean region, and Jamapa, domesticated in the Mesoamerican region, and we examined their differential patterns of carbon assimilation responses to light and CO_2 and how these variable patterns could be explained by their anatomical differences.

Materials and methods

Plant materials and growth conditions

We selected for comparative analysis a representative genotype from each of the two *Phaseolus vulgaris* L. gene pools. Jamapa is a small, black-seeded landrace from Mesoamerica with an indeterminate growth habit, and Calima is a mottled large-seeded

Andean bean with a determinate growth pattern (Egesa et al., 2024b). In addition, these genotypes exhibit contrasting photoperiod sensitivity (Bhakta et al., 2017), and are the parents of a recombinant inbred family (Bhakta et al., 2015).

Seeds from both genotypes were germinated in a 72-well nursery tray custom black (Nursery Supplies, FL) and transplanted at ten days into one-gallon black molded nursery cans. Three-week-old plants from each genotype were used for all the experiments. This age was selected to avoid other potential confounding effects such as differences in the timing of juvenility-to-maturity transitions as well as the rapid sink-source tissue relocation of photo-assimilates normally happening during reproduction. The media used in the nursery and transplanting was PRO-MIX HP Mycorrhizae planting media (Premier Horticulture, Canada). After transplanting, 17 g of Osmocote (N:P: K 18:6:12) were added to each pot. Greenhouse temperatures were maintained at 26±3 °C/20±3 °C day/night respectively, relative humidity of 50±5% and daylight illumination of 1000±200 µmol m^{-2} s^{-1} photosynthetic photon flux density (PPFD). Irrigation was provided daily by applying water to the field capacity.

Physiological measurements

The uppermost completely expanded mature trifoliate leaf of each genotype was used to measure CO_2 assimilation (A), transpiration rate (E), stomatal conductance to water vapor (g_{sw}), intercellular CO_2 (C_i), and total conductance to CO_2 (g_{tc}), using the LI-COR Li-6800 machine (Begcy et al., 2019; LI-COR, 2023). The temperature inside the leaf chamber was maintained at 25°C.

CO_2 conductance measurements

We exposed the mature trifoliate leaf of each genotype to three levels (200, 400, and 600 µmol mol^{-1}) of CO_2 in the Li-6800 leaf chamber using a photosynthetic photon flux density (PPFD) of 1000 µmol m^{-2} s^{-1} and 25°C as set temperature. We then compared the patterns of leaf conductance using the measured values of A, E, g_{sw}, C_i, and g_{tc}. We then used A, C_a, and C_i values to estimate the CO_2 conductance from outside into the leaves using the formula g_c=A/(C_a-C_i) (Boyer and Kawamitsu, 2011).

Light response curves

Responses to light were measured at 25°C and relative humidity of 60% ± 2% at two levels of CO_2: ambient (400 µmol mol^{-1}) and elevated (600 µmol mol^{-1}) CO_2. The light levels were gradually increased from 0 to 1800 µmol m^{-2} s^{-1} (PPFD) (Begcy et al., 2019). The second level of CO_2 (600 µmol mol^{-1}) in the experiment was to test the potential impact of the rising CO_2 levels on the two common bean genotypes. The measurements were collected in the morning from 8 to 10 am, during the midday from 11 am to 1 pm and in the afternoon, from 2 to 4 pm.

CO_2 response (A–Ci) curves

CO_2 response (A–Ci) curves were obtained at moderate PPFD (1000 µmol $m^{-2}s^{-1}$) for both bean genotypes. The ambient CO_2 (C_a) was adjusted between 50 and 600 µmol mol^{-1}. The measurements were collected in the morning from 8 to 10 am, during the midday from 11 to 1 pm and in the afternoon, from 2 to 4 pm (afternoon) V_{cmax} and J_{max} were estimated using a modified Farquhar-von Caemmerer-Berry model as described in the plantecophys package (Duursma, 2015).

$$Am = \frac{Ac + Aj - \sqrt{(Ac + Aj)^2 - 4\theta AcAj}}{2\theta} - R_d$$

Where:

A_m = the hyperbolic minimum of A_c and A_j.

A_n = min (A_c, A_j) - R_d.

A_n = Net CO_2 assimilation.

A_c = Photosynthesis rate when Rubisco activity is limiting.

A_j = Photosynthesis rate when RuBP –regeneration is limiting.

R_d = the rate of mitochondrial respiration.

θ =theta = 0.85.

A_c, the rubisco-limited photosynthesis rate was estimated as previously described (Duursma, 2015), and estimated as:

$$A_c = V_{cmax}(C_i - \Gamma^*)/[C_i + K_c(1 + O_i/K_o)]$$

Where V_{cmax} is the maximum rate of Rubisco activity, C_i and O_i are the intercellular concentrations of CO_2 and O_2, K_c and K_o are the Michaelis–Menten coefficients of Rubisco activity for CO_2 and O_2, respectively, and Γ* is the CO_2 compensation point in the absence of mitochondrial respiration.

A_j, the photosynthesis rate when ribulose-1,5-bisphosphate (RuBP)-regeneration is limiting was estimated as previously described (Laĭsk et al., 2009; Duursma, 2015), and according to:

$$A_j = (J/4) \times (Ci - \Gamma^*)/Ci + 2\,\Gamma^*)$$

Where J is the rate of electron transport which is related to incident photosynthetically active photon flux density, Q, by:

$$qJ^2 - (aQ + J_{max})J + aQJ_{max} = 0(when\ J < J_{max})$$

where;

q = is the quantum energy state.

a = absorbance by leaf photosynthetic pigments.

We modeled the A-Ci curves using the Duursma approach to estimate the photosynthesis rate for ribulose-1,5-bisphosphate (RuBP) saturated and RuBP-regeneration limited conditions (Duursma, 2015).

Chlorophyll quantification

A set of leaf discs measuring 2.01 cm^2 from fresh leaf tissue were harvested from each genotype. After fresh weight determination, discs were finely ground in liquid nitrogen and dissolved in four volumes of 100% of ice-cold acetone. The homogenate was brought

up to 1 mL with 80% ice-cold acetone and mixed by vortexing for 20 seconds. The mixture was centrifuged at 20,000 g for 5 minutes, and the supernatant was obtained. Afterward, 150 µL of the chlorophyll extract was used to read the absorbance using a plate reader at 645nm and 663nm wavelengths to estimate chlorophyll a (ChlA) and chlorophyll b (ChlB), respectively. Total chlorophyll was calculated by the sum of Chlorophyll a and Chlorophyll b as described previously (Warren, 2008; Begcy et al., 2012).

Total protein quantification

An additional set of leaf discs measuring 2.01 cm^2 each from fresh leaf tissue were harvested for the total protein quantification. Discs were finely ground in liquid nitrogen and dissolved with equal volume (v/v) of the 2X Protein Extraction buffer (PE buffer: 0.1 M tris-HCl, pH 8; 2% SDS; 0.05 mL 1M DTT). Followed by the addition of 1X PE buffer to obtain a 1 mL sample-PE buffer mixture before further mixing by vortexing and progressing with the protein extraction. The mixture was then heated in a water bath at 100°C for 10 minutes, then allowed to cool at room temperature for 10 minutes, then pelleted at 20,000 g for 10 minutes at 23±1°C. 200 µL of the supernatant was transferred to new centrifuge tubes and mixed with 800 µL of 100% acetone. The mixture was centrifuged at 20,000 g at 23±1°C for 10 minutes and the supernatant was discarded. The pellet was allowed to dry at room temperature for 2 mins, then dissolved in 50 µL of 0.2 N NaOH and neutralized with an equal volume of 0.2 N HCl. The total protein content was determined using the colorimetric Bio-Rad Protein Assay Kit II (Bio-Rad Laboratories, CA). Seven dilutions of a protein standard containing 0 to 30 µg/mL of the total protein content were used. A standard curve was prepared each time the assay was performed. The absorbance at 595 nm (A595nm) was then measured with a microplate spectrophotometer (Epoch Microplate Spectrophotometer; BioTek, Winooski, VT), and the normalized absorbance values were plotted versus the mass concentration (µg of protein/mg of leaf tissue) as previously described (Kalaman et al., 2022; Egesa et al., 2024a).

Stomatal density

To quantify stomatal density, plants were transferred from the greenhouse to the lab (light ~ 10 µmol $m^{-2}s^{-1}$ PPFD). Then, leaf samples were prepared using the modified leaf peel method (Lawrence et al., 2018). In brief, intact leaves were carefully covered with clear adhesive tape on the abaxial and adaxial sides to obtain a leaf tissue peel with intact cuticle, epidermal, and guard cells. Before imaging, the peels were kept moist in 1% PBS and a small area (5 cm by 1.5 cm) was excised and mounted on a glass slide. A total of 34 plants per genotype were used and 10 excised peels were taken per plant from the abaxial and the adaxial side. Imaging was performed on a Leica compound microscope (Wetzlar, Germany) at a magnification of 10X. The microscope was fitted with Leica microsystems CMS camera calibrated with Leica Application Suite X LAS X (3.7.4.23463) for imaging. We used 25 µL of 5% propidium iodide to enhance the boundaries of the epidermal and guard cells. The images depicted the pavement cells with the closed stomata. The image J software (Schneider et al., 2012) was then used to determine stomatal density and leaf epidermal cell sizes.

Stomata and guard cell size estimation

To quantify stomata size, guard cells size, and fully open stomata aperture area, detached fresh leaf samples were incubated in 150 mL of stomata opening buffer (50 mM KCl, 10 mM MES-KOH, pH 6.2) (Lawrence et al., 2018) for 30 min. Following incubation, a section (5 cm by 1.5 cm) was excised and mounted on a glass slide. Imaging was performed on a Leica compound microscope (Wetzlar, Germany) at magnifications of 40X objective lens. We used 34 plants from each genotype and obtained 10 images from the Abaxial and the adaxial side of the leaf per plant. The images obtained from each genotype were used to determine the size of stomata, guard cells, and full stomata aperture area using the image J software (Schneider et al., 2012).

Cell layer measurements

Fresh leaf samples from three-week-old plants from each genotype were used to prepare cross-sections by hand. Sections were mounted on glass slides using thin forceps. The sections were stained with 25 µL of 5% propidium iodide and imaged at 10X objective lens on a Leica compound microscope (Wetzlar, Germany). Images were used to count the number of cell layers using the Leica microsystems CMS camera calibrated with Leica Application Suite X LAS X (3.7.4.23463).

Palisade and mesophyll cell size characteristics

Fresh leaf samples from three-week-old plants were obtained from each genotype and used for cell isolation. The palisade and mesophyll cells were isolated using a modified leaf cell isolation protocol (Endo et al., 2016). Excised leaf discs (0.5-inch diameter) with their epidermal cell layer peeled off were incubated in 1.7 mL Eppendorf tubes containing 1 mL of ice-cold cell isolation enzyme buffer (75% (wt/vol) cellulase 'Onozuka' R-10, 0.25% (wt/vol) macerozyme R-10, 0.4 M, mannitol, 8 mM $CaCl_2$ and 5 mM MES-KOH) for 20 minutes on a rotating Biometra OV4 Compact Line Hybridization Oven Incubator set at 24°C. Macerated discs were removed from the Eppendorf tubes before centrifugation at 200 g for 5 min at 4°C. The supernatant was discarded, then the isolated cells were gently re-suspended in 500 µL of the ice-cold wash buffer (2 mM MES,125 mM $CaCl_2$,154 mM NaCl, 5 mM KCl) before another round of centrifugation at 200 g for 5 min at 4°C. The supernatant was discarded, and the pellets were resuspended in 100 µL of the cell flotation buffer (4 mM MES, 0.4 M mannitol, and 15 mM $MgCl_2$ at pH 5.7) (Yoo et al., 2007; Nanjareddy et al., 2016), before imaging on a compound microscope at 40X objective lens.

Dimensions of the isolated cells were obtained using the Image J software (Schneider et al., 2012). Side projections of palisade cells were used to obtain the diameter (D), radius (r=D/2), and length (L). The volume of palisade cells was estimated as $v = \pi r^2 L$, and the surface area was estimated as $SA = 2\pi r^2 + 2\pi rL$. Spongy mesophyll cell size was calculated by estimating an average radius of a sphere from three diameter estimates (d1, d2, d3) then the volume was estimated as $V= 4/3\pi r^3$ and the surface area was estimated as $SA = 4\pi r^2$.

Statistical analysis

Differences between photosynthetic parameters, anatomical and physiological traits of the two genotypes were statistically tested using the Welch's t-test ($\alpha = 0.05$). The CO_2 response data was subjected to Farquhar—von Caemmerer—Berry using the FvCB model for C_3 photosynthesis as implemented by Duursma (2015). The model was used to estimate V_{cmax}, J_{max}, R_d, and to determine the intercellular CO_2 levels at which the carboxylation-limited to RuBP regeneration-limited photosynthesis occurred.

Results

Genotypes from the Andean and Mesoamerican gene pools display different photosynthetic performance under high light and CO_2 conditions

To characterize the influence of transient changes in light intensity on photosynthetic capacity in *P. vulgaris*, we used two common bean genotypes from the Andean (Calima) and Mesoamerican (Jamapa) gene pools. First, we subjected both genotypes to low and moderate light intensity, 600 and 1000 µmol m^{-2} s^{-1} Photosynthetic Photon Flux Density (PPFD), respectively (Figures 1A, B). We did not find significant differences between Jamapa and Calima in their photosynthetic levels (A). However, the transpiration rate (E) and stomatal conductance (gsw) levels were significantly higher in Jamapa at moderate light levels (Figure 1B). At a higher light intensity, specifically 1800 µmol m^{-2} s^{-1} (PPFD) (Figure 1C) and 2000 µmol m^{-2} s^{-1} (PPFD) (Figure 1D), Jamapa showed consistently statistically significant higher A, E and gsw than Calima. Based on their origin, these results suggest that both genotypes have adapted to different light intensities, with Calima adapting to the low light while Jamapa to high light intensity.

Diurnal patterns of net assimilation in the Andean and Mesoamerican genotypes

To further characterize the impact on transient light adaptation of these two common bean genotypes, we analyzed their light compensation point and maximum rate of light-unlimited photosynthesis by using light curve measurements at ambient (400 µmol mol^{-1}) and elevated (600 µmol mol^{-1}) CO_2 levels. We subjected both genotypes to increasing light intensity levels from 0 to 1800 µmol m^{-2} s^{-1} PPFD (Figure 2). We used a modified hyperbolic function for the light response curve (LRCs) using data from Calima and Jamapa to estimate the light compensation points (l_c; x-axis intercept), the maximum photosynthetic rate at light-saturating conditions (V_{lmax}; horizontal asymptote), the l_c or PPFDs needed to attain 0.5 V_{lmax} and the quantum use efficiency (QUE= $\Delta A/\Delta PPFD$). In general, Jamapa exhibited a higher V_{lmax} compared to Calima at both ambient and elevated CO_2 (Figure 2). The light compensation points (l_c) for both genotypes were consistently lower in Calima (Figures 2A-C). However, a shift from ambient to elevated CO_2 resulted in a considerable drop in the light compensation point for both Calima and Jamapa (Figures 2D-F).

Higher carboxylation and electron transfer efficiencies in the Mesoamerican genotype

To further characterize CO_2 conductance and carboxylation efficiencies of Calima and Jamapa, we subjected both genotypes to gradually changing levels of CO_2 (A-Ci curve), using CO_2 levels ranging from 50 to 600 µmol mol^{-1}. We estimated the maximum carboxylation (V_{cmax}), Maximum rate of photosynthetic electron transport (J_{max}), rate of dark respiration (R_d), the amount of CO_2 for the transition from ribulose-1,5-bisphosphate saturated to limited ($RuBP_{sa\text{-}li}$) photosynthesis (Figure 3). Jamapa exhibited a higher Carboxylation rate (V_{cmax}) and a higher linear electron transfer rate (J_{max}) compared to Calima. These results were likely due to the prevailing e-transfer rate or better CO_2 conductance across the stomata and through the mesophyll cells in Jamapa compared to Calima. Since efficient CO_2 diffusion into the chloroplast envelopes can significantly reduce the potential of photorespiration, promoting higher net photosynthesis in a plant.

Calima's V_{cmax} increased from the morning to midday and then dropped in the afternoon, and the J_{max} values changed in a similar fashion. Dark respiration in Calima fluctuated between 2.12 and 2.84 µmol m^{-2} s^{-1} throughout the day with an apparent dip at mid-day (Figures 3A-C). The intercellular CO_2 concentration at which Calima switched from carboxylation-limited to RuBP-limited photosynthesis was stable in the morning and midday but decreased in the afternoon by 38 µmol mol^{-1} (Figures 3A-C). In contrast, Jamapa's V_{cmax} increased from morning to midday from 71.28 to 85.65 µmol m^{-2} s^{-1}, and remained stable in the afternoon, while its J_{max} had a net increase throughout the day (Figures 3D-F). Jamapa's dark respiration fluctuated between 1.97 in the morning to 2.52 µmol m^{-2} s^{-1} in the afternoon (Figures 3D, E). Interestingly, Jamapa transitioned from RuBP-saturated to RuBP-limited CO_2 assimilation at a C_i of 341 µmol mol^{-1} in the morning and a C_i of 249 µmol mol^{-1} at midday, then remained stable through the afternoon (Figures 3D-F). In general, the V_{cmax} and J_{max} values of Jamapa were larger than those of Calima throughout the day, except for J_{max} at midday (Figures 3A-F). However, the greatest difference between these genotypes was the daily dynamics of the transitions from RuBP saturated to RuBP limited photosynthesis (Figures 3B, E).

10.3389/fpls.2024.1422814

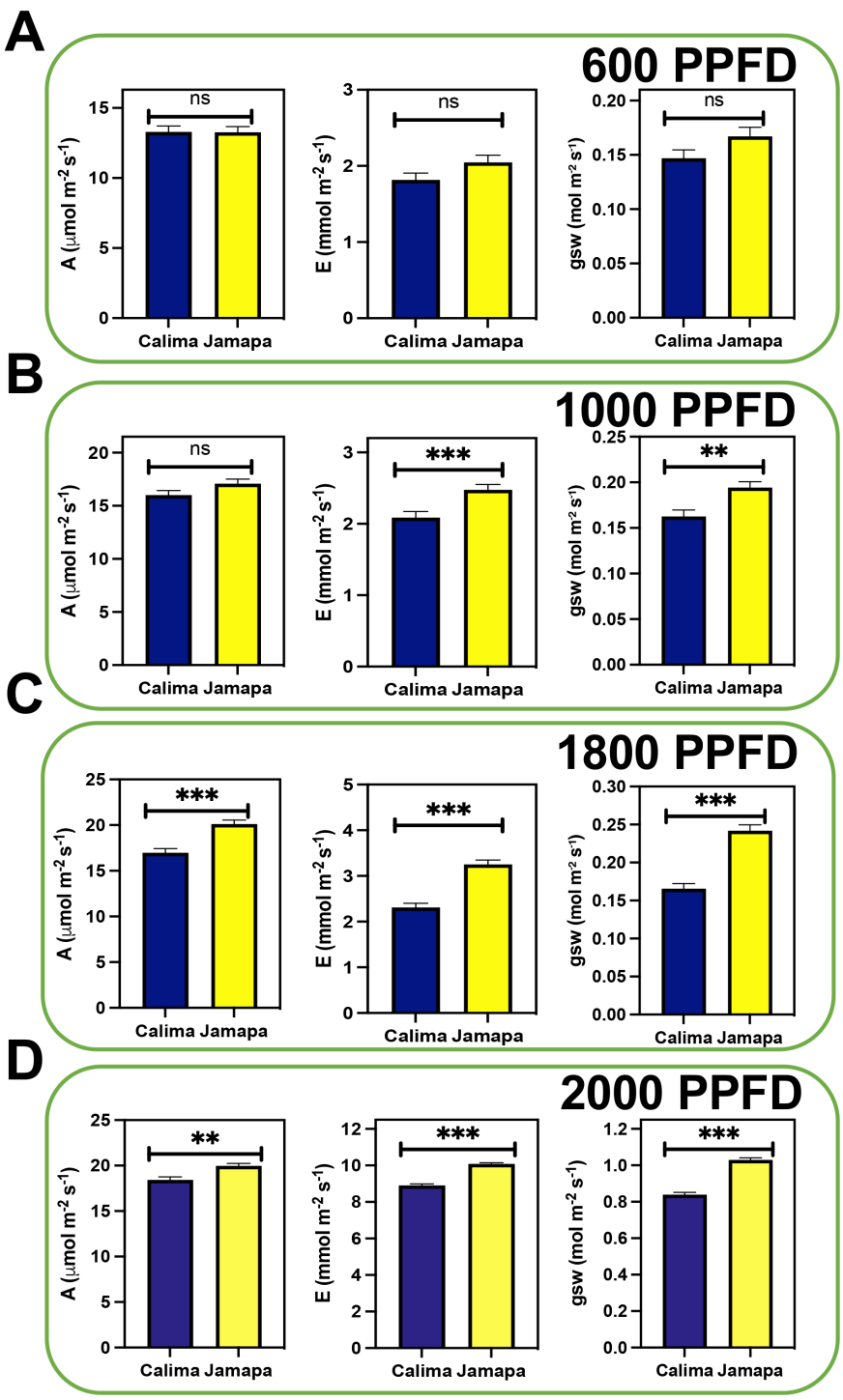

FIGURE 1
Photosynthetic capacity increases in the Mesoamerican genotype under higher light intensity. Photosynthetic gas exchange parameters (Assimilation [A], Transpiration [E], and Stomata conductance to water vapor [gsw]) were measured under different levels of light intensity at ambient CO_2 (400 µmol mol^{-1}). The light levels comprised Photosynthetic Photon Flux Density (PPFD) levels of **(A)** 600 µmol m^{-2} s^{-1}, **(B)** 1000 µmol m^{-2} s^{-1}, **(C)** 1800 µmol m^{-2} s^{-1} and **(D)** 2000 µmol m^{-2} s^{-1}. n = 20. Significant differences were calculated based on Welch's t-test at an alpha of 0.05. Non-significant (ns) $P > 0.05$; **$P \leq 0.01$, and *** $P \leq 0.001$.

The ratio of J_{max}/V_{cmax} in Calima changed very little over the day, which was reflected in the narrow range of the C_i's at which the transition occurred. In Jamapa this ratio dropped from 1.9 to 1.6 throughout the day. Increased photosynthesis rate with increasing light in Jamapa compared to Calima suggested a better capture of light energy by the leaf which may have increased the availability of e^- and H^+ to drive the photosynthesis reactions. These results indicated that Jamapa had a greater capacity to regenerate RuBP

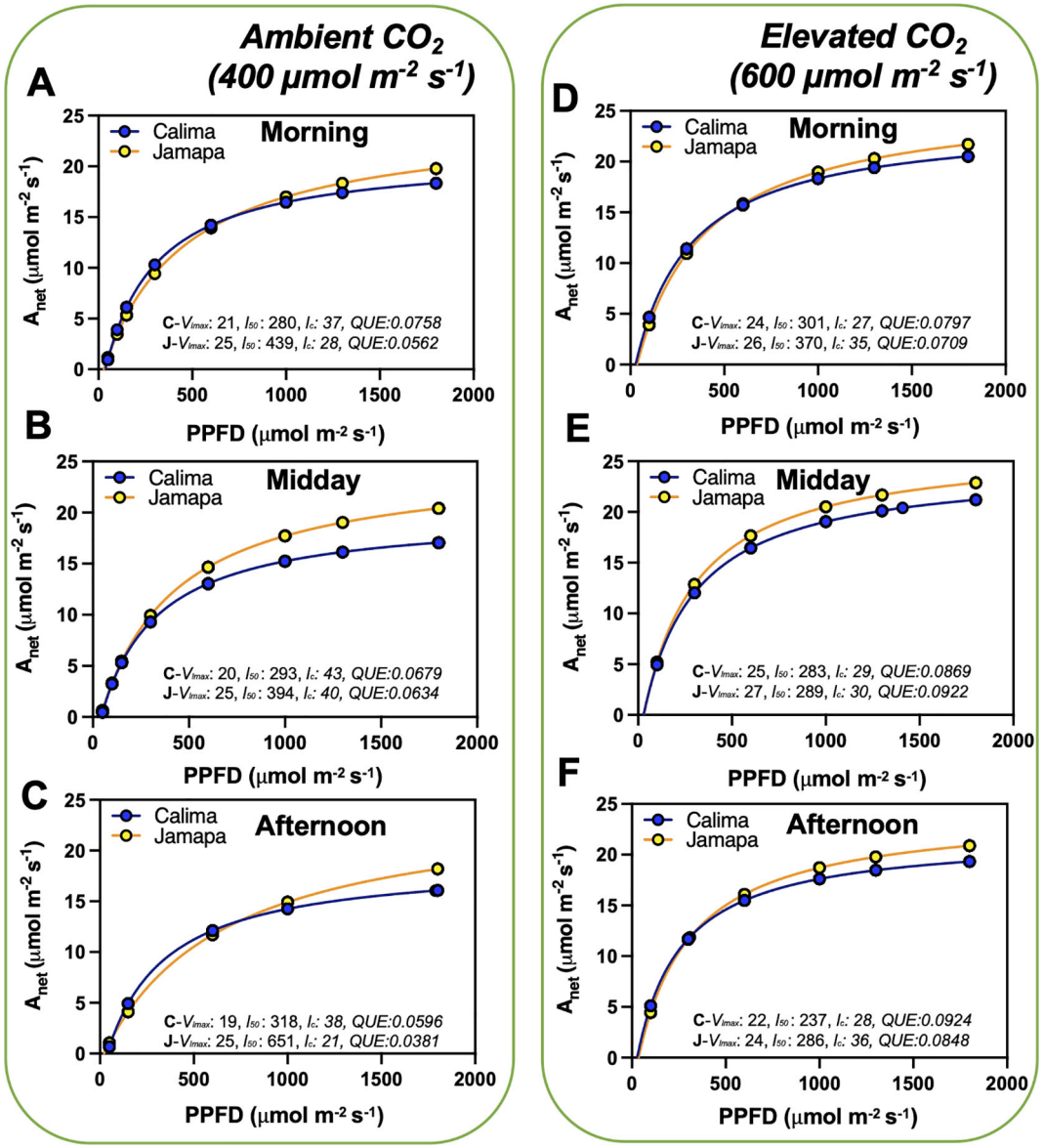

FIGURE 2
Diurnal photosynthetic light use efficiency characteristics are variable from Andean and Mesoamerican common bean genotypes. We used a modified hyperbolic function from light response curves (LRCs) to estimate the light compensation points (I_c; x-axis intercept), the maximum photosynthetic rate at light-saturating conditions (V_{Imax}; horizontal asymptote), the I_{50} or PPFDs needed to attain 0.5 $V_{Imax}$and the quantum use efficiency (QUE= ΔA/ΔPPFD). These data were collected from 8 to 10 am (morning), 11 to 1 pm (midday), and 2 to 4 pm (afternoon) **(A-C)** ambient CO_2 (400 µmol mol^{-1}) and at **(D-F)** elevated CO_2 (600 µmol mol^{-1}). n = 36.

in the morning and that this capacity decayed during the day, in contrast to Calima, which, comparatively, did not display such a dramatic change.

Leaf anatomy as a predictor of photosynthetic efficiency in Calima and Jamapa

We hypothesized that some of the differences in photosynthetic characteristics observed between the two common bean genotypes could be explained by their anatomical differences. To test this hypothesis, we performed comparative anatomical analyses of the leaf epidermis and the mesophyll.

First, we calculated the stomatal density using closed and opened stomata in Calima (Figure 4A) and Jamapa (Figure 4B). The stomatal density on the abaxial side of Jamapa leaves was 225 ±4.12/mm^2 (Figure 4C) and 66±2.08/mm^2 (Figure 4D) on the adaxial side. In contrast, the corresponding densities for Calima were 141±2.44/mm^2 and 44±2.14/mm^2 (Figures 4C, D). Both genotypes exhibited comparable abaxial to adaxial density ratios – 3.4 and 3.2 for Calima and Jamapa, respectively – and consequently similar intergenotypic ratios (Figure 4E). As a proxy to guard cell sizes, we measured the projected surface areas. On the abaxial side,

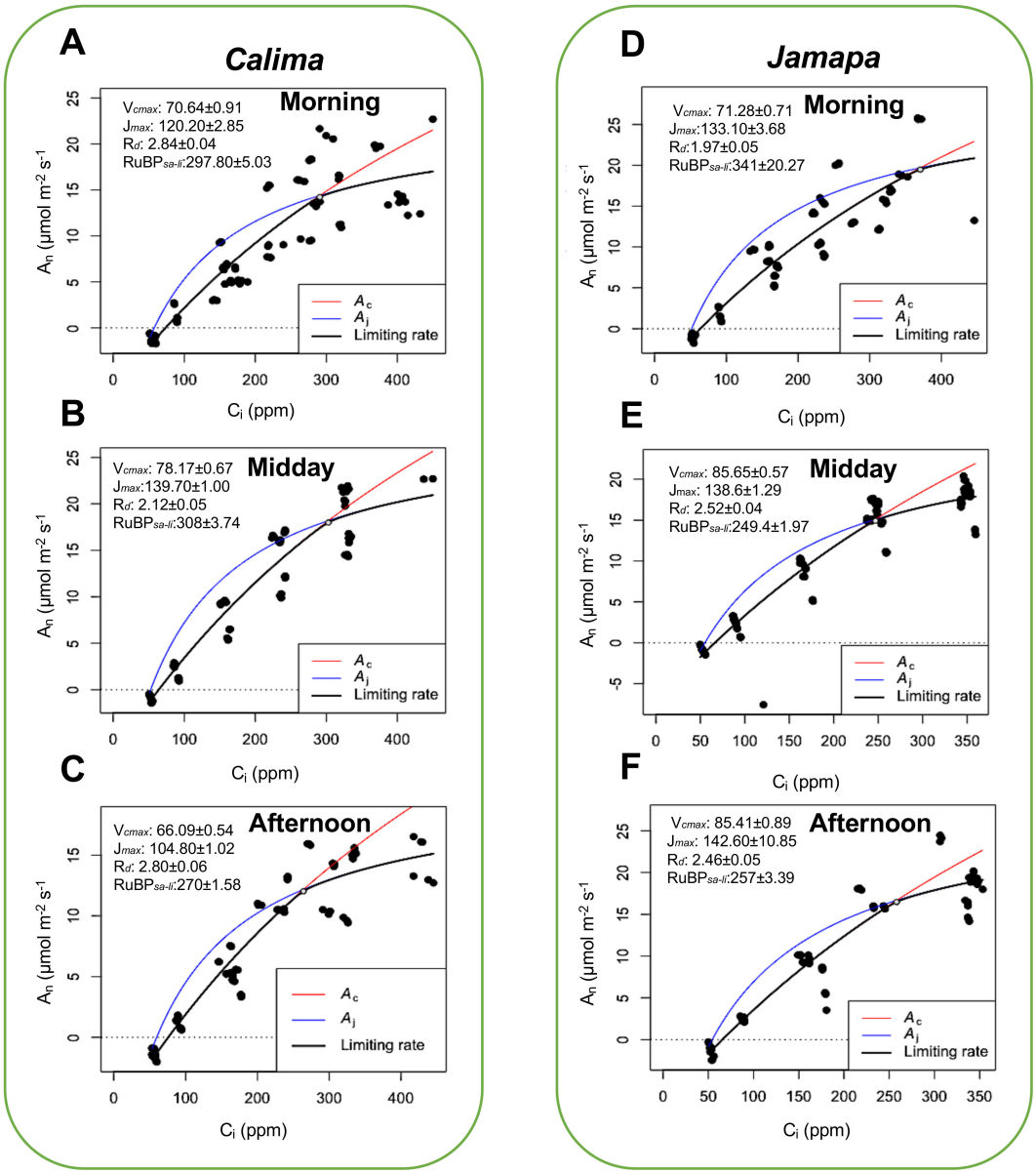

FIGURE 3
Diurnal patterns of carboxylation and electron transfer efficiencies are consistently higher in the Mesoamerican genotype and peak at different periods of the day. Maximum carboxylation (V_{cmax}), Maximum rate of photosynthetic electron transport (J_{max}), rate of dark respiration (R_d), the amount of CO_2 for the transition from ribulose-1,5-bisphosphate saturated to limited ($RuBP_{sa-li}$) photosynthesis was estimated by fitting the A-Ci curves from photosynthesis data collected from Calima and Jamapa, where CO_2 is the substrate in the reaction adopting the Farquhar—von Caemmerer—Berry (The FvCB model for C3 photosynthesis) as described in Plantecophys package (Duursma, 2015). Estimated carboxylation electron transfer efficiencies, dark respiration, and CO_2 levels for $RuBP_{sa-li}$ transition of Calima in the morning **(A)**, midday **(B)**, and afternoon **(C)**, and Jamapa in the morning **(D)**, midday **(E)**, and afternoon **(F)**. Photosynthesis data was collected at 1000 µmol m^{-2} s^{-1} PPFD, temperature of 25 °C, and relative humidity of 60%. n = 36.

Calima's guard cells (204±1.35 µm^2) were 15% larger than those of Jamapa (176±0.98 µm^2) (Figure 4F). On the adaxial side of the leaf, the estimated surface area of Calima's guard cells (211.0±7.42 µm^2) was not significantly different from those of Jamapa (232±8.56 µm^2) (Figure 4G). Furthermore, the apertures of fully open Calima stomata (76±0.81 µm^2) on the abaxial side were 37% larger than those of Jamapa (55±0.51µm^2) (Figure 4H). However, on the adaxial side the stomata apertures were not significantly different, Calima 44.6±2.99 µm^2 and Jamapa 47.32±4.48 µm^2, data that agree with the guard cell sizes (Figure 4I). Moreover, the stomata size was significantly larger in Calima than Jamapa on the abaxial side (Figure 4J), but not in the adaxial side (Figure 4K).

To further elucidate whether the differences in photosynthetic capacity could be explained by their anatomical differences, we

10.3389/fpls.2024.1422814

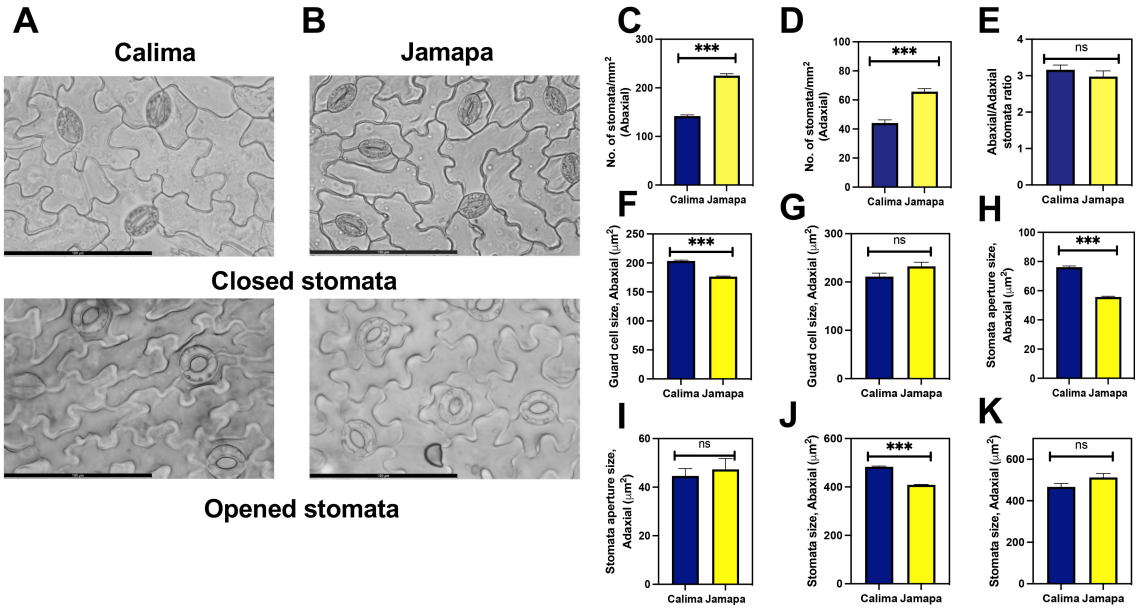

FIGURE 4
Andean common bean genotype exhibits lower stomatal density per unit area than its Mesoamerican counterpart. Light microscopy images of **(A)** Calima and **(B)** Jamapa depicting closed and opened stomata. Number of stomata on the **(C)** abaxial and **(D)** abaxial sides of the leaf. **(E)** Ratio of stomata per unit area on the abaxial to the adaxial side. Guard cell size on the **(F)** abaxial and the **(G)** adaxial side of the leaf. Open stomata aperture size on the **(H)** abaxial and the **(I)** adaxial side. Stomata size on the **(J)** abaxial and the **(K)** adaxial sides. Fresh mature leaves from three-week-old plants were incubated in 150 mL of stomata opening buffer for 30 mins to open the stomata. Significant differences were calculated based on Welch's t-test at an alpha of 0.05. ns $P > 0.05$ and *** $P \leq 0.001$. n = Abaxial: 346, Adaxial: 340. Scale bar = 100 µm.

measured epidermal, palisade and mesophyll cells from both genotypes (Figure 5A). First, we analyzed the size of the epidermal pavement cells (Figure 5B). The average surface area of abaxial and adaxial pavement cells of Jamapa leaves was 1,502±31 and 2,940±82 µm^2 and those of Calima 1,674±32 and 3,493±78 µm^2, respectively (Figures 5B, C). Thus, Calima pavement cells were 11 to 18% larger than Jamapa cells. Furthermore, we quantified the number of epidermal cells on the abaxial (Figure 5D) and the adaxial side (Figure 5E). Jamapa had higher quantity in both. An anatomical normalization or calculation of the number of pavement cells per stoma showed while Jamapa had 3 pavement cells per stoma on the abaxial side and 5 pavement cells per stoma on the adaxial side (Figures 5F, G), the corresponding ratios in Calima were 4 and 6 (Figures 5F, G). In summary, physically and anatomically, Jamapa had a higher stomatal density than Calima.

Examination of a cross-section of the leaf blade showed that the two genotypes had three layers of spongy parenchyma cells arranged below a single palisade cell layer. We then isolated leaf palisade and spongy parenchyma cells, measured their lateral projections and used them to obtain first-order approximations of their cell volume and surface area (Supplementary Figure S1). Calima palisade cells (53.52±1.10 µm) were shorter than Jamapa cells (65±0.96 µm) (Figure 5H), but significantly wider (17±0.42 µm) than Jamapa cells (13.14±0.3 µm) (Figure 5I). These dimensions were used to estimate cell volumes (Figure 5J), and surface areas (Figure 5K) assuming palisade cells as cylindrical and spongy parenchyma cells as spherical bodies. The average volume of Calima palisade cells (14,038±760.6 µm^3) was 32% larger than those of Jamapa (9,482±544.1µm^3) (Figure 5J), and the average surface area for Calima cells (3,556±122.4 µm^2) was 14.99% larger than that of Jamapa cells (3,023±102.8 µm^2) (Figure 5K). Using these values, we calculated the surface-to-volume ratio, and the results showed that Jamapa cells had 23% more surface area than Calima cells per unit of volume in the palisade cells (Figure 5L).

On the other hand, the average diameter of spongy parenchyma cells was larger in Calima (31.45±0.43 µm) than in Jamapa (26.79±0.63 µm) (Figure 5M). Similarly, the average volume of spongy parenchyma cells of Calima (152,037±6,624 µm^3) was 35% larger than those of Jamapa cells (98,185±6,421 µm^3) (Figure 5N), and the surface area of Calima cells (3,146 ±85.50 µm^2) was 26% greater than that of Jamapa cells (2,318 ±104.8 µm^2) (Figure 5O). Similarly, Jamapa cells had 19% more surface area per unit of volume in their spongy parenchyma than Calima cells (Figure 5P). Collectively, these results indicated that mesophyll cells in Jamapa had a larger surface area for CO_2 diffusion than those of Calima.

Effects of anatomical differences on physiological parameters

Following the A-Ci results, we considered the gas exchange parameters at three atmospheric CO_2 concentrations (low C_a = 200, ambient C_a = 400, and high C_a = 600 µmol mol^{-1}) to assess the effect of the anatomical differences on gas exchange characteristics (Table 1). Both genotypes displayed similar responses to the

10.3389/fpls.2024.1422814

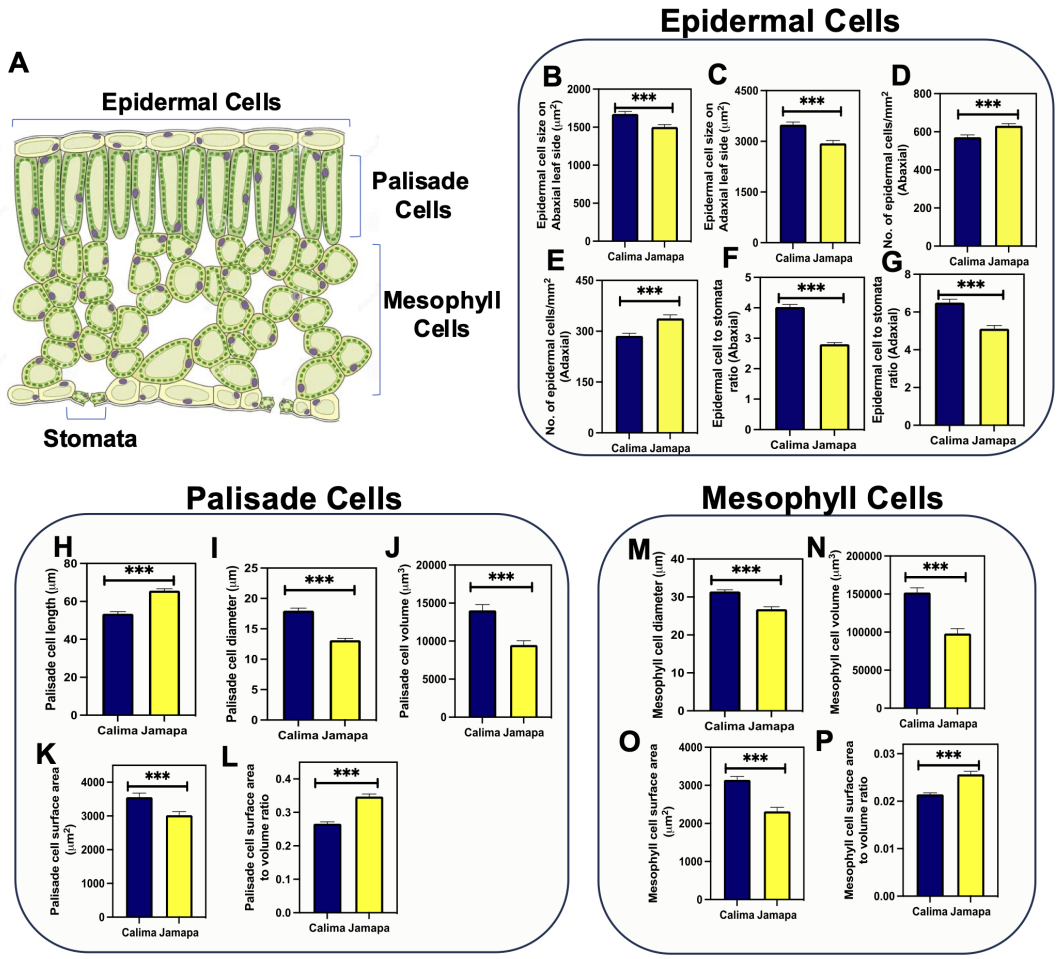

FIGURE 5
Epidermal, palisade, and mesophyll cell size is different between the Andean and the Mesoamerican genotypes. **(A)** Schematic representation of a cross section of a leaf indicating the location of stomata, epidermal, palisade and mesophyll cells. Epidermal cell sizes on the **(B)** abaxial and **(C)** adaxial sides. Number of epidermal cells on the **(D)** abaxial and **(E)** adaxial sides. Epidermal cells to stomata ratio on the **(F)** abaxial and **(G)** adaxial side in Calima and Jamapa. Palisade cells **(H)** length, **(I)** diameter and **(J)** volume. Palisade cells surface area **(K)** and surface area to volume ratio **(L)**. Mesophyll cells **(M)** diameter, **(N)** volume, **(O)** total surface area and **(P)** surface area to volume ratio. Lateral projections of palisade cells were used to obtain the diameter **(D)**, radius (r=D/2), and length **(L)**. The volume of palisade cells was estimated as $v = \pi r^2 L$, and the surface area was estimated as $SA = 2\pi r^{2+} 2\pi rL$. Spongy mesophyll cell size was calculated by estimating the average radius of a sphere. The surface area was estimated as $SA = 4\pi r^2$. Significant differences were calculated based on the Welch's t-test at an alpha of 0.05. *** $P \leq 0.001$. n = 45.

different C_a levels. Stomatal conductance to water vapor (g_{sw}) increased when C_a was raised from low to ambient CO_2, but decreased when C_a reached the highest level. Changes in E mirrored changes in stomatal conductance to water vapor (g_{sw}). However, Jamapa displayed statistically significant greater g_{sw} and higher E rates than Calima at all C_a levels.

Like g_{sw}, stomatal conductance to CO_2 (g_c) increased in both genotypes as C_a increased from low to mid-level, but dropped significantly when C_a reached the highest level (Table 2). Unlike E rates, CO_2 assimilation rates (A) increased to the highest level in both genotypes as CO_2 levels increased (Table 1). Jamapa displayed statistically significant higher A rates than Calima at low and mid C_a levels, however, these differences disappeared at the highest C_a as C_i reached saturation in both genotypes, although Jamapa showed statistically higher C_i values than Calima at all C_a levels. The intercellular CO_2 concentrations (C_i) increased in both genotypes proportionally to the increases in C_a maintaining a Ci/Ca ratio of around 0.8. However, this ratio was lower in Calima than in Jamapa, particularly at the mid and high C_a levels. In summary, the response pattern of E, C_i, A, g_{sw}, and g_c to different levels of C_a was similar in both genotypes, but Jamapa displayed significantly higher values throughout. These differences could be explained largely by the fact that the total stomata aperture per unit of leaf area of Jamapa was 15% larger than that of Calima. However, Jamapa's g_{sw} and g_c exceeded those of Calima's by 44 to 78%. The disproportionality between total stomatal aperture per unit of leaf area and the estimated conductance strongly suggested other functional differences in addition to those of their epidermal anatomies.

10.3389/fpls.2024.1422814

An analysis of leaf-level water use efficiency (WUE) under the then atmospheric CO_2 level (400 µmol mol^{-1}) and possible future higher level (600 µmol mol^{-1}) showed that Calima outperformed Jamapa by about 30%, an advantage that could increase to 50% under the high CO_2 level (Table 1).

Jamapa has higher chlorophyll and total protein content per unit area but carboxylation reactions in Calima are more efficient

We measured chlorophyll and protein content per unit of leaf area to investigate whether the differences in cell size between the genotypes could give rise to differences in the density of components of the photosynthetic apparatuses; these differences, if any, could also explain to some extent differences in photosynthetic capacities. Protein analysis indicated that there were statistically significant differences between Calima (399.9 mg/m^2) and Jamapa (630.10 mg/m^2) (Table 2). We found that both genotypes had similar chlorophyll a/b ratios: Calima (2.82) and Jamapa (2.65). However, the total chlorophyll content in Jamapa (169.02 mg/m^2) was significantly higher than Calima's (149.41 mg/m^2) (Table 3).

TABLE 1 Leaf assimilation and conductance in Calima and Jamapa.

Parameter	Genotype	200 µmol mol^{-1} CO_2	400 µmol mol^{-1} CO_2	600 µmol mol^{-1} CO_2
A (µmol m^{-2} s^{-1})	Calima	6.20±0.23^b	15.42±0.48^b	17.81±0.45^a
	Jamapa	8.04±0.27^a	17.16±0.32^a	18.22±0.37^a
C_i (µmol mol^{-1})	Calima	161.10 ±1.14^b	306.48 ±3.67^b	458.72 ±5.28^b
	Jamapa	165.01±1.27	327.44±3.75	494.80 ±6.47 ^{a}
g_{sw} (µmol m^{-2} s^{-1})	Calima	0.34±0.01^b	0.38±0.02^b	0.28±0.02^b
	Jamapa	0.51±0.02^a	0.65±0.03^a	0.50±0.03^a
E (mmol m^{-2} s^{-1})	Calima	4.14±0.15^b	4.45±0.2^b	3.47±0.18^b
	Jamapa	5.64±0.17^a	6.51±0.25^a	5.33±0.28^a
g_{tc} (mol m^{-2} s^{-1})	Calima	0.20 ±0.0077^b	0.22 ±0.0126^b	0.17 ±0.0098^b
	Jamapa	0.29 ±0.0097^a	0.36±0.017^a	0.28 ±0.01784^a
g_c (mol m^{-2} s^{-1})	Calima	0.18 ±0.0064^b	0.20 ±0.0107^b	0.15 ±0.0083^b
	Jamapa	0.26 ±0.0088 ^{a}	0.31±0.01^a	0.24±0.013^a
WUE (µmol $mmol^{-1}$)	Calima	1.50	3.46	5.13
	Jamapa	2.63	2.63	3.41

Conductance to CO_2 (g_c) was calculated using the formula g_c=A/(Ca-Ci) Boyer and Kawamitsu (2011). n = 60. For each parameter, a different letter within a column indicates significant differences based on the Welch's t-test at an alpha of 0.05 comparing both genotypes. The same letter indicates no significant differences.

After estimating chlorophyll and protein content per unit of leaf area, we recalculated A_{net} based on either mg of protein or mg of chlorophyll instead of leaf area. Next, we fitted a modified hyperbolic function for the light response curves (LRCs) of Calima and Jamapa to compare their patterns of light dependance on net CO_2 assimilation as a function of chlorophyll content (Figure 6A) and protein content (Figure 6B). After normalizing A_{net} for chlorophyll content (Figure 6A), Jamapa's V_{lmax} (129) and l_{50} (264) were higher than Calima's V_{lmax} (146) and l_{50} (409), but Calima displayed a higher l_c value (41) than Jamapa's (35). In contrast, after normalizing A_{net} for protein content (Figure 6B), Calima's V_{lmax} (50) was significantly higher than Jamapa's V_{lmax} (39), but the estimated l_{50s} and l_{cs} remained almost unchanged for both genotypes (Figure 6). In general, the estimated QUE values were higher in both genotypes when calculated based on chlorophyll content than when calculated on protein basis. This is not surprising because light harvesting is primarily carried out by chlorophyll. Interestingly though, regardless of how A_{net} was expressed, Calima appeared to have a higher QUE value than Jamapa.

Considering this difference, we calculated the maximum rate of CO_2 fixation based on protein content. Accordingly, Calima's V_{cmax} rate (167.8 µmol g^{-1} sec^{-1}) was 26% greater than Jamapa's (125.0 µmol g^{-1} sec^{-1}) (Table 3). However, when the results were expressed on a leaf area basis, Jamapa exceeded Calima by 12%. Regarding the electron transport efficiency J_{max}, Jamapa (251.9 µEq g^{-1} sec^{-1}) retained significantly higher values than Calima (137.9 µEq g^{-1} sec^{-1}). The rate of dark respiration remained higher in Calima (4.72 µmol g^{-1} s^{-1}) compared to Jamapa (3.31 µmol g^{-1} s^{-1}). At the same time, the intercellular CO_2 concentration at which these plants switched from carboxylation-limited to RuBP-limited was lower in Calima (55.56 µmol mol^{-1}) and significantly higher in Jamapa (259 µmol mol^{-1}) (Table 3). These results indicated that the carboxylation reactions in Calima are more efficient than those in Jamapa, while photosynthetic electron transport efficiency is higher in Jamapa.

Discussion

Our analysis showed that the Mesoamerican bean (Jamapa) had higher photosynthesis at light-saturating conditions with a V_{lmax} that was 22% greater than that of the Andean bean (Calima) (Figures 1, 2). Furthermore, this genotype exhibited a higher carboxylation efficiency with a $V_{cmax,}$ which was 12% greater than that of Calima (Figure 3). However, when the V_{cmax} was expressed on the basis of total protein instead of leaf area, Jamapa's advantage was nullified, and Calima had more efficient carboxylation reactions. These comparisons suggested that these genotypes have comparable photochemical capacities, but the structural differences that control CO_2 diffusion, protein and chlorophyll content per unit of leaf area have a significant effect on their photosynthetic capacities.

The selection of a specific plant age was based on the observation that leaf anatomy and morphology normally changes

TABLE 2 Leaf chlorophyll and protein characteristics between Calima and Jamapa.

Genotype	chlorophyll a (mg/m^2)	chlorophyll b (mg/m^2)	chlorophyll a/ b ratio	Total chlorophyll (mg/m^2)	Total protein (mg/m^2)
Calima	108.0 ± 3.76^b	41.42 ± 2.35^a	2.82 ± 0.19^a	149.41 ± 0.76^b	399.90 ± 25.84^b
Jamapa	122.3 ± 3.95^a	46.74 ± 1.86^a	2.65 ± 0.06^a	169.02 ± 1.13^a	630.10 ± 50.65^a

Chlorophyll and total protein were measured in mature fully expanded leaves (n = 8). A different letter within a column indicates significant differences for each parameter based on Welch's t-test at an alpha of 0.05 comparing both genotypes. The same letter indicates no significant differences.

during plant development (Wu and Poethig, 2006). In addition, several reports have documented increased phenotypic plasticity of leaves in older plants (Dorken and Barrett, 2004; Barton, 2008; Niinemets, 2016). Thus, we chose to use plants of similar age to ensure sample uniformity, and to avoid developmental factors increasing the number of variables for our study.

Several enzymes and proteins that function in photosynthesis are redox proteins whose activation changes with illumination and the circadian rhythm (Miyake et al., 2005; Thormählen et al., 2017; Cardona et al., 2018; Tan et al., 2021; Chen et al., 2022; Okegawa et al., 2022, 2023). As such, variable activation patterns in the redox proteins could explain the increasing trends in photosynthetic parameters from morning to the afternoon. However, in the afternoon, other factors could also affect the patterns, especially the stomatal closures to reduce the water loss, a situation likely to explain the drop in photosynthetic parameters (V_{cmax} and J_{max}) of Calima compared to Jamapa. Other studies have shown that small stomata responded efficiently to fluctuating environments and could fine-tune gas exchange roles in limited conditions with less cost to the plant (Drake et al., 2013; Zhang et al., 2019). Smaller stomata at a higher density could contribute to higher rates of CO_2 assimilation as it appeared to be the case for Jamapa. However, these features may become a liability under conditions of higher CO_2 levels. In contrast to Jamapa, Calima showed a drastic increase in WUE at higher CO_2 levels, which are expected as a result of climate change. These results suggest that we must examine in greater details the components of stomata conductance, such as stomata density and their responsiveness to external CO_2 concentrations, when considering the development of cultivars for the future.

Our data showed that differences in stomatal and mesophyll cell sizes between the two genotypes had the most consequential effect on photosynthetic capacity. Calima had larger pavement cells than Jamapa which in effect lowered the stomatal densities on the abaxial and adaxial sides of the leaf (Figure 4). Evidence from other studies have indicated the importance of plant leaf anatomy on photosynthesis capacity. For instance, stomatal density controls the flow of CO_2 into the intercellular spaces (Tomás et al., 2013; Harrison et al., 2020), as a result higher stomatal density promotes a better stomatal conductance (g_s) compared to lower densities (Harrison et al., 2020). Furthermore, other studies have also shown that the stomatal density and stomata sizes are essential in fine-tuning the CO_2 flow and managing the plant water balance (Drake et al., 2013; Tanaka et al., 2013). While smaller stomata exhibited faster responses to the environment, larger stomata have been observed to lag in the opening and closing (Drake et al., 2013). Our results indicated significant differences in the sizes of the stomata between the two genotypes. The larger guard cells and stoma opening of Calima were not able to counteract the low CO_2 diffusion caused by a low stomatal density of this genotype (Figure 4, Table 1). In summary, total stomatal openings in Jamapa's abaxial and adaxial leaf sides were 13% and 8% greater than in Calima's, significantly contributing to enhanced differences in CO_2 diffusion between the two plants.

As expected, the differences in cell sizes and stomatal apertures had a significant effect on stomatal conductance to water vapor and CO_2. As a result of the higher stomatal conductance, Jamapa displayed greater rates of transpiration and CO_2 assimilation than Calima. However, by the same token, Calima displayed greater WUE than Jamapa. This phenomenon should not be overlooked in light of climate change upon us where higher CO_2 levels and temperatures are expected, conditions in which Calima is likely to have an advantage. Hence, Calima could be a source of unique genetic markers for breeding water use efficiency in common beans and other C3 legumes, especially under increasing challenges of inadequate water for agricultural production. However, substantial changes in stomatal conductance, especially through reduced stomatal density, could negatively impact assimilation, limiting the potential for higher benefits from this trait (Flexas, 2016; Ghannoum, 2016; Leakey et al., 2019; Israel et al., 2022). Our results are based on intrinsic water use efficiency (Flexas, 2016; Israel et al., 2022) and do not factor in the variation in leaf sizes of the genotypes and the total surface exposed for water loss.

Cell sizes are critical to mesophyll conductance in the diffusion of CO_2 across several membranes into of chloroplast for CO_2 fixation (Flexas et al., 2008; Tomás et al., 2013; Théroux-Rancourt and Gilbert, 2017; Elferjani et al., 2021; Momayyezi et al., 2022a). We also detected significant cell size differences in parenchyma and spongy mesophyll cells. Overall, Jamapa's smaller cells resulted in larger cellular surface area per unit of leaf volume than Calima (Figure 5). In other studies, mesophyll cells' surface area, density, and geometry affected the diffusion of CO_2 into the chloroplast for photosynthesis (Flexas et al., 2008; Tomás et al., 2013; Peguero-Pina et al., 2017; Ren et al., 2019). Our results indicated that Jamapa mesophyll cells provided a larger area for CO_2 diffusion into the cells

10.3389/fpls.2024.1422814

TABLE 3 Carboxylation and electron transfer efficiencies of an Andean and a Mesoamerican common bean genotypes on total protein per unit area basis.

Genotype	A-Ci			
	V_{cmax} (µmol g^{-1} s^{-1})	J_{max} (µEq g^{-1} sec^{-1})	R_d (µmol g^{-1} s^{-1})	$RuBP_{sa-li}$ (µmol mol^{-1})
Calima	167.8±1.44[a]	137.9±2.68[a]	4.72±0.19[a]	55.56±4.01[b]
Jamapa	125.0±0.26[b]	251.9±1.12[b]	3.31±0.03[b]	259.0±1.17[a]

The carboxylation efficiency on a total protein basis was estimated at moderate light (1000 µmol m^{-2} s^{-1} PPFD). Maximum carboxylation (V_{cmax}), Maximum rate of photosynthetic electron transport (J_{max}), rate of dark respiration (R_d) was estimated by fitting the A-Ci curves from photosynthesis data collected from Calima and Jamapa, where CO_2 was the substrate in the reaction adopting the Farquhar—von Caemmerer—Berry; FvCB model for C3 photosynthesis as implemented by Duursma (2015). Photosynthesis data was obtained under a standard light intensity of 1000 µmol m^{-2} s^{-1} PPFD, temperature of 25°C, and relative humidity of 60%. (n = 9). For each parameter, different letter indicates significant differences based on the Welch's t-test at an alpha of 0.05 comparing both genotypes.

than Calima cells. These results also suggested that the difference in chlorophyll content per unit of leaf area may be due to the differences in the size of mesophyll cells, provided the number and size of chloroplasts in the cells of each genotype are very similar.

There were differences in the size of pavement and guard cell between the abaxial and adaxial sides of the leaf in both genotypes. However, we noticed a lack of proportionality between genotypes. This result suggests that the developmental controls of the two sides could be independent to some extent. In addition, the differences in the number of pavement cells per stomata between genotypes also suggested another developmental polymorphism between the genotypes. Thicker leaves have previously been linked to an adaptation to lowlands in Juglans (Momayyezi et al., 2022b). Thus, longer palisade cells in Jamapa might be an adaptation to lower altitudes in the Mesoamerican region. Such thick leaves offer a double advantage of utilizing more light energy through increased number of chloroplasts and a higher mesophyll conductance (Momayyezi et al., 2022b). Therefore, leaf anatomical structure in Jamapa facilitates the efficient utilization of increasing light intensity, resulting in higher net photosynthesis. Therefore, while larger palisade and mesophyll cells surface area to volume ratio appear to be an adaptation to high light intensity, the opposite could be suitable for low light intensity.

Apart from the role of the anatomical differences in enhancing carboxylation rates in Jamapa, these differences also impacted their J_{max} throughout the day (Figure 3). Previous studies have shown that stomatal conductance is affected by the photosynthetic electron transport (Lawson et al., 2008), thus, impacting the PSI redox state (Li et al., 2021), changing the cyclic electron transport, influencing the NPQ system, and in general impacting the overall J_{max}. Our results showed that Jamapa, which had higher stomatal density and smaller cell sizes, had higher stomatal conductance. In addition, these genotypes had significant differences in their chlorophyll content (Table 2). This agrees with previous studies that integrated chlorophyll content with the photosynthetic paraments and improved the empirical estimation of J_{max} from V_{cmax} (Song et al., 2021). Therefore, the better CO_2 conductance in Jamapa could be explained by the anatomical and chlorophyll differences between the two genotypes and contributed to the high J_{max} stability in the afternoon.

A comparative analysis of Mesoamerican and Andean cultivars detected significant differences in organ size (Sexton et al., 1997). A cluster analysis of 427 bean genotypes from both gene pools documented that the main difference between the pools is yield potential, with the Mesoamerican lines excelling over the Andean lines (Amongi et al., 2023). The results presented here strongly suggest that the yield differences between the gene pools are most likely due to differences in photosynthetic capacity as influenced by their differences in anatomic characteristics. Furthermore, the availability of a genotyped recombinant inbred

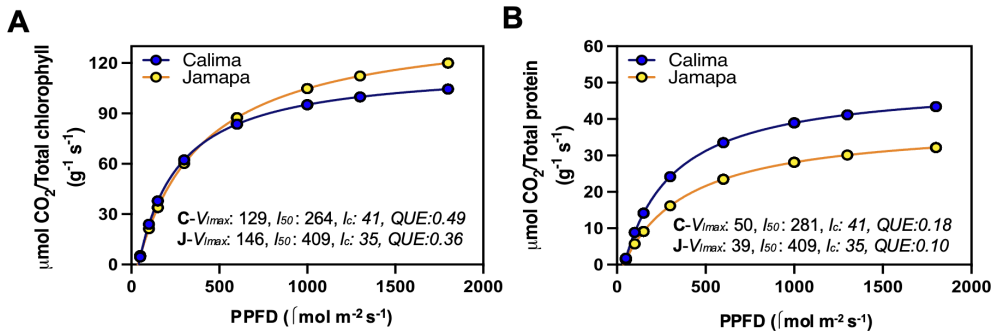

FIGURE 6
Photosynthetic light use efficiency after accounting for differences in chlorophyll and protein content between Andean and Mesoamerican common bean genotypes. LRCs from photosynthesis estimated per unit chlorophyll **(A)** and unit protein **(B)** from Calima and Jamapa. Fitting a modified hyperbolic function from light response curve (LRCs) data from Calima and Jamapa to estimate the light compensation points (I_c; x-axis intercept), maximum photosynthetic rate at light-saturating conditions (V_{lmax}; horizontal asymptote), the I_{50} or PPFDs needed to attain 0.5 V_{lmax} and an estimated quantum use efficiencies (QUE) by calculating the first derivative of the light function at I_c. These estimates were from data collected between 8 am to 2.00 pm during the day at ambient CO_2 400 µmol mol^{-1}. n = 36.

family produced between Jamapa and Calima (Bhakta et al., 2015), will facilitate the genetic analysis of cell size and testing of the hypothesis that cell size exerts significant control over photosynthetic performance.

Data availability statement

The original contributions presented in the study are included in the article/Supplementary Material. Further inquiries can be directed to the corresponding author.

Author contributions

AE: Data curation, Investigation, Methodology, Validation, Visualization, Writing – original draft. CV: Conceptualization, Methodology, Resources, Writing – review & editing. KB: Conceptualization, Funding acquisition, Supervision, Writing – review & editing.

Funding

The author(s) declare financial support was received for the research, authorship, and/or publication of this article. This work was supported by Hatch project FLA-ENH-005853 from the United States Department of Agriculture to KB.

Acknowledgments

We thank Simon Riley from the IFAS statistics consulting unit for guidance on the statistical analysis for the manuscript.

Conflict of interest

The authors declare that the research was conducted in the absence of any commercial or financial relationships that could be construed as a potential conflict of interest.

Publisher's note

Supplementary material

The Supplementary Material for this article can be found online at: https://www.frontiersin.org/articles/10.3389/fpls.2024.1422814/full#supplementary-material

References

Amongi, W., Nkalubo, S. T., Ochwo-Ssemakula, M., Badji, A., Dramadri, I. O., Odongo, T. L., et al. (2023). Phenotype based clustering, and diversity of common bean genotypes in seed iron concentration and cooking time. *PLoS ONE* 18, e0284976. doi: 10.1371/journal.pone.0284976

Baker, N. R., Harbinson, J., and Kramer, D. M. (2007). Determining the limitations and regulation of photosynthetic energy transduction in leaves. *Plant Cell Environ.* 30, 1107–1125. doi: 10.1111/j.1365-3040.2007.01680.x

Barton, K. E. (2008). Phenotypic plasticity in seedling defense strategies: compensatory growth and chemical induction. *Oikos* 117, 917–925. doi: 10.1111/j.0030-1299.2008.16324.x

Begcy, K., Mariano, E. D., Gentile, A., Lembke, C. G., Zingaretti, S. M., Souza, G. M., et al. (2012). A novel stress-induced sugarcane gene confers tolerance to drought, salt and oxidative stress in transgenic tobacco plants. *PloS One* 7, e44697. doi: 10.1371/journal.pone.0044697

Begcy, K., Mariano, E. D., Lembke, C. G., Zingaretti, S. M., Souza, G. M., Araújo, P., et al. (2019). Overexpression of an evolutionarily conserved drought-responsive sugarcane gene enhances salinity and drought resilience. *Ann. Bot.* 124, 691–700. doi: 10.1093/aob/mcz044

Bhakta, M. S., Gezan, S. A., Clavijo Michelangeli, J. A., Carvalho, M., Zhang, L., Jones, J. W., et al. (2017). A predictive model for time-to-flowering in the common bean based on QTL and environmental variables. *G3 GenesGenomesGenetics.* 7, 3901–3912. doi: 10.1534/g3.117.300229

Bhakta, M. S., Jones, V. A., and Vallejos, C. E. (2015). Punctuated distribution of recombination hotspots and demarcation of pericentromeric regions in Phaseolus vulgaris L. *PloS One* 10, e0116822. doi: 10.1371/journal.pone.0116822

Boyer, J. S., and Kawamitsu, Y. (2011). Photosynthesis gas exchange system with Internal CO2 directly measured. *Env. Control. Biol.* 49, 193–207. doi: 10.2525/ecb.49.193

Büssis, D., Von Groll, U., Fisahn, J., and Altmann, T. (2006). Stomatal aperture can compensate altered stomatal density in Arabidopsis thaliana at growth light conditions. *Funct. Plant Biol.* 33, 1037. doi: 10.1071/FP06078

Cackett, L., Luginbuehl, L. H., Schreier, T. B., Lopez-Juez, E., and Hibberd, J. M. (2022). Chloroplast development in green plant tissues: the interplay between light, hormone, and transcriptional regulation. *New Phytol.* 233, 2000–2016. doi: 10.1111/nph.17839

Cardona, T., Shao, S., and Nixon, P. J. (2018). Enhancing photosynthesis in plants: the light reactions. *Essays. Biochem.* 62, 85–94. doi: 10.1042/EBC20170015

Chen, C.-Q., Tian, X.-Y., Li, J., Bai, S., Zhang, Z.-Y., Li, Y., et al. (2022). Two central circadian oscillators OsPRR59 and OsPRR95 modulate magnesium homeostasis and carbon fixation in rice. *Mol. Plant* 15, 1602–1614. doi: 10.1016/j.molp.2022.09.008

Cichy, K. A., Porch, T. G., Beaver, J. S., Cregan, P., Fourie, D., Glahn, R. P., et al. (2015). Phaseolus vulgaris diversity panel for Andean bean improvement. *Crop Sci.* 55, 2149–2160. doi: 10.2135/cropsci2014.09.0653

Dorken, M. E., and Barrett, S. C. H. (2004). Phenotypic plasticity of vegetative and reproductive traits in monoecious and dioecious populations of *Sagittaria latifolia* (Alismataceae): a clonal aquatic plant. *J. Ecol.* 92, 32–44. doi: 10.1111/j.1365-2745.2004.00857.x

Drake, P. L., Boer, H. J., Schymanski, S. J., and Veneklaas, E. J. (2019). Two sides to every leaf: water and CO_2 transport in hypostomatous and amphistomatous leaves. *New Phytol.* 222, 1179–1187. doi: 10.1111/nph.15652

Drake, P. L., Froend, R. H., and Franks, P. J. (2013). Smaller, faster stomata: scaling of stomatal size, rate of response, and stomatal conductance. *J. Exp. Bot.* 64, 495–505. doi: 10.1093/jxb/ers347

Duursma, R. A. (2015). Plantecophys - An R package for analysing and modelling leaf gas exchange data. *PloS One* 10 (11), e0143346. doi: 10.1371/journal.pone.0143346

Egesa, A. O., Davidson, M. T., Pérez, H. E., and Begcy, K. (2024a). Biochemical and physical screening using optical oxygen-sensing and multispectral imaging in Sea oat seeds. *Agriculture* 14, 875. doi: 10.3390/agriculture14060875

Egesa, A. O., Puengchanchaikul, V., Vallejos, C. E., and Begcy, K.. (2024b). Contrasting DynamicPhotoprotective Mechanisms under Fluctuating Light Environments between anAndean and a Mesoamerican Genotype of Phaseolus vulgaris L. *Agronomy.* 14, 1907. doi: 10.3390/agronomy14091907

Elferjani, R., Benomar, L., Momayyezi, M., Tognetti, R., Niinemets, Ü., Soolanayakanahally, R. Y., et al. (2021). A meta-analysis of mesophyll conductance to CO2 in relation to major abiotic stresses in poplar species. *J. Exp. Bot.* 72, 4384–4400. doi: 10.1093/jxb/erab127

Endo, M., Shimizu, H., and Araki, T. (2016). Rapid and simple isolation of vascular, epidermal and mesophyll cells from plant leaf tissue. *Nat. Protoc.* 11, 1388–1395. doi: 10.1038/nprot.2016.083

Flexas, J. (2016). Genetic improvement of leaf photosynthesis and intrinsic water use efficiency in C3 plants: Why so much little success? *Plant Sci.* 251, 155–161. doi: 10.1016/j.plantsci.2016.05.002

Flexas, J., Ribas-Carbó, M., Diaz-Espejo, A., Galmés, J., and Medrano, H. (2008). Mesophyll conductance to CO $_2$: current knowledge and future prospects. *Plant Cell Environ.* 31, 602–621. doi: 10.1111/j.1365-3040.2007.01757.x

Gaut, B. S. (2014). The complex domestication history of the common bean. *Nat. Genet.* 46, 663–664. doi: 10.1038/ng.3017

Gepts, P. (2001). "Phaseolus vulgaris (Beans)," in *Encyclopedia of Genetics* (Elsevier), 1444–1445. doi: 10.1006/rwgn.2001.1749

Ghannoum, O. (2016). How can we breed for more water use-efficient sugarcane? *J. Exp. Bot.* 67, 557–559. doi: 10.1093/jxb/erw009

González, A., Lynch, J., Tohme, J. M., Beebe, S. E., and Macchiavelli, R. E. (1995). Characters related to leaf photosynthesis in wild populations and landraces of common bean. *Crop Sci.* 35, 1468–1476. doi: 10.2135/cropsci1995.0011183X003500050034x

Harrison, E. L., Arce Cubas, L., Gray, J. E., and Hepworth, C. (2020). The influence of stomatal morphology and distribution on photosynthetic gas exchange. *Plant J.* 101, 768–779. doi: 10.1111/tpj.14560

Israel, W. K., Watson-Lazowski, A., Chen, Z.-H., and Ghannoum, O. (2022). High intrinsic water use efficiency is underpinned by high stomatal aperture and guard cell potassium flux in C3 and C4 grasses grown at glacial CO2 and low light. *J. Exp. Bot.* 73, 1546–1565. doi: 10.1093/jxb/erab477

Kalaman, H., Wilson, S. B., Mallinger, R. E., Knox, G. W., Kim, T., Begcy, K., et al. (2022). Evaluation of native and nonnative ornamentals as pollinator plants in Florida: II. Floral resource value. *HortScience* 57, 137–143. doi: 10.21273/HORTSCI16124-21

Keller, B., Soto, J., Steier, A., Portilla-Benavides, A. E., Raatz, B., Studer, B., et al. (2024). Linking photosynthesis and yield reveals a strategy to improve light use efficiency in a climbing bean breeding population. *J. Exp. Bot.* 75, 901–916. doi: 10.1093/jxb/erad416

Kollist, H., Nuhkat, M., and Roelfsema, M. R. G. (2014). Closing gaps: linking elements that control stomatal movement. *New Phytol.* 203, 44–62. doi: 10.1111/nph.12832

Laïsk A. K., Nedbal L. and Govindjee, (Eds.) (2009). *Photosynthesis in silico: understanding complexity from molecules to ecosystems* (Dordrecht, Netherlands ; [New York]: Springer).

Lawrence, S., Pang, Q., Kong, W., and Chen, S. (2018). Stomata tape-peel: An improved method for guard cell sample preparation. *J. Vis. Exp.* 137, 57422. doi: 10.3791/57422

Lawson, T., Lefebvre, S., Baker, N. R., Morison, J. I. L., and Raines, C. A. (2008). Reductions in mesophyll and guard cell photosynthesis impact on the control of stomatal responses to light and CO2. *J. Exp. Bot.* 59, 3609–3619. doi: 10.1093/jxb/ern211

Leakey, A. D. B., Ferguson, J. N., Pignon, C. P., Wu, A., Jin, Z., Hammer, G. L., et al. (2019). Water use efficiency as a constraint and target for improving the resilience and productivity of C $_3$ and C $_4$ Crops. *Annu. Rev. Plant Biol.* 70, 781–808. doi: 10.1146/annurev-arplant-042817-040305

Li, T.-Y., Shi, Q., Sun, H., Yue, M., Zhang, S.-B., and Huang, W. (2021). Diurnal response of photosystem I to fluctuating light is affected by stomatal conductance. *Cells* 10, 3128. doi: 10.3390/cells10113128

LI-COR, B. (2023). *Using the Li-6800 Portable photosynthesis system.*

Lin, M. T., Salihovic, H., Clark, F. K., and Hanson, M. R. (2022). Improving the efficiency of Rubisco by resurrecting its ancestors in the family Solanaceae. *Sci. Adv.* 8, eabm6871. doi: 10.1126/sciadv.abm6871

Lynch, J., González, A., Tohme, J. M., and García, J. A. (1992). Variation in characters related to leaf photosynthesis in wild bean populations. *Crop Sci.* 32, 633–640. doi: 10.2135/cropsci1992.0011183X003200030012x

McAusland, L., Vialet-Chabrand, S., Davey, P., Baker, N. R., Brendel, O., and Lawson, T. (2016). Effects of kinetics of light-induced stomatal responses on photosynthesis and water-use efficiency. *New Phytol.* 211, 1209–1220. doi: 10.1111/nph.14000

Miyake, C., Miyata, M., Shinzaki, Y., and Tomizawa, K. (2005). CO2 response of cyclic electron flow around PSI (CEF-PSI) in tobacco leaves—relative electron fluxes through PSI and PSII determine the magnitude of Non-photochemical quenching (NPQ) of Chl fluorescence. *Plant Cell Physiol.* 46, 629–637. doi: 10.1093/pcp/pci067

Momayyezi, M., Borsuk, A. M., Brodersen, C. R., Gilbert, M. E., Théroux-Rancourt, G., Kluepfel, D. A., et al. (2022a). Desiccation of the leaf mesophyll and its implications for CO $_2$ diffusion and light processing. *Plant Cell Environ.* 45, 1362–1381. doi: 10.1111/pce.14287

Momayyezi, M., Rippner, D. A., Duong, F. V., Raja, P. V., Brown, P. J., Kluepfel, D. A., et al. (2022b). Structural and functional leaf diversity lead to variability in photosynthetic capacity across a range of *Juglans regia* genotypes. *Plant Cell Environ.* 45, 2351–2365. doi: 10.1111/pce.14370

Müller, M., and Munné-Bosch, S. (2021). Hormonal impact on photosynthesis and photoprotection in plants. *Plant Physiol.* 185, 1500–1522. doi: 10.1093/plphys/kiaa119

Nanjareddy, K., Arthikala, M.-K., Blanco, L., Arellano, E. S., and Lara, M. (2016). Protoplast isolation, transient transformation of leaf mesophyll protoplasts and improved Agrobacterium-mediated leaf disc infiltration of Phaseolus vulgaris: tools for rapid gene expression analysis. *BMC Biotechnol.* 16, 53. doi: 10.1186/s12896-016-0283-8

Niinemets, Ü. (2016). Leaf age dependent changes in within-canopy variation in leaf functional traits: a meta-analysis. *J. Plant Res.* 129, 313–338. doi: 10.1007/s10265-016-0815-2

OECD (2019). *Safety assessment of foods and feeds derived from transgenic crops, Volume 3: Common bean, rice, cowpea and apple compositional considerations* (OECD). doi: 10.1787/f04f3c98-en

Okegawa, Y., Sakamoto, W., and Motohashi, K. (2022). Functional division of f-type and m-type thioredoxins to regulate the Calvin cycle and cyclic electron transport around photosystem I. *J. Plant Res.* 135, 543–553. doi: 10.1007/s10265-022-01388-7

Okegawa, Y., Sato, N., Nakakura, R., Murai, R., Sakamoto, W., and Motohashi, K. (2023). *x* - and *y* -type thioredoxins maintain redox homeostasis on photosystem I acceptor side under fluctuating light. *Plant Physiol.* 193, 2498–2512. doi: 10.1093/plphys/kiad466

Peguero-Pina, J. J., Sisó, S., Flexas, J., Galmés, J., García-Nogales, A., Niinemets, Ü., et al. (2017). Cell-level anatomical characteristics explain high mesophyll conductance and photosynthetic capacity in sclerophyllous Mediterranean oaks. *New Phytol.* 214, 585–596. doi: 10.1111/nph.14406

Ren, T., Weraduwage, S. M., and Sharkey, T. D. (2019). Prospects for enhancing leaf photosynthetic capacity by manipulating mesophyll cell morphology. *J. Exp. Bot.* 70, 1153–1165. doi: 10.1093/jxb/ery448

Rodriguez, M., Rau, D., Bitocchi, E., Bellucci, E., Biagetti, E., Carboni, A., et al. (2016). Landscape genetics, adaptive diversity and population structure in *Phaseolus vulgaris*. *New Phytol.* 209, 1781–1794. doi: 10.1111/nph.13713

Sakoda, K., Adachi, S., Yamori, W., and Tanaka, Y. (2022). Towards improved dynamic photosynthesis in C3 crops by utilizing natural genetic variation. *J. Exp. Bot.* 73, 3109–3121. doi: 10.1093/jxb/erac100

Schmutz, J., McClean, P. E., Mamidi, S., Wu, G. A., Cannon, S. B., Grimwood, J., et al. (2014). A reference genome for common bean and genome-wide analysis of dual domestications. *Nat. Genet.* 46, 707–713. doi: 10.1038/ng.3008

Schneider, C. A., Rasband, W. S., and Eliceiri, K. W. (2012). NIH Image to ImageJ: 25 years of image analysis. *Nat. Methods* 9, 671–675. doi: 10.1038/nmeth.2089

Sexton, P. J., Boote, K. J., White, J. W., and Peterson, C. M. (1997). Seed size and seed growth rate in relation to cotyledon cell volume and number in common bean. *Field Crops Res.* 54, 163–172. doi: 10.1016/S0378-4290(97)00046-4

Siddiq, M., Butt, M. S., and Sultan, M. T. (2011). "Dry beans: production, processing, and nutrition," in *Handbook of vegetables and vegetable processing* (Wiley-Blackwell, Ames), 545–564.

Singh, S. P. (1981). *A key for identification of different growth habits of Phaseolus vulgaris L* (Cali, Colombia: Centro Internacional de Agricultura Tropical (CIAT). Available at: https://hdl.handle.net/10568/72290.

Singh, S. P., Gutiérrez, J. A., Molina, A., Urrea, C., and Gepts, P. (1991). Genetic diversity in cultivated common bean: II. Marker-based analysis of morphological and agronomic traits. *Crop Sci.* 31, 23–29. doi: 10.2135/cropsci1991.0011183X003100010005x

Song, G., Wang, Q., and Jin, J. (2021). Including leaf trait information helps empirical estimation of jmax from vcmax in cool-temperate deciduous forests. *Plant Physiol. Biochem.* 166, 839–848. doi: 10.1016/j.plaphy.2021.06.055

Tan, S.-L., Huang, X., Li, W.-Q., Zhang, S.-B., and Huang, W. (2021). Elevated CO2 concentration alters photosynthetic performances under fluctuating light in Arabidopsis thaliana. *Cells* 10, 2329. doi: 10.3390/cells10092329

Tanaka, Y., Adachi, S., and Yamori, W. (2019). Natural genetic variation of the photosynthetic induction response to fluctuating light environment. *Curr. Opin. Plant Biol.* 49, 52–59. doi: 10.1016/j.pbi.2019.04.010

Tanaka, Y., Sugano, S. S., Shimada, T., and Hara-Nishimura, I. (2013). Enhancement of leaf photosynthetic capacity through increased stomatal density in Arabidopsis. *New Phytol.* 198, 757–764. doi: 10.1111/nph.12186

Théroux-Rancourt, G., and Gilbert, M. E. (2017). The light response of mesophyll conductance is controlled by structure across leaf profiles. *Plant Cell Environ.* 40, 726–740. doi: 10.1111/pce.12890

Thormählen, I., Zupok, A., Rescher, J., Leger, J., Weissenberger, S., Groysman, J., et al. (2017). Thioredoxins play a crucial role in dynamic acclimation of photosynthesis in fluctuating light. *Mol. Plant* 10, 168–182. doi: 10.1016/j.molp.2016.11.012

Tomás, M., Flexas, J., Copolovici, L., Galmés, J., Hallik, L., Medrano, H., et al. (2013). Importance of leaf anatomy in determining mesophyll diffusion conductance to CO2

across species: quantitative limitations and scaling up by models. *J. Exp. Bot.* 64, 2269–2281. doi: 10.1093/jxb/ert086

Uebersax, M. A., Cichy, K. A., Gomez, F. E., Porch, T. G., Heitholt, J., Osorno, J. M., et al. (2022). Dry beans (*Phaseolus vulgaris* L.) as a vital component of sustainable agriculture and food security—A review. *Legume. Sci.* 5 (1), e155. doi: 10.1002/leg3.155

Warren, C. R. (2008). Rapid measurement of chlorophylls with a microplate reader. *J. Plant Nutr.* 31, 1321–1332. doi: 10.1080/01904160802135092

Wu, G., and Poethig, R. S. (2006). Temporal regulation of shoot development in *Arabidopsis thaliana* by *miR156* and its target *SPL3*. *Development* 133, 3539–3547. doi: 10.1242/dev.02521

Yoo, S.-D., Cho, Y.-H., and Sheen, J. (2007). Arabidopsis mesophyll protoplasts: a versatile cell system for transient gene expression analysis. *Nat. Protoc.* 2, 1565–1572. doi: 10.1038/nprot.2007.199

Zhang, Q., Peng, S., and Li, Y. (2019). Increase rate of light-induced stomatal conductance is related to stomatal size in the genus Oryza. *J. Exp. Bot.* 70, 5259–5269. doi: 10.1093/jxb/erz267

frontiers | Frontiers in Plant Science

TYPE Original Research
PUBLISHED 07 October 2024
DOI 10.3389/fpls.2024.1465004

OPEN ACCESS

EDITED BY
Sina Fallah,
Shahrekord University, Iran

REVIEWED BY
Yuqi Zhang,
Chinese Academy of Agricultural Sciences, China
Yuqing Ye,
Rice University, United States
Kevin Begcy,
University of Florida, United States

*CORRESPONDENCE
Fang Ji
jifang@cau.edu.cn

RECEIVED 15 July 2024
ACCEPTED 13 September 2024
PUBLISHED 07 October 2024

CITATION
Chen J, Ji F, Gao R and He D (2024) Reducing red light proportion in full-spectrum LEDs enhances runner plant propagation by promoting the growth and development of mother plants in strawberry. *Front. Plant Sci.* 15:1465004. doi: 10.3389/fpls.2024.1465004

Reducing red light proportion in full-spectrum LEDs enhances runner plant propagation by promoting the growth and development of mother plants in strawberry

Jian Chen, Fang Ji*, Rongwei Gao and Dongxian He

Key Laboratory of Agricultural Engineering in Structure and Environment of Ministry of Agriculture and Rural Affairs, College of Water Resources & Civil Engineering, China Agricultural University, Beijing, China

Full-spectrum light-emitting diodes (LEDs) have gradually replaced narrow-spectrum LEDs and are widely used in plant factories with artificial lighting (PFALs). However, the specific effect of LED light quality on dry mass allocation in runner plant propagation remains unclear. Hence, we cultivated "Akihime" strawberries as mother plants for 115 days to conduct runner plant propagation experiment under white LEDs (W_{100}), white and red LEDs ($W_{84}R_{16}$ and $W_{55}R_{45}$), red and blue LEDs (RB_{100}), and red, blue and green LEDs ($RB_{80}G_{20}$) in PFALs, and determined key factors affecting dry mass accumulation and allocation among mother plants and runner plants based on growth component analysis. The results showed that the net photosynthetic rate and total leaf area in mother plants in W_{100} increased by 11% and 31%, respectively, compared with $W_{55}R_{45}$. In comparison to $W_{84}R_{16}$ and $W_{55}R_{45}$, W_{100} increased the dry mass (23%–30%) of runner plants mainly by increasing the total dry mass (TDM) (23%) of strawberry plants, without significantly affecting the fraction of dry mass partitioning to runner plants. However, the number of runners in $W_{55}R_{45}$ was 5.1 per plant, representing only 78% of that in W_{100}. Compared with RB_{100}, $RB_{80}G_{20}$ significantly increased the number of runner plants and runner numbers by 16% and 19% to 13.0 per plant and 5.8 per plant, respectively. The partial replacement of blue light with green light in $RB_{80}G_{20}$ induced a shade avoidance response in runner plants, resulting in a 55% increase in the total leaf area of runner plants compared with RB_{100}. Data from growth component analysis showed that compared with red and blue LEDs, white LEDs increased the TDM of runner plants by 83% by increasing the plant TDM accumulation (44%) and the fraction of dry mass partitioning to runner plants (37%). Additionally, the dry mass (g) of runner plants per mol and per kilowatt-hour under in W_{100} were 0.11 and 0.75, respectively, significantly higher than other treatments. Therefore, reducing red light proportion in full-spectrum LEDs is beneficial for strawberry runner plant propagation in PFALs.

KEYWORDS

strawberry, LED light quality, runner plant propagation, dry mass partitioning, photon yield

1 Introduction

Cultivated strawberries (*Fragaria* × *ananassa* Duch.) are a globally important cash crop. In commercial production, seed propagation is uncommon due to genetic variation and difficulty in seed germination. Vegetative propagation by runners is the main method of asexual propagation for strawberries, which produces offspring with the desirable traits of the mother plants (Hytönen and Kurokura, 2020). Unrooted runner plants are generated from long stems called runners that sprout from virus-free plants selected as strawberry mother plants (Lieten, 1998), which are used as cuttings to produce transplants. Therefore, the propagation of a significant number and quality of runner plants is crucial. Plant factories with artificial lighting (PFALs) play a vital role in the runner plant propagation of strawberries, as they effectively isolate pests and diseases and enable efficient annual crop production (Kozai, 2019). The technologies for runner plant propagation of strawberries in PFALs have been steadily advancing. Chun et al. (2012) proposed a method for autotrophic production of strawberry transplants in PFALs to enhance propagation efficiency. Zheng et al. (2022) suggested a method for efficient production of high-quality runner plants using light-emitting diodes (LEDs) in plant factories, which can enhance the uniformity of strawberry transplants. However, electricity costs account for more than 30% of the total operating costs, with light sources consuming 70%–75% of the total electricity consumption (Fang, 2019). Therefore, optimizing the spectrum compositions of LEDs in PFALs becomes crucial for reducing power consumption, improving energy efficiency, and promoting plant growth.

The light absorption peaks of chlorophyll are located at 430 nm and 660 nm, making red and blue light effective in driving plants for photosynthesis and biomass accumulation (Chory, 2010). Red and blue LEDs are widely used in PFALs. With the increasing efficiency of green LEDs, it is important to understand the effect of green light on plants. Green light can penetrate deep into the tissues of leaves, reach the plant canopy, stimulate photosynthesis in the entire plant (Nishio, 2000; Terashima et al., 2009), and improve water use efficiency within the canopy (Smith et al., 2017). Several studies have shown that applying green light in PFALs can enhance plant biomass accumulation (Kim et al., 2004; Dou et al., 2019). However, using combinations of LEDs, such as red, green, and blue light, for plant cultivation can make visual assessment of plant disorders challenging for diagnosis (Park and Runkle, 2018; Kusuma et al., 2020), which also is harmful to human eyes.

Throughout their long-term evolution, plants have developed photosynthetic systems adapted to a broad-wide wavelength spectrum. Full-spectrum light, such as white light, has a comparable effect on lettuce, and ornamental plant seedlings as red and blue light, while significantly improving the visual colour quality of the lighting (Lin et al., 2013; Park and Runkle, 2018). This has led to an increasing interest in white light. Statistical analysis revealed that 27% of the studies used white light, 21% used red and blue light, followed by 12% using white and red light, and 10% supplementing green light to red and blue light (Nájera et al., 2023). White LEDs are usually achieved by mixing emission from blue LEDs with the excited light from yellow phosphor, resulting in a low percentage of red light. Hence, horticultural lighting companies often incorporate red LEDs into white LED fixtures, which not only meet the specific growth requirements of plants but also improve the energy efficacy of the fixtures (Chen et al., 2016; Yan et al., 2020; Kusuma et al., 2020). Moreover, the packaging cost of white LEDs is only 20% of that of red LEDs, which has led to its increasing share of applications in horticulture (Kusuma et al., 2020). White or white and red LEDs are now commonly used in the production of leafy vegetables in PFALs, including lettuce and sweet potato seedlings (He et al., 2020; Yan et al., 2020). As a value-added plant, it is essential to conduct research on the effects of full-spectrum LEDs on strawberries at different development stages. In order to improve the light photon efficacy of LED lamps and to promote plant growth, it is necessary to explore the effects of red LEDs and white LEDs on strawberry vegetative propagation by runners in the context of full-spectrum LEDs.

The overall performance of LED fixtures in PFALs relies on both the efficacy of the fixtures and the response of plants to different spectrum compositions. Light energy use efficiency (LUE), electric energy use efficiency (EUE), energy yield (EY), and photon yield (PY) are quantitative evaluation indices used to measure the effectiveness of electric light sources for crop growth in PFALs (Kozai, 2019; Fang, 2019). EY represents the amount of target product produced per kilowatt hour in the plant production cycle, while PY represents the amount of target product produced per mole of photon (Fang, 2019). The spectrum composition of LEDs can significantly impact the efficiency of runner plant propagation of strawberries, as well as the EY and PY of strawberries. Previous studies by Wu et al. (2011) and Lee et al. (2023) separately investigated the effects of narrow-spectrum and full-spectrum LEDs on runner plant propagation efficiency. However, the impact of LEDs with different spectrum compositions in PFALs on long-term strawberry runner plant propagation is still unclear, especially why and what kind of differences are caused by full-spectrum LEDs and narrow-spectrum LEDs. At the same time, issues such as power consumption and light energy efficiency need to be fully discussed.

Growth component analysis is a method that breaks down growth into basic morphological and physiological components (Jolliffe and Courtney, 1984). This allows for an effective evaluation of how each component contributes to the growth of target plant parts. In our study, we focused on the relationship between the strawberry mother plant, runners, and runner plants. Our aim was to identify the key components influenced by different LED spectrum compositions during the propagation of strawberry runner plants. We also investigated the impact of LED spectrum compositions on the PY and EY of the strawberry runner plants. To achieve these, we conducted a 115-day experiment in a plant factory using white, white and red LEDs, and narrow-spectrum LEDs to measure plant growth components of strawberry vegetative propagation. The findings from this study will be valuable for the light environment regulation and high-quality production of strawberry runner plants in PFALs.

2 Materials and methods

2.1 Plant materials and environmental conditions

The experiment was conducted in the LED plant factory experimental room of China Agricultural University (116.3 E, 40.0 N). Sixty strawberry plants (*Fragaria* × *ananassa* Duch. cv. "Akihime") with three fully expanded leaves and 9.4 ± 0.6 mm crown diameter were selected as mother plants for runner plant propagation. Strawberry mother plants were planted in 1.5 L pots (L100 mm × W100 mm × H150 mm) with the mixed substrate (vermiculite: perlite: peat = 1:1:1, V/V/V). Twelve pots were placed evenly in two rows on the long side of the cultivation bed (L1200 mm × W900 mm × H70 mm), keeping the spacing between plants and rows at 15 cm. The rest of the cultivation bed was covered with a cultivation cover for horizontal extension of the runners and runner plants produced by the mother plant. During the experiment, the produced runner plants with three leaves were harvested promptly based on a single runner-plant excision method (He et al., 2018; Figure 1B). The nutrient solution was prepared according to Yamazaki strawberry formulation (N 77, P 15.5, K 117, Ca 40, Mg 12, S 16, Fe 2, Mn 0.2, B 0.2, Zn 0.02, Cu 0.01, Mo 0.005 mg L^{-1}), and EC and pH were maintained in the range of 0.6–0.8 mS cm^{-1} and 6.0–6.5, respectively, with sub-irrigation once a day for 30 min. Environmental conditions for the growth of strawberry mother plants were set as follows: air temperature was controlled at 25 ± 1°C in the photoperiod and 20 ± 1°C in the dark period; relative humidity was 75% ± 10%; CO_2 concentration was controlled at 800 ± 50 μmol mol^{-1} in the photoperiod and without control in the dark period.

2.2 LED lighting treatments

The photoperiod of LED lighting treatments was set to 16 h d^{-1} with the photosynthetic photon flux density (PPFD) of 200 μmol m^{-2} s^{-1} and 8 h d^{-1} in the dark period. The LED plant growth lamps (the information was shown in Supplementary Table S1) were installed 15 cm from the top of the mother plants' canopy in different LED lighting treatments. The full-spectrum LED lighting treatments were labelled as W_{100} (white LEDs provided the PPFD of 200 μmol m^{-2} s^{-1}), $W_{84}R_{16}$ (White LEDs provided the PPFD of 168 μmol m^{-2} s^{-1}, red LEDs provided the PPFD of 32 μmol m^{-2} s^{-1}), and $W_{55}R_{45}$ (White LEDs provided the PPFD of 110 μmol m^{-2} s^{-1}, red LEDs provided the PPFD of 90 μmol m^{-2} s^{-1}), respectively. On the basis of the red and blue LEDs lighting treatment (RB_{100}: the PPFD provided by red LEDs was 156 μmol m^{-2} s^{-1}, the PPFD provided by blue LEDs was 44 μmol m^{-2} s^{-1}), the blue LEDs were partly replaced with the green LEDs to obtain the treatment labelled $RB_{80}G_{20}$ (the PPFD provided by red LEDs was 156 μmol m^{-2} s^{-1}, the PPFD provided by blue LEDs was 35 μmol m^{-2} s^{-1}, and green LEDs provided the PPFD of 9 μmol m^{-2} s^{-1}). The spectrum compositions between 300 and 800 nm were measured at 15 cm below the lamps using a fiber spectrometer (AvaField-2, Avates, Apeldoorn, the Netherlands). The PPFD was measured by the quantum meter (LI-250A, LI-COR Inc., Lincoln, NE, USA). According to the spectrum composition, the photon flux densities of ultraviolet light (UV, 300–399 nm), blue light (B, 400–499 nm), green light (G, 500–599 nm), red light (R, 600–700 nm), and far-red light (Fr, 701–800 nm) were integrally calculated, and the red light to blue light ratio (R: B ratio) and the red light to far-red light ratio (R: Fr ratio) were calculated by the photon flux of red light waveband to blue light waveband, the photon flux of red light

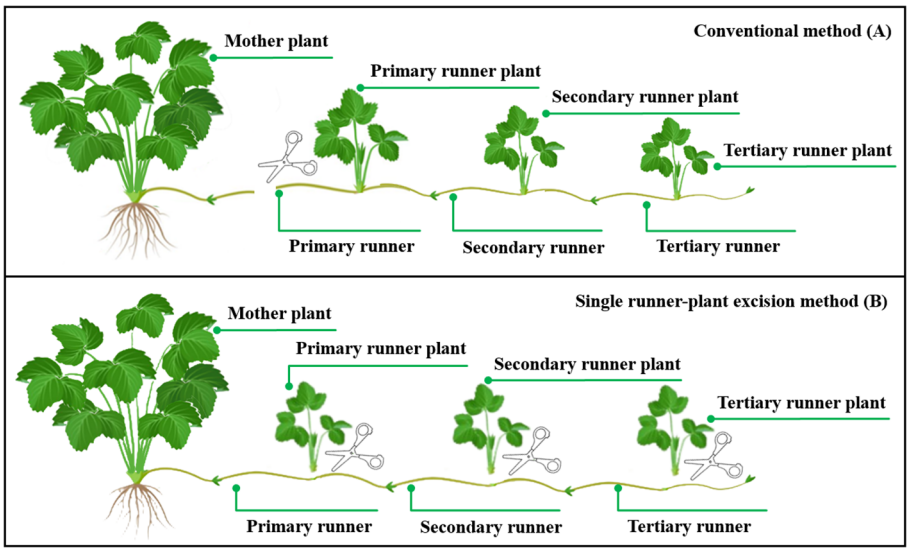

FIGURE 1
Different methods of runner plant harvesting: Conventional method **(A)** and single runner plant excision method **(B)**. Relationships between the strawberry mother plant, the runner, and the runner plant. A runner is a chain-like runner community consisting of a primary runner and subsequent runners in different orders in our study. A runner can produce a plurality of runner plants, the number of runner plant being less than or equal to the number of orders. This figure was drawn with reference to https://strawberryplants.org/.

waveband to far-red light waveband, respectively. The spectrum compositions and PPFD of different LED lighting treatments in this study were shown in Figure 2. The entire experimental period was 115 days.

2.3 Measurement parameters

2.3.1 Growth characteristics of mother plants, runners, and runner plants

The relationship between the strawberry mother plant, the runner, and the runner plant is shown in Figure 1. During the experiment, the newly expanded complete leaves and runners of the mother plant were counted every month, and the number and biomass of old and diseased leaves removed was recorded. The first runner sprouted from the mother plant was selected for measurement after the experiment started, and the length (cm) of the primary runner was measured daily using a ruler. The harvesting time (d) of primary trifoliate runner plants was calculated from the sprout of runners selected for measurement. The crown diameter (mm) and the fresh mass (g) of harvested primary runner plants were measured using vernier callipers and centesimal balance, respectively. Runners collected at the end of experiment and trifoliate runner plants were dried at 105°C for 3 h, then dried at 80°C to constant mass, and the dry mass (g) was measured by an electronic analytical balance (FA1204B, Bioon Group, Shanghai, China). Before destruction, all leaves of runner plants were scanned using a scanner (LiDE 110, Canon Inc, Beijing, China) for calculating the leaf area through image processing. Throughout the experiment, the number and dry mass of trifoliate runner plants harvested from each test area was recorded on time. At the end of the experiment, the crown diameter (mm) of the mother plants was measured using vernier callipers. The shoot and root parts of the mother plant were separated, where the shoot parts were separated into leaves, petioles, and a crown. Moreover, their dry mass and fresh mass were measured in the same way as the runner plants described above.

2.3.2 Photosynthetic and chlorophyll fluorescence characteristics of plant leaves

The net photosynthetic rate and chlorophyll fluorescence were measured every 28 days in the third unfolded leaf from the central leaf of mother plants and primary runner plants. The average photosynthetic rate of strawberry mother plants was calculated by averaging leaf photosynthetic rates measured every 28 days. The net photosynthetic rate was measured using a portable photosynthesis system (LI-6400XT, LI-COR Biosciences, Lincoln, NE, USA) with the following parameters set in the leaf chamber (PPFD, temperature, CO_2 concentration, air flow rate were set at 200 μmol m^{-2} s^{-1}, 25°C, 800 μmol mol^{-1}, and 500 μmol s^{-1}, respectively). The light quality of the leaf chamber was set at 90% red light and 10% blue light mixture. Subsequently, a chlorophyll fluorescence monitoring system (PEA, Hansatech Instruments Ltd., Norfolk, UK) was used to measure the chlorophyll fluorescence of the leaves dark-adapted for more than half an hour. Fluorescence measurements were recorded up to 2 s by illumination with a continuous red light (3,000 μmol m^{-2} s^{-1}, 650 nm) by an array of LEDs focused on the leaf surface.

2.3.3 Growth component analysis of runner plants

The effect of LED light quality on strawberry runner plant propagation was analysed and verified by decomposing the basic components related to plant growth (Figure 3). The total runner plant dry mass (RPDM) was determined by multiplying the plant total dry mass (TDM) with the fraction of dry mass partitioning to runner plants ($P_{runner\ plant}$). $P_{runner\ plant}$ was further divided into the total runner plant number (RPN_{plant}) and runner plant relative sink strength (RPSS). However, our research did not calculate or analyze RPSS. RPN_{plant} was explained by the total runner number (RN_{plant}) and the number of runner plants produced by a single runner (RPN_{runner}). The total leaf area of the strawberry plant (LA_{plant}) consisted of the leaf of the mother plant ($LA_{mother\ plant}$) and the leaf area of total runner plants ($LA_{runner\ plant}$). The data

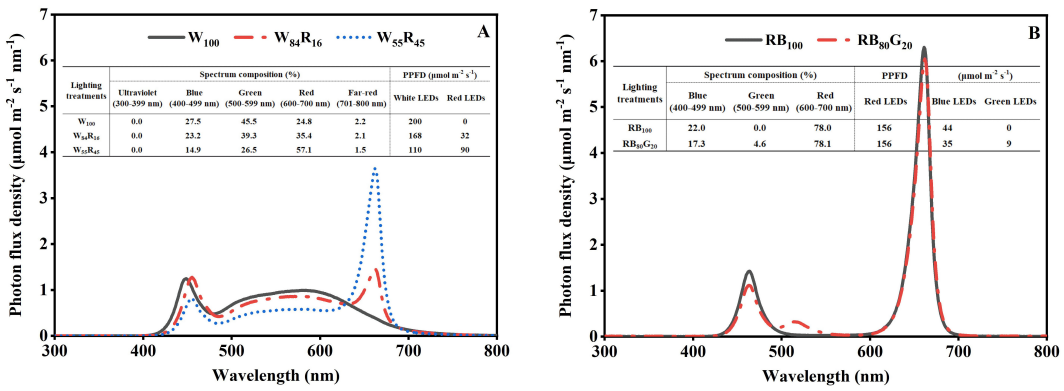

FIGURE 2
The spectrum composition and photosynthetic photon flux density (PPFD) of LED lighting treatments provided by different LEDs measured at the top of the strawberry mother plant canopy. The four LED lighting treatments contained 200 μmol m^{-2} s^{-1} white (W_{100}), 168 μmol m^{-2} s^{-1} white and 32 μmol m^{-2} s^{-1} red ($W_{84}R_{16}$), 110 μmol m^{-2} s^{-1} white and 90 μmol m^{-2} s^{-1} red ($W_{55}R_{45}$), 156 μmol m^{-2} s^{-1} red and 44 μmol m^{-2} s^{-1} blue (RB_{100}), 156 μmol m^{-2} s^{-1} red, 35 μmol m^{-2} s^{-1} blue, and 9 μmol m^{-2} s^{-1} green ($RB_{80}G_{20}$) LEDs.

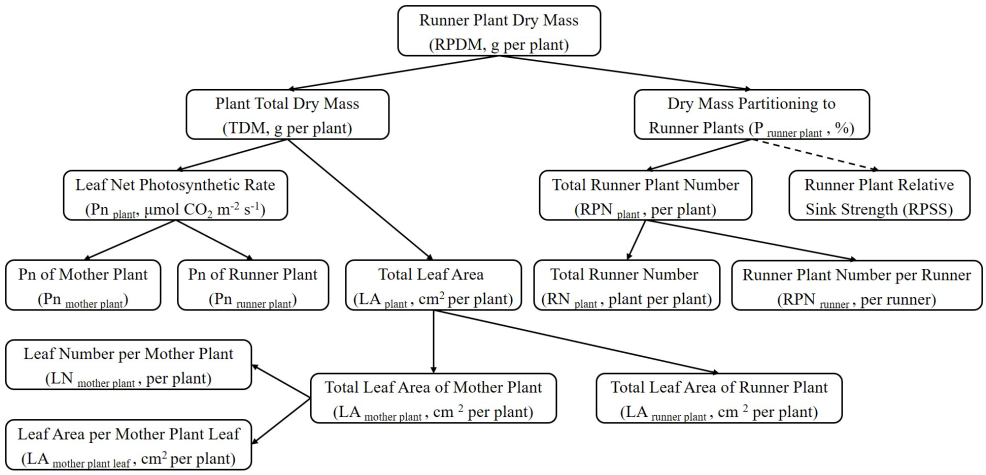

FIGURE 3
The figure illustrated a general scheme of a top-down growth component analysis of total runner plant dry mass. Abbreviations and units were provided in brackets. Dotted lines indicated components that were not calculated or included in the growth component analysis.

including the total leaf area of the mother plant ($LA_{mother\ plant}$), the total number of leaves of the mother plant ($LN_{mother\ plant}$), and the leaf area of a single mother plant leaf (LA_{leaf}) were obtained by destructively sampling at the end of the experiment. The leaf area of total runner plants ($LA_{runner\ plant}$) was determined by the sum of leaf area of each harvested runner plants. The net photosynthetic rate of the strawberry plant (Pn_{plant}) contained the net photosynthetic rate of the mother plant leaves ($Pn_{mother\ plant}$) and the runner plant leaves ($Pn_{runner\ plant}$). The instantaneous net photosynthetic rate of the mother plant leaves ($Pn_{mother\ plant}$) was calculated as the average value of the three measurement periods: 28 days, 56 days, 84 days, and 115 days after the start of the experiment. $Pn_{runner\ plant}$ was the net photosynthetic rate of primary runner plants.

2.3.4 Photon yield and energy yield in runners and runner plants

Referring to the study of Zheng et al. (2019), the PY in runner plants was defined as the number of runner plants produced per mole photons throughout the propagation cycle; its EY was defined as the number of runner plants produced per kilowatt-hour electricity consumed by the light source. The PY and EY in dry mass of all runner plants per mother plant were defined as above for runner plants. The graphs plotted with PY as the horizontal axis and EY as the vertical axis represent the total performance evaluation to evaluate the overall performance differences of different LED lamps on runner plant propagation of strawberries.

2.4 Data statistics and analysis

A total of 5 LED lighting treatments was used in this experiment, with 12 strawberry mother plants planted in each treatment. The experiment was replicated twice. One-way analysis of the variance (ANOVA) of the data was based on Duncan's multiple comparison method for the comparison of means ($P < 0.05$). The significance analysis for the growth component analysis was conducted using an independent samples t-test. Statistical analysis and graphing of the data were done using SPSS 23.0 software (IBM SPSS Statistics for Windows, version 23.0, Armonk, NY, USA), Microsoft Excel 2016, and Origin Pro software, respectively.

3 Results

3.1 Growth parameters and photosynthetic characteristics of strawberry mother plants

White LEDs contributed to the morphogenesis and biomass accumulation of strawberry mother plants (Table 1). The mother plants W_{100} exhibited a total of 11.3 new leaves per plant and the crown diameter was 14.3 mm, both of which were substantially higher compared with those under white and red LEDs and/or narrow-spectrum LEDs. The TDM per mother plant in W_{100} increased by 20%, 22% to 13.66 g compared with $W_{55}R_{45}$ and RB_{100}, respectively. The net photosynthetic rates of mother plants in W_{100} were consistently higher than those of the other treatments (Figure 4A). The average net photosynthetic rates of strawberry mother plants throughout the experiment under narrow-spectrum combination LEDs were only 82% of that under white LEDs, which were at 6.0 μmol m^{-2} s^{-1} (Figure 5B). Moreover, the Fv/Fm values of mother plants under different LED light qualities remained consistently above 0.80 (Figure 4B). In full-spectrum LED lighting treatments, the total leaf area of strawberry mother plants was significantly reduced when replacing white light with red light. The total leaf area of mother plants in $W_{55}R_{45}$ was only 76% of that in W_{100} (Figure 5A). In contrast, there were no significant differences in the total leaf area and net photosynthetic rate of mother plants in RB_{100} and $RB_{80}G_{20}$ (Figure 5).

10.3389/fpls.2024.1465004

TABLE 1 Effect of LED light quality on morphogenesis and biomass accumulation of strawberry mother plants at end of the experiment.

LED lighting treatment	Number of new leaves (per plant)	Crown diameter (mm)	Dry mass of crown (g)	Dry mass of mother plant (g)
RB_{100}	10.8 ± 0.4 ab	13.2 ± 0.5 b	1.53 ± 0.08 b	11.23 ± 1.08 b
$RB_{80}G_{20}$	11.0 ± 0.5 ab	13.1 ± 0.7 b	1.52 ± 0.08 b	11.21 ± 1.04 b
W_{100}	11.3 ± 0.8 a	14.3 ± 0.9 a	1.69 ± 0.11 a	13.66 ± 1.63 a
$W_{84}R_{16}$	10.5 ± 0.5 b	13.5 ± 0.9 b	1.56 ± 0.13 b	11.18 ± 0.97 b
$W_{55}R_{45}$	10.5 ± 0.7 b	13.5 ± 0.8 b	1.57 ± 0.16 ab	11.35 ± 1.04 b

Different letters in the same column indicate significant differences ($p < 0.05$). All values are "mean ± standard deviation".

3.2 Growth characteristics of runners and the number of runner plants

The length of the primary runner was increased by red and blue LEDs, which were approximately 13% longer compared with white LEDs (Figure 6). The partial replacement of blue light by green light also significantly reduced the length of the primary runner. The harvesting time of primary runner plants was the shortest in W_{100} and $RB_{80}G_{20}$, significantly shorter than in $W_{84}R_{16}$ and $W_{55}R_{45}$. Red light replacing white light was not favourable for early runner plant harvesting. Figure 6 showed that a shorter runner length can reduce the time required for harvesting runner plants.

The total number of runner plants produced by a strawberry mother plant was determined by the number of runners produced by it and the number of runner plants produced by a single runner. In this experiment, the earliest runner sprout from strawberry mother plants in different LED lighting treatments produced four runner plants. Under full-spectrum LEDs, excessive increase in red light reduced the number of runners. The number of runners in W_{100} was significantly higher than that in $W_{55}R_{45}$, reaching 6.6 per mother plant (Figure 7). Narrow-spectrum LEDs did not have a significant effect on the number of runners. Full-spectrum LEDs did not affect the production of runner plants, but the number was higher than under red and blue LEDs. The total number of runner plants in W_{100} was 1.3 times that in RB_{100}, reaching 15.0 per mother plant. Additionally, partial replacement of blue light by green light significantly increased the number of runner plants produced by mother plants under narrow-spectrum LEDs.

3.3 Growth component analysis of runner plants

Compared with $W_{84}R_{16}$ and $W_{55}R_{45}$, W_{100} increased the dry mass of total runner plants by 30% and 23%, respectively (Figures 8A, B). Under full-spectrum LEDs, W_{100} significantly enhanced the TDM of strawberry plants. Still, it did not significantly impact the fraction of dry mass partitioning to runner plants. As the proportion of white light replaced by red light increased, W_{100} significantly boosted the increase in the total leaf area of strawberry plants from 21% to 33%. This was the main reason for the increase in the TDM of strawberry plants in W_{100}. Compared with narrow-spectrum LEDs, W_{100} significantly increased the dry mass of total runner plants by 28% to 83% (Figures 8C, D). Taking Figure 8D as an example, the increase in the TDM of strawberry plants (+44%) and the fraction of dry mass partitioning to runner plants (+37%) together contributed to the 83% increase in the dry mass of total runner plants. Additionally, compared with RB_{100}, $RB_{80}G_{20}$ did not result in significant differences in the net photosynthetic rate and total leaf area of mother plants. However, $RB_{80}G_{20}$ significantly increased the leaf area of total runner plants by 55%, ultimately leading to a 15% increase in the TDM of strawberry plants (Figure 8E).

3.4 Growth parameters of primary runner plants

White LEDs improved the quality of runner plants. The crown diameter, leaf area, and dry mass of a single primary runner plant under white LEDs (W_{100}) represented an increase of 7%, 16%, and 14% compared with $W_{55}R_{45}$ (Table 2). The partial replacement of blue light by green light significantly increased the leaf area and dry mass of primary runner plants under narrow-spectrum LEDs. In contrast, the leaf area and dry mass of primary runner plants under red and blue LEDs were significantly lower than those under full-spectrum LEDs, measuring only about 75% of those under white LEDs.

3.5 Total performance evaluation based on photon yield and energy yield

The vertical axis and horizontal axis of Figure 9 represented PY and EY, respectively. The closer the value of the LED lighting treatment was to the upper right of the chart, the more suitable the light source was for plant growth in PFALs. As shown in Figure 9A, the difference in EY of runner plants under full-spectrum LEDs was small but significantly higher than that of narrow-spectrum LEDs. Additionally, more runner plants were produced in W_{100} and $RB_{80}G_{20}$, resulting in a better PY compared with RB_{100}. The changing trend of the dry mass of total runner plants per mother plant under each LED lighting treatment was consistent with the number of runner plants. The dry mass of total runner plants per mother plant under white LEDs was close to the upper right, while it

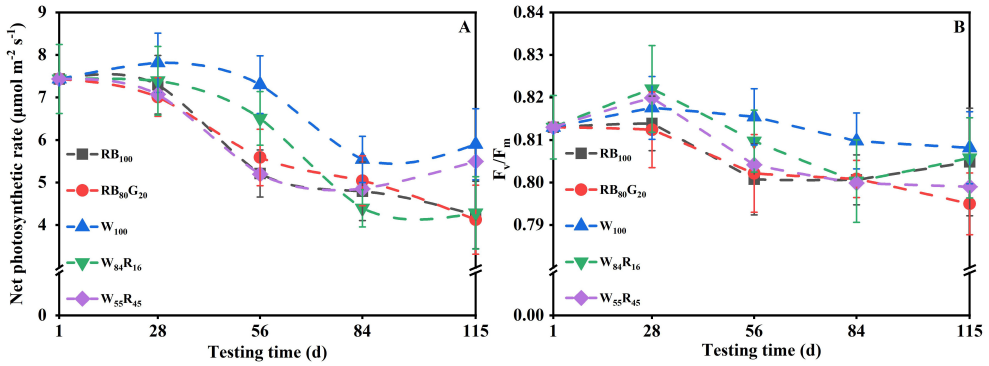

FIGURE 4
Changes in net photosynthetic rate **(A)** and Fv/Fm **(B)** of strawberry mother plants leaves under different LED lighting treatments during the experiment. The vertical bars represent standard deviations.

under red and blue LEDs was close to the lower left (Figure 9B). In full-spectrum LED lighting treatments, the partial replacement of white light by red light reduced PY and EY in the number and dry mass of the runner plant.

4 Discussion

4.1 White LEDs increased biomass accumulation of strawberry plants compared with other treatments

The accumulation of biomass in plants is primarily determined by the net photosynthetic rate of the leaves and the total leaf area influencing the plant's light interception capacity (Higashide, 2022). Our study demonstrated that under full-spectrum LEDs, an increase in the proportion of red light at the expense of white light significantly reduced both the leaf net photosynthetic rate and leaf area in strawberry mother plants and runner plants (Figures 4, 5), ultimately leading to decreased biomass. In the context of supplemental lighting for strawberry greenhouse production, the addition of red light significantly reduced the maximum net photosynthetic rate of leaves by inhibiting processes such as the mesophyll conductance and the maximum rate of carboxylation of Rubisco (Lauria et al., 2021). On the other hand, the daily photosynthetic rate of strawberry leaves increased significantly under white light (23% red light) compared with full-spectrum light with a high proportion of red light (43% and 59% red light, respectively) (Wu et al., 2012). This increase in photosynthetic rate under white light can be attributed to the ability of lower red light proportions to maintain higher stomatal conductance, thereby enhancing CO_2 uptake. Similarly, the net photosynthetic rate change of strawberry mother plant leaves was significantly higher under white LED compared with white and red LEDs ($W_{84}R_{16}$ and $W_{55}R_{45}$) in this experiment (Figure 4). It is notable to note that while supplementing red light under white light has been reported to reduce the leaf area of plants like green onions (Gao et al., 2021) and strawberries (Wu et al., 2012), the addition of white and red LEDs increased the leaf area of wheat seedlings (Li et al., 2022) and lettuce (Lin et al., 2013). Therefore, this experiment concluded that

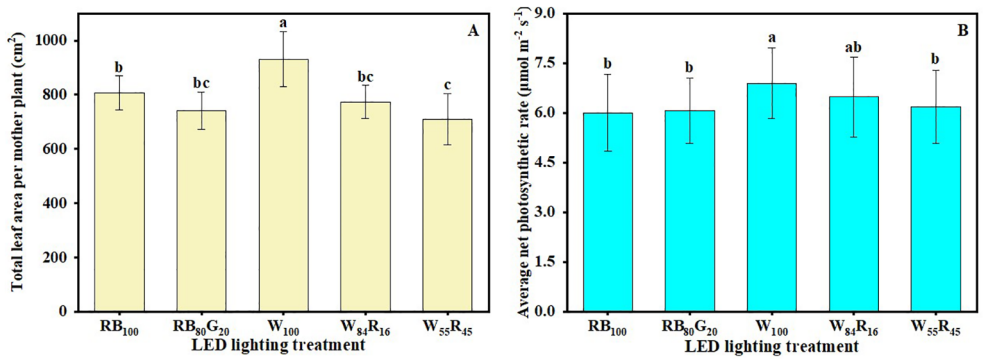

FIGURE 5
Effect of LED light quality on total leaf area **(A)** and average net photosynthetic rate **(B)** of strawberry mother plants leaves at end of the experiment. Letters a–b indicate significant differences according to Duncan's multiple range test at $p < 0.05$. The vertical bar represents standard deviations.

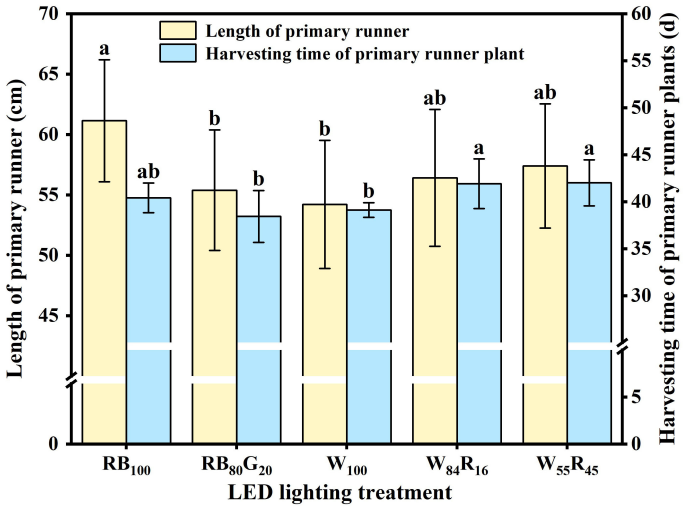

FIGURE 6
Effect of LED light quality on length of primary runners and harvesting time of primary runner plants. Letters a–b indicate significant differences according to Duncan's multiple range test at $p < 0.05$. The vertical bar represents standard deviations.

replacing white light with red light did not enhance the photosynthetic rate or expansion of leaf area in plants, ultimately leading to a reduction in biomass accumulation.

The average leaf net photosynthetic rate of mother plants in $W_{55}R_{45}$ was similar to RB_{100}, but the leaf area was significantly lower in $W_{55}R_{45}$ (Figure 5). It is worth noting that the TDM of mother plants in $W_{55}R_{45}$ was not significantly different from RB_{100} (Table 1). We hypothesize that the green light in the 500–599 nm range of the full-spectrum light enhances photosynthesis in plant leaves and/or the middle and lower parts of the canopy, leading to increased plant dry mass accumulation. Nishio (2000) has shown that photosynthesis is enzyme limited rather than light limited in the upper one-third of the leaf, while photosynthesis at the abaxial surface of the leaf is light limited. Difference in transmittance between red light and green light in the leaves can result in a 15% difference in biomass accumulation (Ptushenko et al., 2015). Hence, wavelengths in the 500–599 nm range may compensate for or even exceed the losses caused by the reduction of red and blue light. The absence of green light likely contributes to the lower dry mass under red and blue LEDs compared with full-spectrum LEDs. In narrow-spectrum LEDs, the partial replacement of blue light by green light also significantly increased the TDM of runner plants (Table 2). Green light also induces shade avoidance responses, such as stem elongation and leaf expansion (Meng et al., 2019). In this experiment, replacing part of the blue light with green light significantly increased the leaf area of runner plants, contributing to increased dry mass, though it did not affect the mother plants (Figure 8E). Thus, green light plays a crucial role in promoting

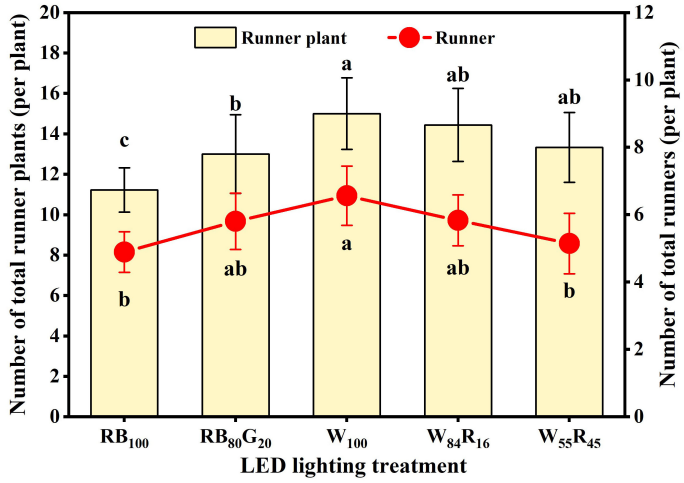

FIGURE 7
Total number of runners and runner plants produced by strawberry mother plants in different LED lighting treatments at end of the experiment. Letters a–c indicate significant differences according to Duncan's multiple range test at $p < 0.05$. The vertical bar represents standard deviations.

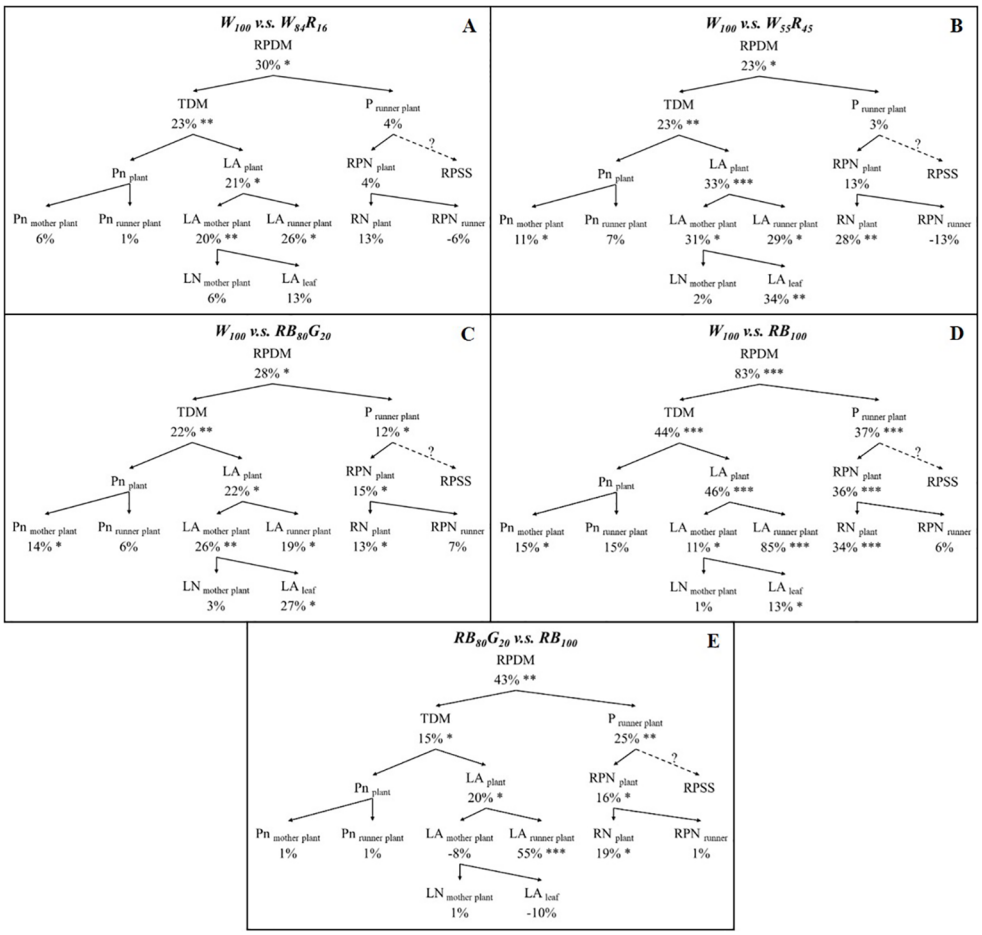

FIGURE 8
Effect of LEDs with different spectrum composition on the growth component of strawberry. **(A–D)** are the results of the comparison of W_{100} with $W_{84}R_{16}$, $W_{55}R_{45}$, $RB_{80}G_{20}$, RB_{100}, respectively. **(E)** is the results of the comparison of $RB_{80}G_{20}$ with RB_{100}. RPDM, runner plant dry mass; TDM, total dry mass; P $_{runner\ plant}$, the proportion of dry mass partitioning to runner plant; Pn $_{plant}$, the net photosynthetic rate of the strawberry plant; Pn $_{mother\ plant}$, leaf net photosynthetic rate of mother plants; Pn $_{runner\ plant}$, leaf net photosynthetic rate of runner plants; LA $_{plant}$, total leaf area of strawberry plant; LA $_{mother\ plant}$, total leaf area of mother plants; LA $_{runner\ plant}$, leaf area of total runner plants; LN $_{mother\ plant}$, leaf number per mother plant; LA $_{leaf}$, leaf area per mother plant leaf; RPN $_{plant}$, total runner plant number; RN $_{plant}$, total runner number; RPN $_{runner}$, runner plant number per runner; RPSS, runner plant relative sink strength. Asterisks indicate significant effect of LEDs tested by independent samples t-test (*$P < 0.05$, **$P < 0.01$, ***$P < 0.001$). The runner plant relative sink strength was not determined.

canopy dry mass accumulation and enhancing light interception through shade avoidance responses.

4.2 White LEDs promoted runner plant propagation of strawberry compared with white and red LEDs

The emergence of runners and the production of runner plants are key indicators of vigorous vegetative growth in strawberries. During the process of vegetative propagation, runners served as the main reproductive organs and their formation involved two stages: axillary bud germination and axillary bud growth (Liang et al., 2022). The direction and growth of axillary buds were regulated by signals such as light and hormones (Hytönen et al., 2009). Our study discovered that the partial replacement of white light by red light had a negative impact on the germination of axillary buds into runners. For example, the number of runners in W_{100} was 1.3 times higher than in $W_{55}R_{45}$ (Figure 7). In contrast, partially replacing white light with blue light had no significant effect on runner numbers (Lee et al., 2023). This suggested that red light had a greater influence on runner formation than blue light, with higher proportions of red light inhibiting this process. Red light and far-red light often worked together in hormone-mediated pathways that regulate runner formation. The low R: FR (rich in far-red light) upregulated gibberellic acids (GAs) anabolism and downregulate catabolic genes in plants, leading to an increase in GAs levels (Yamaguchi et al., 1998; Seo et al., 2006). Elevated GA levels induced cell division in axillary buds, promoting runner formation (Hytönen et al., 2009). In this experiment, the low R: FR (W_{100}) significantly increased the number of runners compared with high R: FR ($W_{55}R_{45}$) and red and blue LEDs (without far-red

TABLE 2 The morphology and biomass accumulation of single primary runner plant and dry mass of total runner plants in different LED lighting treatments.

LED lighting treatment	Crown diameter (mm)	Leaf area of a single primary runner plant (cm^2)	Dry mass of a single primary runner plant (g)	Dry mass of total runner plants (g)
RB_{100}	6.2 ± 0.3 ab	61.4 ± 7.0 c	0.59 ± 0.05 c	6.50 ± 0.79 c
$RB_{80}G_{20}$	6.2 ± 0.5 ab	69.7 ± 6.8 b	0.71 ± 0.06 b	10.10 ± 1.83 b
W_{100}	6.5 ± 0.3 a	81.2 ± 8.5 a	0.83 ± 0.10 a	13.38 ± 1.21 a
$W_{84}R_{16}$	6.1 ± 0.3 b	71.4 ± 8.0 b	0.73 ± 0.06 b	10.32 ± 1.70 b
$W_{55}R_{45}$	6.1 ± 0.3 b	70.0 ± 8.8 b	0.73 ± 0.08 b	10.92 ± 1.65 b

Dry mass of total runner plants per mother plants was calculated. Letters a–c indicate significant differences according to Duncan's multiple range test at $p < 0.05$.

light) (Figure 7). White LEDs, which contain more far-red light, may have a greater advantage in promoting runner formation compared with narrow-spectrum LEDs.

White LEDs significantly promoted strawberry runner growth by increasing dry mass accumulation in crowns. Experimental data showed that the dry mass of crowns treated with white LEDs was significantly higher than in other treatment groups (Table 1). Crowns acted as major carbohydrate storage sites, with fructose, glucose, and sucrose playing crucial roles in plant development (Macías-Rodríguez et al., 2002). Higher biomass in crowns could more effectively mobilize reserves, promoting leaf and axillary bud sprouting while temporarily increasing sugar content (Rivero et al., 2022). This rise in sugar content helped break axillary bud dormancy and was positively correlated with runner numbers (Li et al., 2020). However, the number of runner plants was influenced by both the number of runners and the number of runner plants produced per runner. Compared with $W_{84}R_{16}$ and $W_{55}R_{45}$, W_{100} reduced the number of runner plants produced per runner, although there was no significant difference in total runner plant numbers among the three treatments (Figures 8A, B). Fewer runner plants per runner facilitated the concentrated supply of dry mass, thereby improving the quality of primary runner plants in W_{100} (Table 2), which was one reason why it outperformed white and red LEDs.

4.3 Possible reasons for white LEDs to increase the dry mass of runner plants

Our study revealed that partially replacing white light with red light in full-spectrum LEDs significantly reduced the TDM of strawberry runner plants (Figures 8A, B). This reduction was primarily attributed to the high proportion of red light, which significantly decreased the total leaf area of both mother plants and runner plants, ultimately leading to diminished overall photosynthetic productivity. Compared with blue and red LEDs, the increase in TDM observed in runner plants under white LEDs could only be partially linked to the increase in the overall dry mass of the strawberry plants. The increased the fraction of dry mass partitioning to runner plants contributed to more than 40% of the total runner plant dry mass (Figure 8D). Enhancing the fraction of dry mass partitioning to the sinks (runner plants), it was crucial to

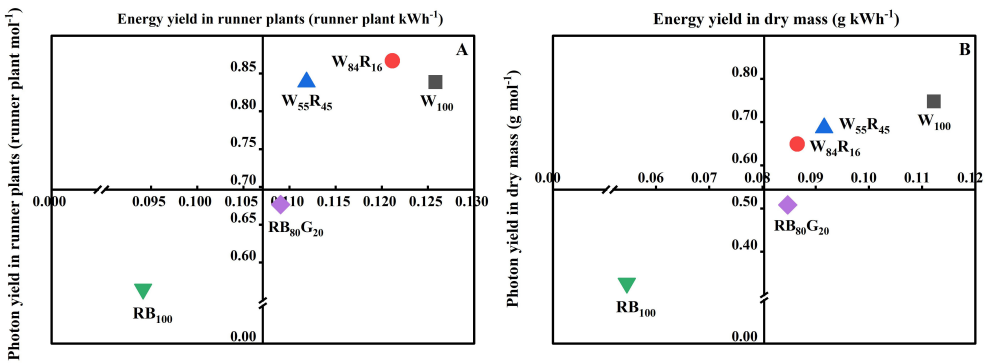

FIGURE 9
Effect of LED light quality on number **(A)** and biomass accumulation **(B)** of runner plants based on PY and EY. Taking panel **(A)** as an example, the horizontal axis value for W100 represented the PY (the number of runner plants produced per mole photons throughout the propagation cycle) of the runner plant number, while the vertical axis value indicates the EY (the number of runner plants produced per kilowatt-hour electricity) of the runner plant number. The closer a treatment is to the upper right corner of the graph, the better its overall performance in simultaneously increasing both the PY and EY of the runner plant number.

enhance the sink strength and numbers (Marcelis, 1996; Heuvelink, 1997). The relative sink strength of a sink organ could be determined by its dry mass. Strawberry runner plants acted as sinks and relied on the mother plant for their water, minerals, and photosynthate supply before they took roots (Caraco and Kelly, 1991). As the leaves of runner plants mature and initiate photosynthesis, the proportion of photosynthates transported from the mother plant decreases, complicating the assessment of the sink strength of runner plants. Unlike reproductive organs such as fruits, dry mass was not an ideal indicator of sink strength for photosynthetically active vegetative organs.

The number of runner plants significantly influenced the fraction of dry mass partitioning to runner plants. While the number of runner plants per runner affected the total number of runner plants produced by the mother plant, this effect was not statistically significant. Therefore, under full-spectrum LEDs, a substantial increase in the number of runners led to an overall increase in the number of runner plants, which in turn increased the fraction of dry mass partitioning to runner plants. Wu et al. (2011) found that partially replacing blue light with green light promoted runner growth. Similarly, our experiment showed that, compared with RB_{100}, the $RB_{80}G_{20}$ treatment significantly increased the number of runners by 19%. This increase in runner number was a primary factor in the significant rise in the fraction of dry mass partitioning to runner plants under this treatment, contributing to the overall increase in total runner plant dry mass. Neither the $RB_{80}G_{20}$ nor the RB_{100} significantly affected dry mass accumulation in mother plants (Table 1). It remained unclear whether the $RB_{80}G_{20}$ treatment increased the transport of photosynthates from the mother plant to the runner plants, resulting in no significant change in the mother plant's dry mass. However, it was evident that the 55% increase in leaf area observed under $RB_{80}G_{20}$, compared with RB_{100}, positively impacted dry mass accumulation in runner plants.

4.4 Photon yield and energy yield under full-spectrum LEDs were better than narrow-spectrum LEDs

PY and EY are valuable for assessing the effectiveness and energy efficiency of LED lamps in PFALs for crop cultivation (Fang, 2019). This study demonstrated that white LEDs outperformed white and red LEDs, with their performance improving as the proportion of red light decreased (Figure 9). This improvement was primarily due to the positive effect of white LEDs with a low red light proportion on the growth of strawberry runners and runner plant. Although the addition of red LEDs increased the photon efficacy of white and red LEDs, the cost was significantly higher compared with white LEDs. Therefore, optimizing the light spectrum must balance energy efficiency with the potential to maximize crop production. Our findings suggested that for strawberry runner plant propagation, low-cost, high-efficiency white LEDs satisfied these essential requirements. Full-spectrum LEDs generally outperformed narrow-spectrum LEDs, providing advantages in terms of growth promotion and energy savings. These results were consistent with the increasing popularity of white LEDs as light sources for horticultural production.

5 Conclusions

Our study demonstrates that partially substituting white light with red light inhibits leaf expansion in strawberry mother and runner plants, while reducing net photosynthetic rate. This reduction is detrimental to the accumulation of dry mass in strawberry plants. The application of red light also suppresses runner formation, leading to fewer runner plants and a lower partitioning of dry mass to runner plants. Under full-spectrum LEDs, a higher proportion of green light enhances overall carbon assimilation, contributing to significantly greater dry mass accumulation in mother plants compared with those under red and blue LEDs. Furthermore, under narrow-spectrum LEDs, replacing a portion of the blue light with green light significantly increases the number of runners and induces a shade avoidance response in runner plants, thereby enhancing light capture efficiency and substantially boosting dry mass accumulation. Full-spectrum LEDs with a lower proportion of red light (white LEDs) achieve the highest photosynthetic yield (0.11 g per mol) and energy yield (0.75 g per kWh) of runner plant dry mass, providing energy-saving benefits in PFALs. Therefore, white LEDs represent a suitable artificial light source for the runner plant propagation in strawberries, as they promote increased dry mass accumulation and a higher number of runner plants.

Data availability statement

The raw data supporting the conclusions of this article will be made available by the authors, without undue reservation.

Author contributions

JC: Investigation, Validation, Writing – original draft, Data curation, Formal analysis. FJ: Conceptualization, Funding acquisition, Project administration, Supervision, Writing – review & editing. RG: Investigation, Validation, Writing – original draft. DH: Funding acquisition, Supervision, Writing – review & editing.

Funding

The author(s) declare financial support was received for the research, authorship, and/or publication of this article. This work was supported by the Beijing Training Program of Innovation and Entrepreneurship for Undergraduates (No. S202110019162) and the earmarked fund for China Agriculture Research System (CARS-21).

Conflict of interest

The authors declare that the research was conducted in the absence of any commercial or financial relationships that could be construed as a potential conflict of interest.

Publisher's note

All claims expressed in this article are solely those of the authors and do not necessarily represent those of their affiliated organizations, or those of the publisher, the editors and the reviewers. Any product that may be evaluated in this article, or claim that may be made by its manufacturer, is not guaranteed or endorsed by the publisher.

Supplementary material

The Supplementary Material for this article can be found online at: https://www.frontiersin.org/articles/10.3389/fpls.2024.1465004/full#supplementary-material

References

Caraco, T., and Kelly, C. K. (1991). On the adaptive value of physiological integration in clonal plants. *Ecol. (Durham)* 72, 81–93. doi: 10.2307/1938904

Chen, X. L., Xue, X. Z., Guo, W. Z., Wang, L. C., and Qiao, X. J. (2016). Growth and nutritional properties of lettuce affected by mixed irradiation of white and supplemental light provided by light-emitting diode. *Scientia Hortic.* 200, 111–118. doi: 10.1016/j.scienta.2016.01.007

Chory, J. (2010). Light signal transduction: an infinite spectrum of possibilities. *Plant J.* 61, 982–991. doi: 10.1111/j.1365-313X.2009.04105.x

Chun, C., Park, S. W., Jeong, Y. W., and Ko, K. D. (2012). *Strawberry Propagation Method Using Closed Transplant Production Systems*. Korean Patent NO 10-1210680. Daejeon: Korean Intellectual Property Office.

Dou, H. J., Niu, G. H., and Gu, M. M. (2019). Photosynthesis, morphology, yield, and phytochemical accumulation in basil plants influenced by substituting green light for partial red and/or blue light. *HortScience* 54, 1769–1776. doi: 10.21273/HORTSCI14282-19

Fang, W. (2019). "Total Performance Evaluation in Plant Factory with Artificial Lighting," in *Plant Factory Using Artificial Light*, eds. M. Anpo, H. Fukuda and T. Wada (Boston, USA: Academic Press Elsevier), p155–165. doi: 10.1016/B978-0-12-813973-8.00014-2

Gao, S., Liu, X. N., Liu, Y., Chen, Z. J., and Xu, K. (2021). Comparison of the effects of LED light quality combination on growth and nutrient accumulation in green onion (*Allium fistulosum* L.). *Protoplasma* 258, 753–763. doi: 10.1007/s00709-020-01593-y

He, D. X., Yan, Z. N., Sun, X., and Yang, P. (2020). Leaf development and energy yield of hydroponic sweetpotato seedlings using single-node cutting as influenced by light intensity and LED spectrum. *J. Plant Physiol.* 254, 153274. doi: 10.1016/j.jplph.2020.153274

He, D. X., Zheng, J. F., and Du, W. F. (2018). *A New Method for Harvesting Unrooted Runner Plantlets in Strawberry Plug Plant Production*. China Patent NO 10474655.02018. Beijing: China National Intellectual Property Administration.

Heuvelink, E. (1997). Effect of fruit load on dry matter partitioning in tomato. *Scientia Hortic.* 69, 51–59. doi: 10.1016/S0304-4238(96)00993-4

Higashide, T. (2022). Review of dry matter production and growth modelling to improve the yield of greenhouse tomatoes. *Horticulture J.* 91, 247–266. doi: 10.2503/hortj.UTD-R019

Hytönen, T., Elomaa, P., Moritz, T., and Junttila, O. (2009). Gibberellin mediates daylength-controlled differentiation of vegetative meristems in strawberry (*Fragaria× ananassa* Duch). *BMC Plant Biol.* 9, 1–12. doi: 10.1186/1471-2229-9-18

Hytönen, T., and Kurokura, T. (2020). Control of flowering and runnering in Strawberry. *Horticulture J.* 89, 96–107. doi: 10.2503/hortj.UTD-R011

Jolliffe, P. A., and Courtney, W. H. (1984). Plant growth analysis: additive and multiplicative components of growth. *Ann. Bot.* 54, 243–254. doi: 10.1093/oxfordjournals.aob.a086788

Kim, H. H., Goins, G. D., Wheeler, R. M., and Sager, J. C. (2004). Green-light supplementation for enhanced lettuce growth under red-and blue-light-emitting diodes. *HortScience* 39, 1617–1622. doi: 10.21273/HORTSCI.39.7.1617

Kozai, T. (2019). Towards sustainable plant factories with artificial lighting (PFALs) for achieving SDGs. *Int. J. Agric. Biol. Eng.* 12, 28–37. doi: 10.25165/j.ijabe.20191205.5177

Kusuma, P., Pattison, P. M., and Bugbee, B. (2020). From physics to fixtures to food: Current and potential LED efficacy. *Horticulture Res.* 7, 56. doi: 10.1038/s41438-020-0283-7

Lauria, G., Lo Piccolo, E., Pellegrini, E., Bellini, E., Giordani, T., Guidi, L., et al. (2021). Photosynthetic traits and biochemical responses in strawberry (*Fragaria* × *ananassa* Duch.) leaves supplemented with LED lights. *Photosynthetica* 59, 557–569. doi: 10.32615/ps.2021.048

Lee, H., Park, S. W., Cui, M., Lee, B., Pham, D. M., Hwang, H., et al. (2023). Improvement of strawberry transplant production efficiency by supplementary blue light in a plant factory using white LEDs. *Horticulture Environment Biotechnol.* 64, 233–244. doi: 10.1007/s13580-022-00493-9

Li, J. Y., Guo, X. L., Zhang, S. Q., Zhang, Y. H., Chen, L. P., Zheng, W. G., et al. (2022). Effects of light quality on growth, nutritional characteristics, and antioxidant properties of winter wheat seedlings (*Triticum aestivum* L.). *Front. Plant Sci.* 13, 978468. doi: 10.3389/fpls.2022.978468

Li, Y. L., Hu, J. T., Wei, H., and Jeong, B. R. (2020). A long-day photoperiod and 6-benzyladenine promote runner formation through upregulation of soluble sugar content in strawberry. *Int. J. Mol. Sci.* 21, 4917. doi: 10.3390/ijms21144917

Liang, J. H., Wu, Z., Zheng, J., Koskela, E. A., Fan, L. J., Fan, G. X., et al. (2022). The GATA factor *HANABA TARANU* promotes runner formation by regulating axillary bud initiation and outgrowth in cultivated strawberry. *Plant J.* 110, 1237–1254. doi: 10.1111/tpj.15759

Lieten, F. (1998). "Recent advances in strawberry plug transplant technology," in *XXV International Horticultural Congress, Part 3: Culture Techniques with Special Emphasis on Environmental Implications, Acta Hortic.* 513, 383–388. doi: 10.17660/ActaHortic.1998.513.45

Lin, K. H., Huang, M. Y., Huang, W. D., Hsu, M. H., Yang, Z. W., and Yang, C. M. (2013). The effects of red, blue, and white light-emitting diodes on the growth, development, and edible quality of hydroponically grown lettuce (*Lactuca sativa* L. var. *capitata*). *Scientia Hortic.* 150, 86–91. doi: 10.1016/j.scienta.2012.10.002

Macías-Rodríguez, L., Quero, E., and López, M. G. (2002). Carbohydrate differences in strawberry crowns and fruit (*Fragaria* × *ananassa*) during plant development. *J. Agric. Food Chem.* 50, 3317–3321. doi: 10.1021/jf011491p

Marcelis, L. F. M. (1996). Sink strength as a determinant of dry matter partitioning in the whole plant. *J. Exp. Bot.* 47, 1281–1291. doi: 10.1093/jxb/47.Special_Issue.1281

Meng, Q. W., Kelly, N., and Runkle, E. S. (2019). Substituting green or far-red radiation for blue radiation induces shade avoidance and promotes growth in lettuce and kale. *Environ. Exp. Bot.* 162, 383–391. doi: 10.1016/j.envexpbot.2019.03.016

Nájera, C., Gallegos-Cedillo, V. M., Ros, M., and Pascual, J. A. (2023). Role of spectrum-light on productivity, and plant quality over vertical farming systems: bibliometric analysis. *Horticulturae* 9, 63. doi: 10.3390/horticulturae9010063

Nishio, J. N. (2000). Why are higher plants green? Evolution of the higher plant photosynthetic pigment complement. *Plant Cell Environ.* 23, 539–548. doi: 10.1046/j.1365-3040.2000.00563.x

Park, Y., and Runkle, E. S. (2018). Spectral effects of light-emitting diodes on plant growth, visual color quality, and photosynthetic photon efficacy: white versus blue plus red radiation. *PloS One* 13, e202386. doi: 10.1371/journal.pone.0202386

Ptushenko, V. V., Avercheva, O. V., Bassarskaya, E. M., Berkovich, Y. A., Erokhin, A. N., Smolyanina, S. O., et al. (2015). Possible reasons of a decline in growth of Chinese cabbage under a combined narrowband red and blue light in comparison with illumination by high-pressure sodium lamp. *Scientia Hortic.* 194, 267–277. doi: 10.1016/j.scienta.2015.08.021

Rivero, R., Sønsteby, A., Heide, O. M., Solhaug, K. A., and Remberg, S. F. (2022). Growth analysis of the everbearing strawberry 'Delizzimo'under controlled temperature and photoperiod conditions. *CABI Agric. Bioscience* 3, 43. doi: 10.1186/s43170-022-00110-w

Seo, M., Hanada, A., Kuwahara, A., Endo, A., Okamoto, M., Yamauchi, Y., et al. (2006). Regulation of hormone metabolism in Arabidopsis seeds: phytochrome regulation of abscisic acid metabolism and abscisic acid regulation of gibberellin metabolism. *Plant J.* 48, 354–366. doi: 10.1111/j.1365-313X.2006.02881.x

Smith, H. L., McAusland, L., and Murchie, E. H. (2017). Don't ignore the green light: exploring diverse roles in plant processes. *J. Exp. Bot.* 68, 2099–2110. doi: 10.1093/jxb/erx098

Terashima, I., Fujita, T., Inoue, T., Chow, W. S., and Oguchi, R. (2009). Green light drives leaf photosynthesis more efficiently than red light in strong white light: revisiting the enigmatic question of why leaves are green. *Plant Cell Physiol.* 50, 684–697. doi: 10.1093/pcp/pcp034

Wu, C. C., Hsu, S. T., Chang, M. Y., and Fang, W. (2011). Effect of light environment on runner plant propagation of strawberry. *Acta Hortic.* 907), 297–302. doi: 10.17660/actahortic.2011.907.48

Wu, C. C., Yen, Y. H., Chang, M. Y., and Fang, W. (2012). Effects of light quality and CO_2 concentration on diurnal photosynthetic characteristics of strawberry. *Acta Hortic.* 956), 247–253. doi: 10.17660/actahortic.2012.956.27

Yamaguchi, S., Smith, M. W., Brown, R. G., Kamiya, Y., and Sun, T. P. (1998). Phytochrome regulation and differential expression of gibberellin 3β-hydroxylase genes in germinating Arabidopsis seeds. *Plant Cell* 10, 2115–2126. doi: 10.1105/tpc.10.12.2115

Yan, Z. N., He, D. X., Niu, G. H., Zhou, Q., and Qu, Y. H. (2020). Growth, nutritional quality, and energy use efficiency in two lettuce cultivars as influenced by white plus red versus red plus blue LEDs. *Int. J. Agric. Biol. Eng.* 13, 33–40. doi: 10.25165/j.ijabe.20201302.5135

Zheng, J. F., He, D. X., and Ji, F. (2019). Effects of light intensity and photoperiod on runner plant propagation of hydroponic strawberry transplants under LED lighting. *Int. J. Agric. Biol. Eng.* 12, 26–31. doi: 10.25165/j.ijabe.20191206.5265

Zheng, J. F., He, D. X., and Ji, F. (2022). Process design and yield simulation for the industrial propagation of strawberry basic transplants. *Trans. Chin. Soc. Agric. Eng. (Transactions CSAE)* 38, 226–231. doi: 10.11975/j.issn.1002-6819.2022.z.026

frontiers | Frontiers in Plant Science

TYPE Original Research
PUBLISHED 10 December 2024
DOI 10.3389/fpls.2024.1467443

OPEN ACCESS

EDITED BY
Sina Fallah,
Shahrekord University, Iran

REVIEWED BY
Sofia D. Carvalho,
Independent researcher, Laramie, United States
Maxwell A. Ware,
Free University of Berlin, Germany

*CORRESPONDENCE
Rhuanito Soranz Ferrarezi
ferrarezi@uga.edu

†These authors have contributed equally to this work

RECEIVED 19 July 2024
ACCEPTED 06 November 2024
PUBLISHED 10 December 2024

CITATION
Mayorga-Gomez AM, van Iersel MW and Ferrarezi RS (2024) Lowering the target daily light integrals following days with excessive lighting can reduce lettuce production costs. *Front. Plant Sci.* 15:1467443. doi: 10.3389/fpls.2024.1467443

Lowering the target daily light integrals following days with excessive lighting can reduce lettuce production costs

Andres M. Mayorga-Gomez†, Marc W. van Iersel† and Rhuanito Soranz Ferrarezi*

Department of Horticulture, University of Georgia, 1111 Miller Plant Sciences, Athens, GA, United States

Given the fluctuating availability of natural lighting throughout the year, supplemental light is frequently employed to maintain the optimal daily light integral (DLI) levels necessary for adequate plant growth. However, the use of supplemental light translates into higher operational costs. Recent reports suggest that plants can tolerate a day with low DLI following exposure to a day with high DLI from natural light. This was referred to as the 'carryover' effect. In such cases, supplemental lighting may not be necessary, resulting in energy savings. In this study, we determined if plants can withstand such DLI fluctuations over multiple days without compromising plant growth. Additionally, we calculated the energy requirements for trese treatments to evaluate the potential energy savings of the carryover effect. To test this, we cultivated lettuce plants (*Lactuca sativa* cv. 'Waldmand's Dark Green' and 'Rouxai') in a walk-in grow chamber, subjecting them to six different lighting treatments. Each treatment consisted of a day with a high DLI of 22.5 mol·m^{-2}·d^{-1} followed by a varying number of consecutive days with low DLI, ranging from 1 to 5 days, with DLIs of 7.5, 11.25, 12.5, 13.13, and 13.5 mol·m^{-2}·d^{-1} respectively. The combined DLI for each treatment, calculated as the average DLI across high and low DLI days, was maintained at 15 mol·m^{-2}·d^{-1}. Additionally, we included a control treatment where plants were exposed to a constant DLI of 15 mol·m^{-2}·d^{-1}. We measured plant growth rate, final fresh and dry weights, leaf number, leaf area, specific leaf area, light use efficiency, and relative pigment content to assess differences in plant growth under the different lighting regimes. We observed a decrease in biomass accumulation, as indicated by a 13% reduction in final dry weight only for the treatment involving one day of high DLI followed by one day of low DLI, compared to our control. We discovered that plants can tolerate multiple days of low DLI following a day with high DLI, in contrast to the optimal values reported in the literature. This finding can lead to reduced energy consumption for supplemental lighting and consequent operational cost savings.

KEYWORDS

***Lactuca sativa*, light levels, energy, supplemental light, daily light integral**

1 Introduction

Daily light integral (DLI) refers to the amount of photosynthetically active radiation provided to plants in 24 hours (Faust et al., 2005). DLI has been used as a reference point for the required light for optimal plant growth. Runkle (2019) reported a guideline specifying the essential DLI for cultivating different crops in controlled environments. However, the availability of light varies based on geographical locations since light levels differ significantly in the northern parts of the U.S. compared to southern locations. Additionally, there is less sunlight available in winter compared to summer overall. Supplemental lighting becomes essential to ensure consistent production throughout the year (Korczynski et al., 2022). Not only supplemental light is implemented to achieve DLIs reported to be optimal. For instance, Albright et al. (2000) developed a lighting control that includes shadings and supplemental light to maintain optimal DLI for plant growth. However, the cost for supplemental lighting in a vegetable greenhouse may amount to USD $200,000 per hectare, constituting 30% of the annual farm gate value (van Iersel and Gianino., 2017). Studies have focused on reducing electricity consumption and energy pricing associated with supplemental light. In 2017, van Iersel and Gianino (2017) proposed an adaptive control system for light-emitting diode (LED) lights. This system adjusts photosynthetic photon flux density (PPFD) levels by considering the natural sunlight to achieve the target DLIs. They claim electricity consumption reductions of 20-92%. In 2021, Bhuiyan and van Iersel (2021) conducted a study testing lettuce growth under fluctuating PPFD levels every 15 minutes. They observed that when these PPFD fluctuations were not extreme, lettuce plants exhibited normal growth without significant adverse effects. This suggests that lettuce can tolerate fluctuations in PPFD levels, potentially leading to energy cost savings if paired with variable electricity prices.

Most recently, Jayalath et al. (2024). reported that plants can grow unaffectedly with extended lighting fluctuations. They conducted experiments growing lettuce in greenhouses and indoor conditions (growth chamber), varying the target DLI from one day to the next. The DLI fluctuation between two consecutive days ranged from 5 to 25 $mol{\cdot}m^{-2}{\cdot}d^{-1}$. Interestingly, plants exposed to DLI fluctuations with a difference of 10 $mol{\cdot}m^{-2}{\cdot}d^{-1}$ showed no negative effects on their growth. They propose the existence of a 'carryover' effect from days with high DLI (exceeding the target) to days with low DLI (falling below the target). This suggests that in agriculture setups utilizing supplemental light, it might not be always necessary to reach a specific DLI for lettuce if plants get exposed to a higher DLI than the target the day before, generating a reduction in electricity consumption.

The present study assessed whether plants can tolerate DLI fluctuations over consecutive days without compromising growth in an indoor growth chamber. Specifically, our goal was to investigate the viability of the 'carryover' effect for plants exposed to a high DLI for one day, followed by multiple days of a low DLI (falling below the target DLI). If plants can tolerate such lighting fluctuations, potential significant electricity savings exist. Additionally, we determined the energy requirements for trese treatments to evaluate the potential energy savings of the carryover effect.

2 Results

2.1 Plant growth rate

We determined the time needed to reach different coverage levels in a specific area to analyze plant growth rates by estimating the days based on the sigmoidal curves fitted to the projected canopy size (PCS) information. Plants growing under different lighting regimes needed different days to achieve specific sizes indicated by the coverage percentage of a reference area. For example, to cover 25% of the said area, plants growing with 0, 1, 2, 3, 4, and 5 days with low DLI following a day with high DLI needed an average of 11.46, 12.41, 11.81, 11.86, 11.6, and 11.54 days, respectively (Figure 1A). We did not find a significant interaction between the lettuce cultivars and lighting treatment ($F_{5,24}$ = 0.028, P=0.99). The time taken to achieve this level of coverage showed significant differences ($F_{5,29}$ = 3.91, P=0.007) between plants growing with one day of low DLI compared to the control treatment (P=0.007) (0 days with low DLI) and plants with 4 (P=0.029) and 5 (P=0.017) days with low DLI.

Likewise, to cover 50% of the reference area, plants subjected to 0, 1, 2, 3, 4 and 5 days with low DLI following a day with high DLI needed 14.25, 15.22, 14.58, 14.6, 14.26, and 14.24 days, respectively (Figure 1B). The interaction between cultivar and lighting treatment was not significant ($F_{5,24}$ = 0.26, P=0.92). Once again, the time needed to attain this coverage level exhibited significant differences ($F_{5,29}$ = 3.62, P=0.011) when comparing plants subjected to one day of low DLI when compared with the control (P=0.017) and plants with 4 (P=0.023) and 5 (P=0.018) days with low DLI.

To achieve 75% coverage, plants growing with 0, 1, 2, 3, 4 and 5 days with low DLI following a day with high DLI needed 16.75, 17.68, 17.1, 16.97, 16.76, and 16.96 days, respectively (Figure 1C). Here, significant differences were found ($F_{5,29}$ = 2.59, P=0.046) (Tukey's test did not show differences when comparing means) with no interaction between lighting treatments and cultivars ($F_{5,24}$ = 0.9, P=0.49). Since Tukey's test did not show differences when comparing means, we used Fisher's LSD test. Here, plants growing with one day of low DLI needed significantly more days to achieve 75% of coverage when compared to plants growing under 0 (P=0.005), 3 (P=0.0087), 4 (P=0.0064) and 5 (P=0.028) days with low DLI.

Finally, to cover 100% of the reference area, plants growing under 0, 1, 2, 3, 4 and 5 days with low DLI following a day with high DLI needed 19.3, 19.96, 19.5, 19.72, 19.14, and 19.27 days, respectively (Figure 1D). There were no significant differences among treatments regarding covering the equivalent of the entire reference area ($F_{5,29}$ = 0.76, P=0.26) ($F_{5,29}$ = 1.35, P=0.26). Interaction between cultivar and lighting treatments was not found ($F_{5,24}$ = 1.35, P=0.29). ($F_{5,24}$ = 1.304, P=0.29).

2.2 Leaf area and specific leaf area

We measured the final leaf area on three plants situated at the central transverse position of each tray, yielding a total count of six plants. The average leaf area for plants growing under the least amount of days with low DLI (T0) ascendingly to 5 days with DLI was as follows: 1436.09, 1276.86, 1342.12, 1388.37, 1409.01 and 1452.79 cm^2

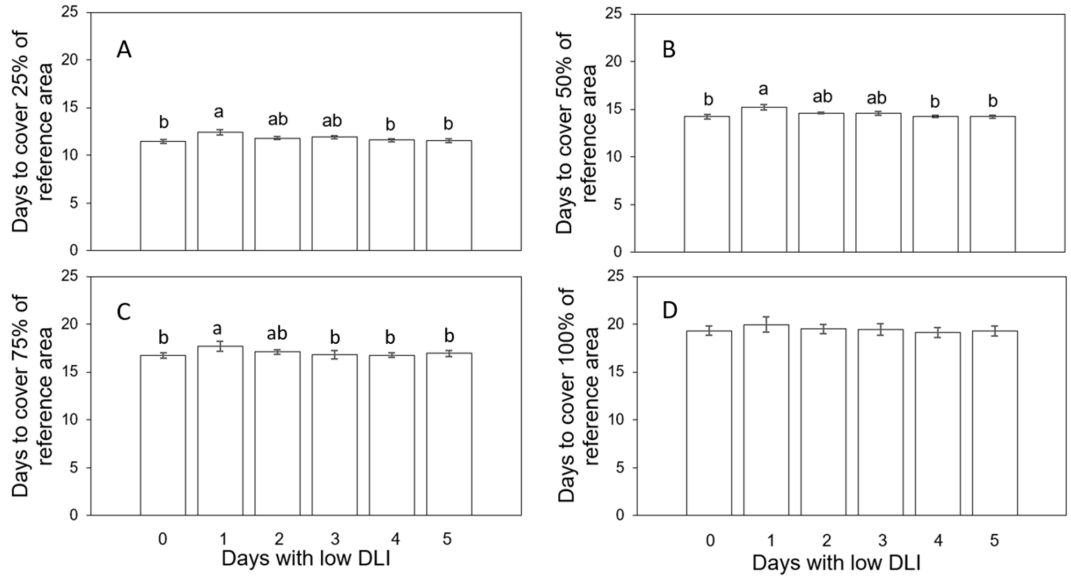

FIGURE 1
Number of days that plants growing under different daily light integral (DLI) treatments needed to achieve the coverage of a reference area of 25% **(A)**, 50% **(B)**, 75% **(C)**, and 100% **(D)**. Error bars denote standard error (n=6). Different letters on top of error bars show significant differences at α=0.05 from Tukey's test for **A, B**. Different letters on top of error bars show significant differences at α=0.05 from Fisher's LSD test for **(C)** Absence of letters on top of error bars show no significant differences.

respectively (Figure 2). However, we did not find significant differences in this parameter ($F_{5,29}$ = 1.65, P=0.17). Furthermore, there was no interaction between light treatment and cultivar ($F_{5,24}$ = 0.36, P=0.88).

We did not find significant differences ($F_{5,29}$ = 0.79, P=0.56) in specific leaf area (SLA) among plants growing under different lighting treatments, and there was no interaction between SLA and lettuce cultivar ($F_{5,24}$ = 0.74, P=0.59). The average SLA per plant from treatment 0 to 5 days were as follows: 407.86, 371.18, 386.29, 370.17, 355.63, and 370.17 $cm^2 \cdot g^{-1}$ (Figure 3).

2.3 Pigment content

We conducted pigment content measurements on both lettuce varieties. For 'Rouxai', the leaf anthocyanin content varied from 7.36 to 7.46 anthocyanin content index (ACI) across treatments with varying low DLI days (Figure 4), with no significant differences found ($F_{5,12}$ = 0.36, P=0.86). Additionally, the leaf chlorophyll content in sequence from treatment T0 to T5 were 8.36, 8.05, 8.06, 8.41, 8.11, and 7.98 chlorophyll content index (CCI) (Figure 5). However, no

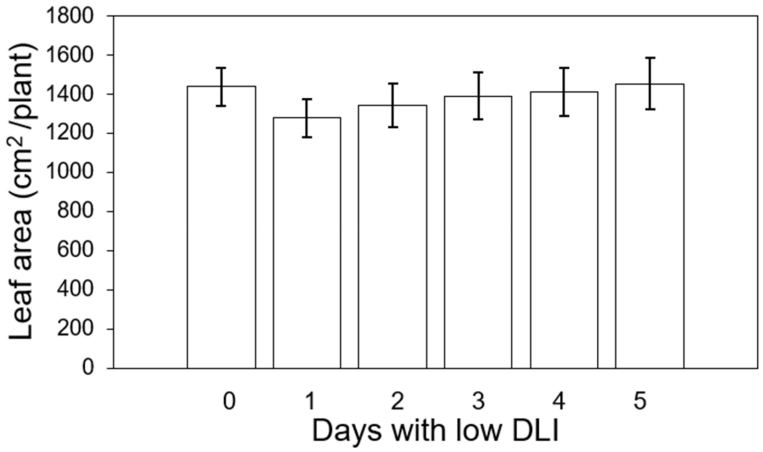

FIGURE 2
Final leaf area of 'Rouxai' and 'Walmand's dark green' lettuce plants growing under different lighting treatments. Lighting treatments are described by the number of days with low daily light integral (DLI) after a day with high DLI. Error bars denote standard error (n=6). Absence of letters on top of error bars show no significant differences at α=0.05 from Tukey's test.

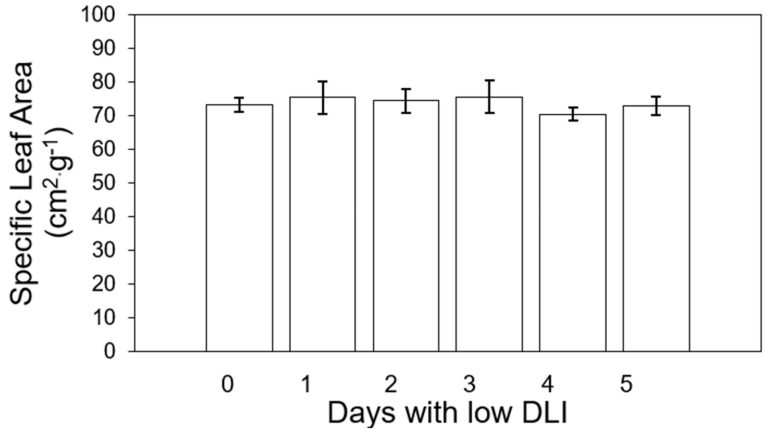

FIGURE 3
Specific leaf area of 'Rouxai' and 'Walmand's dark green' lettuce plants growing under different lighting treatments. Specific leaf area was calculated as the ratio of final leaf area and final fry weight. Lighting treatments are described by the number of days with low daily light integral (DLI) after a day with high DLI. Error bars denote standard error (n=6). Absence of letters on top of error bars show no significant differences at α=0.05 from Tukey's test.

significant differences were found ($F_{5,29}$ = 1.02, P=0.42) nor interaction between cultivar and treatment ($F_{5,29}$ = 0.74, P=0.59).

2.4 Shoot dry weight

We averaged the final shoot dry weight for the different lighting treatments for both cultivars. The values in sequence from treatment T0 to T5 were recorded as follows: 3.91, 3.4, 3.6, 3.75, 3.87, and 3.83 g per plant (Figure 6). The number of days of low DLI significantly affected the final shoot dry weight ($F_{5,29}$ = 3.29, P=0.017). Compared to the control treatment, plants growing with one day of low DLI showed a significant decrease in dry weight of 13% (P=0.022). The other significant differences were between plants growing under T1 and T4 (P=0.047). In addition, we did not find a significant interaction between light treatment and cultivar ($F_{5,24}$ = 0.33, P=0.88).

2.5 Shoot fresh weight

On the other hand, we also assessed the final fresh weight of shoots across both cultivars. The values were the following from the treatment with less amount of days with low DLI (T0 days) to the

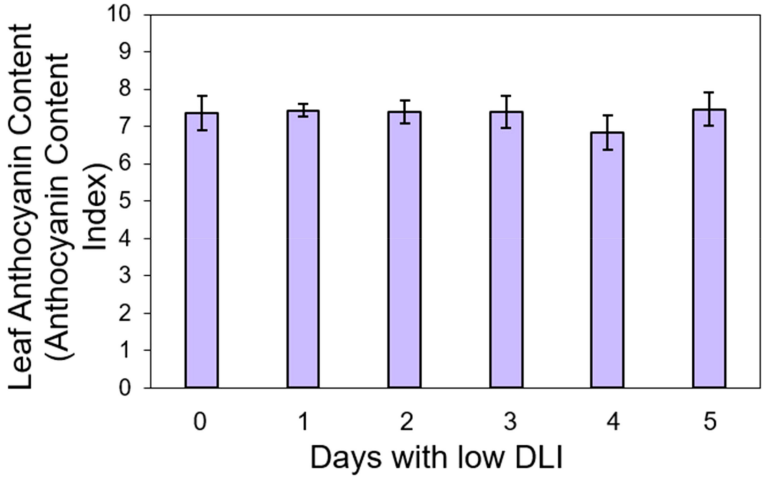

FIGURE 4
Leaf anthocyanin content of 'Rouxai' lettuce plants growing under different lighting treatments. Lighting treatments are described by the number of days with low daily light integral (DLI) after a day with high DLI. Error bars show standard error (n=3). Absence of letters on top of error bars show no significant differences at α=0.05 from Tukey's test.

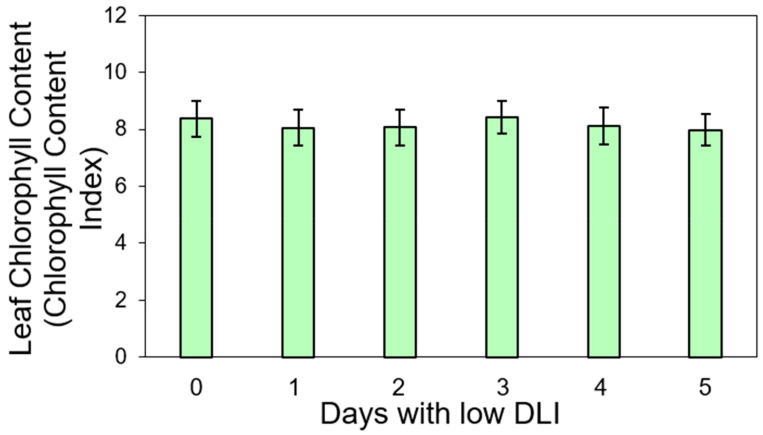

FIGURE 5
Leaf chlorophyll content in 'Walmand's dark green' and 'Rouxai' plants (both cultivars averaged) growing under different lighting treatments. Lighting treatments are described by the number of days with low daily light integral (DLI) after a day with high DLI. Error bars show standard error (n=6). Absence of letters on top of error bars show no significant differences at α=0.05 from Tukey's test.

one with more days with low DLI (T5): 80, 73, 76.07, 78.85, 80.42, and 77.95 g per plant respectively (Figure 7). Lighting treatments did not show significant differences ($F_{5,29}$ = 1.48, *P*=0.22), and there was no significant interaction between cultivar type and lighting treatment ($F_{5,24}$ = 0.49, *P*=0.77).

2.6 Light use efficiency

We calculated light use efficiency (LUE) for both cultivars for their whole growing cycle. The LUE for treatment from T0 to T5 were 0.56, 0.5, 0.51, 0.54, 0.55, and 0.54 g·mol^{-1}, respectively (Figure 8). We did not find significant differences among lighting treatments on LUE ($F_{5,29}$ = 1.92, *P*=0.121) or interaction between cultivar and treatment ($F_{5,24}$ = 0.63, *P*=0.147). ($F_{5,24}$ = 0.69, *P*=0.63).

2.7 Leaf number

We counted the leaf number of three plants in the middle transversely of each tray, resulting in six plants counted (three per cultivar per treatment). The average leaf count per treatment, ranging from the lowest to the highest number of days with low DLI, was as follows: 19, 18.5, 18.44, 18.77, 19.72, and 19.55 leaves (Figure 9). The analysis of variance (ANOVA) test showed a significant difference in leaf number ($F_{5,29}$ = 2.79, *P*=0.035). However, Tukey's test did not show significant differences among the treatments. Additionally, we did not find an interaction between treatment and cultivar ($F_{5,24}$ = 0.45, *P*=0.8). Then, we used the Fisher DLS test since Tukey's test did not show the significant differences announced by the ANOVA. Significant differences were found between plants growing under T1 in comparison to T4 and

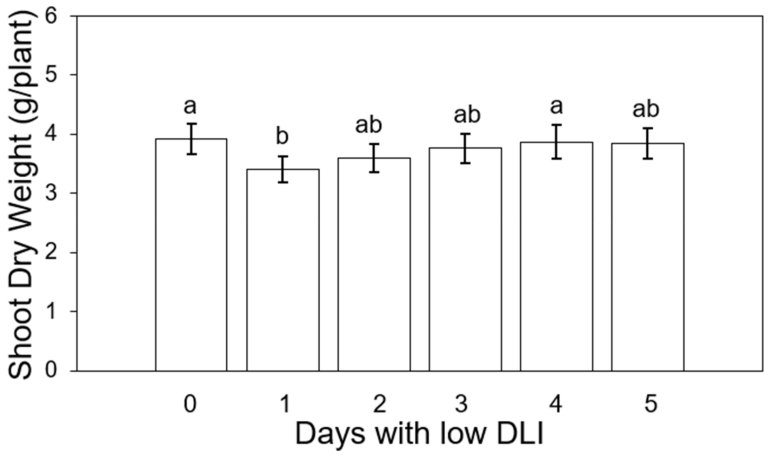

FIGURE 6
Final shoot dry weight of 'Rouxai' and 'Walmand's dark green' lettuce plants growing under different lighting treatments. Lighting treatments are described by the number of days with low daily light integral (DLI) after a day with high DLI. Error bars denote standard error (n=6). Different letters on top of error bars show significant differences at α=0.05.

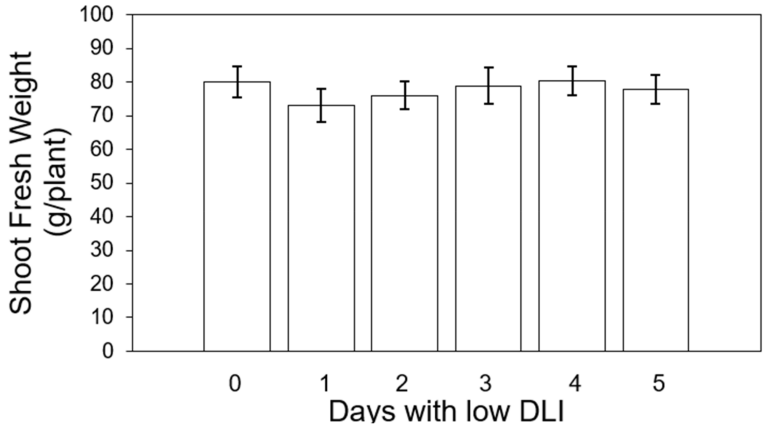

FIGURE 7
Final shoot fresh weight of 'Rouxai' and 'Walmand's dark green' lettuce plants growing under different lighting treatments. Lighting treatments are described by the number of days with low daily light integral (DLI) after a day with high DLI. Error bars denote standard error (n=6). Absence of letters on top of error bars show no significant differences at α=0.05 from Tukey's test.

T5, among plants growing under T2 in comparison to T4 and T5. Finally, there was a significant difference in leaf number between plants growing under T3 and T4. However, no significant differences existed between the treatment and the control treatment or plants growing with zero days with low DLI or no DLI fluctuations.

2.8 Energy requirement

In the first hypothetical scenario about energy needs, we assessed the energy required to generate the additional DLI needed to reach the target DLI of 15 mol·m^{-2}·d^{-1} on days with low DLI, considering the number of low DLI days in our treatments over a 30-day period. The energy requirements were as follows: 113.6 MWh/ha when the additional DLI was 3.75 (1 low DLI days), 86.1 MWh/ha for an extra DLI of 2.5 mol·m^{-2}·d^{-1} (2 low DLI days), 68 MWh/ha for 1.87 mol·m^{-2}·d^{-1} (3 low DLI days), and 56.9 MWh/ha for 1.5 mol·m^{-2}·d^{-1} (1 low DLI days) (Figure 10).

In the second hypothetical case of energy savings, we calculated the energy required to produce an additional DLI of 5 mol·m^{-2}·d^{-1} (to reach the optimal 15 mol·m^{-2}·d^{-1}) on days with low DLI, assuming that sunlight provided a DLI of 10 mol·m^{-2};·d^{-1} over 30 days. The energy requirements were as follows: 152.7 MWh/ha for 2 days with low DLI after each day with high DLI, 171.8 MWh/ha for 3 days, 183.3 MWh/ha for 4 days, and 190.9 MWh/ha for 5 days of low DLI following a day with high DLI. Additionally, we assessed the energy needed to produce extra DLIs of 1.25, 2.5, 3.13, and 3.5 mol·m^{-2};·d^{-1} for 2, 3, 4, and 5 days of low DLI, respectively, following a day with high DLI. The resulting energy values were 38, 81.6, 114, and 133.3 MWh/ha for the additional DLI levels during the 30-day period (Figure 11).

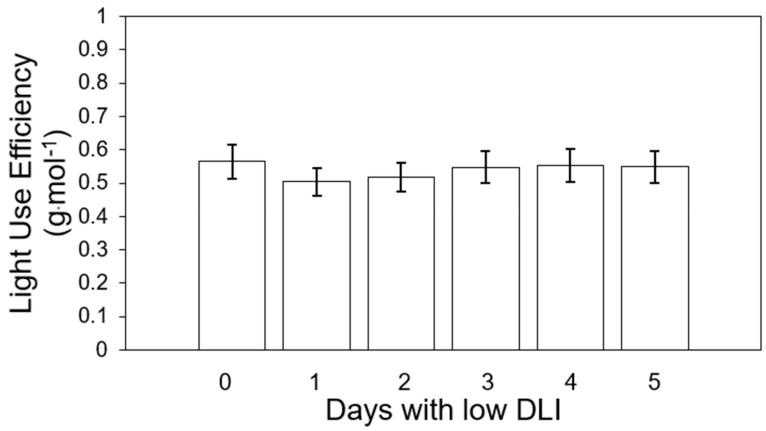

FIGURE 8
Light use efficiency of 'Rouxai' and 'Walmand's dark green' lettuce plants growing under different lighting treatments. Lighting treatments are described by the number of days with low daily light integral (DLI) after a day with high DLI. Error bars denote standard error (n=6). Absence of letters on top of error bars show no significant differences at α=0.05 from Tukey's test.

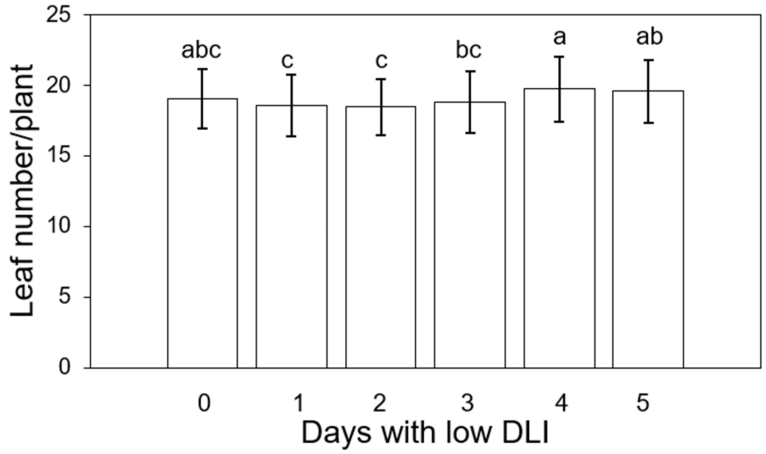

FIGURE 9
Final leaf number per plant of 'Rouxai' and 'Walmand's dark green' lettuce plants growing under different lighting treatments. Lighting treatments are described by the number of days with low daily light integral (DLI) after a day with high DLI. Error bars denote standard error (n=6). Different letters on top of error bars show significant differences at α=0.05.

3 Discussion

3.1 Plant growth rate

Plants growing under treatment1 day with high DLI followed only by 1 day with low DLI (T1) grew at a slower rate in comparison to plants growing with 4 (T4) and 5 days with low DLI (T5). We observed this while determining the time required for plants to reach 25%, 50%, and 75% coverage of a reference area. We assessed the plant growth rate using the PCS registered and calculated at various time points throughout the plant growth cycle. This means that when plants required more days to attain a specific coverage, they had a lower PCS, implying a slower growth rate. According to Klassen et al. (2003), plant growth is influenced by the quantity of light reaching the plant, which is directly tied to PCS and LUE (Legendre and van Iersel, 2021). Then, faster plant growth can be associated with a high PCS value. Plants with higher PCS intercept more light (Weaver and van Iersel, 2020), leading to more photosynthesis and biomass accumulation (Klassen et al., 2003). Said differences in biomass accumulation can be observed in Figure 6, what explains the differences in canopy sizes and plant growth rate in our study (Figures 1A–C).

As indicated by Jayalath and van Iersel (2021), LUE was one factor that plays a role in plant growth. LUE is a measure of the plant's efficiency in producing biomass with light reaching its canopy (Legendre and van Iersel, 2021). Then, differences in LUE between the plants growing under distinct light treatments are expected to contribute to differences in PCS or growing rates. However, those significant differences disappear when calculating the number of days needed to cover 100% (Figure 1D) of the reference area, a consequence of the overlapping canopies of the plants (Figure 12).

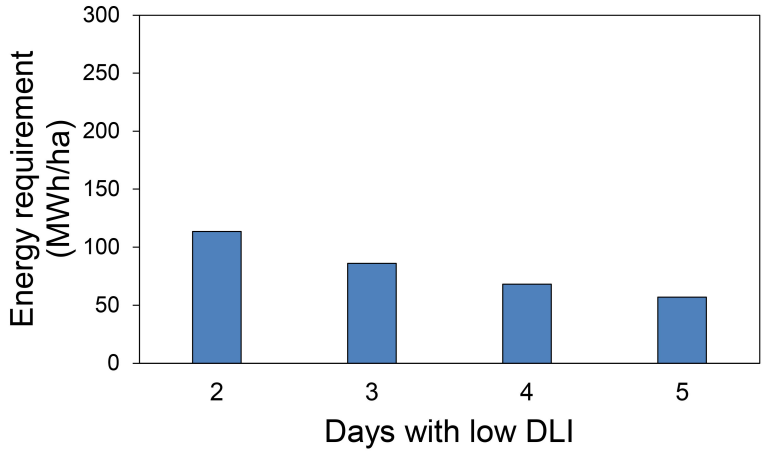

FIGURE 10
Energy requirement in 30 days used in supplemental lighting to provide extra daily light integral (DLI) to achieve a DLI of 15 mol·m^{-2}·d^{-1} for days with low DLI for the first hypothetical case presented.

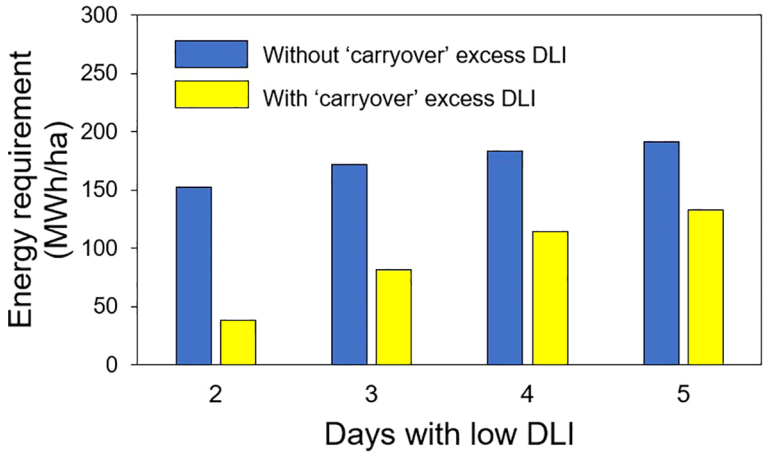

FIGURE 11
Energy requirement in 30 days used in supplemental lighting to provide extra daily light integral (DLI) to achieve a DLI of 15 mol·m^{-2}·d^{-1} (without carryover) to obtain a lower DLI (with carryover depending on the number of days with low DLI) for days with low DLI for the second hypothetical case presented.

3.2 Light use efficiency

LUE (Figure 8) followed a similar trend to fresh and dry weight despite the absence of significant differences. This means that plants, regardless of the treatment, had the same efficiency in producing biomass with the incident light provided (Jayalath and van Iersel, 2021). The intensity of light may influence variations in LUE. Elevated light levels lead to a greater closure of the reaction centers within the photosystem II (PSII). With an increased closure of these centers, a higher proportion of absorbed light by the PSII light-harvesting complex remains unused for electron transport in PSII (van Iersel, 2017). Excess of absorbed light might be dissipated in different ways (Bassi and Dall'Osto, 2021). Consequently, when the photosynthetic machinery does not utilize light, more photons are being redirected to other routes and not used by photosynthesis, resulting in lower LUE values. On the contrary, reduced light levels produced an inverse effect and a higher LUE. The treatments in our study were made up of a combination of days with low DLI or low light intensity and days with high DLI or high light intensity, which would mean different LUE depending on the day. However, said variations in light intensities across treatments did not significantly affect the final cumulative utilization of absorbed light for electron transport or dissipation, as evidenced by the absence of significant differences in LUE.

3.3 Shoot dry weight

Plants growing under 1 day with high DLI (22.53 mol·m^{-2}·d^{-1}) followed by 1 day with low DLI (7.53 mol·m^{-2}·d^{-1}) showed the lowest final dry shoot weight, meaning that the group of plants had a lower biomass accumulation (Figure 6). Dry weight increased when the number of days with low DLI increased, and at the same time, the DLI for those days increased (11.25, 12.5, 13.17, and 13.52 mol·m^{-2}·d^{-1}, respectively). As far as we know, most studies that look into DLI and biomass accumulation have grown plants under fixed DLI, even if that DLI is composed of a different combination of PPFD and photoperiod (Elkins and van Iersel, 2020). Jayalath et al.

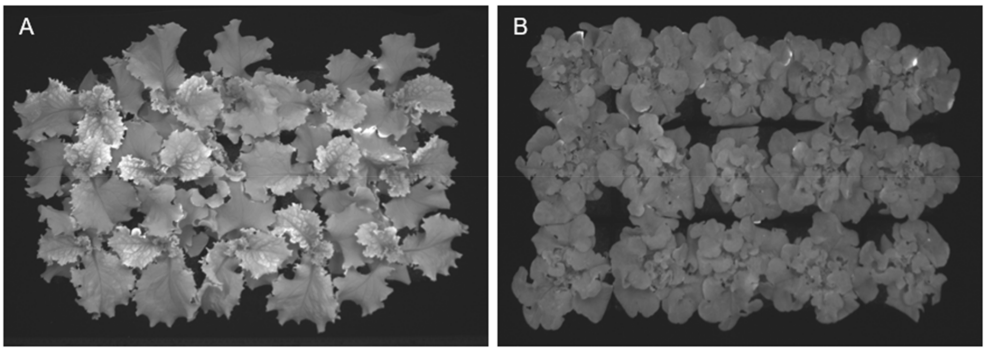

FIGURE 12
Picture of projected canopy size at 17 days after seeds were sowing shows how the canopy of individual plants overlaps with others. **(A)** 'Walmand's dark green' plants. **(B)** 'Rouxai' plants.

(2024) recently experimented with DLI changes only for two consecutive days. In our study, our treatments had variable DLIs for more than two following days, making it more challenging to compare results. Yan et al. (2019b) showed an increasing direct relationship between leaf dry weight and DLIs between 5.04 to 15.12 $mol{\cdot}m^{-2}{\cdot}d^{-1}$. Furthermore, Pennisi et al. (2020) reported the highest value in shoot dry weight for plants growing under a DLI of 14.4 $mol{\cdot}m^{-2}{\cdot}d^{-1}$ made of a photoperiod of 16 hours and a PPFD of 250 $\mu mol{\cdot}m^{-2}{\cdot}s^{-1}$. Plants growing under lower DLIs (5.8, 8.6, 11.5 $mol{\cdot}m^{-2}{\cdot}d^{-1}$) and a higher DLI (17.3 $mol{\cdot}m^{-2}{\cdot}d^{-1}$) showed significantly lower final biomass values for lettuce. This relationship of higher dry weight with high light levels has been also observed on dwarf tomato (*Lycopersicon esculentum*) 'Micro-Tom' (Ke et al., 2023), common purslane (*Portulaca oleracea*) (Kudirka et al., 2023), petunia (*Petunia* × *hybrida*) 'Wave Blue', geranium (*Pelargonium* × *hortorum*) 'Pinto Premium Orange Bicolor', and coleus (*Solenostemon scutellariodes*) 'Wizard Golden' (Park and Runkle, 2018).

In addition, differences in photosynthesis rates and canopy size may explain differences in final shoot dry weight in our study. Zhou et al. (2020) observed an increase in photosynthesis rates of lettuce plants with increasing PPFD levels, ranging from 0 to 350 $\mu mol{\cdot}m^{-2}{\cdot}s^{-1}$ (12-hour photoperiod of about DLI 15$mol{\cdot}m^{-2}{\cdot}d^{-1}$), reaching a plateau phase at approximately 500 $\mu mol{\cdot}m^{-2}{\cdot}s^{-1}$. In our study, plants exposed to 1 day of low DLI (T1) received around 104 $\mu mol\ m^{-2}{\cdot}s^{-1}$, while those subjected to 5 days of low DLI (T5) received approximately 187 $\mu mol{\cdot}m^{-2}{\cdot}s^{-1}$. This difference in incident light could signify variations in photosynthesis rates, and greater photosynthesis is associated with increased biomass accumulation (Klassen et al., 2003). However, all treatments were also exposed to a day with a high DLI of approximately 14.4 $mol{\cdot}m^{-2}{\cdot}d^{-1}$, achieved by subjecting plants to PPFD of around 312 $\mu mol{\cdot}m^{-2}{\cdot}s^{-1}$. Specifically, plants growing with just 1 day with low DLI (T1) had a DLI of 22 $mol{\cdot}m^{-2}{\cdot}d^{-1}$ during half of the growing cycle. This might suggest that these plants could have exhibited a higher photosynthetic rate during days with elevated PPFDs than other treatments (Zhou et al., 2020). However, it is crucial to note that, for the other half of the growing cycle, plants under T1 experienced lower DLI values (approximately 7.53 $mol{\cdot}m^{-2}{\cdot}d^{-1}$ and PPFD of 104 $\mu mol{\cdot}m^{-2}{\cdot}s^{-1}$). The potential reduction in the photosynthetic rate at these lower light levels could account for a decrease in the final biomass. Zhou et al. (2020) showed reduced photosynthetic values when light intensity was low. Additionally, Pennisi et al. (2020) showed lower values of biomass accumulation for plants growing under a DLI of 8.6 $mol{\cdot}m^{-2}{\cdot}d^{-1}$ and PPFD of 150 $\mu mol{\cdot}m^{-2}{\cdot}s^{-1}$.

When the number of days with low DLI increased, the minimum DLI also increased. Plants growing for 4 and 5 days with low DLI had an average DLI of 13.17 and 13.52 $mol{\cdot}m^{-2}{\cdot}d^{-1}$, respectively. Hence, those plants were growing most of the days under a DLI that was close to the control treatment (14.88 $mol{\cdot}m^{-2}{\cdot}d^{-1}$), which is close to the ideal DLI for lettuce between 12 and 16$mol{\cdot}m^{-2}{\cdot}d^{-1}$ depending on the cultivar (Zhang et al., 2018; Yan et al., 2019a; Kelly et al., 2020; Pennisi et al., 2020; Modarelli et al., 2022). Consequently, the photosynthetic rates, LUE, and biomass accumulation of plants growing under T4 and T5 are higher (in comparison to T1) and similar to the control treatment. Jayalath et al. (2024) reported a decrease in final dry weight when the DLI fluctuation from one day to the next is above 15 $mol{\cdot}m^{-2}{\cdot}d^{-1}$. They also explained this partly due to a lower canopy rate expansion that decreased the incident light available for photosynthesis. In our study, this lower expansion rate on the canopy can be seen in the number of days plants needed to reach different sizes (Figure 1).

These results corroborate the hypothesis the carryover effect exists, wherein higher photosynthesis rates during days with high DLI might compensate for the lower photosynthetic rates observed on days with lower DLI. They also indicate that plants experiencing more days with low DLI maintain similar photosynthetic rates because these lower DLI values are closely aligned with the optimal conditions required for lettuce growth.

3.4 Shoot fresh weight

Despite the significant differences observed in shoot dry weight results among the different lighting treatments, these differences were not found when measuring the final shoot fresh weight (Figure 7). However, the consistent trend of increasing dry weight when the number of days with low DLI increased was also observed in the fresh weight. Changes in significant differences between shoot dry and fresh weight have been reported before. Khwankaew et al. (2018) reported mismatched significant differences between shoot dry and fresh weight on *Ipomoea aquatica* plants growing under LED light with different spectrum combinations. Fresh weight should be assessed promptly after sampling, or plant material should be stored in hermetically sealed recipients, as fresh plant material tends to lose water rapidly (Turner, 1981). Then, if fresh weight is not taken consistently across all the samples, some variation might be induced. In our study, we measured this parameter right after cutting the shoot from the root system. Therefore, we did not expect any variability in fresh weight induced by the sampling process. A possible reason for the differences in dry weight not being reflected in the final fresh weight could be related to the water status of the plants and their water retention capacity. For instance, plants growing under our control conditions showed a fresh weight of around 80 g per plant and a dry weight of approximately 4 g per plant. We can see that the final dry weight represented only 5% of the total fresh weight of the plants. This means that the significant differences observed in dry weight are lost due to the amount of water inside the leaf. Fresh weights have been reported in other studies to be more variable for showing differences among treatments compared to dry weights (Bashan and De-bashan, 2005; Huang et al., 2017).

3.5 Leaf area and specific leaf area

No significant differences were found in final leaf area or SLA in our study (Figures 2, 3). Pennisi et al. (2020) observed an increase in leaf area for lettuce and basil with higher DLI. In contrast, the SLA for

both species decreased as DLI increased. This reduction in SLA was attributed to the denser arrangement of mesophyll cells and the development of thicker and larger leaves. Similarly, Carotti et al. (2021) found that SLA decreased when lettuce plants grew under higher light intensities. However, these results were obtained for plants growing under constant DLI or light intensities. Bhuiyan and van Iersel (2021) grew lettuce plants under variable PPFD levels every 15 minutes (400/0, 360/40, 320/80, 280/120, 240/160, and 200/200 $\mu mol \cdot m^{-2} \cdot s^{-1}$), and observed that leaf area decreased when plants were subjected to high PPFD fluctuations but increased when the PPFD fluctuations were minimized between light levels. In contrast, SLA was higher under high PPFD fluctuations, whereas it was lower when the fluctuations were smaller at their respective light levels. They argue that extreme fluctuations in light prevent plants from reaching a steady state of photosynthesis. Consequently, this leads to reduced carbon gain by leaves, resulting in decreased dry weight and increased SLA. In our study, the DLI and PPFD fluctuations occurred over an extended period, suggesting that plants could reach a steady state of photosynthesis. This likely contributed to the production of similar biomass across treatments, resulting in comparable SLA values. Given the similar biomass production, we expected similar leaf area values regardless of our lighting treatments.

For plants growing under DLI fluctuations that happened during extended periods, specifically focusing on day-to-day variations, Jayalath et al. (2024) found that DLI fluctuations above 15 $mol \cdot m^{-2} \cdot d^{-1}$ significantly reduced leaf area. Lower PCS and LUE may explain these differences. A larger PCS captures more light, and higher LUE transforms that light more efficiently into biomass. While our study also observed differences in PCS initially, we found that PCSs became similar across all treatments once canopies started to overlap. This suggests that plants reached similar leaf area values with similar PCS and LUE. Nonetheless, our treatment involving a single day with low DLI exhibited a DLI fluctuation from one day to the next of approximately 15 $mol \cdot m^{-2} \cdot d^{-1}$, consistent with findings reported for lettuce (Jayalath et al., 2024). Despite this fluctuation, we did not observe significant differences in leaf area under the same lighting treatment.

3.6 Leaf number

Even when we found significant differences in leaf number among the treatments involving a DLI fluctuation, none showed a significant difference compared to the control treatment (Figure 9). Changes in leaf number depending on different light levels have been reported before. Kang et al. (2013) found a higher leaf number for lettuce plants growing under high PPFD (290 $\mu mol \cdot m^{-2} \cdot s^{-1}$) levels when their photoperiod was 6/2 (light/dark) in 3 cycles per day. On the other hand, the least number of leaves was found when the plant grew at a low PPFD (200 $\mu mol \cdot m^{-2} \cdot s^{-1}$) with a photoperiod of 18/6 (light/dark). Also, Zervoudakis et al. (2012) found a significant reduction of leaf number in common sage (*Salvia officinalis* L.) when they grew under 25% ambient light compared to plants growing under full ambient light. These results suggest that plants growing under lower light levels generally produce fewer leaves. In our study, even plants that grew under different PPFD levels depending on the number of days with low DLI; they had, on average, the same light levels when taking into account the days with DLI and the days with low DLI. This might explain the lack of differences in leaf number compared to the control treatment (T0).

3.7 Relative pigment content

3.7.1 Anthocyanins

We did not see any differences in leaf anthocyanin content on 'Rouxai' plants regardless of the lighting treatment those plants were growing under (Figure 4). Hwang et al. (2023) demonstrated that elevating light intensity and extending the photoperiod increased anthocyanin content in *Brassica juncea* cultivated in a plant factory. The highest concentrations of anthocyanins were observed in plants exposed to 300 $\mu mol \cdot m^{-2} \cdot s^{-1}$ for 18 hours daily. Likewise, Jones-Baumgardt et al. (2020) reported a higher concentration of anthocyanins in arugula (*Eruca vesicaria* subsp. *sativa* (Mill.) Thell.), cabbage (*Brassica oleracea* L.), kale (*Brassica napus* L. subsp. *napus* var. *pabularia* (DC.) Alef.), and mustard (*Brassica juncea* (L.) Czern) plants when cultivated under 600 $\mu mol \cdot m^{-2} \cdot s^{-1}$, as opposed to those grown under 100 $\mu mol\ m^{-2} \cdot s^{-1}$. Similar results were found on arugula (Veremeichik et al., 2023), pak-choi (*Brassica campestris* ssp. Chinensis Makino) (Zhu et al., 2017), sweet basil (*Ocimum basilicum*) 'Opal' and lettuce (*Lactuca sativa*) 'Nikolaj' (Sutulienė et al., 2022), lettuce 'Outredgeous' (Massa et al., 2015) and red mustard (Hwang et al., 2023). One potential role of anthocyanins in plants is safeguarding the photosynthetic machinery against high light intensities (Landi et al., 2015). Anthocyanins are believed to play a role in partially mitigating the impacts of de-epoxidation of violaxanthin within the photo-protective xanthophyll cycle (Cavender-Bares et al., 1999; Landi et al., 2015; Logan et al., 2015).

The plants in our study experienced comparable high PPFD levels during the high DLI day. Those subjected to 1 to 5 days with low DLI received approximately 312 $\mu mol \cdot m^{-2} \cdot s^{-1}$ intermittently throughout their growth cycle, potentially leading to a similar production of anthocyanins. However, under the control treatments, plants did not have days with low DLI or PPFD levels. Then, plants probably still needed protection for their photosynthetic machinery.

Temperature changes have been linked to variations in anthocyanin levels. According to Gazula et al. (2005) 'Lollo Rosso' lettuce exhibited a notable increase in anthocyanin content when grown at lower temperatures than plants cultivated under higher temperatures. Similar response was observed on Chinese cabbage (*Brassica rapa* L.) (He et al., 2020), strawberry (*Fragaria* × *ananassa* Duch. cv. Toyonoka) (Zhang et al., 2018), Japanese parsley (*Oenanthe stolonifera*, DC.) (Hasegawa et al., 2001), and grape (*Vitis labrusca* L. × *Vitis vinifera* L.) (Gao-Takai et al., 2019). Lower temperatures are believed to lead to elevated transcript levels for enzymes like phenylalanine ammonia-lyase and chalcone isomerase, which play a role in anthocyanin biosynthesis (Dela et al., 2003). Plants in our investigation experienced uniform temperature conditions, which

could partly account for the absence of significant differences in anthocyanin content.

3.7.2 Chlorophyll

Similar to anthocyanins in 'Rouxai' plants, we did not find significant differences in chlorophyll content for either 'Rouxai' or 'Walmand's dark green' plants, regardless of the lighting treatment (Figure 5). Chlorophyll content per unit area indicates the plant's photosynthetic capacity could have been influenced by environmental factors (Palta, 1990). For instance, chlorophyll may degrade in excess light (De Carvalho Gonçalves et al., 2005) due to photo-oxidation (Kramer and Kozlowski, 1979), while under low light conditions, the content of this pigment might increase (Czeczuga, 1987). Zervoudakis et al. (2012) reported an increase of chlorophyll content on *Salvia officinalis* when growing under low light conditions. Similarly happened to sweet pepper (*Capsicum annuum* L.) (Sui et al., 2012). In our study, plants were subjected to varying light levels (high and low) across different days without any differences in chlorophyll content. This could indicate that the plants might have reached a balance in their suitable chlorophyll content for both conditions. Conversely, two rice (*Oryza sativa*) phenotypes growing under different lighting conditions, 600 and 1200 $\mu mol \cdot m^{-2} \cdot s^{-1}$, did not show significant differences in chlorophyll content despite the light intensity (Zhao et al., 2017). This suggests that variations in chlorophyll content in response to light conditions might vary among different species.

3.8 Energy requirement

DLI fluctuations only from one day to another or "carryover" effect has been reported to potentially reduce energy cost related to supplemental lighting in green gouses set up (Jayalath et al., 2024). In this study, we tested how plants behave when said DLI fluctuations happen during multiple days. We proposed two hypothetical cases to assess the energy requirements for supplemental light when fluctuating DLI levels during various days. For the first case, we assumed that plants would be subjected to DLI of 11.25, 12.5, 13.13, and 13.5 $mol \cdot m^{-2} \cdot d^{-1}$ (provided by sunlight) during 2, 3, 4, and 5 days after a day with high DLI (22.5 $mol \cdot m^{-2} \cdot d^{-1}$) respectively. Under the conditions of our study, said plants did not require a DLI of 15 $mol \cdot m^{-2} \cdot d^{-1}$ after a day with high DLI to not show significant differences in plant growth compared to plants growing consistently under the optimal DLI of 15 $mol \cdot m^{-2} \cdot d^{-1}$. It has been showed that plants could be allowed to get a high DLI on sunny days, and this could compensate for a day with a low DLI immediately after, and this concept was called the carryover effect (Jayalath et al., 2024). Then, if we experience one day with a high daily light integral (DLI) of 22.5 $mol \cdot m^{-2} \cdot d^{-1}$, followed by subsequent days with lower DLIs of 11.25, 12.5, 13.13, or 13.5 $mol \cdot m^{-2} \cdot d^{-1}$ over the next 2, 3, 4, or 5 days respectively, all under natural light conditions (as described in our first hypothetical case), the use of energy for supplemental lighting (Figure 10) to achieve an optimal DLI of 15 $mol \cdot m^{-2} \cdot d^{-1}$ may not be necessary. This is due to the carryover effect from the initial high DLI day.

In our second hypothetical case, we calculated the energy requirements assuming that days with a high DLI of 22.5 $mol \cdot m^{-2} \cdot d^{-1}$ (from sunlight) would be followed by periods of 2, 3, 4, and 5 days with low DLI. Additionally, we assumed that these low DLI days would receive only 10 $mol \cdot m^{-2} \cdot d^{-1}$ (also from sunlight). We estimated the energy needed to supplement an extra 5 $mol \cdot m^{-2} \cdot d^{-1}$ to achieve the optimal 15 $mol \cdot m^{-2} \cdot d^{-1}$, as well as the energy required to generate additional DLI to reach 11.25, 12.5, 13.13, and 13.5 $mol \cdot m^{-2} \cdot d^{-1}$ (depending on the number of consecutive days with low DLI) to take advantage of the 'carryover' effect. In our study, the contrast in energy requirements between achieving the optimal DLI and the energy to use the 'carryover' effect could indicate potential energy savings.

4 Materials and methods

4.1 Experimental set up and treatments

This research was conducted in a walk-in growth chamber (vertical farm) at the University of Georgia (College of Agriculture and Environmental Sciences, Department of Horticulture, Horticultural Physiology Laboratory), in Athens, GA, USA. The environmental conditions during the experiment, without distinguishing between light and dark periods, were: (mean ± standard deviation): temperature 24.35 ± 0.673°C, relative humidity 65.22% ± 7.56%, CO_2 concentration 847.64 ± 43.52 mg/L, and vapor pressure deficit 1.0201 ± 0.235 kPa.

Inside the growth chamber, there were three metal racks (2.4 m long × 0.6 m wide × 2.2 m high), each serving as a separate replication. Each rack had three horizontal shelves, and each shelf was divided into two equal parts vertically, resulting in six growing spaces per rack and 18 growing spaces in total, each with dimensions of 1.2 m long × 0.6 m wide × 0.6 m high. Each growing space was equipped with two LED fixtures (SPYDRx Plus with PhysioSpec indoor spectrum; Fluence Bioengineering, Austin, TX, USA) (Supplementary Figure 1). Furthermore, four small fans (AD0412HB-C50; ADDA, Orange, CA, USA), evenly distributed, were positioned on the sides of each growing space to ensure proper lateral airflow.

We tested six lighting treatments randomly assigned to the growing spaces. These lighting treatments were controlled by a datalogger (CR6; Campbell Scientific, Logan, UT, USA) and six dimmable drivers (4009715; Intertek/Fluence, Arlington, VA, USA), with each driver responsible for controlling three growing spaces that shared the same lighting treatment, one space per rack or replication.

PPFD levels were assessed in the middle of every cultivation area using a quantum sensor (MQ-500; Apogee Instruments, Logan, UT, USA). Each treatment consisted of two DLI levels, called high and low, with a photoperiod of 20 hours. Plants were exposed to one day under high DLI, followed by varying numbers of days under low DLI, denoted as T0 (Control), T1, T2, T3, T4, and

T5, indicating the respective number of days with low DLI in each treatment (Figure 13). DLI and PPFD for each treatment are shown in Table 1.

4.2 Plant material

Ten-cm square plastic pots were filled with soilless substrate (Metro-Mix® 830; SunGro Horticulture, Agawam, MA, USA) up to about 1 cm below the top rim. Three pelleted 'Waldmann's dark green' or 'Rouxai' (Johnny's Selected Seeds, Winslow, ME, USA) seeds were planted in each pot. The substrate was then covered with calcined clay or metakaolin (Turface MVP; Turface Athletics, Buffalo Grove, IL, USA) to avoid algae growth affecting PCS measurement. These pots were organized in trays, with fifteen pots arranged in a 5×3 configuration and placed in the designated growing spaces. Once the seeds germinated, a thinning process was carried out to keep only one seedling per pot. The plants received irrigation and nutrients through an ebb-and-flow subirrigation system, which delivered a 15N–2.2P–12.45K nutrient solution containing 100 mg·L^{-1} of nitrogen using a water-soluble fertilizer (15-5-15 Ca-Mg Professional LX; J.R. Peters, Allentown, PA, USA).

4.3 Data collection and calculations

4.3.1 Projected canopy size and plant growth rates

Canopy photos of 15 plants from each tray were captured initially 7 days following seed sowing and then twice a week, employing the setup detailed in Jayalath and van Iersel (2021). These images were analyzed using a custom Python script to calculate the PCS at the time said images were taken. The PCS data was then plotted against the number of days after sowing (DAS), and a sigmoidal curve of the form PCS = a/[1 + e$^{-(DAS-x0)/b}$] was applied to fit the data (SigmaPlot 11.0; Systat Software, San Jose, CA, USA). From the regression equations, we estimated the PCS for each day during the growth cycle, spanning from day 1 to day 30 for 'Wadmands' dark green' and to day 35 for 'Rouxai' (30 and 35 DAS were the harvest point respectively). Additionally, we calculated the number of days required for the crops to achieve specific sizes, such as 25%, 50%, 75%, and 100% coverage of the trays holding the plants (equivalent to 0.15 m^2), based on the estimated PCS for each day throughout the growth cycle.

4.3.2 Incident light and light use efficiency

To determine the daily incident light received by each group of plant' canopies on each day of the growth cycle, we multiplied the daily PCS by the DLI for each light treatment, as expressed by the formula: Incident Daily Light Integral (mol·d^{-1}) = PCS (mm^2) × DLI (mol·m^{-2}·d^{-1}). Using these values, we calculated the cumulative incident light on the canopy over the entire growth cycle. Subsequently, the cumulative incident light was divided by the final dry weight of the shoot to calculate LUE.

4.3.3 Leaf area and leaf specific area

We measured the leaf area of three plants per cultivar per growing space using a leaf area meter (LI-3100; LI-COR Biosciences, Lincoln, NE, USA) at harvesting day. The chosen plants were located transversally in the middle of each tray containing the pots. Then, we calculated SLA as the ratio between dry weight and leaf area.

4.3.4 Pigment content

At harvesting (30 DAS for 'Wadmands' dark green' and 35 DAS for 'Rouxai), we assessed the relative pigment content of chlorophyll and anthocyanins. The measurement involved randomly selecting 10 plants (sub-samples) per growing space per cultivar for pigment content evaluation. Meassurements were taken on uppermost fully

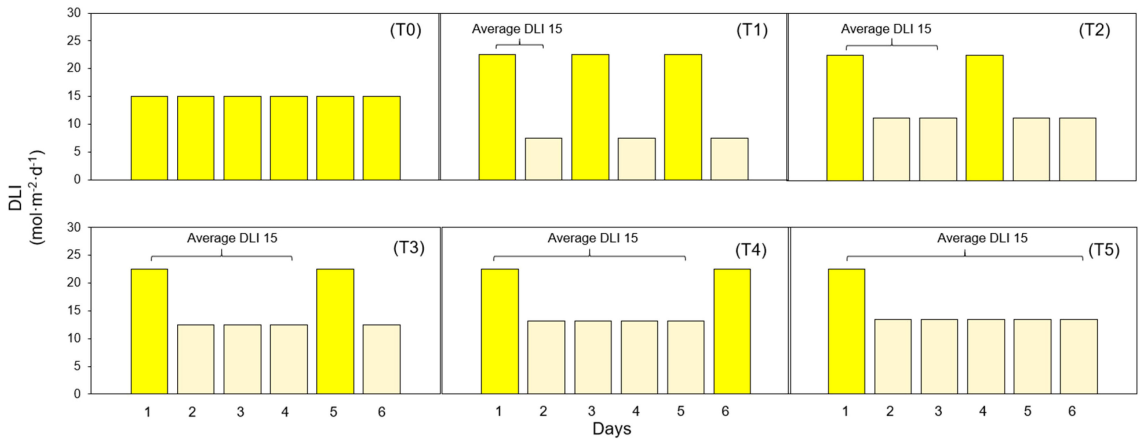

FIGURE 13
Diagram showing different lighting treatments. (T0) Treatment with zero days with low DLI. (T1) Treatment with one day with high DLI followed by one day with low DLI. (T2) Treatment with one day with high DLI followed by two days with low DLI. (T3) Treatment with one day with high DLI followed by three days with low DLI. (T4) Treatment with one day with high DLI followed by four days with low DLI. (T5) Treatment with one day with high DLI followed by five days with low DLI. The average DLI for each combination of days with high DLI and low DLI is 15 mol·m^{-2}·d^{-1}.

TABLE 1 Photosynthetic Photon Flux Density (PPFD) levels and corresponding daily light integral (DLI).

Treatment	High DLI	Low DLI	Average DLI	Days with low DLI	Photo-period	High PPFD	Low PPFD
	—— (mol·m^{-2}·d^{-1}) ——				(h)	— (µmol·m^{-2}·s^{-1}) —	
0 (Control)	14.88 ± 0.27	14.88 ± 0.27	14.88	–	20	206.66 ± 3.78	206.66 ± 3.78
1	22.53 ± 0.21	7.53 ± 0.18	15.03	1	20	313.00 ± 3	104.66 ± 2.51
2	22.48 ± 0.18	11.25 ± 0.18	15.00	2	20	312.20 ± 2.51	156.33 ± 2.51
3	22.44 ± 0.34	12.50 ± 0.2	14.98	3	20	311.66 ± 4.75	173.66 ± 3.78
4	22.51 ± 0.21	13.17 ± 0.19	15.04	4	20	312.66 ± 3.05	183.00 ± 2.64
5	22.48 ± 0.1	13.51 ± 0.14	15.01	5	20	312.33 ± 1.52	187.66 ± 2.08

High DLI, low DLI, high PPFD, and low PPFD are averages of three lighting fixtures with ± SD. Average DLI is the average of one day with high DLI and a different number of days with low DLI, depending on the treatment.

expanded leaves. The respective devices averaged the final value from each set of 10 measurements. Chlorophyll content for both cultivars was measured using a chlorophyll content meter (MC-100; Apogee Instruments, Logan, UT, USA) measuring the ratio of optical transmission at 931 to 653 nm. Anthocyanin measurement for 'Rouxai' was taken with an anthocyanin content meter (ACM 200 plus; Opti-sciences, Hudson, NH, USA) measuring the optical absorbancy at 530 and 931 nm.

4.3.5 Fresh and dry weight

Following the harvest of plant shoots in each cultivation area at 30 DAS for 'Wadmands' dark green' and 35 DAS for 'Rouxai', all of the plants (15 per cultivar per treatment) were weighed to obtaintheir fresh weight, and subsequently, dried in an oven at 80°C for 72 hours for final dry weight determination. We computed LUE as the ratio of shoot biomass to the total incident light.

4.3.6 Energy requirement assessment

Finally, using two hypothetical scenarios, we assessed the theoretical energy requirements of implementing the lighting strategy of reducing the target DLI for multiple days after a sunny day or day with high DLI. In the first one, we assumed that DLI was obtained only from natural light (sunlight). Here the DLI were the same as the ones provided in the treatments of this study. Days with high DLI had a DLI of 22.5 mol·m^{-2}·d^{-1}, and the days with low DLI had a DLI of 11.25, 12.5, 13.13, and 13.5 mol·m^{-2}·d^{-1} for treatments T2 to T5 respectively. Since 15 mol·m^{-2}·d^{-1} is the optimal DLI reported to grow lettuce, we calculated the DLI needed to provide during the days with low DLI to achieve said ideal number. In this case, for every day with low DLI, T2 would need an extra 3.75 mol·m^{-2}·d^{-1}, T3 would need an extra 2.5 mol·m^{-2}·d^{-1}, T4 would need an extra 1.87 mol·m^{-2}·d^{-1}, and T5 would need an extra 1.5 mol·m^{-2}·d^{-1} (Supplementary Table 1). To calculate the energy needed to produce the extra DLI, we followed the steps explained by Mattson (2017) and adopted the same assumptions. However, for this study, we used a light output of 1100 µmol·s^{-1}, and an energy requirement of 600 watts for this light source and area to cover one hectare during 30 days. The count of days with low DLI over 30 days, as per our lighting regimes, was as follows: 20 days of low DLI when having two days of low DLI after a day with high DLI, 22.5 days when having three days with low DLI after a day with high DLI, 24 days if there were four days with low DLI after a day with high DLI, and 25 days when having five days with low DLI after a day with high DLI.

In the second hypothetical case, days with high DLI also experienced a DLI of 22.5 mol·m^{-2}·d^{-1} naturally. However, the days with low DLI only received 10 mol·m^{-2}·d^{-1} from the sun. We chose a DLI of 10 mol·m²·d-¹ because this represents the average daily amount of light received in a northern U.S. state such as Washington, during December, January, and February when light availability is lower (Faust and Logan, 2018). The average DLI for these months in this region typically ranges between 5 and 15 mol·m^{-2}·d^{-1}. For simplicity, we used the midpoint value of 10 mol·m^{-2}·d^{-1} in our calculations. Then, the extra DLI would be provided with supplemental light either to obtain a DLI of 15 mol·m^{-2}·d^{-1} to achieve the optimal literature value, or to achieve DLI of 11.25, 12.5, 13.13, and 13.5 mol·m^{-2}·d^{-1} (depending on the number of days with low DLI) to use the 'carryover' effect (Supplementary Table 2). The energy required to produce the extra DLI to get the optimal value and to take advantage of the carryover was calculated as mentioned before.

All previous calculations were based on hypothetical DLI values provided by natural light (sunlight) and the hypothetical DLI values for each specific case using artificial lighting. The calculations considered only the DLI and did not account for the length of the day or night. It was assumed that the hypothetical DLIs from natural and supplemental light were provided over a period of 20 hours per day to provide a period of darkness even though lettuce does not respond to photoperiod.

4.4 Data analysis and experimental design

The experimental setup followed a randomized split-block design with three blocks and six lighting treatments. Each experimental unit consisted of 15 plants. We used ANOVA by using an statistical software (R version 4.1.2; R Project for Statistical Computing, Vienna, Austria) to compare differences in the number of days plants need to reach specific sizes, differences in shoot-dry weight, pigment content, leaf area, relative leaf area, dry and fresh weights, leaf number and light use efficiency.

5 Conclusions

After comparing plant responses under the lighting conditions tested in our study, we found that plants can tolerate multiple days with suboptimal DLI if they have been preceded by a day with higher-than-optimal DLI. This study suggests that plants can use the high DLI from one day to compensate for subsequent days with lower DLI. This finding implies that growers might not always need to achieve a specific DLI through supplemental lighting if similar lighting patterns are provided by sunlight. Consequently, this could reduce the need for supplemental lighting and result in economic benefits. However, the precise energy savings may vary depending on factors such as geographical location, weather conditions, and supplemental lighting systems. Additionally, determining the optimal DLI levels and acceptable DLI fluctuations for different crops is necessary if the findings of this study are to be applied more broadly.

Data availability statement

The raw data supporting the conclusions of this article will be made available by the authors, without undue reservation.

Author contributions

AMM-G: Conceptualization, Data curation, Formal analysis, Investigation, Methodology, Project administration, Supervision, Validation, Visualization, Writing – original draft, Writing – review & editing. MvI: Conceptualization, Data curation, Formal analysis, Funding acquisition, Investigation, Resources, Supervision, Validation, Writing – original draft, Writing – review & editing. RSF: Project administration, Resources, Supervision, Visualization, Writing – original draft, Writing – review & editing.

Funding

The author(s) declare financial support was received for the research, authorship, and/or publication of this article. This study was funded by the U.S. Department of Agriculture-National Institute of Food and Agriculture-Specialty Crop Research Initiative Award No. 2018-51181-28365 (Project LAMP "Lighting Approaches to Maximize Profits").

Acknowledgments

We thank Dr. Marc van Iersel for his important role in obtaining the funding and providing input in all the stages of the research. We also thank Dr. Lynne Seymour for support with the statistical analysis and all the members of the Horticultural Physiology and Controlled Environment Agriculture Crop Phisiology and Production Laboratories at the University of Georgia for their technical support.

Conflict of interest

The authors declare that the research was conducted in the absence of any commercial or financial relationships that could be construed as a potential conflict of interest.

Publisher's note

Supplementary material

The Supplementary Material for this article can be found online at: https://www.frontiersin.org/articles/10.3389/fpls.2024.1467443/full#supplementary-material

References

Albright, L. D., Both, A. J., and Chiu, A. J. (2000). Controlling greenhouse light to a consistent daily integral. *Trans. ASAE.* 43, 421–431. doi: 10.13031/2013.2721

Bashan, Y., and De-bashan, L. E. (2005). Fresh-weight measurements of roots provide inaccurate estimates of the effects of plant growth-promoting bacteria on root growth: a critical examination. *Soil Biol. Biochem.* 37, 1795–1804. doi: 10.1016/j.soilbio.2005.02.013

Bassi, R., and Dall'Osto, L. (2021). Dissipation of light energy absorbed in excess: the molecular mechanisms. *Annu. Rev. Plant Biol.* 72, 47–76. doi: 10.1146/annurev-arplant-071720-015522

Bhuiyan, R., and van Iersel, M. W. (2021). Only extreme fluctuations in light levels reduce lettuce growth under sole source lighting. *Front. Plant Sci.* 12. doi: 10.3389/fpls.2021.619973

Carotti, L., Graamans, L., Puksic, F., Butturini, M., Meinen, E., Heuvelink, E., et al. (2021).). Plant factories are heating up: hunting for the best combination of light intensity, air temperature and root-zone temperature in lettuce production. *Front. Plant Sci.* 11. doi: 10.3389/fpls.2020.592171

Cavender-Bares, J., Apostol, S., Moya, I., Briantais, J. M., and Bazzaz, F. A. (1999). Chilling-induced photoinhibition in two oak species: are evergreen leaves inherently better protected than deciduous leaves? *Photosynthetica.* 36, 587–596. doi: 10.1023/A:1007000406399

Czeczuga, B. (1987). Carotenoid contents in leaves grown under various light intensities. *Biochem. Sys. Ecol.* 15, 523–527. doi: 10.1016/0305-1978(87)90098-6

De Carvalho Gonçalves., J. F., De Sousa Barreto, D. C., Dos Santos, U. M., Fernandes, A. V., Barbosa Sampaio, P. D. T., and Buckeridge, M. S. (2005). Growth, photosynthesis and stress indicators in young rosewood plants (*Aniba rosaeodora* Ducke) under different light intensities. *Braz. J. Plant Physiol.* 17, 325–334. doi: 10.1590/S1677-04202005000300007

Dela, G., Or, E., Ovadia, R., Nissim-Levi, A., Weiss, D., and Oren-Shamir, M. (2003). Changes in anthocyanin concentration and composition in 'Jaguar'rose flowers due to transient high-temperature conditions. *Plant Sci.* 164, 333–340. doi: 10.1016/S0168-9452(02)00417-X

Elkins, C., and van Iersel, M. W. (2020). Longer photoperiods with the same daily light integral increase daily electron transport through photosystem II in lettuce. *Plants.* 9, 1172. doi: 10.3390/plants9091172

Faust, J. E., Holcombe, V., Rajapakse, N. C., and Layne, D. R. (2005). The effect of daily light integral on bedding plant growth and flowering. *HortScience.* 40, 645–649. doi: 10.21273/HORTSCI.40.3.64523

Faust, J. E., and Logan, J. (2018). Daily light integral: A research review and high-resolution maps of the United States. *HortScience.* 53, 1250–1257. doi: 10.21273/HORTSCI13144-18

Gao-Takai, M., Katayama-Ikegami, A., Matsuda, K., Shindo, H., Uemae, S., and Oyaizu, M. (2019). A low temperature promotes anthocyanin biosynthesis but does not accelerate endogenous abscisic acid accumulation in red-skinned grapes. *Plant Science.* 283, 165–176. doi: 10.1016/j.plantsci.2019.01.015

Gazula, A., Kleinhenz, M. D., Streeter, J. G., and Miller, A. R. (2005). Temperature and cultivar effects on anthocyanin and chlorophyll b concentrations in three related lollo rosso lettuce cultivars. *HortScience HortSci.* 40, 1731–1733. doi: 10.21273/HORTSCI.40.6.1731

Hasegawa, H., Fukasawa-Akada, T., Okuno, T., Niizeki, M., and Suzuki, M. (2001). Anthocyanin accumulation and related gene expression in Japanese parsley (*Oenanthe stolonifera*, DC.) induced by low temperature. *J. Plant Physiol.* 158, 71–78. doi: 10.1007/s11738-018-2767-8

He, Q., Ren, Y., Zhao, W., Li, R., and Zhang, L. (2020). Low Temperature promotes anthocyanin biosynthesis and related gene expression in the seedlings of purple head chinese cabbage (*Brassica rapa* L. *). Genes* 11, 81. doi: 10.3390/genes11010081

Huang, P., de-Bashan, L., Crocker, T., Kloepper, J. W., and Bashan, Y. (2017). Evidence that fresh weight measurement is imprecise for reporting the effect of plant growth-promoting (rhizo) bacteria on growth promotion of crop plants. *Biol. Fertility Soils.* 53, 199–208. doi: 10.1007/s00374-016-1160-2

Hwang, H. S., Jeong, H. W., Jeong, J. H., Jo, D. H., and Hwang, S. J. (2023). Changes in growth and anthocyanin content of Brassica juncea L. affected by light intensity and photoperiod in plant factory with artificial lighting. *Hortic. Sci. Technology.* 40, 586–594. doi: 10.7235/HORT.20220053

Jayalath, T. C., and van Iersel, M. W. (2021). Canopy size and light use efficiency. *explain Growth Dif. between lettuce mizuna vertical farms.* 10, 704. doi: 10.3390/plants10040704

Jayalath, T. C., van Iersel, M. W., and Ferrarezi, R. S. (2024). The energy requirement for supplemental greenhouse lighting can be reduced by considering 'excess' light from the previous day. *Plants.* 13, 652. doi: 10.3390/plants13050652

Jones-Baumgardt, C., Ying, Q., Zheng, Y., and Bozzo, G. G. (2020). The growth and morphology of microgreens is associated with modified ascorbate and anthocyanin profiles in response to the intensity of sole-source light-emitting diodes. *Can. J. Plant Science.* 101, 212–228. doi: 10.1139/cjps-2020-0060

Kang, J. H., KrishnaKumar, S., Atulba, S. L. S., Jeong, B. R., and Hwang, S. J. (2013). Light intensity and photoperiod influence the growth and development of hydroponically grown leaf lettuce in a closed-type plant factory system. *Horticulture Environment Biotechnol.* 54, 501–509. doi: 10.1007/s13580-013-0109-8

Ke, X., Yoshida, H., Hikosaka, S., and Goto, E. (2023). Photosynthetic photon flux density affects fruit biomass radiation-use efficiency of dwarf tomatoes under LED light at the reproductive growth stage. *Front. Plant Sci.* 14. doi: 10.3389/fpls.2023.1076423

Kelly, N., Choe, D., Meng, Q., and Runkle, E. S. (2020). Promotion of lettuce growth under an increasing daily light integral depends on the combination of the photosynthetic photon flux density and photoperiod. *Sci. Horticult.* 272, 109565. doi: 10.1016/j.scienta.2020.109565

Khwankaew, J., Nguyen, D. T., Kagawa, N., Takagaki, M., Maharjan, G., and Lu, N. (2018). Growth and nutrient level of water spinach (*Ipomoea aquatica* Forssk.) in response to LED light quality in a plant factory. *Acta Hortic.* 1227, 653–660. doi: 10.17660/ActaHortic.2018.1227.83

Klassen, S. P., Ritchie, G. L., Frantz, J. M., Pinnock, D. R., and Bugbee, B. (2003). Real-time imaging of ground cover: Relationships with Radiation capture, canopy photosynthesis, and daily growth rate. In: Digital imaging and spectral techniques: Applications to precision agriculture and crop physiology. *Am. Soc. Agronomy.* 66, 1–14. doi: 10.2134/asaspecpub66.c1

Korczynski, P. C., Logan, J., and Faust, J. E. (2022). Mapping monthly distribution of daily light integrals across the contiguous United States. *HortTechnology.* 12, 12–16. doi: 10.21273/HORTTECH.12.1.12

Kramer, P. I., and Kozlowski, T. T. (1979). *Physiology of woody plants* (New York: Academic Press), 67–71.

Kudirka, G., Viršilė, A., Laužikė, K., Sutulienė, R., and Samuolienė, G. (2023). Photosynthetic photon flux density effects on *Portulaca oleracea* in controlled-environment agriculture. *Plants* 12, 3622. doi: 10.3390/plants12203622

Landi, M., Tattini, M., and Gould, K. S. (2015). Multiple functional roles of anthocyanins in plant-environment interactions. *Environ. Exp. Botany.* 119, 4–17. doi: 10.1016/j.envexpbot.2015.05.012

Legendre, R., and van Iersel, M. W. (2021). Supplemental far-red light stimulates lettuce growth: disentangling morphological and physiological effects. *Plants.* 10, 166. doi: 10.3390/plants10010166

Logan, B. A., Stafstrom, W. C., Walsh, M. J. L., Reblin, J. S., and Gould., K. (2015). Examining the photoprotection hypothesis for adaxial foliar anthocyanin accumulation by revisiting comparisons of green- and red-leafed varieties of coleus (*Solenostemon scutellarioides*) Photosynth. *Res.* 124, 267–274. doi: 10.1007/s11120-015-0130-0

Massa, G., Graham, T., Haire, T., Flemming, C. II, Newsham, G., and Wheeler, R. (2015). Light-emitting diode light transmission through leaf tissue of seven different crops. *HortScience.* 50, 501–506. doi: 10.21273/HORTSCI.50.3.501

Mattson, N. (2017). How many light fixtures do I need? *e-Gro Edible Alert* 2, 5.

Modarelli, G. C., Paradiso, R., Arena, C., De Pascale, S., and Van labeke, M. C. (2022). High light intensity from blue-red LEDs enhance photosynthetic performance, plant growth, and optical properties of red lettuce in controlled environment. *Horticulturae.* 8, 114. doi: 10.3390/horticulturae8020114

Palta, J. P. (1990). Leaf chlorophyll content. *Remote Sens. Rev.* 5, 207–213. doi: 10.1080/02757259009532129

Park, Y., and Runkle, E. S. (2018). Far-red radiation and photosynthetic photon flux density independently regulate seedling growth but interactively regulate flowering. *Environ. Exp. Botany.* 155, 206–216. doi: 10.1016/j.envexpbot.2018.06.033

Pennisi, G., Pistillo, A., Orsini, F., Cellini, A., Spinelli, F., Nicola, S., et al. (2020). Optimal light intensity for sustainable water and energy use in indoor cultivation of lettuce and basil under red and blue LEDs. *Sci. Hortic.* 272, 109508. doi: 10.1016/j.scienta.2020.109508

Runkle, E. (2019). "DLI Requirements," in *Greenhouse product news*, vol. 29. (Sparta, MI), 50.

Sui, X. L., Mao, S. L., Wang, L. H., Zhang, B. X., and Zhang, Z. X. (2012). Effect of low light on the characteristics of photosynthesis and chlorophyll a fluorescence during leaf development of sweet pepper. *J. Integr. Agriculture.* 11, 1633–1643. doi: 10.1016/S2095-3119(12)60166-X

Sutulienė, R., Laužikė, K., Pukas, T., and Samuolienė, G. (2022). Effect of light intensity on the growth and antioxidant activity of sweet basil and lettuce. *Plants.* 11, 1709. doi: 10.3390/plants11131709

Turner, N. C. (1981). Techniques and experimental approaches for the measurement of plant water status. *Plant Soil.* 58, 339–366. doi: 10.1007/BF02180062

van Iersel, M. W. (2017). "Optimizing LED lighting in controlled environment agriculture," in *Light Emitting Diodes for Agriculture*, vol. 2017Ed. S. Dutta Gupta (Springer, Singapore: SpringerSingapore), 59–80. doi: 10.1007/978-981-10-5807-3_4

van Iersel, M. W., and Gianino., D. (2017). An adaptive control approach for light-emitting diode lights can reduce the energy costs of supplemental lighting in greenhouses. *Hortscience.* 52, 72–77. doi: 10.21273/HORTSCI11385-16

Veremeichik, G. N., Grigorchuk, V. P., Makhazen, D. S., Subbotin, E. P., Kholin, A. S., Subbotina, N. I., et al. (2023). High production of flavonols and anthocyanins in *Eruca sativa* (Mill) Thell plants at high artificial LED light intensities. *Food Chem.* 408, 135216. doi: 10.1016/j.foodchem.2022.135216

Weaver, G., and van Iersel, M. W. (2020). Longer photoperiods with adaptive lighting control can improve growth of greenhouse-grown 'Little Gem' lettuce (*Lactuca sativa*). *HortScience.* 55, 573–580. doi: 10.21273/HORTSCI14721-19

Yan, Z., He, D., Niu, G., and Zhai, H. (2019a). Evaluation of growth and quality of hydroponic lettuce at harvest as affected by the light intensity, photoperiod and light quality at seedling stage. *Sci. Hortic.* 248, 138–144. doi: 10.1016/j.scienta.2019.01.002

Yan, Z., He, D., Niu, G., Zhou, Q., and Qu, Y. (2019b). Growth, nutritional quality, and energy use efficiency of hydroponic lettuce as influenced by daily light integrals exposed to white versus white plus red light-emitting diodes. *HortScience.* 54, 1737–1744. doi: 10.21273/HORTSCI14236-19

Zervoudakis, G., Salahas, G., Kaspiris, G., and Konstantopoulou, E. (2012). Influence of light intensity on growth and physiological characteristics of common sage (*Salvia officinalis* L.). *Braz. Arch. Biol. technology.* 55, 89–95. doi: 10.1590/S1516-89132012000100011

Zhang, X., He, D., Niu, G., Yan, Z., and Song, J. (2018). Effects of environment lighting on the growth, photosynthesis, and quality of hydroponic lettuce in a plant factory. *Int. J. Agric. Biol. Eng.* 11, 33–40. doi: 10.25165/j.ijabe.20181102.3420

Zhang, Y., Liu, Y., Hu, W., Sun, B., Chen, Q., and Tang, H. (2018). Anthocyanin accumulation and related gene expression affected by low temperature during strawberry coloration. *Acta Physiologiae Plantarum* 40, 1–8. doi: 10.1007/s11738-018-2767-8

Zhao, X., Chen, T., Feng, B., Zhang, C., Peng, S., Zhang, X., et al. (2017). Non-photochemical quenching plays a key role in light acclimation of rice plants differing in leaf color. *Front. Plant Sci.* 7. doi: 10.3389/fpls.2016.01968

Zhou, J., Wang, J. Z., Hang, T., and Li, P. P. (2020). Photosynthetic characteristics and growth performance of lettuce (*Lactuca sativa* L.) under different light/dark cycles in mini plant factories. *Photosynthetica.* 58, 740–747. doi: 10.32615/ps.2020.013

Zhu, H., Li, X., Zhai, W., Liu, Y., Gao, Q., Liu, J., et al. (2017). Effects of low light on photosynthetic properties, antioxidant enzyme activity, and anthocyanin accumulation in purple pak-choi (*Brassica campestris* ssp. *Chinensis Makino). PloS One* 12, e0179305. doi: 10.1371/journal.pone.0179305

frontiers | Frontiers in Plant Science

TYPE Original Research
PUBLISHED 25 February 2025
DOI 10.3389/fpls.2025.1496790

OPEN ACCESS

EDITED BY
Meijian Yang,
Cornell University, United States

REVIEWED BY
Ferit Kocacinar,
Kahramanmaras Sütçü Imam University, Türkiye
Zhenqi Luo,
Cornell University, United States

*CORRESPONDENCE
Uma Maheswari Rajagopalan
uma@shibaura-it.ac.jp

RECEIVED 15 September 2024
ACCEPTED 13 January 2025
PUBLISHED 25 February 2025

CITATION
Igarashi H, Baba T, Takemura K, Kono T, Kadono H, Yamada J and Rajagopalan UM (2025) Laser biospeckle as a method to investigate the short-term effects of far-red light on an arugula (*Eruca sativa* Mill) plant. *Front. Plant Sci.* 16:1496790. doi: 10.3389/fpls.2025.1496790

Laser biospeckle as a method to investigate the short-term effects of far-red light on an arugula (*Eruca sativa* Mill) plant

Hibiki Igarashi[1], Takeshi Baba[1], Kairi Takemura[1], Takahiro Kono[2], Hirofumi Kadono[3,4], Jun Yamada[1] and Uma Maheswari Rajagopalan[1,5]*

[1]Department of Mechanical Engineering, Shibaura Institute of Technology, Tokyo, Japan, [2]Shibaura Institute of Technology, Tokyo, Japan, [3]Tokyo Metropolitan University, Hino, Japan, [4]Graduate School of Science and Engineering, Saitama University, Saitama, Japan, [5]Innovative Global Program, Shibaura Institute of Technology, Tokyo, Japan

With rapid climate change, it has been increasingly difficult to grow different crops, and as an alternative method, artificial cultivation in controlled environments has evolved into a new sustainable agriculture practice. However, the cost of having a controlled environment has become a major issue, and investigations have been conducted to develop cost-saving and efficient cultivation techniques. One research focus is on the utilization of stimulating appropriate photoreceptors for a certain time by far-red (FR) light to influence plant development. Here, we propose a novel laser biospeckle method, a non-destructive and real-time measurement method for the speedy evaluation of FR effects on arugula (*Eruca sativa* Mill) plants. Laser biospeckles are formed from the interference of scattered light from the organelles within the biological tissue, and the intensity of such speckles varies due to displacements within the tissue. In the experiment, while illuminating with FR and red (R) LED light of 735 nm and 630 nm, respectively, for a duration of 120 s to 300 s, the leaves of an arugula plant were irradiated simultaneously with laser light of 852 nm to obtain biospeckles. Video clips were recorded using a complementary metal-oxide-semiconductor (CMOS) camera at 15fps for 20 s. Correlations between the first and the subsequent frames were calculated to investigate the differences in the internal activity with exposure to FR and were characterized by a parameter named biospeckle activity (BA). Experiments were done with the healthiness and the age of the plant as parameters. It was found that depending on the healthiness of the plants, under short durations of 120s FR, BA and thus the internal activity within the leaves increased compared to the long duration of 300s FR. Further, a 1-month-old plant was found to have a faster decay of correlation and thus a steep increase in BA compared to that for a 3-month-old plant. Our results suggest that BA could be used as a measure to investigate the effects of FR or FR plus R in plant development within a timeframe of a few minutes, and thus can be employed as a complementary measurement technique for the speedier investigation of FR effects on plants.

KEYWORDS

laser, biospeckle, plant development, photoreceptor, short-term effects, far-red

1 Introduction

Global environmental changes, such as global warming, drought, and acid rain, are known to significantly impact plant growth and thus food yield (Prasad et al., 2002; Wong, 1990; Flannigan et al., 2000; Huang et al., 2022). With such climate change on the rise, sustainable agriculture is expected to become difficult in terms of plant resources and food security, which is a significant problem (Craufurd and Wheeler, 2009; Benke and Tomkins, 2017). In addition, the problem of the food supply is expected to accelerate further as the land available to grow plants is steadily decreasing due to reforestation, declining water supply, population growth, and climate change (Thomaier et al., 2015; Rajan et al., 2019; Hoenecke et al., 1992).

Vertical farms, where plants are grown in high-rise buildings with complete control of the surrounding environment, including light, temperature, and water, have attracted attention for their ability to significantly increase plant productivity. In such modern artificial agriculture, light is a key parameter, and control of parameters such as light intensity, duration, and wavelength composition is a challenge to increase the yield and value of products (Paradiso and Proietti, 2022 and references therein) (Demotes-Mainard et al., 2016; Tan et al., 2022). For instance, red light affects the photosynthetic apparatus development, and red and blue light are most efficiently utilized for photosynthesis (Hoenecke et al., 1992). Blue light influences stomatal opening, plant height, and chlorophyll biosynthesis, while far-red light (FR) stimulates flowering in long-day plants, and the red/far-red ratio regulates stem elongation and branching, leaf expansion, and reproduction (Jin et al., 2021). However, the cost of maintaining the environment is enormous, especially the cost related to lighting, which is a major obstacle to expanding the vertical farms (Jin et al., 2021; Zhen, 2020).

There existing research into improving the efficiency of plant growth through the use of fertilizers, improved lighting, and genetic improvement (Benke and Tomkins, 2017). Among these, irradiating plants with FR in the wavelength range of 700 to 800 nm has recently attracted increased attention to improve growth efficiency through the action of photoreceptors (Tan et al., 2022). However, it has been reported that the effect is higher when FR and red light are mixed than when FR alone is used due to the Emerson reaction (Emerson et al., 1957; Pettai et al., 2005).

Recently, it has been shown that in addition to the general photosynthetic wavelength range of 400~700 nm, irradiation with FR can increase growth efficiency. For example, Jin et al. reported that in lettuce cultivation, adding FR light to red and blue LEDs increased the dry leaf weight and leaf area of lettuce after 30 days of growth (Jin et al., 2021). Zhen (2020) also reported that adding FR to photosynthetic wavelengths (400~700 nm) during lettuce cultivation increased carbon gain and biomass by approximately 30% (Zhen, 2020). Kalaitzoglou et al. (2019) reported that adding FR treatments during tomato cultivation during the early growth stages increased productivity while mixing FR/R at a larger ratio than the natural light had a negative effect on growth.

The growth evaluation in the above cases is based on the measurement of plant growth in terms of physiological measures such as photosynthetic rate and physical measures, for example, plant height, leaf size, and weight of cut and dried leaves (Demotes-Mainard et al., 2016). However, it is a challenge to observe plants in a living state and also monitor short-time changes as the existing methods take considerable time with the need to wait for the plants to grow to a size that can be measured (Yadava, 2022; Lazzarin et al., 2024). In contrast, the laser biospeckle method is a technology that enables the non-destructive and non-contact evaluation of biological objects (Braga et al., 2009; Pandiselvam et al., 2020; Rajagopalan et al., 2021).

Minute irregularities comparable to the wavelength of the illuminating laser light in static objects cause light to scatter in different directions. When the scattered light reaches a screen or a camera, the scattered light then interferes, forming a random granular pattern of light-dark patches called speckles. When the laser light irradiates biological structures such as a leaf, light gets scattered from the surface, including internal structures. Here, the internal structures refer to cellular structures such as the nucleus and mitochondria that are involved in the functioning, and the sizes are in the order of wavelength of light or much smaller. Such organelles scatter light and the scattered light interferes with producing speckles on the observation plane, for example, on the camera plane. Because the structures within the tissue are changing, the speckle pattern also changes in relation to the movement within the leaf or seed itself. Such speckles obtained from a living organism are called biospeckles (Aizu and Asakura, 1996).

Here, biospeckles are considered to be related to cellular activities resulting in changes in the shape of the organelles themselves, for example, cell expansion or related to movement such as nutrient transport (Zdunek et al., 2014; Silva et al., 2018). The intensity of the biospeckle changes with the movement of organelles within the tissue. These changes are proportional to the movements with larger change in response to more significant movements. By analyzing the intensity changes of the speckles, it is possible to infer changes within the plant tissue. It should be pointed out that although the biospeckles change with the changes in biological activity due to environmental factors, the exact origin of biospeckles remains unknown.

Biospeckles have been used to evaluate the quality of fruits and vegetables with a few root-related studies in the agricultural field (Zdunek and Cybulska, 2011; Zdunek et al., 2014; Singh et al., 2020; Costa et al., 2017). Our group has recently demonstrated the application of laser speckles in the investigation of plants. Hirai et al. demonstrated that the response of plants to different sound frequencies could be rapidly evaluated by laser biospeckles (Hirai et al., 2020; Rajagopalan et al., 2021), indicating the potential of laser biospeckles in speedy monitoring in plant studies.

The objective of the current study is to investigate the applicability of the laser biospeckle method in the speedy evaluation of the short-term effects of far-red light on arugula plants [an extension of a report in a conference (Igarashi et al., 2023). To demonstrate the feasibility of the proposed method, we have used the healthiness and the age of the plants as parameters and conducted an investigation on short exposure of FR for 2 or 5 minutes. Compared with the existing techniques of measurement by CO_2 assimilation, the proposed method is non-invasive and could be complementary to the existing techniques.

2 Materials and methods

2.1 Plant sample

Arugula or rocket plant (*Eruca sativa* Mill), which grows quickly, is easy to cultivate, and can be grown in a variety of environments, was used as the plant sample in the experiments. A 3 cm square cube of hydroponic rockwool (0138-008, Grotop Grodan) was cut crosswise, and 3 to 4 seeds were sowed. The rockwool was placed in a 100 ml disposable cup with three holes in the bottom to absorb water, and approximately 10 plants were grouped in a tray and filled with enough water for the rockwool to absorb. The seeds were soaked in 3% oxindole for 10 minutes immediately before planting and then rinsed twice with water.

A custom-made cultivation chamber equipped with a temperature and humidity controller (APISTE, PAU-300S) a fluorescent lamp (SMILE, XFX2-20W), and a plant lamp [HUJIKURA plant light (HUJIKURA, KY-08W-SC) at a temperature of 23 ± 5°C and a humidity of 70 ± 5% was used for growing the plants. A day-night cycle of 12 h/12 h with photosynthetic photon flux density (PPFD) levels of 186 µmol/m^2s for the day period was used. The nutrient solution was given once a week, and it was made with 1.5 g of fertilizer (OAT House No. 1) and 1.0 g of manure (OAT House No. 2) dissolved in approximately 20 L of water to have a conductivity of 1.0 ds/m as measured by a water quality meter (FUSO Corporation, Model-7200).

We conducted two sets of experiments, one investigating healthiness with different health conditions and the other investigating the effects of age with two different age groups. Representative examples used in both the experiments are shown in Figures 1 and 2. We selected (a) healthy individuals with green leaves and (b) weak individuals with yellow leaves from arugula grown from seed in the laboratory for approximately 1 month as samples. Hereafter, (a) and (b) will be referred to as healthy and weak, respectively. Figure 2 shows the different-aged plants with a, b, and c representing, respectively, a 1-month-old, a 3-month-old, and a dying plant. Here, a leaf that had turned yellow and detached

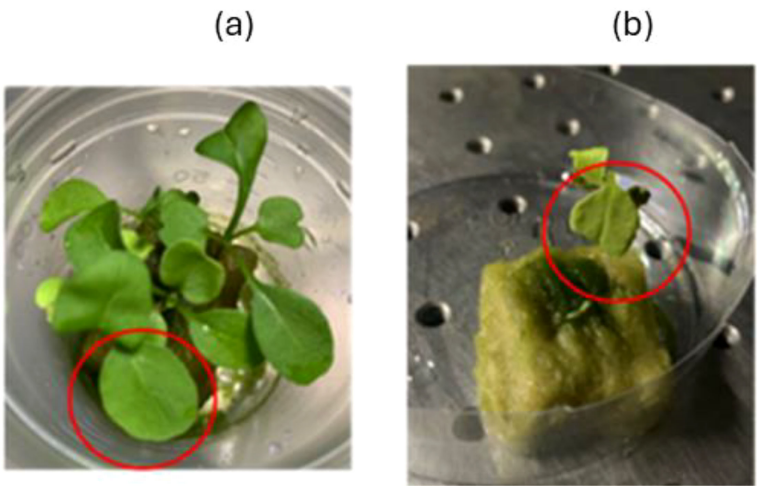

FIGURE 1
Argula samples of different health conditions with **(A)** healthy and **(B)** weak individuals. Red circles indicate the measured leaf region. Both were grown in the custom-made plant chamber in the laboratory under controlled conditions.

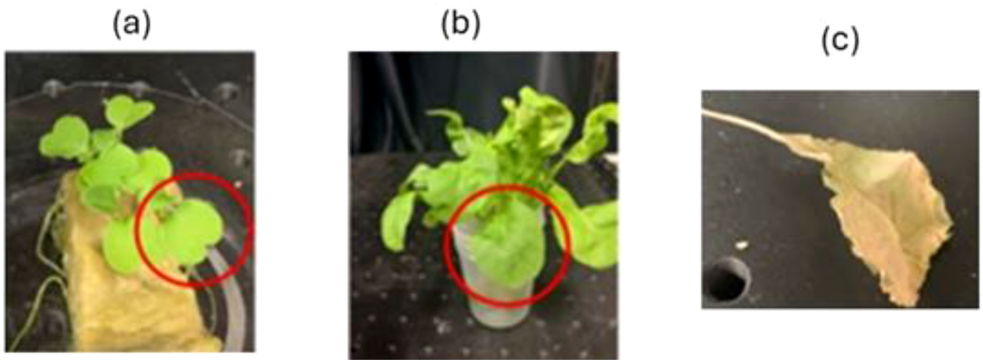

FIGURE 2
Argula samples used to study age effects with pictures of seedlings at **(A)** 1 month old and **(B)** 3 months old and **(C)** a dying leaf turning yellow that was detached from the plant just before the experiment. Red circles indicate the measured leaf region.

from the plant was referred to as a dying leaf. For both experiments, three replicates were prepared for each of the sample conditions.

2.2 Experimental system and protocol

Figure 3 shows an overview of the experimental system. The system contained two light systems, one for illuminating the plant sample and the other for measurement by laser speckle. The illuminating system consisted of an FR LED light with a wavelength of 735 nm fixed with an arm stand that irradiated a leaf of the sample plant. A red LED of 630nm was also used for experiments done for the FR plus R condition. The system for measuring speckles consisted of a laser diode (LD) (THORLABS, CPS series, NewJersey, USA) with a wavelength of 852 nm, a beam diameter of 1 mm × 2 mm, and a power of 1.26 mW. The plant leaf was gently held by sandwiching the sides of the leaf to magnetic sheets, as shown in the inset of Figure 3. The scattered light from the leaf interfered to produce speckles on the surface of the CMOS camera (THORLAB, DCC1545M-GL, NewJersey, USA; pixels: 1024 × 1280). The distances between the laser and the sample and between the sample and the CMOS camera were each 150 mm.

Laser light was made to an incident on the leaf at 45 degrees with respect to the normal of the leaf, and the scattered light was collected by the CMOS camera. Here, the basic configuration of the optical system was adjusted so that the light reflected from the sample leaf interfered. As for the distances, the distance from the leaf has to be far enough that the scattered field interfering with the camera plane produces fully-developed speckles (Dainty, 1984). A sharp-cut filter (IR82, cutoff wavelength: 820 nm or less, Fujifilm, Japan) was placed between the plant sample and the camera to block unwanted light other than the scattered LD light from the sample entering the camera.

Figure 4 shows the experimental protocol used to acquire the images. The CMOS camera recorded speckle video clips at a frame rate of 15 fps. Before the start of the experiment, the plant was taken out of the chamber and kept in the dark for 10 min, followed by the acquisition of biospeckle videos. This was followed by exposure to FR. The FR exposure experiment consisted of two investigations. The first investigated the healthiness and FR effects and the second age effects under FR plus R. In both cases, the FR or the FR plus R exposure periods were varied and done at an exposure period of 120 s or 300 s.

In both experimental cases, biospeckle acquisition was done in a consecutive sequence of three sets, with each set lasting for 20 s, totaling 60 s. FR and R light PFD levels were set at 78 μmol m^{-2} s^{-1} and 186 μmol m^{-2} s^{-1}, respectively. All the light levels used during the growth and FR exposure conditions are given in Table 1. Here, the FR and R PFD light levels were chosen based on the previous research of Jin et al. (2021). Furthermore, the timing of 120 seconds and 300 seconds for the laser speckle study was chosen based on our previous laser speckle response of plants to sound study (Hirai et al., 2020) and the short-term effects investigated by Lazzarin et al. (2024). The conditions for the experiments are summarized in Table 1.

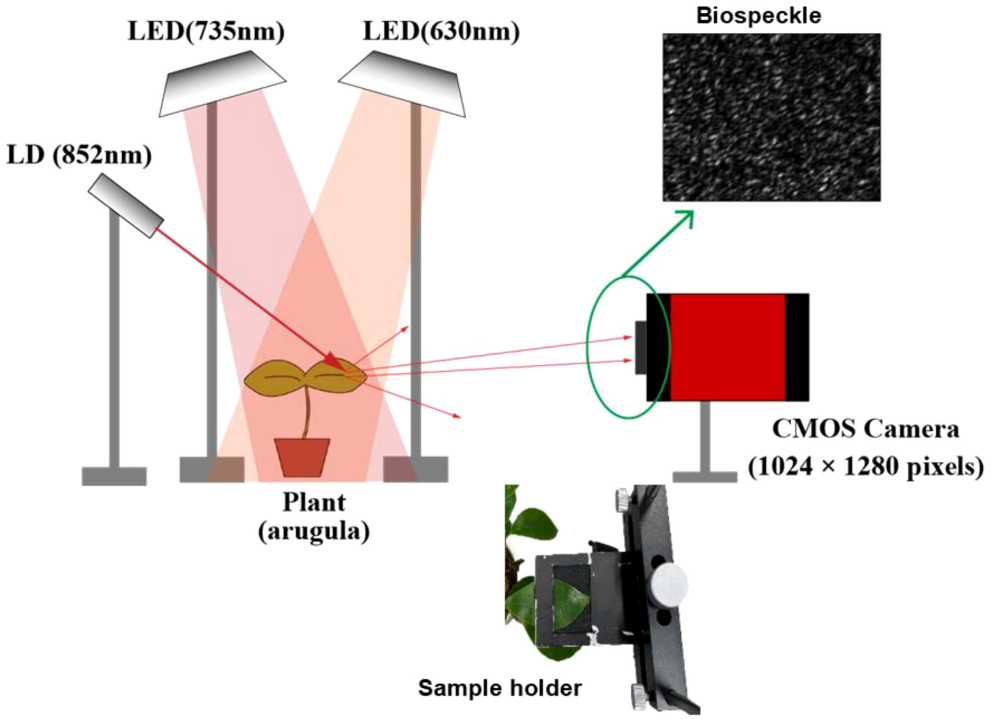

FIGURE 3
Experimental system for measuring the short-term FR response of plants using the laser biospeckle method with an inset of the sample holder with a mounted leaf. Laser light of 852 nm was made to illuminate the leaf of the plant, and the scattered light from the leaf was acquired by a CMOS camera. The plant was illuminated either by FR (735 nm) alone when investigating the healthiness effect or FR plus R (630 nm) illumination in the age effect experiment. The biospeckles shown in the inset formed on the camera plane were recorded as videos to be analyzed.

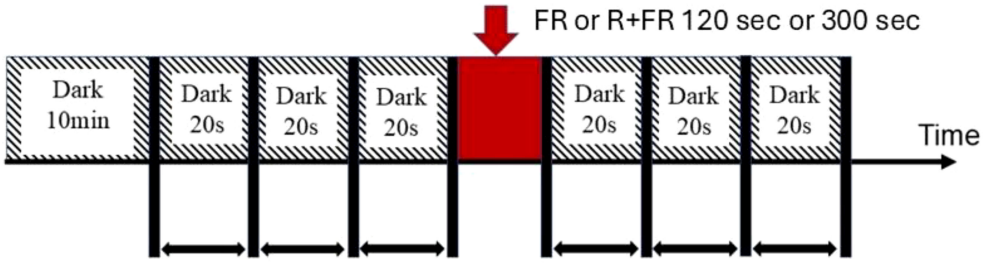

FIGURE 4
Experimental protocols for comparing biospeckles at different FR or FR plus R irradiation. Following an initial dark period of 10 min, the biospeckles were recorded. Similarly, following FR or FR plus R radiation for a period of 120 s or 300s, the biospeckles were recorded. In both cases, the recording was done in sets of three with each set lasting for 20s and thus for a total of 60s.

2.3 Laser biospeckles and analysis

As explained in the introduction, biospeckles are formed when living tissue, such as plant leaves, is irradiated with laser light. This is because the light scattered from the surface and from the internal structures of the leaves interfere to produce speckles on the camera surface. Several methods exist for analyzing biospeckles, including a contrast-based evaluation of each acquired speckle image and assessment of the uniformity of speckle images using the second-order moment (IM) (Alves Braga Junior et al., 2007). In this study, we conducted cross-correlation between the frames of the acquired biospeckles (Ansari and Nirala, 2013) to evaluate the response of the plants to light.

The frame rate of the camera during the measurement was 15 fps, and video data was acquired in three sets, with each set lasting 20s for an overall period of 60 s. The video data were analyzed using analysis software (MATHWORKS, Natick, MA, USA version: R2023b). Here, each 20-s video was analyzed individually (Supplementary Information S1, S2), and the first 20-s video was used for comparison between different conditions, namely the healthiness and the age of the plants. Supplementary Videos for the dead leaf and 1-month-old leaves under no FR and FR are given in S3, S4, and S5, respectively.

In the analysis, the correlation coefficient denoted by γ was calculated between the first frame, which is reference frame A, and the subsequent frame, B. A_{mn} and B_{mn} are the intensities, where m and n specify the pixels in the frame. $\bar{A}$ and $\bar{B}$ indicate the average of the intensities of each of the frames A and B, respectively.

$$\gamma = \frac{\sum_m \sum_n (A_{mn} - \bar{A})(B_{mn} - \bar{B})}{\sqrt{\{\sum_m \sum_n (A_{mn} - \bar{A})^2\}\{\sum_m \sum_n (B_{mn} - \bar{B})^2\}}} \quad (1)$$

When there is greater movement within the leaf, there is higher decorrelation and *vice versa*. Thus, a decrease in correlation and an increase in correlation relate to large and small changes, respectively. In other words, a decrease in correlation corresponds to increased plant movement and an increase in correlation corresponds to decreased plant movement. Therefore, to create a positive measure that can relate to the activity of the plant, we used a quantity, the biospeckle activity (BA), which is calculated as the value that remains after the correlation coefficient is subtracted from unity. BA makes it easier to see changes over time.

$$BA = 1 - \gamma \quad (2)$$

For stationary objects, BA is zero, while for an object that moves, BA decreases with the slope of variation depending on the motion of the object. When the object is moving fast, the slope is steep, and when the object moves relatively slow, then the slope of BA is gentle. For comparison with the plant leaf, a paper object, as a stationary object, has been introduced to assess the relative activity between the reference or the first frame and the rest of the recorded video frames.

To quantitatively evaluate the slope of the BA variation, the variation within the first 0 to 2 s was used, and the slope over this region was calculated by fitting a straight line. The fitted slope was

TABLE 1 Illumination conditions under different conditions of laser biospeckle recording in experiments with healthiness and age parameters and the summary of results.

Experimental parameters	FR/R PFD (μmol $m^{-2}s^{-1}$)	Sample details	Exposure time (s)	BA slope results at 2 sec
Healthiness of the plant	78/0	Healthy	120	Increase
			300	Decrease
		Weak	120	Decrease
			300	Decrease
Age of the plant	78/186	1 month old	120	Increase
		3 months old	120	Decrease

used as a parameter and is indicated as a shaded area in all the graphs. Based on the slope, we can discern when the initial slope of BA variation is steeper, the speckle frames are then decorrelated faster, and thus, the activity or movement of the organelles within the leaf is faster. In contrast, when the slope of the initial variation is gentler, the neighbouring frames are then correlated, and thus, there is slower movement or there could be more coordinated displacements of the organelles within the leaf. When there is zero movement between the frames, then the correlation becomes close to one and the object could be considered as stationary.

2.4 Statistical analysis

Statistical analysis was done using Excel (Microsoft, Seattle, DC, USA). A paired t-test was performed to assess whether there was a significant difference, set at $p< 0.05$. For each of the conditions, BA was averaged across three samples. Statistical significance was tested between the treatment conditions of before FR or FR+R and after FR or FR+R treatments. In the healthiness effects experiment, significance tests were conducted between healthy and non-healthy plants. Similarly, for the age effects experiment, significance tests were conducted between 1-month-old and 3-month-old healthy plants under no FR and FR+R.

3 Results

3.1 Healthiness of plant and FR

The results of the BA obtained for the healthy and weak plants that were identified from the leaves as indicated in Figure 1 are shown in Figures 5A–D, respectively, under FR-only irradiation of 120 s (a,c) and 300 s (b,d). In all the plants, the BA increased with the increase in time. However, the slope of the rise of BA was different depending on the healthiness of the sample and the FR exposure times. When comparing the 120 s and 300 s FR exposures, there was a clear difference in the increase of BA depending on the healthiness of the sample.

Under 120s FR irradiation, the BA variation before and after FR exposure differed for healthy and weak plants (Figures 5A, C). For the healthy sample, the slope of the variation of BA was steeper after exposure than before, indicating a stronger activity within the healthy leaf (Figure 5A). In comparison, for the weak sample, the slope of the variation of BA was steeper before than after exposure to FR (Figure 5C). This implies that FR exposure could be causing less activity within the leaf of a weaker plant or slowing it down, possibly because of less biological activity within the leaf.

In contrast, under 300 s exposure to FR radiation, BA variation before and after exposure was similar for both the healthy and weak

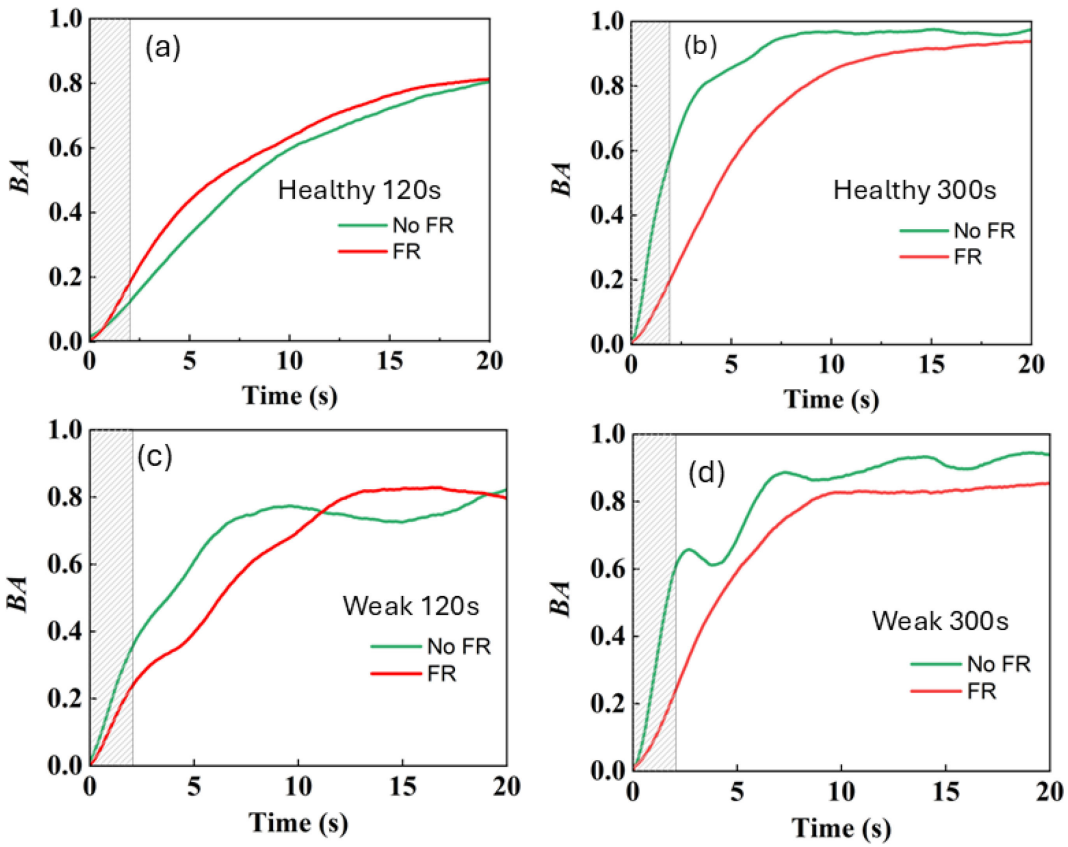

FIGURE 5
Average BA as a function of recording time for healthy **(A, B)** and weak **(C, D)** plants at different FR irradiation times of 120 s **(A, C)** and 300s **(B, D)**. Green and red lines indicate NoFR and FR exposure conditions. The shaded area corresponds to the region used for slope evaluation.

samples, with the slope being lesser for the FR-exposed ones (Figures 5B, D). In other words, the BA before exposure was steeper than that after exposure. Moreover, the variation in slope was also statistically significantly different depending on the healthiness of the plant. For the healthy plant, there was a significant difference in the slope between the NoFR and FR exposed samples. These results indicate that the effect of FR was different depending on the health status of the plant.

3.1.1 Results obtained with paper as a control

For comparison with the plant leaf, a stationary paper object was introduced to assess the relative activity between the reference or the first frame and the rest of the recorded video frames. Figure 6 shows the results obtained under the absence and presence of FR. Under no FR, as shown by the green line, BA was zero or, in other words, the correlation was one all the time as expected. Under FR, although we expected the paper to show null activity because of the absorption of FR light by paper, the activity for the paper was not zero. There was a finite correlation between the recorded frames and there was a finite BA that increased slowly with time. This was believed to be due to the heating up of the paper due to heat from the FR radiation.

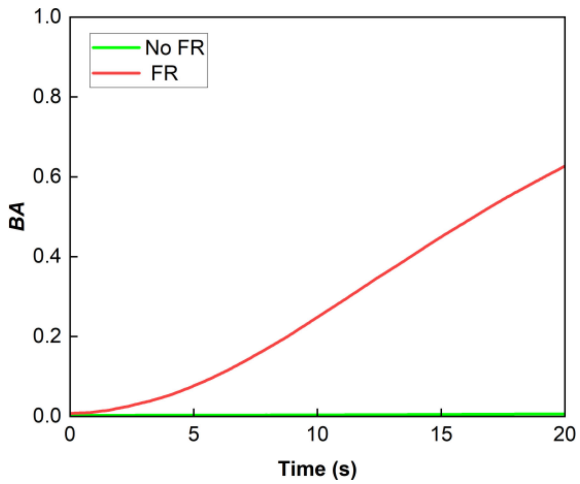

FIGURE 6
Average BA as a function of time for paper. Although we expected the paper to show null activity because of the absorption of FR light by paper, the activity within the paper was not zero, but there was a finite correlation between the recorded frames. Under no FR, the correlation was one all the time or, in other words, BA was zero.

3.2 Evaluation based on the slope of BA variation

Next, the slopes of BA variation in Figures 5A–D were quantitatively compared. To evaluate the difference in the steepness of the variation of BA under different conditions, the slope of the BA variation was estimated as defined in the analysis section and was used. As stated previously, the steeper the variation, the faster the correlation between successive frames vanishes, and thus, the motion could be more extensive, and the activity could be stronger. In contrast, the slower variation or lower value of the slope could be the result of a slowdown of the activity and could be from sustained correlated activity. It thus could be the result of displacement activity within the plant tissues, such as expansion and elongation growth.

In fact, a plant consists of thousands of cells of different shapes, sizes, and so on, and the growth is uniform across the plant. At the same time, plant growth is a complex and highly dynamic process and is stringently regulated with proper balance between turgor and wall extensibility. Turgor pressure makes the cell swell. Turgor occurs because the osmotic water uptake causes the cells to become turgid, leading to internal pressure. Thus, it is because of the turgor pressure that a cell grows or elongates. The turgor-driven cell wall expansion is irreversible and involves a slow reorganization of the cell wall (Hamant and Traas, 2010); (Taiz and Zeiger, 2003).

The slope under different FR exposure times, i.e., 120 s and 300 s, is shown in the histogram plots in Figure 7. The vertical axis represents the slope within a period of 2s, and the horizontal axis represents the sample condition, with the green and red bars indicating the before and after FR conditions, respectively. For 120 s of FR irradiation, for the healthy young plant, the slope of BA following FR exposure was large in comparison to that in the absence of FR. In contrast, for the weak sample, it is *vice versa* with a larger slope under no FR than that of under FR exposure. A paired t-test revealed that there was a significant difference between the healthy and weak plants and between the exposure conditions for 120 s. For the 300s experiment, there was a significant difference between the exposure conditions but not between the weak and healthy conditions.

For the 300 s FR exposure, irrespective of the healthiness of the leaves, the slope of BA was smaller under FR than that under the absence of FR. The steepness of the slope indicates the activity within the tissue, and the results indicated that longer FR exposure slows down the activity. When comparing 120 s and 300 s FR exposure times, longer FR exposure led to a decrease in the slope irrespective of the healthiness of the plant. For both healthy and weak samples, the decrease was almost two-fold. One possibility was that, with longer exposure, there could be an effect of heat generated from longer FR exposure, which may slow down the internal activity within the leaf tissue and possibly influence growth.

3.3 Plant age and FR plus R

The influence of FR plus R exposure on the age of the plant was also investigated. Figures 8A, B show the BA results obtained under the presence and absence of FR plus R, respectively, for 1-month-old and 3-month-old plants. The vertical axis represents BA and the horizontal axis represents the measurement time. FR plus R exposure was given for 120 s. For comparison, the dying plant leaf is also shown in Figure 9, and it can be seen that the activity of the dying leaf was much slower. Here, the dying leaf is the one that had fallen off and is no longer attached to the plant, and the appearance was also yellow. Thus, a clear correlation between the age of the plant and FR plus R effects can be seen from a comparison

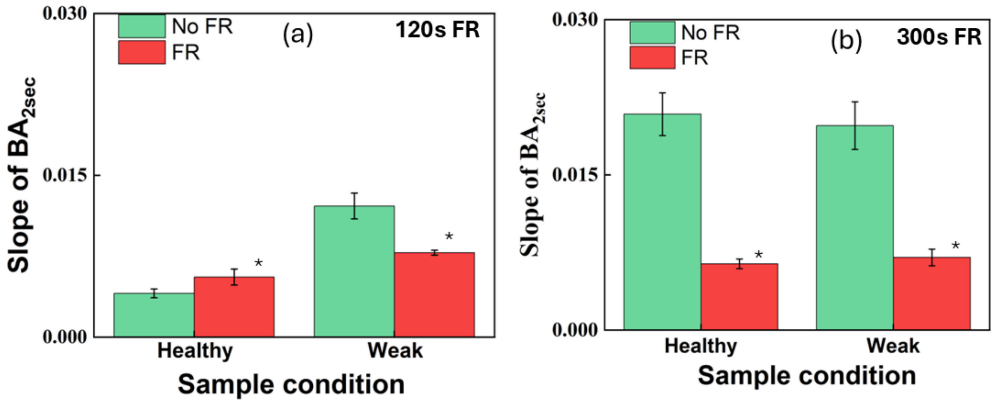

FIGURE 7
Comparison of the initial slope of average BA up to 2 s at different FR irradiation times shown in red for **(A)** 120s and **(B)** 300s compared to no FR irradiation shown in green. Error bars correspond to standard error. Here, the slope was calculated from the initial 2s by fitting a line to the region within the shaded area of Figure 5. * indicates a significant difference between the NoFR (green bar) and FR exposure conditions (red bar) for both **(A, B)**. Further, we expected the slopes of the healthy and weak plants under no FR to behave in the same fashion. However, the weak set and the healthy sets were prepared separately; it is possible that there existed large differences.

of the BA variation. For a plant of a younger age, the slope was steep with exposure to FR plus R. In contrast, for a plant of old age, the slope and the variation in BA are gentler, indicating the slowing effect of FR plus R for older plants. These results indicate that there is a clear effect of age on the FR plus R exposure.

The results for the initial slope within the first 2 s for two different ages are shown in Figure 10. In the case of young leaves from a 1-month-old plant, the FR plus R treatment increased the slope while the slope decreased for the 3-month-old plant. This indicates that FR plus R exposure for a younger plant had the effect of increasing activity within the tissue. In contrast, for the 3-month-old plant, FR plus R had the effect of reducing the slope with increased age, indicating that there was a slowing down of activity within the plant. Significance tests using paired t-tests revealed that the slopes between the exposure conditions for both age groups were significantly different. * indicates a significant difference between age groups and ** indicates a significant difference between the NoFR and FR+R exposure conditions. This may be due to the fact that the younger leaves (1 month old) were more vigorous and responded more actively to the FR plus R stimulation. The other possibility is that, with age, the plants themselves stop making use of the FR and, thus, there was a reduction in the relative activity (review work of Tan et al., 2022).

4 Discussion

In this study, our aim was to investigate the short-term effects of far-red light on plants using the laser biospeckle method. In comparison to the existing techniques of physiological measurements by photosynthesis and physical measurements, we have shown that our non-invasive and non-contact laser biospeckle method can detect the variation response in the plant after a few minutes of exposure to FR and red light, and it can work as a complementary technique to the existing techniques. To our knowledge, the application of laser biospeckles to investigate

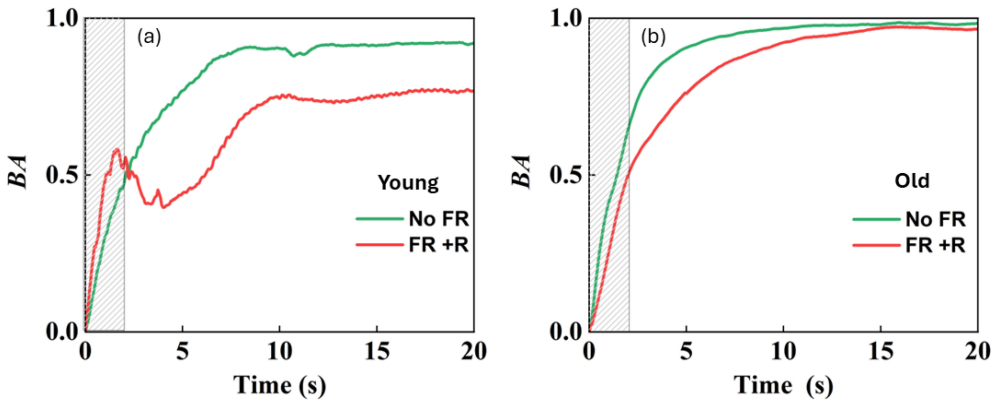

FIGURE 8
Average BA results under no FR and FR plus red light for 1-month-old **(A)** and 3-month-old plants **(B)**. Paired t-tests were done between 1-month-old and 3-month-old plants under NoFR and FR+R and the results differed significantly.

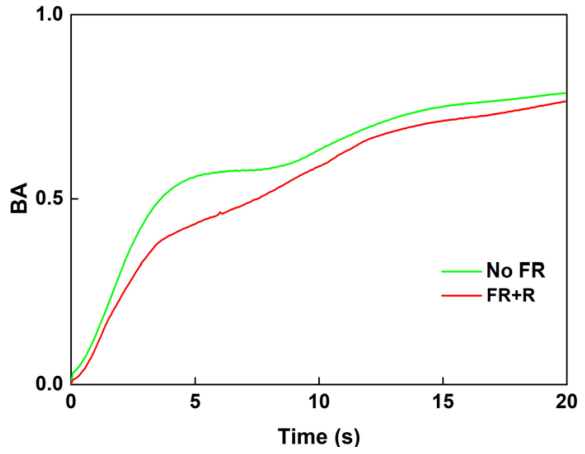

FIGURE 9
BA as a function of time in seconds for a dying leaf under NoFR and FR plus R. Despite the leaf having fallen off, there was some difference in the BA activity depending on the exposure to FR+R compared to no FR. The dying leaf experiment was done to confirm the aging effect.

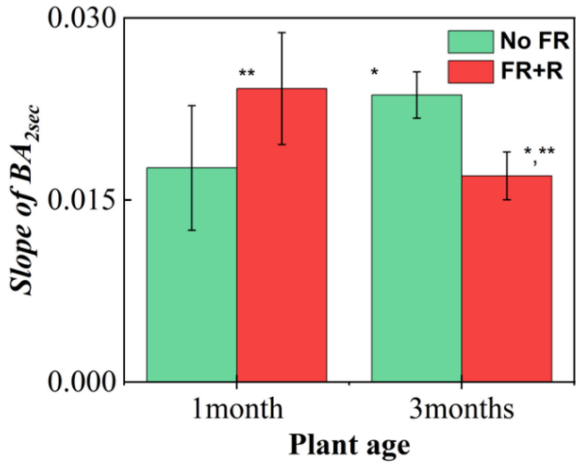

FIGURE 10
Slope of BA up to 2 s for two different plant ages, namely 1-month-old and 3-month-old plants. Green and red indicate the conditions of NoFR and FR+R exposure. In this experiment, FR was irradiated in conjunction with red LED light. Error bars correspond to the standard errors. * indicates the existence of a significance difference in the slope of BA between the ages of the plant. ** corresponds to a significant difference between the NoFR and FR+R treatments. Here, the slope was calculated from the initial 2s as shown by fitting a line to the region within the shaded area of Figure 8.

instantaneous spatially localized changes after FR or FR plus R exposure has never been done before.

In our study, exposure of arugula to FR (735 nm) and FR plus R (630 nm) against NoFR were compared. To investigate the effects of FR plus R using laser biospeckles, a near IR laser light from a laser diode of 852 nm was used to obtain a video of biospeckles for a period of 20 s from the leaf of the arugula plant *in vivo*. Laser biospeckles are generated when scattered light from biological tissues interferes, and the intensities of such speckles change over time. Investigating the temporal correlation of speckles reflects the structural changes of the scattered structures within the biological tissue. When there is considerable variation, there will be less correlation and *vice versa*. In other words, by examining the decorrelation time of the time-varying speckles for a period of 2 s, we could differentiate the effects of healthiness and age when exposed to FR. The results obtained are summarized in Table 1, along with the conditions of the experiments.

We found that for healthy plants, there was a faster decay of the speckle correlation or steep increase in BA in comparison with an unhealthy plant of almost the same age (Figure 5). By investigating the slope within a 2 s window, under 120 s FR exposure, we found that FR has the effect of increasing the slope for a healthy plant (Figure 7A) but it decreases for a weak plant. Under longer FR exposure, there was a decrease in slope for both the healthy and weak plants (Figure 7B). As for the age comparison, a 1-month-old plant was found to have a faster decrease in correlation, and thus a steep increase in BA in comparison to that of a 3-month-old plant (Figure 8). This indicates that with increased age, there is a slowing down of activity within the plant (Figure 10). Thus, based on our results, we demonstrated that our method has significant sensitivity differentiating the response of the plant within minutes after exposure to FR or FR plus R. This is in agreement with our previous studies of plant's response to sound where we could show that the laser speckles are sensitive to a minutes exposure to sounds (Rajagopalan et al., 2021).

Although this study was done with the intention of demonstrating the feasibility of the laser biospeckle method in the evaluation of FR/R illumination effects, it has the potential to extend to different species. FR is known to be species-dependent (Kalaitzoglou et al., 2019; Shibuya et al., 2016; Lazzarin et al., 2024) and also age plays a vital role in the response of a plant to FR. Thus, exposure times of FR are vital for the advantageous use of FR. One more advantage of our method is that it can be applied to investigate the different parts of a plant. The current study was restricted to leaves. Our method allows us to study the effects of localized changes in relation to perception sites and inter-organ relationships and might be useful for applications in horticulture, such as applying supplemental light at precise times and locations, helping to optimize energy use (Demotes-Mainard et al., 2016).

5 Summary

We proposed using laser biospeckles to investigate the short-term effects of FR. The laser biospeckle method is non-contact, non-invasive, and offers the possibility of conducting real-term measurements. Our measurement method could complement the existing tools as a measure to detect the effects due to a few minutes of exposure to FR. Investigations conducted on the healthiness of the plants and the age of the plants revealed that there was faster decay of the speckle correlation or a steep increase in BA in a healthy plant in comparison to an unhealthy plant of almost the same age, and when comparing age, a 1-month-old plant was found to have a faster decay of the correlation and thus a steep increase in BA in comparison to that of a 3-month-old plant. These results indicate that for unhealthy or aged plants, there is a slowing down of

activity within the plant. Thus, based on our results, we demonstrated that our method has significant sensitivity, differentiating the response of the plant within minutes after exposure to FR or FR plus R. Although the mechanism remains elusive because of the complexity of the plant tissue, our method can work as a complementary measurement technique for speedier investigations of FR effects on plants.

Data availability statement

The raw data supporting the conclusions of this article will be made available by the authors, without undue reservation.

Author contributions

HI: Data curation, Formal analysis, Investigation, Writing – original draft. TB: Data curation, Investigation, Writing – review & editing. KT: Methodology, Writing – original draft. TK: Writing – review & editing. HK: Software, Writing – review & editing. JY: Writing – review & editing. UR: Conceptualization, Data curation, Formal analysis, Funding acquisition, Investigation, Methodology, Project administration, Resources, Software, Supervision, Validation, Visualization, Writing – review & editing.

Funding

The author(s) declare that no financial support was received for the research, authorship, and/or publication of this article.

Conflict of interest

The authors declare that the research was conducted in the absence of any commercial or financial relationships that could be construed as a potential conflict of interest.

Publisher's note

Supplementary material

The Supplementary Material for this article can be found online at: https://www.frontiersin.org/articles/10.3389/fpls.2025.1496790/full#supplementary-material

SUPPLEMENTARY FIGURE 1
BA as a function of time obtained in three sets with each lasting a period of 20s after exposure of the plant to FR with FR exposure time of 120 s. Here, the data were not acquired continuously for a minute but in three sets of 20 s each. Correlation and thus BA were obtained for each of the 20 s with the top representing the BA results obtained with speckles obtained within the 1st 20 s. The middle and bottom represent the results of BA obtained with speckles in the set 2 corresponding to 20 to 40 s and the third set corresponding to 40 s to 60 s times of recording, respectively. Large changes can be seen in the first 20 s and so the data analysis was restricted to the first set of 20 s.

SUPPLEMENTARY FIGURE 2
BA as a function of time obtained for 60 s after exposure of the plant to FR with FR exposure time of 300 s. Here, the data were not acquired continuously for a minute but in three sets with each set lasting 20 s. The top represents the BA results obtained with speckles obtained within the 1st 20 s. The middle and bottom represent the results of BA obtained with speckles in the 20s to 40 s and 40 s to 60 s times of recording, respectively. Although large changes are seen during all the windows of acquisition, in order to conduct a comparison with the results of 120-s exposure, the data analysis was restricted to the first 20 s.

SUPPLEMENTARY INFORMATION S3
Supplementary video under No FR for deadleaf.

SUPPLEMENTARY INFORMATION S4
Video under NoFR for a 1-month-old leaf.

SUPPLEMENTARY INFORMATION S5
Video under FR for a 1-month-old leaf.

References

Aizu, Y., and Asakura, T. (1996). "Bio-speckles," in *Trends in optics, 1st ed.* Ed. A. Consortini (Academic Press, san diego), 27–49.

Alves Braga Junior, R., Silva, B. O., Rabelo, G., Costa, R. M., Enes, A. M., Cap, N., et al. (2007). Reliability of biospeckle image analysis. *Optics Lasers Eng.* 45, 390–955. doi: 10.1016/j.optlaseng.2006.07.002

Ansari, Z., and Nirala, A. K. (2013). Biospeckle activity measurement of Indian fruits using the methods of cross-correlation and inertia moments. *Optik* 124, 2180–2186. doi: 10.1016/j.ijleo.2012.06.081

Benke, K., and Tomkins, B. (2017). Future food-production systems: vertical farming and controlled-environment agriculture. *Sustainability: Science Pract. Policy* 13, 13–265. doi: 10.1080/15487733.2017.1394054

Braga, R. A., Dupuy, L., Pasqual, M., and Cardoso, R. R. (2009). Live biospeckle laser imaging of root tissues. *Eur. Biophysics J.* 38, 679–865. doi: 10.1007/s00249-009-0426-0

Costa, A. G., Pinto, F. A. C., Braga, R. A., Motoike, S. Y., and Gracia, L. M. N. (2017). Relationship between biospeckle laser technique and firmness of acrocomia aculeata fruits. *Rev. Bras. Engenharia Agricola e Ambiental* 21, 68–735. doi: 10.1590/1807-1929/agriambi.v21n1p68-73

Craufurd, P. Q., and Wheeler, T. R. (2009). Climate change and the flowering time of annual crops. *J. Exp. Bot.* 60, 2529–2539. doi: 10.1093/jxb/erp196

Dainty, J. C. (1984). *Laser speckle and related phenomena*. (Springer-Verlag).

Demotes-Mainard, S., Péron, T., Corot, A., Bertheloot, J., Le Gourrierec, J., Pelleschi-Travier, S., et al. (2016). Plant responses to red and far-red lights, applications in horticulture. *Environ. Exp. Bot.* 121, 4–21. doi: 10.1016/j.envexpbot.2015.05.010

Emerson, R., Chalmers, R., and Cederstrand, C. (1957). Some factors influencing the long-wave limit of photosynthesis. *Proc. Natl. Acad. Sci.* 43, 133–435. doi: 10.1073/pnas.43.1.133

Flannigan, M. D., Stocks, B. J., and Wotton, B. M. (2000). Climate change and forest fires. *Sci. Total Environ.* 262, 221–229. doi: 10.1016/S0048-9697(00)00524-6

Hamant, O., and Traas, J. (2010). The mechanics behind plant development. *New Phytol.* 185, 369–855. doi: 10.1111/j.1469-8137.2009.03100.x

Hirai, M., Endo, D., Gonome, H., Kono, T., Yamada, J., and Rajagopalan, U. M. (2020). Laser biospeckle metrology in investigating plant-sound interactions. *Proc.SPIE* 11238, 1123813. doi: 10.1117/12.2543663

Hoenecke, M. E., Bula, R. J., and Tibbitts, T. W. (1992). Importance of 'blue' Photon levels for lettuce seedlings grown under red-light-emitting diodes. *HortScience : A Publ. Am. Soc. Hortic. Sci.* 27, 427–430. doi: 10.21273/hortsci.27.5.427

Huang, W., Duan, W., and Chen, Y. (2022). Unravelling lake water storage change in central asia: rapid decrease in tail-end lakes and increasing risks to water supply. *J. Hydrology* 614, 128546. doi: 10.1016/j.jhydrol.2022.128546

Igarashi, H., Takemura, K., Kono, T., Kadono, H., Yamada, J., and Rajagopalan, U. M. (2023). Laser biospeckle based novel method in the evaluation of far-red light effects on plant growth. *Proc.SPIE* 12377, 123770C. doi: 10.1117/12.2649031

Jin, W., Urbina, J. L., Heuvelink, Ep., and Marcelis, L. F. M. (2021). Adding far-red to red-blue light-emitting diode light promotes yield of lettuce at different planting densities. *Front. Plant Sci.* 11. doi: 10.3389/fpls.2020.609977

Kalaitzoglou, R., Van Ieperen, W., Harbinson, J., Martinakos, S., Weerheim, K., Nicole, C. C., et al. (2019). Effects of continuous or end-of-day far-red light on tomato plant growth, morphology, light absorption, and fruit production. *Front. Plant Sci.* 10, 373037. doi: 10.3389/fpls.2019.00322

Lazzarin, M., Dupont, K., van Ieperen, W., Marcelis, L. F.M., and Driever, S. M. (2024). Far-red light effects on plant photosynthesis: from short-term enhancements to long-term effects of artificial solar light. *Ann. Botany.* doi: 10.1093/aob/mcae104

Pandiselvam, R., Mayookha, V. P., Kothakota, A., Ramesh, S. V., Thirumdas, R., and Juvvi, P. (2020). Biospeckle laser technique – A novel nondestructive approach for food quality and safety detection. *Trends Food Sci. Technol.* 97, 1–13. doi: 10.1016/j.tifs.2019.12.028

Paradiso, R., and Proietti, S. (2022). Light-quality manipulation to control plant growth and photomorphogenesis in greenhouse horticulture: the state of the art and the opportunities of modern LED systems. *J. Plant Growth Regul.* 41, 742–805. doi: 10.1007/s00344-021-10337-y

Pettai, H., Oja, V., Freiberg, A., and Laisk, A. (2005). Photosynthetic activity of far-red light in green plants. *Biochim. Biophys. Acta - Bioenergetics* 1708, 311–215. doi: 10.1016/j.bbabio.2005.05.005

Prasad, V., Boote, K. J., Hartwell Allen, L. Jr., and Thomas, J. M.G. (2002). Effects of elevated temperature and carbon dioxide on seed-set and yield of kidney bean (Phaseolus vulgaris L.). *Global Change Biol.* 8, 710–215. doi: 10.1046/j.1365-2486.2002.00508.x

Rajagopalan, U. M., Wakumoto, R., Endo, D., Hirai, M., Kono, T., Gonome, H., et al. (2021). Demonstration of laser biospeckle method for speedy *in vivo* evaluation of plant-sound interactions with arugula. *PloS One* 16, 1–15. doi: 10.1371/journal.pone.0258973

Rajan, P., Lada, R. R., and MacDonald, M. T. (2019). Advancement in indoor vertical farming for microgreen production. *Am. J. Plant Sci.* 10, 1397–14085. doi: 10.4236/ajps.2019.108100

Shibuya, T., Endo, R., Kitaya, Y., and Hayashi, S. (2016). Growth analysis and photosynthesis measurements of cucumber seedlings grown under light with different red to far-red ratios. *HortSci.* 51 (7), 843–846. doi: 10.21273/hortsci.51.7.843

Silva, S. H., Lago, A. M. T., Rivera, F. P., Prado, MônicaE. T., Braga, R. A., and de Resende, J. V. (2018). Measurement of water activities of foods at different temperatures using biospeckle laser. *J. Food Measurement Characterization* 12, 2230–2395. doi: 10.1007/s11694-018-9839-8

Singh, P., Chatterjee, A., Bhatia, V., and Prakash, S. (2020). Application of laser biospeckle analysis for assessment of seed priming treatments. *Comput. Electron. Agric.* 169, 105212. doi: 10.1016/j.compag.2020.105212

Taiz, L., and Zeiger, E. (2003). *Plant physiology. 3rd ed* (Sunderland: Sinauer Associates).

Tan, T., Li, S., Fan, Y., Wang, Z., Ali Raza, M., Shafiq, I., et al. (2022). Far-red light: A regulator of plant morphology and photosynthetic capacity. *Crop J.* 10, 300–309. doi: 10.1016/j.cj.2021.06.007

Thomaier, S., Specht, K., Henckel, D., Dierich, A., Siebert, R., Freisinger, U. B., et al. (2015). Farming in and on urban buildings: present practice and specific novelties of zero-acreage farming (ZFarming). *Renewable Agric. Food Syst.* 30, 43–545. doi: 10.1017/S1742170514000143

Wong, S.-C. (1990). Elevated atmospheric partial pressure of CO2 and plant growth. *Photosynthesis Res.* 23, 171–180. doi: 10.1007/BF00035008

Yadava, U. L. (2022). A rapid and nondestructive method to determine chlorophyll in intact leaves. *HortScience* 21, 1449–1450. doi: 10.21273/hortsci.21.6.1449

Zdunek, A., Adamiak, A., Pieczywek, P. M., and Kurenda, A. (2014). The biospeckle method for the investigation of agricultural crops: A review. *Optics Lasers Eng.* 52, 276–855. doi: 10.1016/j.optlaseng.2013.06.017

Zdunek, A., and Cybulska, J. (2011). Relation of biospeckle activity with quality attributes of apples. *Sensors* 11, 6317–6375. doi: 10.3390/s110606317

Zhen, S. (2020). Substituting far-red for traditionally defined photosynthetic photons results in equal canopy quantum yield for CO2 fixation and increased photon capture during long-term studies: implications for re-defining PAR. *Front. Plant Sci.* 11. doi: 10.3389/fpls.2020.581156

Frontiers in
Plant Science

Cultivates the science of plant biology and its applications

The most cited plant science journal, which advances our understanding of plant biology for sustainable food security, functional ecosystems and human health.

Discover the latest Research Topics

See more →

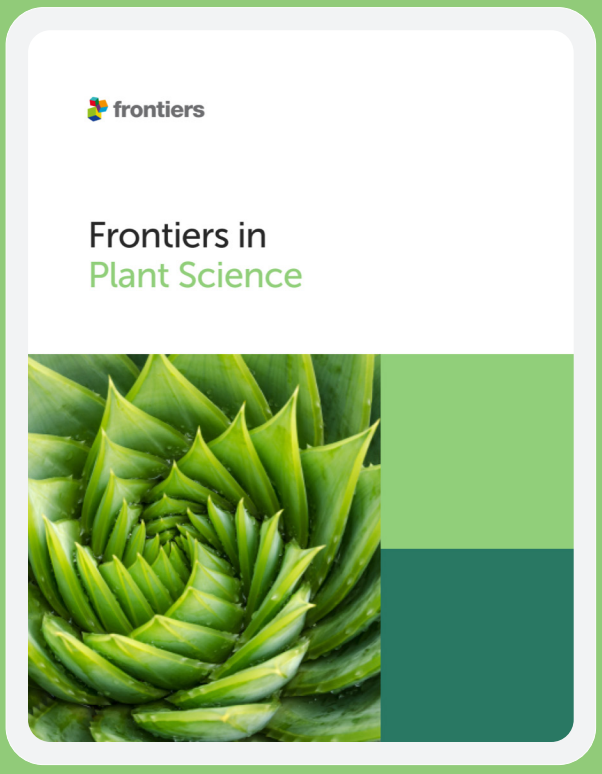

Frontiers

Avenue du Tribunal-Fédéral 34
1005 Lausanne, Switzerland
frontiersin.org

Contact us

+41 (0)21 510 17 00
frontiersin.org/about/contact